# CODED ONE-PORT ACOUSTIC SURFACE-WAVE DELAY LINES

by

A.S. Burgess, B.Sc.,B.E. (Hons.)

A thesis

submitted for the degree of

DOCTOR OF PHILOSOPHY

in the

Electrical Engineering Department

UNIVERSITY OF ADELAIDE

March 1974

TO MY WIFE PATRICIA

CONTENTS

Page No.

CHAPTER 5 - A COMPUTER MODEL FOR SURFACE-WAVE DEVICES



CHAPTER 6 - EXPERIMENTAL AND COMPUTED RESULTS FOR TYPICAL TRANSDUCERS

Page No.

CHAPTER 7 - ONE-PORT DEVICE ADMITTANCE MODEL



CHAPTER 8 - PROPERTIES OF ONE-PORT CODES



CHAPTER 9 - EXPERIMENTAL ONE-PORT CODING SYSTEM

SUMMARY

This thesis describes an investigation into the use of acoustic surface-wave delay lines for the realization of passive coded one-port structures. These devices are of interest for their potential use as coded labels suitable for remote interrogation over a single communication link. The surface-wave mode was selected for this application because of its low velocity compared with electromagnetic radiation and because the correspondence between the spatial geometry and time domain behaviour of interdigital piezoelectric surface-wave transducers, provides a unique method for the production of waveforms coded in the time domain.

The work commences with a description of the general characteristics of the various acoustic modes known collectively as surface-waves, and the development of computer programs to generate basic data on the propagation characteristics and field distributions of surface-waves is described.

A fundamental requirement in both the analysis and operation of a one-port structure which is to function as a read-only information store, is to identify the effective input and output quantities. In this work it is shown how the voltage appearing across the terminals of a one-port connected to a finite source impedance may be determined as a function of the complex one-port input admittance, the source impedance and the source voltage. The input admittance of a complex structure containing many devices (transducers or circuits) connected in parallel may be determined from the admittance matrix defining the coupling between individual devices, and the problem in this situation devolves into one of determining the transfer admittance between individual devices.

Starting from first principles, a general expression has been derived for the frequency transadmittance between a pair of acoustically-coupled interdigital transducers on a weak-coupling substrate by means of a normal mode theory approach. The analysis reveals that the transfer admittance contains the product of the spatial Fourier transforms of the source distributions on the two transducers concerned, multiplied by an additional factor $|\omega|$. This frequency weighting has been verified in the experimental work on frequency-tapered transducers, and also in the published results of other workers.

A simplified model for surface-wave devices permitting the efficient computation of the complete input admittance of a single transducer, and the frequency transadmittance between a pair of transducers has been developed, based on approximate analytic formulae. The model has been tested against experimental results with interdigital transducers in quartz substrates and good agreement obtained.

The functional relationship between the transducer locations and phasing, and the output response waveform of a one-port delay line structure has been analytically derived. The resulting expression is used as a basis for investigation of the general properties of one-port output codes, and the results are illustrated by a detailed survey of three basic coding procedures.

The surface-wave device computer model is used to predict the expected response waveforms for some experimental coded one-port delay devices, and is shown to give good agreement with the experimental observations. The model is then used to explore the dependence of output pulse overlap upon the various delay line parameters, and the results are presented in the form of set of design curves.

The final part of the investigation is concerned with the

computer simulation and experimental modelling of a complete prototype transmitter and receiver system for operation with the experimental devices. Useful coded responses are obtained, demonstrating the feasibility of the coded one-port label concept, and giving good qualitative agreement with the computer model. The limitations presented by the occurrence of second-order effects in lines with a large number of bits in the reply code are examined and it is shown that in general regeneration, and not reflection, causes the major problems in obtaining error-free decoding of the delay line response on weak to moderate-coupling substrates.

## PREFACE

This thesis contains no material which has been accepted for the award of any other degree or diploma in any University. To the best of the author's knowledge and belief, this thesis contains no material previously published or written by another person, except where due reference is made in the text.

(Alan S. Burgess)

ACKNOWLEDGEMENTS

The project described in this thesis was carried out within the Electrical Engineering Department of the University of Adelaide, under the supervision of Dr. P.H. Cole, and later under joint supervision with Dr. D.W. Griffin, over the period from March 1969 to March 1973. The author would like to thank Dr. Cole for suggesting the project, for his many stimulating discussions, unwavering support, and encouragement throughout the course of this work. The author is also indebted to his colleagues, Dr. P.V.H. Sabine, Mr. N.C.V.Krishnamacharyulu and Mr. A.R. Downing for helpful discussions on different aspects of the work.

A number of people made important material contributions to the success of the experimental work. The vacuum chamber used for device fabrication was kindly loaned by Professor D.R. Miller of the Material Science Department, and the experimental receiver unit along with a 50 MHz. power amplifier was made available by Dr. Cole and Dr. R. Vaughan of the University of New South Wales. Dr. Cole also assisted with detailed drawings for the photoreduction cameras. Thanks are also due to the workshop staff of the Electrical Engineering Department who assisted in the construction of the experimental facilities and to Mr. G.W. Pook for assistance in the laboratory.

The author was supported by a Department of Supply Studentship, and finance for the project was provided by the Department of Supply, the Post Master General's Department (Research Contract No. CO/35513), and the University of Adelaide.

# CHAPTER 1

# INTRODUCTION

## 1.1 The One-Port Label Concept

This thesis describes an investigation into the application of acoustic surface-waves for the realization of passive coded one-port delay lines. The motivation behind this study is outlined briefly in this section.

With the advent of the current interest in acoustic surface-wave techniques for practical device development at VHF to microwave frequencies, it was apparent that delay lines of this type were admirably suited to the construction of transversal filters[1] which could utilise the simple relationship between the transducer geometry in the propagation direction, and the device impulse response. The concept of a surface-wave information store may be visualized by means of the example of a transversal filter whose impulse response may be described as a string of pulses in the time domain. It is obvious that the output of such a device could be interpreted as a binary code, for example, and the device could be envisaged as a passive read-only information store, where the information is recorded in the device at the time of manufacture (in the form of the displacement of the transducers). We come thus to the fundamental motivation behind the project: the construction of devices which will produce uniquely coded output pulse trains upon excitation by an input signal. Such devices could be used as labels in any situation requiring identification of separate objects.

The restriction of the field of interest to one-port devices requires further explanation, and arose through a consideration of the following factors. It is envisaged that the most likely application

of such devices would be in the development of automated sorting systems for items such as mail bags in a mail exchange, freight in a warehouse, or baggage at a passenger transport terminal. The operation of sorting implies relative motion of the labelled objects, and poses the problem of how the label reading equipment will communicate with the label. The mechanical problems associated with the arrangement of physical contact between a moving label and the reading equipment would limit both the reliability and speed of sorting, in a system requiring electrical contact. Accordingly attention was focussed on the use of unguided propagation for the communication link.

A number of sorting systems already in existence in the fields of mail sorting, and warehouse container routing employ light beams for the scanning of a suitably coded label, and a recent proposal for the automatic sorting of railway trucks employs microwave radiation to excite a frequency selective transponder.* All these systems require the correct orientation of the label to face the sensing unit and it was felt that a worthwhile improvement would be achieved if this requirement could be relaxed with the surface-wave labels.

The requirement that the label be permitted to adopt random orientation relative to the sensing equipment has a number of direct consequences. The first is that quasi-omnidirectional antennas will be required for the label. If this requirement is accepted then it becomes apparent that the input and output antennas of our coded two-port delay line will <u>both</u> simultaneously receive the excitation signal and retransmit the coded reply waveform. Thus the concept of the one-port delay line was born; the same response will be achieved with a

---

* A description of a typical system employing optically scanned phosphorescent labels may be found in "The Letter Handling System", by H.L. Hulka, D.Y. McFadden and E. Wulf, in The Telecommunications Journal of Australia, Vol.16, 1966, pages 215-235, and a coded microwave transponder is described in "Microwave System for the Automatic Recognition of Freight Car Numbers", by H. Gotz, in Siemens Review, Vol. 37,1970,pages 327-332.

single antenna and the input and output transducers connected in parallel.

It is also possible to make some useful deductions on the desirable frequencies of operation. The requirement for an omni-directional antenna suggests that the propagation wavelength should be greater than the maximum antenna dimensions. If we also wish to minimise shielding of the label by the tagged object then the propagation wavelength should also be greater than the objects to be sorted. These inequalities suggest wavelengths of a few metres, which precludes acoustic propagation, and corresponds to electromagnetic radiation frequencies of around 100 MHz, which of course are well within the efficient operating range of acoustic surface-wave devices.

It thus appeared that acoustic surface-wave devices offered a unique potential for the realization of a general purpose label suitable for electromagnetic interrogation. The following chapters report an investigation of the theoretical aspect of coding one-port structures in general and some of the practical limitations resulting from the employment of acoustic surface-wave technology for the device realization.

## 1.2 A Brief History of Acoustic Surface-Waves

The first recorded reference to an acoustic surface-wave is credited to Rayleigh[2] (1885) who predicted the existence of a wave motion constrained to the surface in isotropic elastic solids. This wave motion, which became known as the Rayleigh wave, was subsequently identified as a significant component of seismic disturbances, and has received detailed study from seismologists since the early part of this century. In this application the interest in the wave motion was restricted to low frequencies and propagation in the earth's crust, usually modelled as a curved laminar structure with macroscopically

isotropic material properties.

Over the years Rayleigh waves also received some attention from various workers who attempted to analyse the wave motion on anisotropic supporting materials, notably Stoneley[3] (1955), Gold[4] (1956), Deresiewicz and Mindlin[5] (1957), Synge[6] (1957), Gazis, Herman and Wallis[7] (1960) and Buchwald[8,9] (1961). In general it was found that analytic solutions were only possible when certain crystal symmetries were invoked.

The first practical application of Rayleigh waves came in the late 1950's when techniques for ultrasonic flaw-detection in metals were developed by a number of workers, including Cook and Van Valkenburg[10] (1954) and Viktorov[11,12] (1962), utilizing the reflection of Rayleigh waves from acoustic discontinuities at or near the surface of the metal. In this work it was not yet possible to launch Rayleigh waves directly and acoustic mode-conversion devices known as comb and wedge transducers were employed.

Then in the early 1960's two factors provided the impetus which precipitated the currect wide interest in the use of surface-waves for an increasingly diverse number of applications. The first was the realization that usefully low propagation losses could be obtained on single crystal materials at frequencies up to and above 100MHz, through the work of Press and Healy[13] (1957), Lamb et al.[14] (1959), and Vinogradov and Ul'yanov[15] (1960).

The second factor was the invention by Mortley[16,17] (1962, 1965), and independently by White and Voltmer[18] (1965), of the inter-digital transducer for the direct generation of surface-waves on piezoelectric materials.* These developments led Ash[19] (1967), and

---

* The publication by White and Voltmer[18] (1965) aroused widespread interest. The independent work of Mortley[16,17] (1962,1965) on the interdigital transducer and Rowen[29] (1964) on the single-phase transducer did not receive general recognition until much later.

others, to conclude that surface-waves might be employed in the realization of circuit components, at frequencies from VHF to micro-waves, by means of techniques similar to those used in the design of conventional waveguide circuit elements.

The development of these proposals required a general method of solution for surface-wave propagation in any prescribed direction on anisotropic and piezoelectric materials of low symmetry. The general case for anisotropic materials had been considered by Deresiewicz and Mindlin[5] (1957) who showed that iterative numerical methods were required to obtain the surface-wave solution, except where the crystal symmetries were such as to permit a reduction in the order of the polynomials to be solved. The resulting particle motion in the general case is three dimensional, and it was found that the decay constants for the motion could be complex, indicating an additional harmonic variation in the expected decay of the particle motion with depth. These solutions were termed 'generalised Rayleigh waves' by Synge[6] (1957) and Gazis et al.[7] (1960), and in the remainder of this work will be simply included under the general term 'surface-waves'.

Coquin and Tiersten[20] (1967) extended the equations of motion to include the effect of piezoelectricity, and employed a digital computer to evaluate numerically the surface-wave velocity curves on several cuts of quartz, but neglected the piezoelectric coupling in their surface-wave solution. This method was extended to include the effect of piezoelectric coupling with open-circuit and short-circuit electrical boundary conditions by Campbell and Jones[21] (1968), who published computed velocity curves for the strongly piezoelectric material lithium niobate, and their computational technique now forms the basis of most surface-wave analysis.

Some of the early investigators in surface-wave propagation

had concluded that in certain directions in certain crystal symmetry classes, it was not possible for the materials to support surface-waves[7,8]. However a detailed survey by Lim and Farnell[22] (1968), using the numerical solution method and a digital computer, failed to find any 'forbidden' directions upon which surface-waves would not propagate and it is now generally believed that surface-waves are always possible.

Lim and Farnell[23] (1969) also described the possibility of pseudo-surface-waves, on certain crystal cuts, which may be confused with the desired surface-wave mode in practical devices. A number of distinct subclasses of surface-waves are known to exist for particular sets of electrical and mechanical boundary conditions at the propagation surface. These are named after their discoverers, and in addition to the well known Love-waves[24] (1911) and Stoneley-waves[25] (1924), we have the recently discovered Bleustein[26] (1968)-Gulyaev[27] (1968)-waves and Maerfeld-Tournois[28] (1971)-waves. These propagation modes only exist for special boundary conditions and in the present investigation attention has been restricted to 'generalised Rayleigh-waves'.

Following the invention of the interdigital transducer there has been a very fruitful period of innovation, which has seen the extension of the transducer concept to the single phase (Rowen[29] (1964), Artz et al.[30] (1967)), grating array (Bahr et al.[31] (1972) ), and multiphase array (Hartmann et al.[32] (1972) ) transducers on piezoelectric materials. These form the basis of most current surface-wave device development, but surface-wave generation has also been demonstrated using the thermal effects of electromagnetic radiation (Lee and White[33] (1968) ), the magnetostrictive effect (Voltmer et al.[34] (1969) ), the travelling domain of Gunn diodes as sources (Lee and White[35] (1970) ), and the electrostrictive effect (Iamsakun and Wilkinson[36](1972).

An even wider variety of techniques have been employed for the detection of surface-waves. The earliest detectors were the volume mode conversion and single phase and interdigital transducers, mentioned previously, operating reciprocally. The alternative surface-wave detectors function by sensing the motion of the surface, the associated electric field of electroacoustic surface-waves, or the surface heating due to the passage of the surface-wave. The surface motion may be detected by the induced voltage in a conductor on the surface which is located in a known magnetic field (Serafin et al.[37] (1967) ), by the diffraction (Ippen[38] (1967) ) or reflection (Korpel et al.[39] (1967) ) of collimated optical radiation at the distorted propagation surface, by the transport of small particles placed upon the surface (Engan[40] (1969) ), by the turbulence created in nematic liquid crystals (Davis and Chambers[41] (1971) ), or by means of the piezoresistance effect in field effect transistors (Bruun[42] (1971) ). The electric field of an electroacoustic surface-wave may be sampled directly with a probe (Richardson and Kino[43] (1970) ), or inferred from its effect upon electron emission (Blackledge and Kaufman[44] (1969) ), and the surface-wave heating effect may be sensed with a bolometer (Gloersen and White[45] (1971) ).

Of the various options available at the commencement of this project (1969) the interdigital transducer appeared to be the most promising and was selected for more detailed study with regard to the production of coded delay lines.

The early work on the development of practical devices was hampered by a lack of suitable analytic tools for the analysis of device behaviour, particularly with respect to transducer design. The early work made use of the obvious analogy between the interdigital grid electrodes and an end-fire antenna (White[46] (1967) ), and obtained

reasonable agreement with the experimental findings. Probably the biggest single advance in this direction came with the publication by Smith et al.[47,48] (1969) of their three-port model intuitively derived by representing each individual section of the grid with the three-port volume-wave equivalent circuit of Mason[49] (1964). This model has been demonstrated to give a very good description of transducer behaviour on both weak- and strong-coupling substrates, but the complete model for multi-transducer structures becomes quite complex. In the simple equivalent circuit representation derived for the input impedance of uniform interdigital grids it provides a very convenient, and in many cases sufficiently accurate, basis for the quick design of simple delay lines.

A general basis for the analysis of surface-wave structures in general, and transducers in particular, was first provided by Auld[50,51] (1969, 1971) who developed convenient formalisms and proved the necessary orthogonality relations to permit the representation of surface-wave fields in terms of an orthogonal set of electroacoustic surface modes (often called the surface-wave normal-mode theory), to permit the use of normal-mode techniques already well established in microwave theory. This development permitted a unified approach to be taken with much of the work which had occurred previously, including the fields of transduction, reflection and scattering ( and also surface-wave amplification which is outside the scope of the present work).

At the time of writing, the field of acoustic surface-wave technology can be said to be approaching a degree of maturity. The theoretical and experimental techniques now available permit the design and manufacture of surface-wave devices with considerable precision. Much of this knowledge has become available during the course of the present investigation and has made a significant contribution to the results achieved.

This historical survey is of necessity rather brief, and for greater detail on the topics mentioned the reader is referred to the excellent review papers by White[52] (1970) and Kino and Matthews[53] (1971).

## 1.3 An Outline of the Thesis

The preceding sections of the present chapter are concerned with an introduction to the concept of a one-port information store, and a brief survey of the historical development of the field of acoustic surface-waves.

Chapter 2 contains a brief description of a computer program developed to provide accurate data on the surface-wave propagation for the later experimental work. The program is based on the method of Campbell and Jones[21], and includes provision for a perfect conductor at a specified height above the propagation surface, to permit determination of the electroacoustic coupling factor $\Delta v/v$ on piezoelectric materials. The program is used to provide basic data for propagation on Y-cut quartz, and also to supply input data to a subsequent program which produces contour and vector field plots of the principal acoustic and electric fields, providing a visual aid to the interpretation of the wave motion and electric coupling mechanisms.

In Chapter 3 the conventions used in setting up an admittance formalism for the characterisation of both one-port and two-port surface-wave structures is described. It is shown that the voltage transfer ratio for such devices may be expressed as a series expansion in terms of the appropriate admittance matrix coefficients, and that the individual terms in the expansion may be identified as the first, second and higher-order responses of the device in question.

The admittance formalism depends upon the availability of suitable formulae to permit the ready calculation of the admittance

coefficients, and these are derived in Chapter 4. By means of the normal mode techniques developed by Auld[50], an expression is derived for the frequency transadmittance between a pair of acoustically coupled interdigital transducers, in the weak-coupling approximation. The resulting expression predicts two features of surface-wave devices not accounted for in the simpler $\delta$-function models, and which are verified in the experimental work. The first is the appearance of a $|\omega|$-factor in the frequency response product, which accounts for the rising sensitivity in log-frequency-tapered transducers, and which is in fact present in all interdigital transducers. The second is the occurrence of polarity inversion in the output of two-port delay lines employing two identical transducers.

The diagonal elements of the admittance matrix are the input admittances of the individual transducers, and an expression for the input admittance has been obtained by Auld and Kino[54]. Their derivation is recast here in terms of the open circuit propagating modes appropriate to the present analysis, and modified slightly to obtain the result in terms of the same transducer source function as used in the transadmittance analysis.

The transadmittance formula is then used as the basis for the derivation of an approximate expression for transducers with variable electrode overlap (apodizing) and spacing, in Chapter 5. This expression is used as the basis of computer programs, written to evaluate the input and transfer admittance parameters for later use in modelling the behaviour of the experimental devices. This approximate expression could also be readily related to the simpler $\delta$-function transducer models, but in view of the efficiency of the computer programs described in Chapter 5, the small computational saving which would be achieved by this simplification did not appear to justify the loss in

modelling accuracy.

In Chapter 6 the fabrication and testing of experimental delay lines to test the accuracy of the computer model are reported. Experiments were performed on both uniform and log-frequency-tapered transducers, on various cuts of $\alpha$-quartz, and good agreement was obtained with the computer model.

In Chapter 7 attention is focussed on the coding capabilities of one-port structures. An analytic expression relating the output response of a coded one-port delay line to the admittance coefficients relating to the individual transducers is obtained, using the expansion techniques described in Chapter 4. The basic relationship between the transducer pattern and the response code is shown to be a modified auto-correlation function.

The properties of this relationship are investigated in more detail in Chapter 8, where it is shown that due to the natural properties of the autocorrelation function it is possible for more than one transducer pattern to produce any particular output response. A systematic method for the classification of coding procedures is introduced and the need for a decoding algorithm is outlined. The particular algorithms used in this study are described and it is demonstrated that the introduction of a decoding procedure results in a further reduction in the number of useful responses available from any particular coding scheme. Comparative curves showing the relative coding efficiencies of the three basic coding schemes investigated are given for various decoders.

The study of coding schemes assumes that each pulse in the reply code is readily discernible, and in Chapter 9 the pulse envelopes obtainable from delay lines employing uniform interdigital transducers are examined both theoretically and experimentally, with particular emphasis on the pulse spreading in the time domain. The results for

a line connected as a simple one-port structure show that it is adequately described by the computer model developed in Chapter 7. The next sections of the investigation are concerned with the detectability of the output code from the line when used with a complete prototype pulsed transmitter and receiver system. It is shown that the system parameters will have a significant role in determining the waveshape of the reply code, and should be matched to the delay line design.

Chapter 10 has a more detailed survey of the factors which limit the packing density of coded information on the delay lines, and the level of second-order effects in the output response. In the trial system examined, regenerated pulses determine the second-order signal levels, and are shown to be the limiting factor in determining the total number of transducers which may be employed on an echo-line, thus limiting the total number of useful codes available in a given coding system.

Some suggested improvements, which might be incorporated into the development of a full scale implementation of the coded one-port acoustic wave delay line concept, are described in Chapter 11.

In Chapter 12, the work is summarized and some conclusions based on the results are presented. The work concludes with a suggestion as to the most logical approach to coded one-port system design.

# CHAPTER 2

## THE ELECTROACOUSTIC SURFACE-WAVE SOLUTION

### 2.0 Introduction

The simplest type of surface-wave occurs in isotropic solids, and is the motion first identified by Lord Rayleigh[2]. This type of wave is characterised by elliptical particle motion in the sagittal plane*, and the relative amplitude of the motion decays exponentially with depth into the medium. The particle motion is two dimensional and the wave may be considered as the sum of a pair of longitudinal and shear waves which each decay exponentially with depth, propagate at the same velocity, and together satisfy the stress free boundary conditions at the surface of the supporting medium. This wave velocity is usually (but not always) slightly lower than the velocity of bulk shear waves in the same material and has the very important property that the velocity is independent of frequency.

When surface-waves are propagated on single crystal materials, which are attractive for their low propagation loss at the higher frequencies, the wave motion becomes more complex due to the anisotropic elastic properties of the substrate material. The particle motion becomes three-dimensional, and each component of the particle velocity is described as a linear sum of three exponential decay terms, instead of a sum of two terms as in the isotropic case. The decay constants may not be purely real, indicating that the phase of the motion varies with depth into the medium, and this type of motion is sometimes referred to as a 'generalized Rayleigh wave'.

Not unexpectedly, the velocity becomes dependent upon the direction of propagation upon a given crystal cut, and the orientation of the surface relative to the crystal axes. The velocity remains

---

* The sagittal plane is the plane containing the wave vector and the surface normal.

independent of frequency, but in general the nett power flow is no longer collinear with the wave vector (defined as the normal to the phase fronts of an infinite width uniform plane wave).

When the crystalline substrate material is also piezoelectric, as is necessary when employing interdigital transducers, the surface-wave has an associated electric field, and the general solution for the particle motion and electric field parameters takes the form of a linear sum of four terms having exponential decay into the medium. As in the basic anisotropic case, the particle motion is again three dimensional, and the nett power flow is not collinear with the wave vector. The associated electric field contributes to the total energy carried by the electroacoustic wave, and this contribution should be taken into account on strong-coupling substrates. Fortunately, the velocity is still independent of frequency.

Another case of interest, which is now assuming considerable practical importance, is the propagation of surface-waves on non-piezoelectric but anisotropic substrates with thin-film piezoelectric overlays. By depositing interdigital transducer electrodes on top of such a substrate, and confining the piezoelectric material to the region of the transducer, it is possible to launch surface-waves on non-piezoelectric substrates with acceptable efficiency. Analysis of the surface-wave propagation in such cases is even more complex than in the cases cited above and will not be considered here in any detail, except to observe that the propagation of surface-waves on laminar structures is normally dispersive i.e. the velocity varies with frequency.

The above discussion has been in terms of the generalised propagation solutions and it should be pointed out that on anisotropic or piezoelectric substrates it is usually possible to find a number of

propagation directions, on any given crystal cut, in which the transverse component of particle motion is zero, and in these cases the particle motion is two-dimensional and the power flow and wave vectors are collinear. (According to Farnell[55] it is also possible to find directions in which the particle motion is three-dimensional but the power flow is collinear.) The directions of two-dimensional particle motion are commonly associated with any symmetries inherent in the crystal material in use, and these directions are usually sought for the design of practical delay lines.

One of the basic problems in the early work on surface-waves was to find a parameter which would simply and accurately quantify the strength with which a given piezoelectric material would provide coupling to electroacoustic surface-waves. The early attempts to use $k^2$, the conventional coupling factor used to define volume wave coupling[56], met with limited success. Then in 1968 Campbell and Jones[21] proposed the use of the parameter $\Delta v$, where $\Delta v$ is the surface-wave velocity change caused by the lowering of a massless perfect conductor onto the surface of the piezoelectric material. Subsequent analysis by Ingebrigtsen[57] showed that the ratio of $\Delta v/v$ can in fact be related in a direct manner with the strength of surface-waves launched, and the ratio is now almost universally adopted as the relevant coupling parameter.

In the early phases of this project there was very little propagation data available for surface-waves on specific materials,and to facilitate the later experimental work, a general purpose computer program was developed to enable the prediction of the surface-wave parameters for propagation in any direction on any specified cut of any required piezoelectric single crystal material. The computer program, named SURF02, is listed in Appendix A1.1, and is based on the published solution method of Campbell and Jones[21]. To assist compre-

hension of the program execution procedure, and the notation used, the analysis of Campbell and Jones is reproduced in Section 2.2.

In Section 2.3 a further program developed by the author, called ASWPLOT, is described. This program makes use of the surface-wave solution parameters provided by program SURF02 to provide contour and vector plots of the propagating surface-wave fields, as an aid to interpretation of surface-wave phenomena. And in Section 2.4 some computed results for surface-wave propagation on Y-cut quartz are presented.

## 2.1 Coordinate Conventions

### 2.1.1 Crystal Axes

The standard adopted in this work for defining the crystallographic axes, specifying particular crystal cuts and specifying particular propagation directions is the 'I.R.E. Standard on Piezoelectric Crystals, 1949'[58]. The application of these conventions is illustrated in Figure 2.1(a) showing the orientation of X,Y and Z cut surfaces, and Figure 2.1(b) showing XY-propagation. Care is needed in specifying crystal cuts because some of the available literature on quartz (including some from suppliers) contains illustrations which appear to relate to the axis conventions prevailing prior to the introduction of the I.R.E. standards mentioned above.

### 2.1.2 Propagation Coordinates

In the analysis in this chapter orthogonal cartesian coordinates are employed. To permit ready interpretation of the wave motion in the medium it is usual to seek a surface-wave solution such that the propagation vector $\underline{\beta}$ is parallel to one of the coordinate axes, and the surface normal $\underline{n}$ is parallel to another. There is no uniformity in the literature on which axes these should be, and the convention chosen

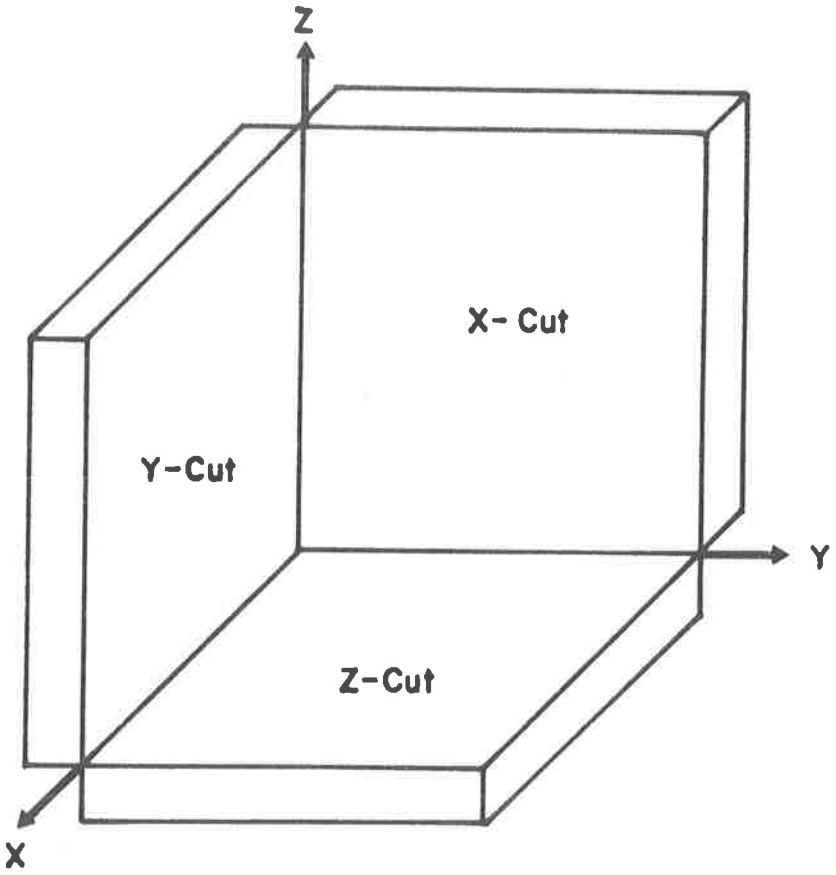


(a)

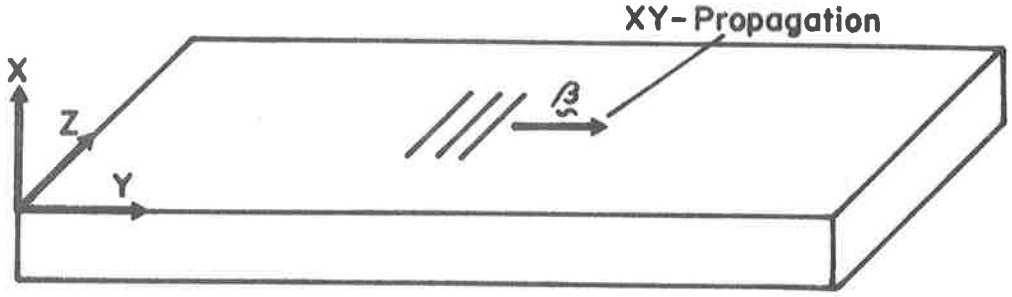


(b)

Figure 2.1 Sketch to illustrate conventions used to specify (a) crystal cuts, and (b) propagation direction on a given crystal cut.

in this work is to assume a spatial dependence of the form $e^{j(\omega t-\beta x_1)}$ as shown in Figure 2.2(a).

To permit analysis of surface-wave propagation at any specified orientation relative to the fundamental crystallographic axes of the substrate material it is necessary to relate all the material parameters to the new axes. This is done using the usual tensor transformation formulae[59],

$$\begin{aligned} \epsilon'_{ij} &= V_{ir}\, V_{js}\, e_{rs} \\ e'_{ijk} &= V_{ir}\, V_{js}\, V_{kt}\, e_{rst} \\ c'_{ijkl} &= V_{ir}\, V_{js}\, V_{kt}\, V_{lu}\, c_{rstu} \end{aligned} \qquad (2.01)$$

where $\epsilon_{rs}$, $e_{rst}$ and $c_{rstu}$ are the dielectric constant, piezoelectric and elastic constants and the $V_{ij}$ are the direction cosines between the old and the new axes. The primed quantities are referred to the new axes and the summation convention for repeated indices is implied.

The version of program SURF02 given in Appendix A1.1 is set up to examine propagation on rotated Y-cuts of quartz, and the angle notation is specified in Figure 2.2(b). The direction cosines for this case are specified by the transformation

$$\begin{bmatrix} x_1 \\ x_2 \\ x_3 \end{bmatrix} = \begin{bmatrix} \cos\Psi & -\sin\Psi\sin\theta & \sin\Psi\cos\theta \\ -\sin\Psi & -\cos\Psi\sin\theta & \cos\Psi\cos\theta \\ 0 & -\cos\theta & -\sin\theta \end{bmatrix} \begin{bmatrix} x \\ y \\ z \end{bmatrix}.$$

## 2.2 The Surface-Wave Solution

The analysis outlined in this section follows the procedure of Campbell and Jones [21]. To enable the determination of the crystal coupling factor, the electrical boundary conditions include a perfect conducting plane at a height h above the surface, as illustrated in Figure 2.2. The theory assumes adiabatic propagation of small-

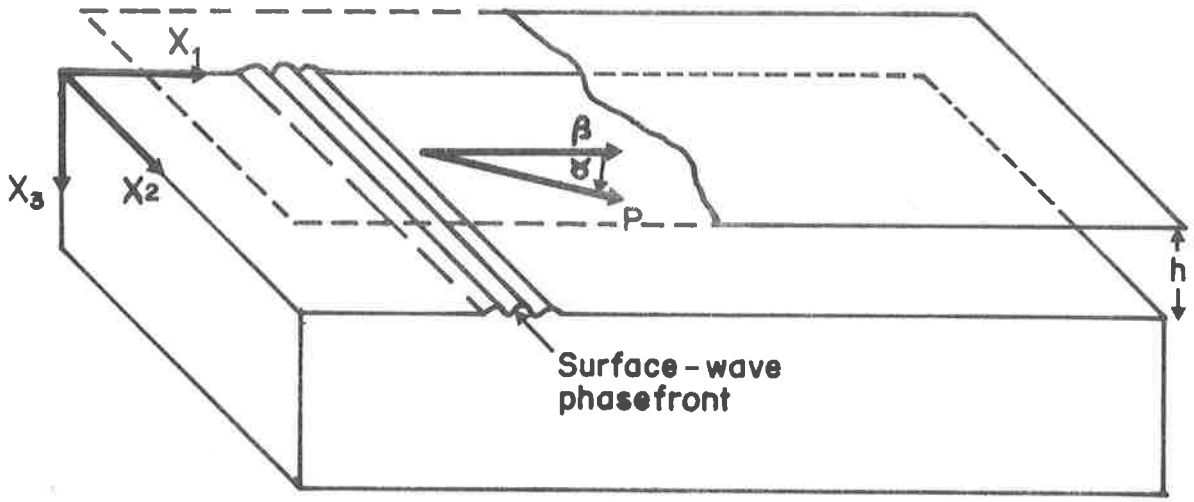


(a)

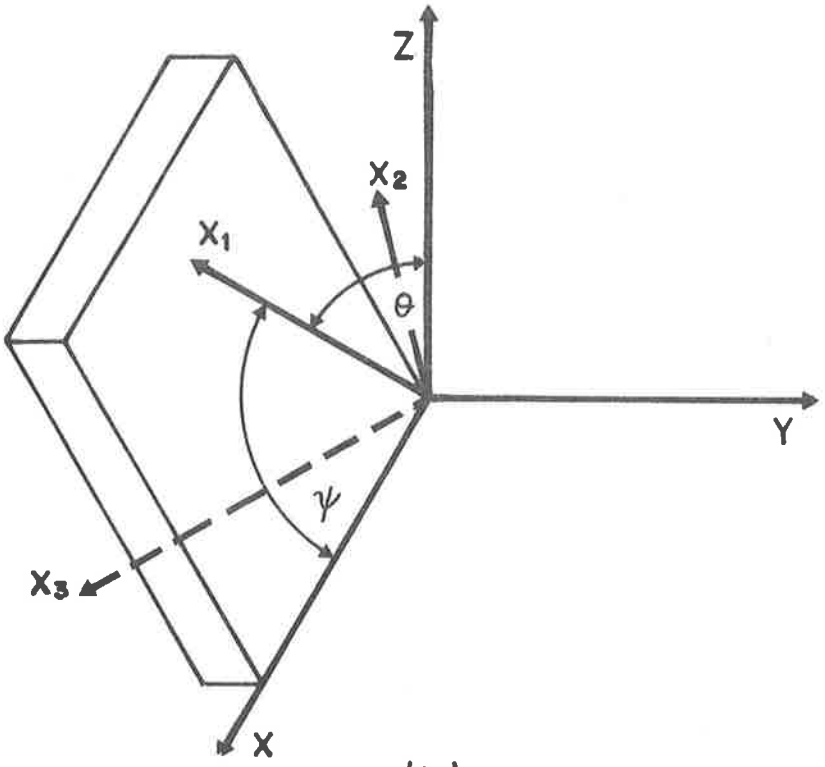


(b)

Figure 2.2 Sketches showing conventions used in the propagation analysis program SURF02 (a) propagation coordinates and location of conducting layer, and (b) orientation of propagation axes $X_1 X_2 X_3$ relative to crystal axes XYZ.

amplitude waves[60] in linear piezoelectric media, and the basic equations within the substrate medium are the linear piezoelectric constitutive relations,

$$T_{ij} = c_{ijkl} S_{kl} - e_{kij} E_k \tag{2.02}$$

$$D_i = e_{ikl} S_{kl} + \varepsilon_{ik}^{S} E_k \tag{2.03}$$

the strain-displacement relations,

$$S_{kl} = \tfrac{1}{2} (u_{k,l} + u_{l,k}) \tag{2.04}$$

the equations of motion,

$$T_{ij,i} = \rho \ddot{u}_j \tag{2.05}$$

the electrostatic charge equation

$$D_{i,i} = 0 \tag{2.06}$$

and the definition of electric potential

$$E_k = -\phi_{,k} \tag{2.07}$$

where $T_{ij}$, $S_{kl}$, $E_k$, $D_i$, $u_k$ are the components of stress, strain, electric field, electric displacement and particle displacement respectively, and $c_{ijkl}^{E}$, $e_{kij}$, $\varepsilon_{ik}^{S}$ are the elastic, piezoelectric and dielectric tensors respectively. Again, the summation convention for repeated tensor indices is employed, the dot notation indicates differentiation with respect to time and an index preceded by a comma indicates differentiation with respect to a space coordinate.

Substituting Equations (2.04) and (2.07) into (2.02) and (2.03) and the resultant equations into Equations (2.05) and (2.06) we obtain four differential equations in the four variables $u_i$, $i = 1,2,3$ and $\phi$.

$$c_{ijhl}^{E} u_{k,li} + e_{kij} \phi_{,ki} = \rho \ddot{u}_j \quad j=1,2,3) \tag{2.08}$$

$$e_{ikl} u_{k,li} - \varepsilon_{ik}^{S} \phi_{,k} = 0 \quad ) \; x_3 > 0 \tag{2.09}$$

In the region above the substrate and below the conducting layer the electric field must satisfy

$$\nabla^2\phi = 0 \qquad -h \leq x_3 \leq 0 \qquad (2.10)$$

We are seeking solutions representing surface-waves so we assume solutions independent of $x_2$ having the general form

$$\left.\begin{aligned} u_i &= B_i \; e^{\frac{-\alpha\omega x_3}{v_s}} \; e^{j\omega(t - \frac{x_1}{v_s})} \\ \phi &= B_4 \; e^{\frac{-\alpha\omega x_3}{v_s}} \; e^{j\omega(t - \frac{x_1}{v_s})} \end{aligned}\right\} \quad i = 1,2,3 \qquad (2.11)$$

where $B_i$ are constants, $\alpha$ is the decay constant, $\omega$ the angular frequency and $v_s$ is the surface-wave velocity.* When these expressions are substituted into Equations (2.08) and (2.09) a set of four linear equations in the unknowns $B_i$, i = 1-4 results and to allow a non-trivial solution for the $B_i$ the determinant of the coefficients of these equations must be zero. The coefficients of the equations are given in Equation (2.12), below, and it is apparent that the expression for the determinant will be an eighth order polynomial in s (where $s = j\alpha$) and the polynomial coefficients are dependent upon the material constants and the velocity $v_s$ i.e.

$$\begin{bmatrix} (A_{11} + \rho v_s^2) & A_{12} & A_{13} & A_{14} \\ A_{21} & (A_{22} + \rho v_s^2) & A_{23} & A_{24} \\ A_{31} & A_{32} & (A_{33} + \rho v_s^2) & A_{34} \\ A_{41} & A_{42} & A_{43} & A_{44} \end{bmatrix} \begin{bmatrix} B_1 \\ B_2 \\ B_3 \\ B_4 \end{bmatrix} = \begin{bmatrix} 0 \\ 0 \\ 0 \\ 0 \end{bmatrix} \qquad (2.12)$$

where

$$A_{ij} = -c_{3ij_3} s^2 + (c_{3ij_1} + c_{1ji_3})s - c_{1ij_1} \quad \text{for } i = 1,2,3 \; j = 1,2,3$$

$$A_{i4} = -e_{33i} s^2 + (e_{13i} + e_{31j})s - e_{11i} \quad \text{for } i = 1,2,3$$

$$A_{4j} = -e_{3j3} s^2 + (e_{1j3} + e_{3j1})s - e_{11i} \quad \text{for } j = 1,2,3$$

$$A_{44} = \varepsilon_{33} s^2 - (\varepsilon_{13} + \varepsilon_{31}) s + \varepsilon_{11}$$

---

* the letter j when used other than as an index represents the imaginary $\sqrt{-1}$.

$$C_8 s^8 + C_7 s^7 + C_6 s^6 + C_5 s^5 + C_4 s^4 + C_3 s^3 + C_2 s^2 + C_1 s + C_0 = 0 \quad (2.13)$$

Since the polynomial coefficients $C_i$ are real, the roots will be real, or occur in conjugate pairs. To satisfy the general surface-wave solution (2.11) the real part of $\alpha$ must be positive, i.e. the imaginary part of the root for s must be negative. Selecting the roots with negative imaginary parts gives four values for $\alpha_i$, i = 1-4 and for each value $\alpha_i$ we can solve the linear Equations (2.12) to obtain a set of four amplitude coefficients $B_{ij}$, j = 1 to 4.

The general surface-wave solution now takes the form of a linear sum of the four exponential decay terms i.e.,

$$\left.\begin{aligned} u_i &= A_j B_{ij} e^{\frac{-\alpha_j \omega x_3}{v_s}} e^{j\omega(t - \frac{x_1}{v_s})} \\ \phi &= A_j B_{4j} e^{\frac{-\alpha_j \omega x_3}{v_s}} e^{j\omega(t - \frac{x_1}{v_s})} \end{aligned}\right\} \quad i = 1,2,3 \quad x_3 > 0 \quad (2.14)$$

where the summation convention over j = 1 to 4 is implied. To determine the coefficients $A_i$ we must match the solution to the boundary conditions. The requirement that the wave amplitude must vanish on $x_3 \to \infty$ has already been mentioned and we now look at the boundary conditions at $x_3 = 0$ and $x_3 = -h$, and we note that the electric field must also be a solution to Equation (2.10) for $-h \leq x_3 \leq 0$. At $x_3 = 0$ the surface is assumed to be free of mechanical stresses, and the normal component of electric displacement must be continuous across the surface, i.e.

$$\left.\begin{aligned} T_{3j}\,|_{x_3 = 0} &= 0 \qquad j = 1,2,3 \\ D_3\,|_{x_3 = 0^-} &= D_3|_{x_3 = 0^+} \end{aligned}\right\} \quad (2.15)$$

At $x_3 = -h$ the electric potential is constant and without loss of generality we can put

$$\phi(-h) = 0 \tag{2.16}$$

The electric potential satisfying the boundary conditions and Equation (2.10) for the region above the surface is given by[21]

$$\phi = A_j B_{ij} \operatorname{csch}\left(\frac{\omega h}{v_s}\right) \sinh\left(\frac{\omega}{v_s}(x_3 + h)\right) e^{j\omega\left(t-\frac{x_3}{v_s}\right)} \qquad -h \leq x_3 \leq 0 \tag{2.17}$$

Substituting for (2.14) and (2.15) in (2.02) we obtain three equations in the coefficients $A_j$. A fourth equation is obtained by equating the normal component of electric displacement in (2.15) using (2.14), (2.03) and (2.17). The resulting set of homogenous linear equations is shown overleaf in Equation (2.18). Again the determinant of the coefficients should be zero, and this will be so only if the chosen velocity $v_s$ is an allowable wave velocity. The need for the use of a computer in obtaining surface-wave solutions is now quite apparent: the correct value for $v_s$ must be found by assuming trial values (for $v_s$) and evaluating the above expressions to obtain a value for the determinant of the coefficients in (2.18), then incrementing $v_s$ until an acceptably small value for the determinant has been achieved. Once a satisfactory velocity has been found Equation (2.18) may be used to determine the relative amplitudes of the coefficients $A_j$ to give the complete solution for $u_i$ and $\phi$ .

A computer program has been written to perform the above analysis, and a flow-chart and listing are given in Appendix A1.1. The program assumes the initial velocity is less than the correct velocity and increments the velocity by specified steps until it detects a change in the sign of either the real part or imaginary part of the determinant of (2.18). It then goes into a different search mode using 'interval halving' to seek a more accurate estimate of the surface-wave velocity, still using the sign of either part of the determinant

$$\sum_{j=1}^{4} A_j\{B_{1j}(jc_{3111} + \alpha_j c_{3113}) + B_{2j}(jc_{3121} + \alpha_j c_{3123}) + B_{3j}(jc_{3131} + \alpha_j c_{3133}) + B_{4j}(je_{131} + \alpha_j e_{331})\} = 0$$

$$\sum_{j=1}^{4} A_j\{B_{1j}(jc_{3211} + \alpha_j c_{3213}) + B_{2j}(jc_{3221} + \alpha_j c_{3223}) + B_{3j}(jc_{3231} + \alpha_j c_{3233}) + B_{4j}(je_{132} + \alpha_j e_{332})\} = 0$$

$$\sum_{j=1}^{4} A_j\{B_{1j}(jc_{3311} + \alpha_j c_{3313}) + B_{2j}(jc_{3321} + \alpha_j c_{3323}) + B_{3j}(jc_{3331} + \alpha_j c_{3333}) + B_{4j}(je_{133} + \alpha_j e_{333})\} = 0$$

$$\sum_{j=1}^{4} A_j\{B_{1j}(je_{311} + \alpha_j e_{313}) + B_{2j}(je_{321} + \alpha_j e_{323}) + B_{3j}(je_{331} + \alpha_j e_{333})$$

$$+ B_{4j}(-j\varepsilon_{31} - \alpha_j \varepsilon_{33} - \varepsilon_0 \coth(\frac{\omega h}{v_s}))\} = 0 \qquad (2.18)$$

to indicate when it has stepped past the correct velocity. The program halts when the size of the interval within which the correct velocity is known to lie is less than some user-specified value. Practical experience indicates that the velocity may be determined to any desired accuracy, limited only by rounding errors in the machine. If the initial starting velocity is higher than the correct surface-wave velocity, the program will usually converge onto a quasi-surface-wave solution at a slightly higher velocity, identifiable as such by the fact that it will have less than four decay constants with positive real parts. It will be noted in the above analysis that the more conventional contracted-index notation[58] has not been employed for the tensor quantities, because it was considered easier to carry the tensors in standard form in the machine, particularly when rotating the axes.

The program also evaluates the components, $W_i$, of the total nett power flow associated with the mechanical stress-field of the wave, using the expression given by Coquin and Tiersten[20] for the nett power flow per unit width,*

$$W_i = -\tfrac{1}{2}\,\mathrm{Re}\int_0^\infty T_{ij}\,\dot{u}_j^*\,dx_3 \qquad (2.19)$$

On substituting the solution obtained above, we get

$$W_i = \mathrm{Re}\,\frac{\omega}{2}\sum_{j=1}^{3}\sum_{n=1}^{4}\sum_{m=1}^{4}\frac{(A_m B_{jm})^*}{(\alpha_n + \alpha_m^*)}\{(e_{1ij} - j\alpha_n e_{3ij})A_n B_{4n} + \sum_{k=1}^{3}(c_{ijk1} - j\alpha_n c_{ijk3})A_n B_{kn}\} \qquad (2.20)$$

The program evaluates the expression for $W_i$ to obtain the acoustic power flow in the direction $\beta$, and then condenses and normalises the amplitude coefficients to correspond to a wave of intensity one watt/metre by means

---

* The power carried by the electric field has been neglected here because the experimental work was carried out on weak-coupling substrates. On strong-coupling materials the Poynting vector[50] must be included.

of the simple substitution

$$B_{ij}' = \frac{A_j B_{ij}}{\sqrt{W_1^2 + W_2^2}} \qquad (2.21)$$

The program also outputs all the rotated material constants onto punched cards to permit a closer examination of the surface-wave fields undertaken in the next section.

## 2.3 The Propagating Surface-Wave Fields

To provide a graphical representation of the mechanical and electrical fields of a propagating surface-wave in detail, a further computer program was written to evaluate the fields for the surface-wave solutions obtained in the above program, and plot them directly on an XY-plotter driven by the computer. A listing of this program ASWPLOT is given in Appendix A1.2, and a number of field plots are included in this section showing, for the purpose of illustration, the surface-wave fields for YX-propagation on α-quartz.

The first example is for YX-propagation on an unmetallized, or free, surface. The values of the decay constants $\alpha_i$ and amplitude coefficients $B_{ij}$ ($\times 10^{11}$) obtained from program SURF02 (based on the material constants given by Bechmann[61]) are,

$\alpha_1 = .164 + j0$

$\alpha_2 = .974 + j0$

$\alpha_3 = .871 - j.617$

$\alpha_4 = .871 + j.617$

| | | | |
|---|---|---|---|
| $B_{11} = 1.43 + j0$ | | $B_{12} = .343 + j0$ | |
| $B_{13} = -9.08 - j4.34$ | | $B_{14} = -9.08 + j4.34$ | |
| $B_{21} = 0 + j14.4$ | | $B_{22} = 0 + j.816$ | |
| $B_{23} = -7.33 - j2.73$ | | $B_{24} = 7.33 - j2.73$ | |
| $B_{31} = 0 - j23.0$ | | $B_{32} = 0 - j.205$ | |
| $B_{33} = -6.17 - j.641$ | | $B_{34} = 6.17 - j.641$ | |

$B_{41} = 4.04 \times 10^{10} + j0.$ $\quad B_{42} = 9.02 \times 10^{10} + j0.$

$B_{43} = -6.53 \times 10^{10} + j5.84 \times 10^{10}$ $\quad B_{44} = -6.53 \times 10^{10} - j5.84 \times 10^{10}$

for a surface wave of intensity of 1 watt/metre at 50 MHz.

The particle displacement field in the sagittal plane is shown plotted to scale over an area one wavelength square in Figure 2.3. The plotting program calculates the magnitude of the displacement vector to be plotted at each of the intersection points of a grid, and then arrows are drawn to indicate the magnitude and direction of the displacement vectors, starting at the unperturbed particle positions. The magnitude of the displacement of any particle may be determined by comparing the length of the relevant displacement vector with the scale drawn at the bottom of the figure. The field shown in the figure is for a surface-wave travelling from left to right evaluated at t = 0, and the elliptical particle motion with the major axis of the ellipse vertical can clearly be seen. The horizontal line in the figure represents the unperturbed surface of the quartz.

The particle velocity field was calculated using the relation

$$v_i = j\omega u_i \qquad (2.22)$$

and the results are shown in Figure 2.4. This figure differs from the previous one in that the field vectors straddle their respective grid points (the exact location of the point at which each vector was evaluated is indicated by the intersection of the cross-bar on the shaft of the arrow). Examination of the figure confirms the particle motion to be retrograde elliptical.

The electric potential associated with the propagating wave was evaluated using Equations (2.14) and (2.17), and is shown in the contour plot in Figure 2.5 for the 'open circuit' case obtained by setting $h \simeq \infty$ (in fact H = 1.E10). In this case the scale factor gives

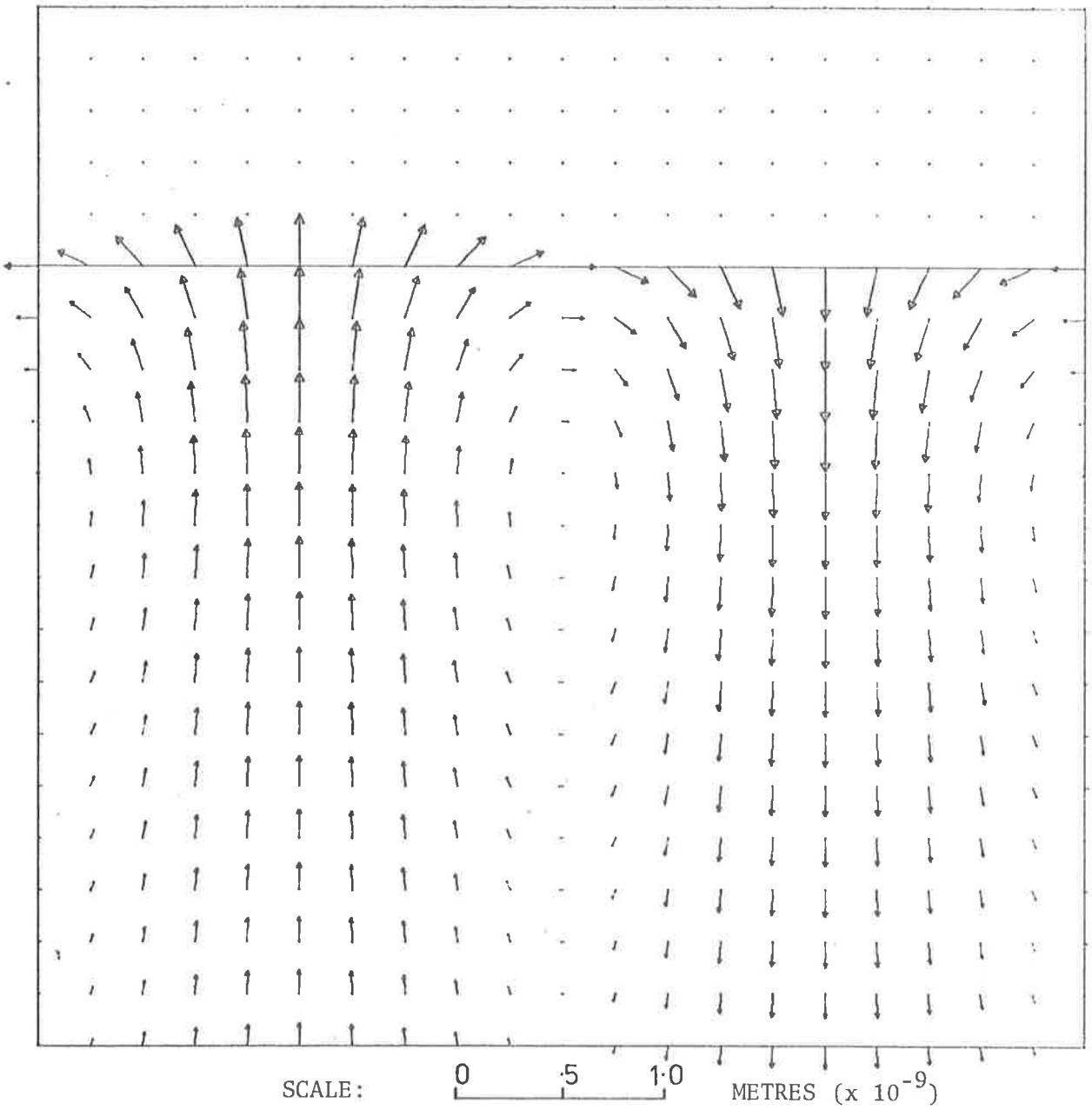


Figure 2.3 The particle displacement field in the sagittal plane for a YX-propagating surface-wave, of intensity 1 watt/metre, on a free surface (h=∞) of quartz. The cross-section shown is 1 wavelength square, and the unperturbed surface location is indicated by the horizontal line.

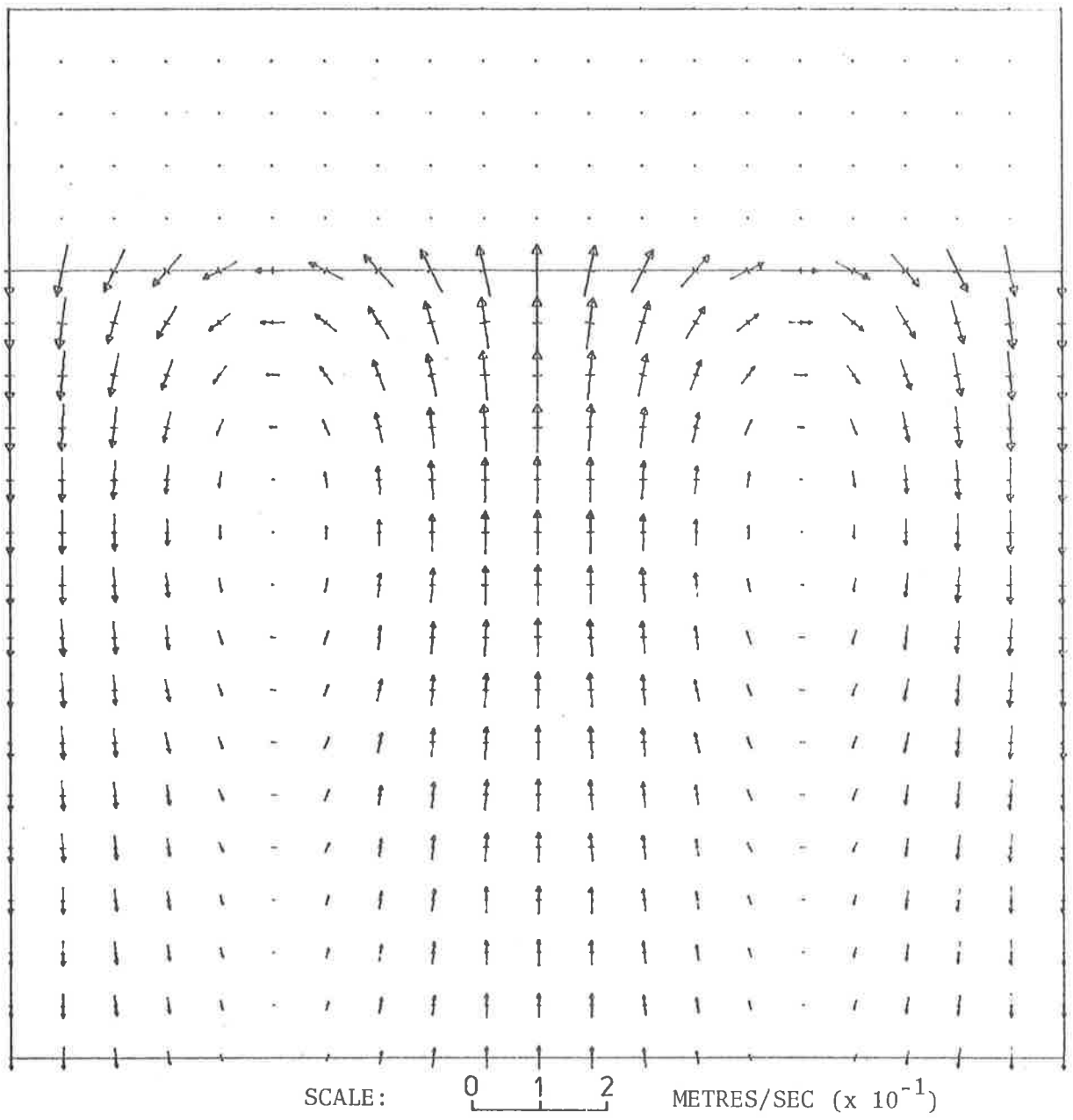


Figure 2.4 Particle velocity field for the surface-wave described in Figure 2.3 ($h=\infty$). In this case the particle velocity is evaluated at the location of the mid-points of the velocity vectors.

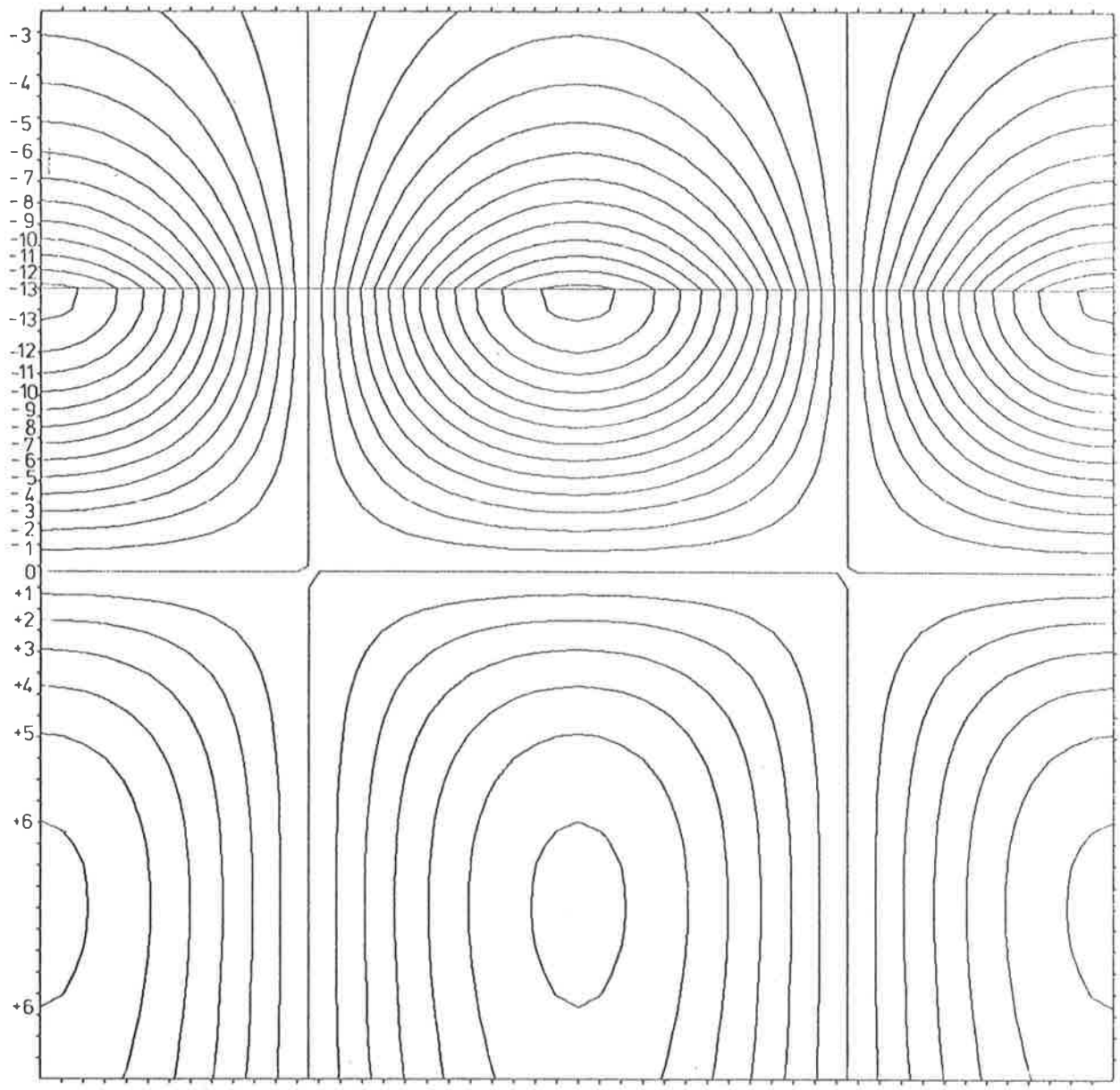


CONTOUR SPACING = 0.037 VOLTS

Figure 2.5 Potential contours for the surface-wave described in Figure 2.3 ($h=\infty$), and as before the surface is indicated by the horizontal line.

the potential between contours in volts.

The other parameter which was plotted was the electric displacement, evaluated within the medium using the relation

$$D_i = e_{ikl}\, u_{k,l} - \varepsilon_{ik}\phi_{,k} \qquad (2.23)$$

$$x_3 \geq 0$$

which after substitution for $u_i$ and $\phi$ becomes,

$$D_i = -\frac{\omega}{v_s} \sum_{k=1}^{4} \{ \sum_{l=1}^{3} (je_{il_1} + \alpha_k e_{il_3})\, B'_{lk} - (je_{i_1} + \alpha_k \varepsilon_{i_3})\, B'_{4k} \}\, E_k \qquad (2.24)$$

$$x_3 \geq 0 \ .$$

The electric displacement field in the region between the crystal surface and the conducting layer is given by

$$\underset{\sim}{D} = -\varepsilon_0 \underset{\sim}{\nabla}\phi \qquad (2.25)$$

and substituting for $\phi$ from Equation (2.17), we obtain,

$$D_1 = \frac{j\varepsilon_0\omega}{v_s} \sum_{j=1}^{4} B'_{4j}\, \operatorname{csch}\left(\frac{\omega h}{v_s}\right) \sinh\left(\frac{\omega}{v_s}(x_3+h)\right) e^{j\omega\left(t-\frac{x_1}{v_s}\right)}$$

$$D_3 = -\frac{\varepsilon_0\omega}{v_s} \sum_{j=1}^{4} B'_{4j}\, \operatorname{csch}\left(\frac{\omega h}{v_s}\right) \cosh\left(\frac{\omega}{v_s}(x_3+h)\right) e^{j\omega\left(t-\frac{x_1}{v_s}\right)} \qquad (2.26)$$

$$-h \leq x_3 < 0$$

The electric displacement field is plotted using the vector-field plotting routine again in Figure 2.6 for t=0, and for 'open circuit' propagation by putting $h \approx \infty$.

These plots indicate the general form of the propagating fields associated with an electroacoustic surface-wave, showing the exponential decay of all fields with depth into the medium, and harmonic dependence in the propagation direction. Examination shows that the horizontal component of particle displacement changes sign at a depth of approximately $0.25\lambda$: the electric displacement exhibits

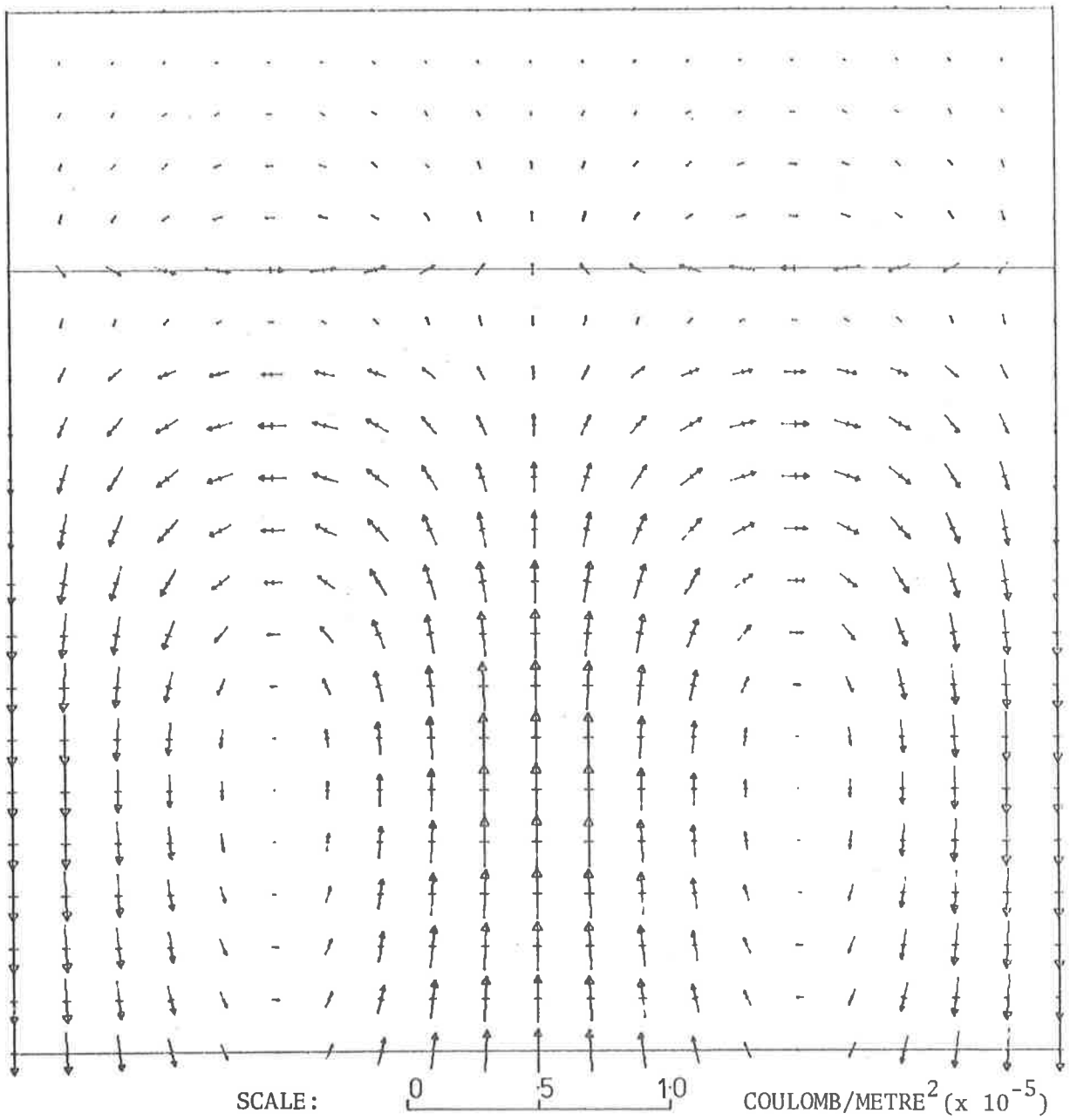


Figure 2.6 The electric displacement field for the surface-wave referred to in Figures 2.3 to 2.5 ($h=\infty$).

similar behaviour, but the sign reversal takes place at the slightly greater depth of 0.4λ. The potential field is interesting in that it shows a line of zero potential o.27λ below the surface, and below this line the potential has the opposite sign to the potential in the region immediately above the line, and the maximum value of the potential below this line is about half the peak potential values near the surface of the crystal. A comparison of the potential and electric displacement plots reveals that the vertical component of electric displacement, which is the dominant component, has opposite sign to the electric field in the regions near the surface, and the same sign deeper within the material, due to the piezoelectric coupling within the crystal.

It is also of some interest to examine the effect of bringing the conducting plane close to the surface. The particle displacement and velocity fields are only sightly affected, but the electric potential and displacement fields are greatly modified and examples are shown in Figures 2.7 and 2.8 for h=λ/4 and in Figures 2.9 and 2.10 for h≈0.

## 2.4 Propagation Data for Y-cut Quartz.

The aims of the above analysis were firstly to obtain a better understanding of electroacoustic surface-wave behaviour, and secondly to obtain accurate data for the experiments described later. The available data on surface-wave propagation on quartz at the commencement of this work consisted of calculated velocities, determined ignoring the piezoelectric coupling factor for X-cut and rotated Y-cuts [20], and measured free-surface propagation velocities on X,Y and Z cut surfaces [62]. The velocity information was presented graphically and it was felt that the accuracy with which these could be read (after the photoreduction involved in printing) was inadequate; hence the computer program SURF02

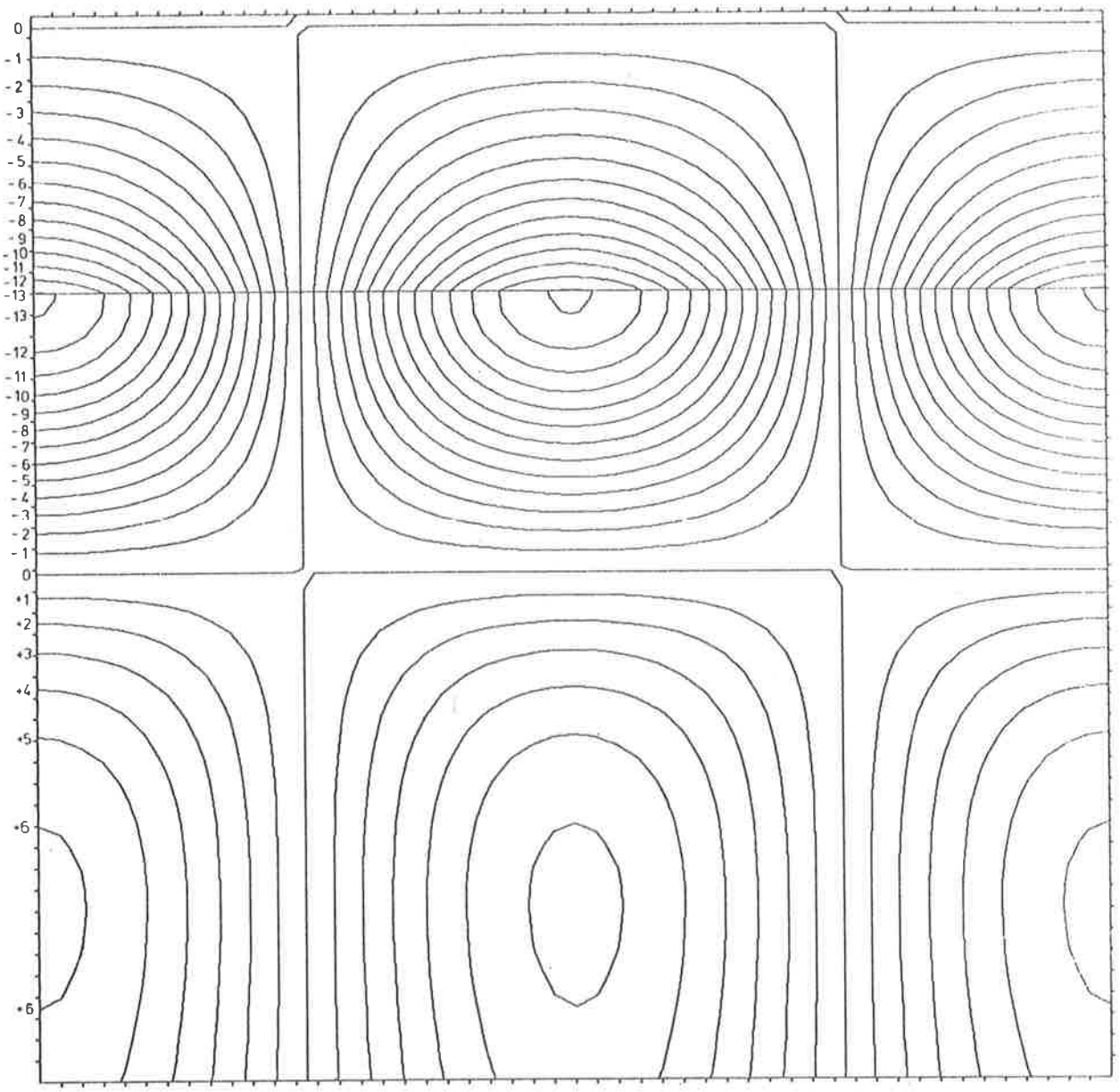


Figure 2.7 Electric potential contours for a YX-propagating surface-wave, of intensity 1 watt/metre, on quartz with a shorting plane h = $\frac{\lambda}{4}$ above the surface. The section shown is one wavelength square in the sagittal plane, and the shorting plane is at the upper boundary of the plot.

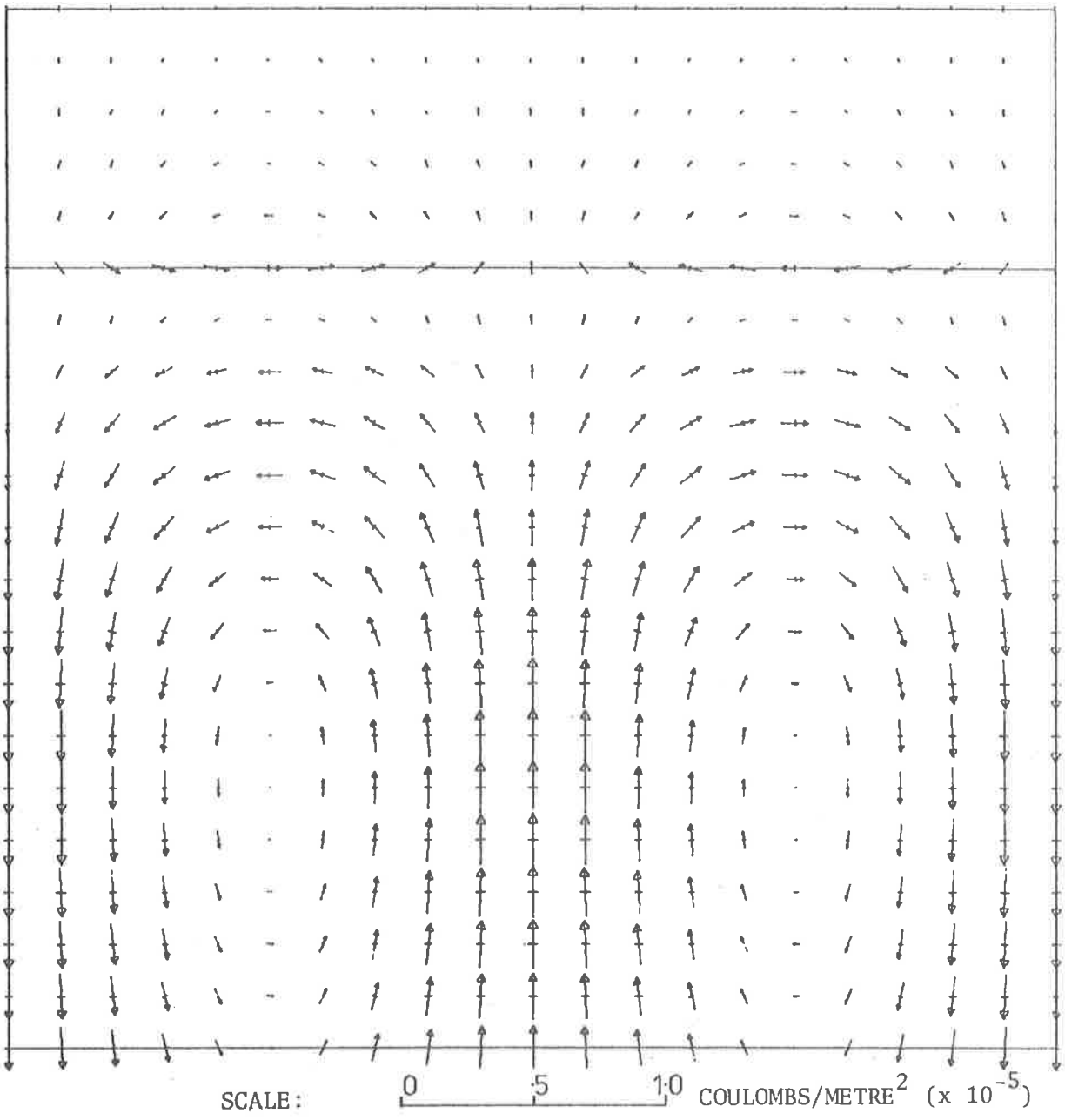


Figure 2.8 The electric displacement field for the surface wave described in Figure 2.7 ($h = \frac{\lambda}{4}$).

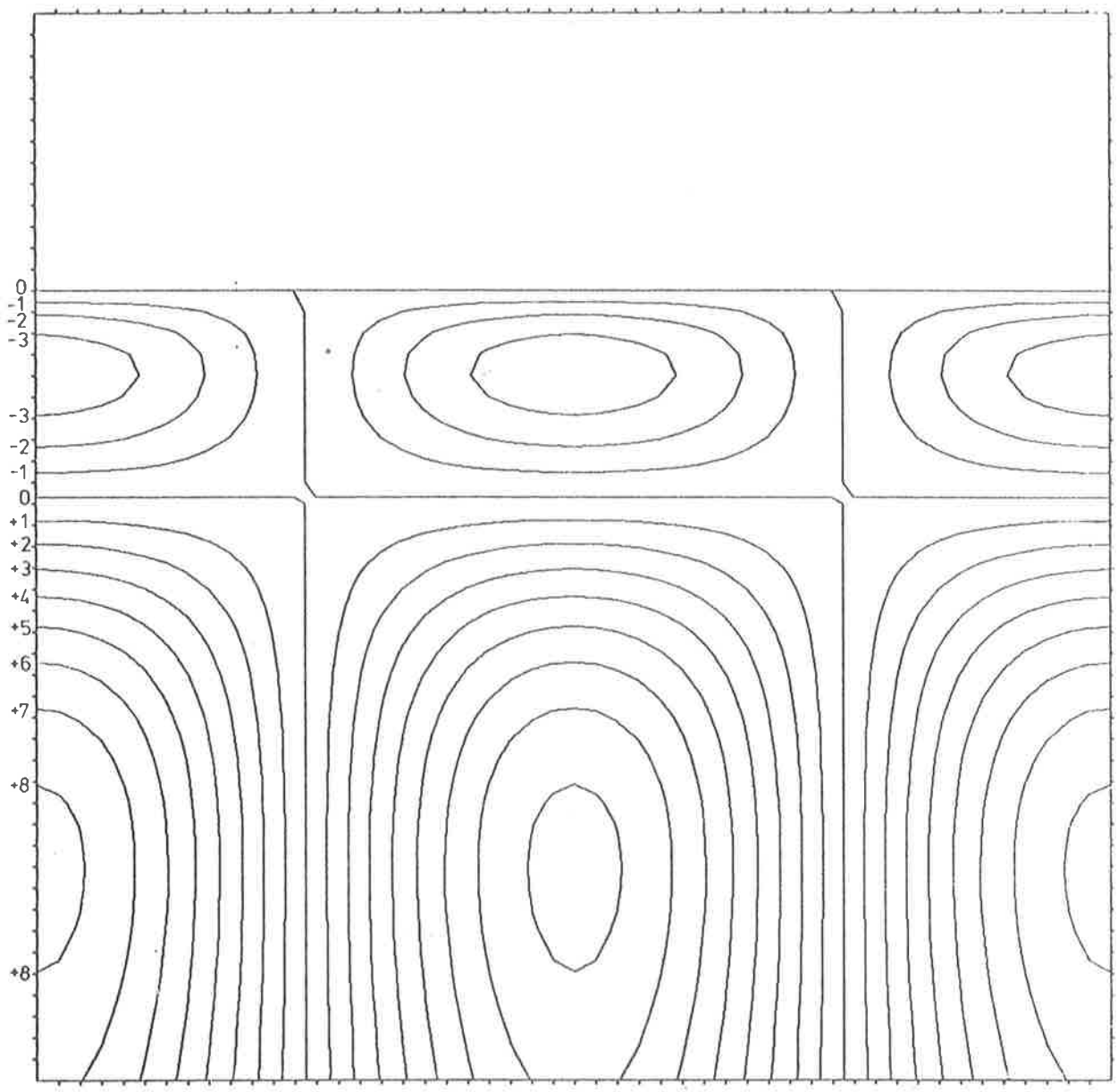


Figure 2.9 Electric potential contours for a YX-propagating surface wave, of intensity 1 watt/metre, on a metallized quartz surface (h=0). As before the section shown is one wavelength square in the sagittal plane.

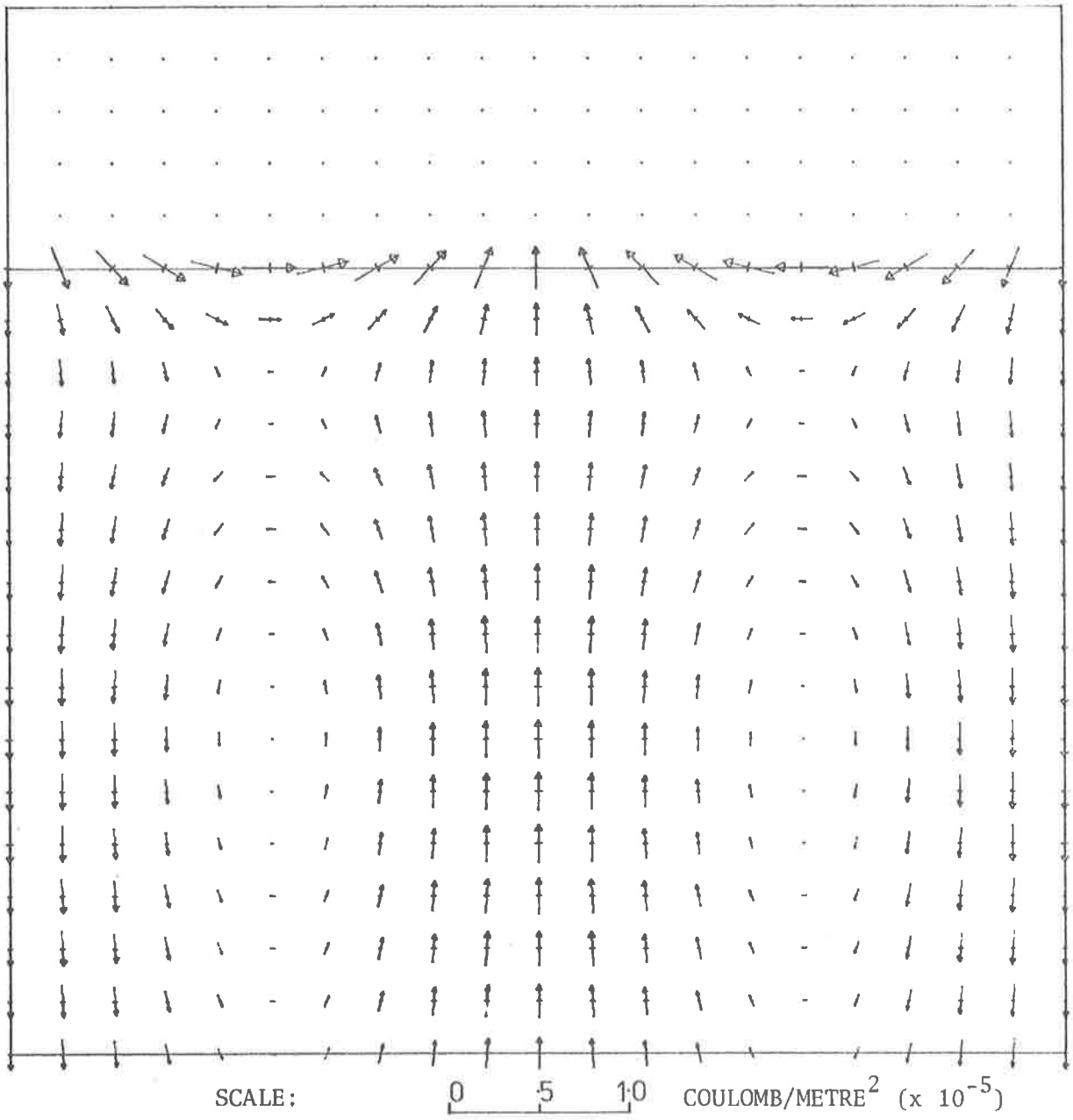


Figure 2.10 The electric displacement field for the surface-wave described in Figure 2.9 (h=0).

was employed to obtain more accurate data. The results for the particular case of a Y-cut quartz plate with 'left-hand' symmetry, are given below.

### 2.4.1. Surface-Wave Velocity

The velocity was calculated for 'open circuit' or free surface propagation on the Y-cut surface and is shown plotted against the angle between the wave vector $\underset{\sim}{\beta}$ and the X-axis, in Figure 2.11.

### 2.4.2. The Short-circuit Velocity Shift $\frac{\Delta v}{v}$

The parameter used to calculate the coupling factor is the velocity shift which occurs when a massless perfectly conducting plane is lowered onto the propagating surface. This is also shown in Figure 2.11, plotted against propagation direction and it should be noted that $\frac{\Delta v}{v}$ is negative. This is always true because the effect of introducing piezoelectric coupling into a material is to 'stiffen' the effective elastic compliance [63], and raise the velocity slightly. The introduction of the shorting layer then reduces this effect, lowering the velocity, and, as mentioned previously, this velocity shift gives a good indication of the relative strength of surface-wave coupling to be expected in any particular direction.

### 2.4.3. The Misalignment Angle

As mentioned earlier in this chapter, the wave-vector and nett power flow vector are not normally collinear, and it is of obvious importance to know what the magnitude of this effect is when designing practical devices. The misfire or misalignment angle is most efficiently computed from the velocity curve obtained above by constructing normals to the 'slowness' surface [55]. The misfire angle $\Upsilon$ is shown plotted against the direction of the wave-vector, measured

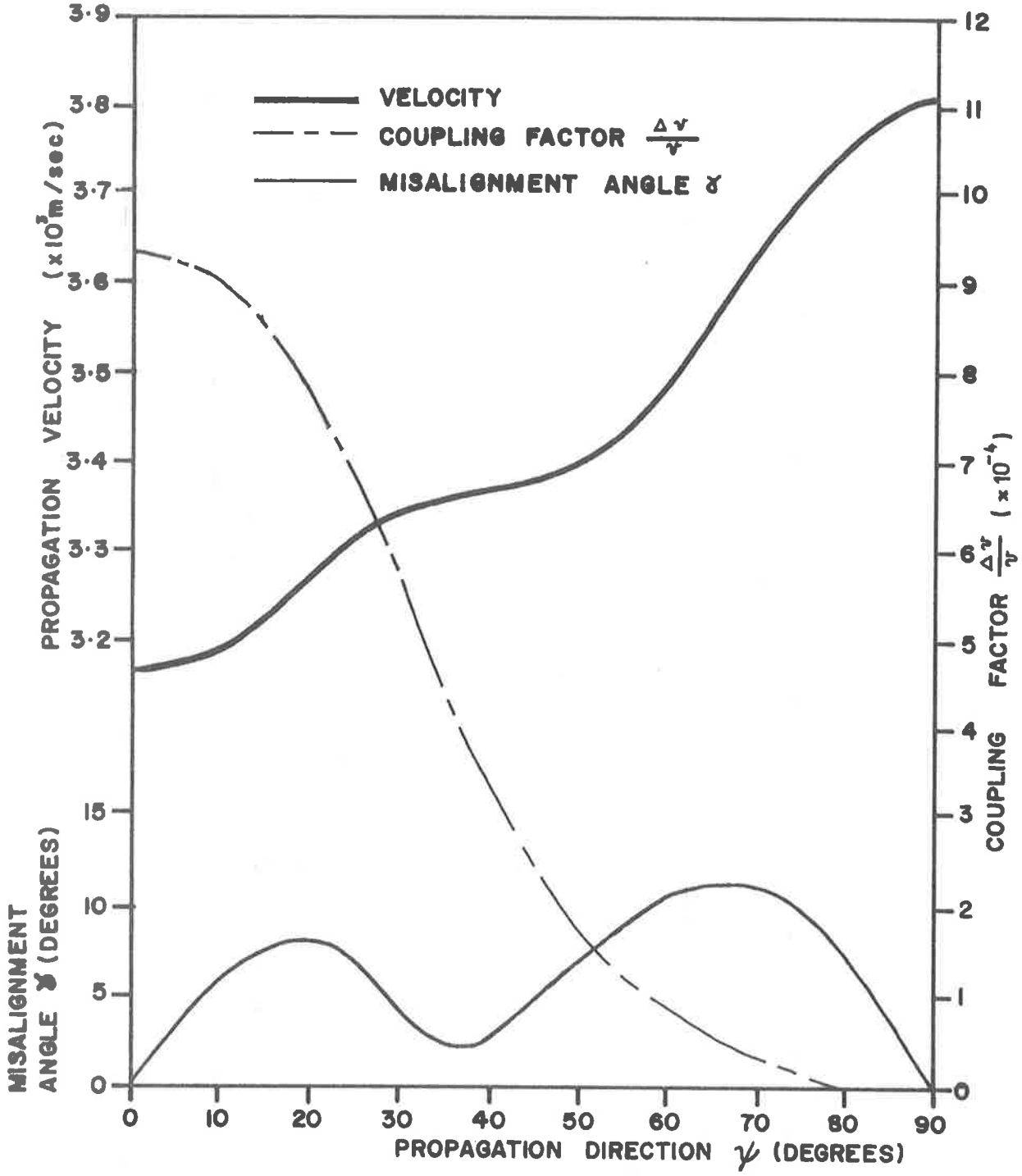


Figure 2.11 Computed curves for the propagation velocity, coupling factor and misalignment angle, on a Y-cut quartz. The values in the other quadrants may be determined from the crystal symmetry. (For the definitions of $\Psi$ and $\gamma$ see Figure 2.2.)

relative to the X-axis in Figure 2.11. As can be seen the misfire angle is zero only at the ends of the range $\psi$ = 0 to 90$^{o}$ on Y-cut quartz.

### 2.4.4. The Accuracy of the Results

Since the programming required to implement the above analysis is fairly complex, some effort was spent in attempting to eliminate any possible occurrence of errors within the program due to programming mistakes. The results are also subject to the accumulation of round-off errors in the calculation, but this was not considered to be a problem as the computer used was a CDC 6400 carrying fifteen significant decimal digits in the calculations.

The computed curves were checked against the computed results of Engan et al.[62], and the later work of Slobodnik and Conway[64], and Sabine[65], and appear to give good agreement. These results, of course, are also heavily dependent upon the accuracy of the assumed values of the material constants which are used in the calculations. The good agreement obtained between the predicted velocities and the measured velocities, observed by Engan et al.[62] and in the experiments reported in later chapters, would appear to confirm the accuracy of both the material constants used and the program SURF02.

# CHAPTER 3

# AN ADMITTANCE FORMALISM FOR SURFACE-WAVE DEVICES

## 3.0 Introduction

A basic need in any study of surface-wave devices is to have a convenient and accurate method for characterising the behaviour of the transducers used to launch and detect the surface-waves. The transducer model should permit easy analysis of the behaviour of existing devices, should relate the transducer geometry to the device response in a manner which aids the designer's understanding, and should be able to be readily extended in the case of structures employing more than one transducer.

The main function of interest in describing a transducer is the signal conversion efficiency, specified in either the frequency or time domains, and most device models are intended to aid the determination of this quantity. The simplest type of model is the one-dimensional model for a interdigital transducer which represents each electrode by a single independent surface-wave source (referring here to the launching situation), and is commonly known as the δ-function model. This approach was used by White[46] in his early work and gives a useful prediction for the amplitude-frequency response of narrow-band transducers. A slightly more sophisticated approach was used by Tancrell and Holland[66] who used two δ-function sources for each electrode, based on the idea that the major component of excitation came from the discontinuity of the horizontal electric field at the surface, which occurs at the edges of the electrode. Other workers have used discrete sources with finite duration impulse responses in the time domain, e.g. Tseng[67] and Atzeni[68] (rectangles) and Hartmann[69] (sine waves), in similar studies. The difficulty in this general approach lay in determining

the amplitudes of the individual sources in terms of the piezoelectric and material constants and the electrode geometry.

An alternative approach which was proposed by Krairojananan and Redwood[70] was to employ the equivalent circuit model developed previously for one-dimensional bulk-wave transducers[49], using one such circuit for each of the active regions within the surface-wave transducer and connecting them with appropriate lengths of acoustic transmission line. This model was an improvement in that it did take into account the electrical coupling between individual sources, and the most versatile version developed using the approach was that of Smith et al.[47], which made use of the short-circuit velocity shift[21] as a measure of the surface-wave coupling factor, following the experimental verification by Collins et al.[71]. Known generally as the three-port model, it has seen further development[72-78] and in complete or simplified form is the basis of much of the present work on the analysis of surface-wave devices.

The need for a suitable equivalent circuit model comes about due to the fact that the electrical source fields are in reality two-dimensional in the sagittal plane (assuming infinite-width transducers) and one is faced with the problem of determining the coupling of this field, via the piezoelectric matrix of the material, to the complex electroacoustic field pattern of the surface-waves and other acoustic modes being launched into the anisotropic substrate. Attempts at direct analysis of surface-wave coupling to a given transducer structure normally involve the assumption that the piezoelectric coefficients are small[20,54,67,79,80]: this permits the independent solution of the electric source field and the acoustic surface-wave field, because the electric field of the surface-wave can be neglected in the determination of the electric field of the electrodes. This assumption is conventionally

referred to as the weak-coupling approximation. Even with this approximation, the problem is still two-dimensional and to simplify things further, the next step is to consider the source and surface-wave fields only at the surface of the substrate. This approach leads to the consideration of surface-waves as modes, defined in terms of the propagating field quantities at the surface, and the concept of a surface impedance [57].

The reciprocity relations and orthogonality relations necessary for the development of a normal mode theory, along with a suitable notation were derived by Auld[50,51]. This theory was successfully used by Auld and Kino[54] to calculate the input impedance of an interdigital transducer over a range of frequencies.

The 3-port model, however, is also suitable for use on relatively strong-coupling substrates (like lithium niobate and the PZT-ceramics) as it includes the effect of regeneration via the electrical coupling of the individual transducer electrodes. Considerable effort has gone into the search for methods of determining the correct parameter values for use in this equivalent circuit, and effective formulae have been deduced by Skeie[75,76] and Lakin[81] using a perturbation technique, and by Milsom and Redwood[82] who employed a variational method of analysis.

The accuracy of the 3-port model for the determination of the fundamental response of interdigital transducers has been convincingly demonstrated, but it has the disadvantage that the complete equivalent circuit of a single transducer is a very complicated 3-port network, particularly in the case of apodized transducers [66], and requires considerable computation before either the frequency or time domain performances can be ascertained for any particular device. Further, the consequences of the presence of second-order effects, such as regeneration within a

transducer or between transducers, although included in the 3-port model, are very difficult to isolate, especially in the case of the multi-transducer structures which are of primary interest in this investigation.

In an effort to circumvent these difficulties it was decided to attempt the development of an admittance model for surface-wave transducers, which it was felt would permit a more convenient analysis of parallel-connected multi-transducer structures. It was also hoped that the model would provide a more direct relation between the transducer geometry and the predicted device response.

In the remainder of this chapter, expressions for the externally measurable responses of a delay line are derived in terms of the elements of an admittance matrix, and a method whereby second and higher-order responses may be individually identified and applied as correction terms to the first-order response, is given. The derivations of integral expressions for the individual elements of the admittance matrix, in terms of the interdigital transducer geometry and material parameters, will be found in Chapter 4.

## 3.1 The Admittance Matrix

We commence with the assumption that our delay line structure has two or more independent surface-wave transducers on the propagating surface, and some or all of them are acoustically coupled. Initially, before the transducers are connected electrically, the device may be represented by the generalised N-port structure shown diagrammatically in Figure 3.1. The admittance matrix for this structure is defined by the relations,

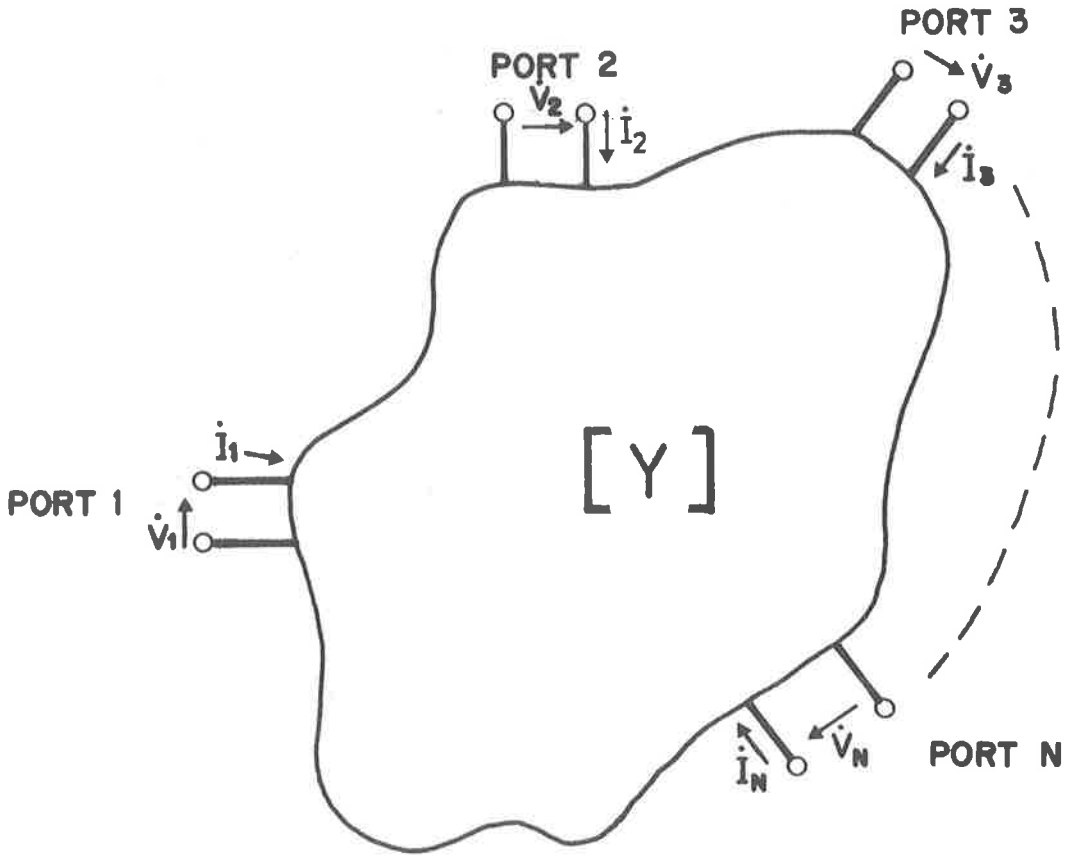


Figure 3.1 A generalised passive N-port structure.

$$\begin{bmatrix} I_1 \\ I_2 \\ \vdots \\ I_N \end{bmatrix} = \begin{bmatrix} Y_{11} & Y_{12} \cdots & Y_{1N} \\ Y_{21} & Y_{22} \cdots & Y_{2N} \\ \vdots & & \vdots \\ Y_{N_1} & Y_{N_2} \cdots & Y_{NN} \end{bmatrix} \begin{bmatrix} V_1 \\ V_2 \\ \vdots \\ V_N \end{bmatrix} \qquad (3.1)$$

where the voltage and current conventions are defined in Figure 3.1

### 3.1.1. Matrix Element Determination

The value of the element $Y_{ij}$ of the matrix may be found by connecting a zero output impedance CW voltage generator to port j, short-circuiting all the other ports, and measuring the current in port i. The element $Y_{ij}$ is then simply given by

$$Y_{ij} = \frac{\dot{I}_i}{\dot{V}_j} \qquad (3.2)$$

The derivation of a method for calculating this parameter is given in the next chapter.

### 3.1.2. Frequency Domain to Time Domain Conversion

In the preceding it was assumed that the measurements were performed with continuous sinusoidal inputs, and by varying the frequency of measurement we may determine the matrix elements as functions of the frequency, f, to obtain $Y_{ij}(f)$. In later work it will be more convenient to work in the time domain and use will be made of the fact that the frequency and time domain functions are related by the familiar Fourier integrals; the definition of the Fourier transform pair which was adopted in this work is,

$$y_{ij}(t) = \int_{-\infty}^{\infty} Y_{ij}(f) \; e^{j2\pi ft} \; df \qquad (3.3)$$

$$Y_{ij}(f) = \int_{-\infty}^{\infty} y_{ij}(t) \; e^{-j2\pi ft} \; dt$$

In practice care must be taken to ensure that the matrix elements are defined in such a way that these integrals are bounded,

and this point will be referred to again in Chapter 7.

## 3.2 One-Port Delay Line Responses.

The general case of an N-transducer delay line connected as a one-port device is shown in Figure 3.2. Devices of this type pose an interesting conceptual problem, in that they do not have separate input and output terminals, as in the more conventional two-port delay lines, and the best means to achieve analytic separation and identification of the input and output signals is not initially apparent. The only externally measureable parameter of a one-port device is its input immittance* so any type of coding, in the form of frequency sensitivity or time-delayed echo pulses must be characterised by a complete description of the input immittance in either the time or frequency domains. A method for separately identifying the input and response signals can be developed as follows.

The input admittance of the one-port structure may be determined from a knowledge of the coefficients of the appropriate N-port matrix, by making use of the relations,

$$\dot{V}_i = \dot{V}_{IN} \quad , \quad i = 1 \text{ to } N \text{ , and}$$

$$\dot{I}_{IN} = \sum_{i=1}^{N} \dot{I}_i \qquad (3.4)$$

for the one-port, and hence

$$Y_{IN} = \sum_{i=1}^{N} \sum_{j=1}^{N} Y_{ij} \qquad (3.5)$$

The reason for the choice of admittance, in preference to impedance, coefficients is at once obvious.

---

* It would be possible to determine a frequency dependent scattering coefficient S = (Z-Zo)/(Z+Zo) for the device, but this would require the introduction of an arbitrary reference impedance, Zo, in the input port which would not be a characteristic of the device.

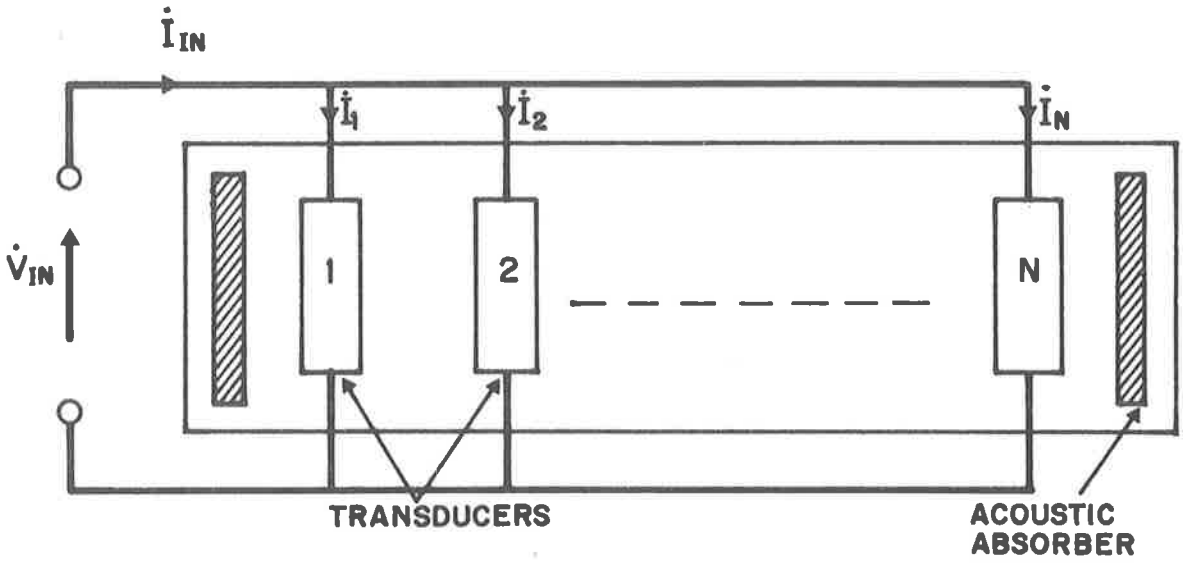


Figure 3.2 A general one-port delay line structure with N (not necessarily identical) transducers.

To observe the response of the line we must use a source with finite output impedance for the excitation of the line, as shown diagrammatically in Figure 3.3(a). In practice a receiver must be connected across the one-port device to monitor $V_o$, and if a high impedance detector is not available, the equivalent circuit is as shown in Figure 3.3(b). This may be reduced to the general case, shown in Figure 3.3(a), by means of the Thevenin equivalent source, defined by

$$\dot{V}_S = \frac{Z'_L \dot{V}'_S}{Z'_S + Z'_L} \quad \text{and,} \quad Z_S = \frac{Z'_S Z'_L}{Z'_S + Z'_L} , \qquad (3.6)$$

for the purposes of analysis.

Returning to Figure 3.3(a), the response of the line to an input signal $\dot{V}_S$ is given by the relation,

$$\frac{\dot{V}_o(\omega)}{\dot{V}_S(\omega)} = \{1 + Z_S Y\}^{-1} \qquad (3.7)$$

In the coding situation it is usual to select weak-coupling substrates, and a suitable choice of source impedance $Z_S$ enables us to satisfy the inequality $|Z_S Y| << 1$ at all frequencies. We may now introduce the binomial expansion for the denominator to rewrite this equation in the form,

$$\dot{V}_o(\omega) = \dot{V}_S(\omega)\{1-(Z_S Y) + (Z_S Y)^2 - (Z_S Y)^3 + ---\} \qquad (3.8)$$

We can now identify the terms, in various powers of the input admittance $Y(\omega)$, as the various 'order' responses of the one-port structure i.e.

| | |
|---|---|
| Zero-order Response | $= V_S(\omega)$ |
| Primary Response | $= -V_S(\omega)\ Z_S(\omega)\ Y(\omega)$ |
| Secondary Response | $= +V_S(\omega)\{Z_S(\omega)\ Y(\omega)\}^2$ |
| Higher-order Responses | = etc. (3.9) |

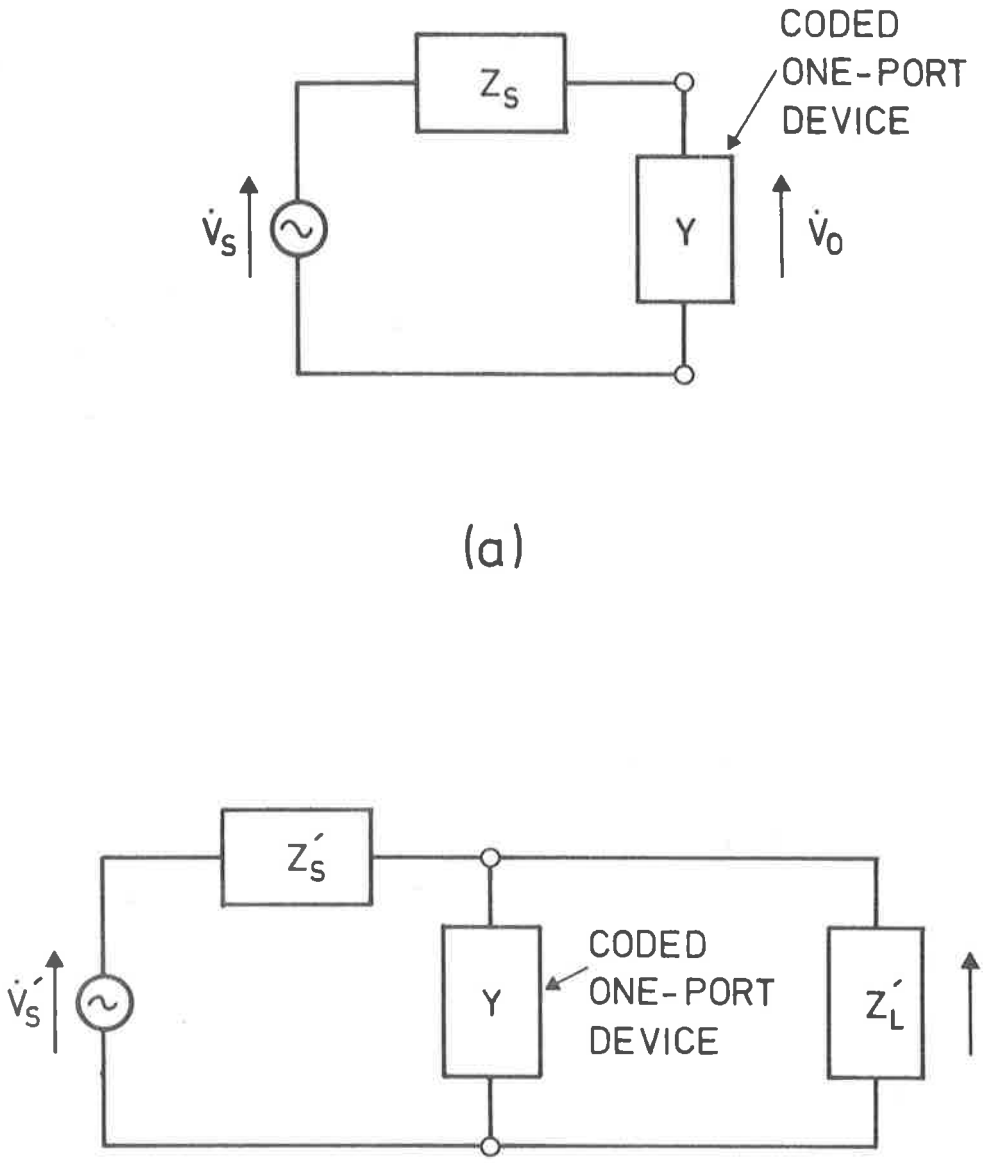


Figure 3.3 Equivalent circuits for the excitation of a coded one-port device, (a) with high-impendance receiver, (b) with inclusion of the finite receiver input impedance, $Z_L'$ .

The zero-order response is simply the input signal appearing across the device terminals. Added to this voltage we have the desired primary or 'first-order' response, containing $Y(\omega)$ to first order. With time domain coding this response will occur after the input excitation to permit observation. The higher-order terms, i.e. the secondary, tertiary, etc. responses, may be neglected in a simple analysis, or included if a more accurate assessment is required. This analysis may be performed in either the time or frequency domains, and in Chapter 7, the time domain analysis is used in a more detailed study of time-coded one-port surface-wave structures: the problems involved in making the above expansion for the voltage ratio are also discussed in more detail.

This brief discussion shows that the admittance formulation appears very attractive for the representation of multitransducer one-port structures, provided suitable expressions for the N-port admittance matrix coefficients are available. The derivation of suitable expressions for these coefficients is described in the next chapter.

## 3.3 Two-Port Delay Line Responses

The initial experiments in this project (Chapter 6) were performed on conventional two-port surface-wave delay lines, and we look now at the characterisation of two-port structures, in terms of the admittance coefficients.

Consider the general case of an N-transducer surface-wave delay line connected as shown in Figure 3.4, to form a two-port device. The appropriate admittance matrix for the two-port structure in terms of the N-port matrix elements is,

$$\begin{bmatrix} \dot{I}_1 \\ \dot{I}_2 \end{bmatrix} = \begin{bmatrix} Y'_{11} & Y'_{12} \\ Y'_{21} & Y'_{22} \end{bmatrix} \begin{bmatrix} \dot{V}_1 \\ \dot{V}_2 \end{bmatrix} \qquad (3.10)$$

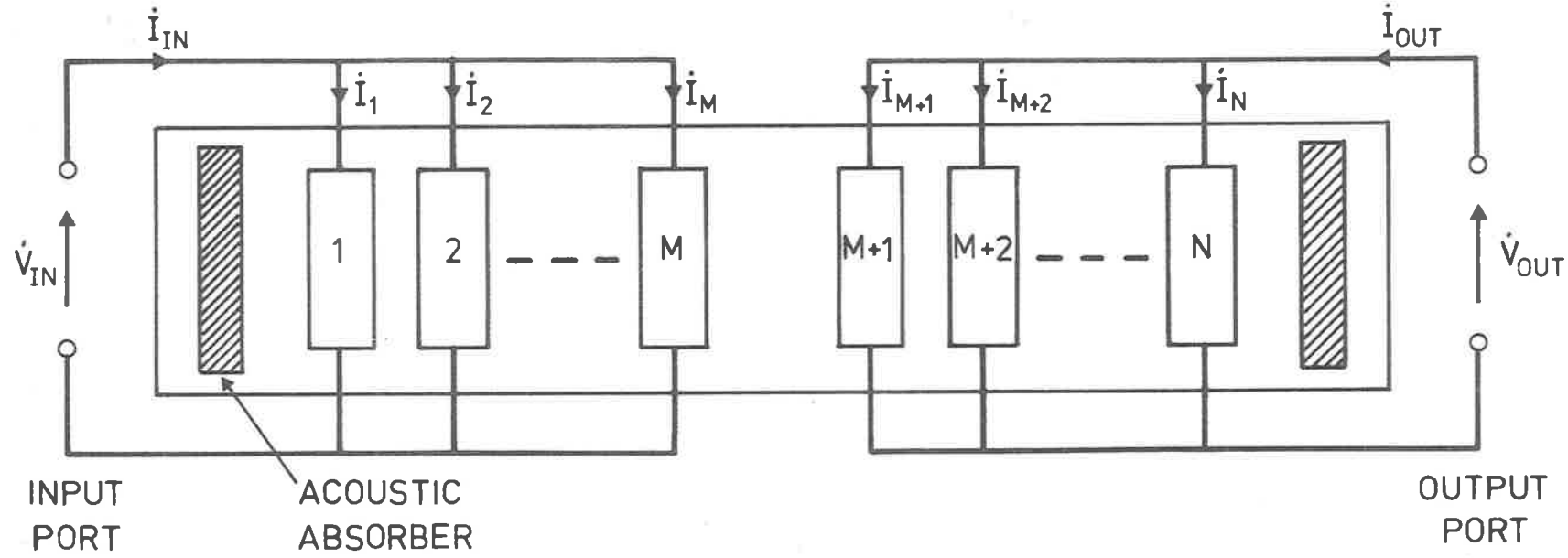


Figure 3.4 Multi-transducer structure connected as a two-port delay line.

where

$$Y'_{11} = \sum_{i=1}^{M}\sum_{j=1}^{M} Y_{ij} \qquad Y'_{12} = \sum_{i=1}^{M}\sum_{j=M+1}^{N} Y_{ij}$$

$$Y'_{21} = Y'_{12} \qquad Y'_{22} = \sum_{i=M+1}^{N}\sum_{j=M+1}^{N} Y_{ij} \tag{3.11}$$

To ascertain the dependence of the observable delay line response upon the admittance parameters we introduce the equivalent circuit, with source and load impedances, shown in Figure 3.5. Dropping the superscripts on the new matrix elements, the frequency transfer function of the delay line is then given by,

$$\frac{\dot{V}_L(\omega)}{\dot{V}_S(\omega)} = \frac{-Y_{21}Z_L}{1 + Y_{11}Z_S + Y_{22}Z_L + Y_{11}Y_{22}Z_SZ_L - Y_{12}Y_{21}Z_SZ_L} \tag{3.12}$$

This expression gives the complete response of the two-port line, but in many cases, e.g. on weak-coupling substrates used for transversal filters, this equation may be simplified by means of the approximation

$$Y_{11}Z_S \approx Y_{22}Z_L \approx Y_{12}Z_L \approx Y_{21}Z_S << 1 \tag{3.13}$$

to give the simple relation,

$$\frac{\dot{V}_L(\omega)}{\dot{V}_S(\omega)} = -Y_{21}(\omega)\, Z_L(\omega) \tag{3.14}$$

This relation in effect states that, with high impedance transducers in a low impedance measurement system, the delay line frequency response is given essentially by the transadmittance of the transducers. This relationship is used in the experiments in Chapter 6 as a means for checking the accuracy of the computed transadmittance curves. The presence of the negative sign in this expression is also of interest and receives further discussion in the next chapter.

It was stated in Section 3.0 that it is desirable to be able to isolate the various second-order effects occurring in delay lines

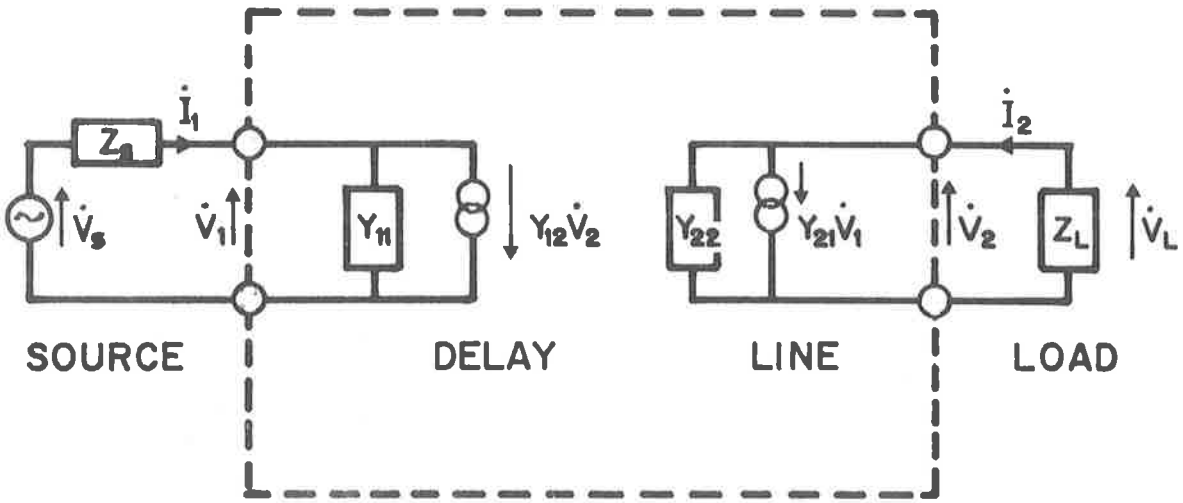


Figure 3.5 Equivalent circuit for a two-port delay line in terms of admittance parameters.

as a result of reflection and regeneration, and this may be achieved using the series expansion technique introduced previously in the one-port case. If the approximations given in Equation (3.13) are valid at all frequencies, then Equation (3.12) may be rewritten, using the binomial expansion, to obtain

$$V_L = - V_S Y_{21} Z_L (1 - E + E^2 - E^3 + \text{---}) \qquad (3.15)$$

where

$$E = Y_{11} Z_S + Y_{22} Z_L + (Y_{11} Y_{22} - Y_{12} Y_{21}) Z_S Z_L . \qquad (3.16)$$

Writing this expression out in full we may collect terms of similar power n, in the factors of the form $(Y_{ij} Z_k)^n$ to identify the responses of various orders, as in the case for the one-port devices, and we get,

$$\begin{aligned}
&\text{Primary Response} && = -Y_{21} Z_L \\
&\text{Secondary Response} && = +Y_{21} Z_L (Y_{11} Z_S + Y_{22} Z_L) \\
&\text{Tertiary Response} && = -Y_{21} Z_L ((Y_{11} Z_S)^2 + (Y_{22} Z_L)^2 \\
& && \quad + (Y_{11} Y_{22} + Y_{12} Y_{21}) Z_S Z_L) \\
&\text{Higher-Order Responses} && = \text{etc.}
\end{aligned} \qquad (3.17)$$

The first point to be noticed here is the absence of the zero-order response which is present in the one-port case. The largest observable response will be the primary response (ignoring here any question of electromagnetic coupling between the input and output wiring) which has the form predicted in Equation (3.14). The terms giving the secondary responses correspond to the regenerated signals arising in the transmitting and receiving transducers. In the case of the source transducer this may be physically interpreted as follows; the launched surface-wave induces an additional voltage $-Y_{11} Z_S V_S$ across the source impedance $Z_S$ as it travels under the launching transducer, and this results in the launching of an additional (regenerated) surface-wave. It should be noted that this is not equivalent to a simple change in

the effective amplitude of the launched wave (except in the case of pure CW operation which is of little interest) because $Y_{11}(\omega)$ (and possibly also $Z_S(\omega)$) is a complex function of frequency. In the time domain this regenerated response will have an impulse response with twice the duration of the primary surface-wave impulse response.

The tertiary responses of a two-port delay line are also listed, and again each of the terms in this expression may be identified with a particular signal path through the device. The first two terms describe double regeneration in the launching and receiving transducers respectively, the third term single regeneration at both transducers, and the last term accounts for what is commonly known as the 'triple-transit' signal. These tertiary responses of a two-port delay line are normally of little interest, being too small to be observed and obscured by the primary and secondary responses. In lines of moderate coupling factor, however, the triple-transit signal may be observed separately because it is delayed relative to the other responses by an interval equal to three times the primary time delay.

From this brief outline it can be seen that the admittance formalism provides a convenient method for the representation of parallel-connected transducer structures. This approach enables the contributions from second and third-order effects to the total device response to be separately identified and individually calculated, in delay lines with moderate coupling factors. The accuracy of this method of analysis is limited only by the validity of the approximation listed above and our ability to obtain the elements of the N-port admittance matrix.

Formulae permitting the ready evaluation of first, second and third-order responses for a two-port structure employing uniform interdigital transducers, operated at the synchronous frequency, have

been published elsewhere[83], based on the admittance formulae derived in the next chapter.

# CHAPTER 4

# DERIVATION OF THE ADMITTANCE COEFFICIENTS

## 4.0 Introduction

In order to apply the admittance formalism developed in the previous chapter to practical problems, methods for the calculation of the admittance matrix coefficients must be available. The diagonal elements of the admittance matrix are the input immittances of the individual transducers, and the off-diagonal elements correspond to the acoustic coupling between individual pairs of transducers (with the uninvolved transducers electrically short-circuited).

In practice the off-diagonal transadmittance and elements are of greater importance for, as was shown in the last chapter, the first-order response of a two-port delay line is specified by the transadmittance $Y_{21}(\omega)$. A similar result is obtained for one-port structures in Chapter 7, where it is shown that the useful part of the primary response of a time domain coded one-port is given by the sum of the transadmittances between acoustically coupled transducers (the diagonal elements also contribute to the primary response of a one-port but are of no use as they represent undelayed pulses obscured by the zero-order response). While the diagonal matrix elements do not contribute to the useful part of the primary responses of one and two-port devices, they do contribute significantly to the second and higher-order responses of both these devices.

The calculation of input admittances by a normal mode theory has been mentioned earlier[54], and it is the purpose of the next section to describe a normal mode theory for the calculation of the transadmittance between a pair of transducers on a weak-coupling substrate. The transadmittance is derived for a pair of transducers separated by a length

of free surface, but the result can also be applied to transducers on a multitap delay line in a situation where the reflections from intermediate transducers which are short-circuited (for the transadmittance calculation) may be neglected in comparison with the regeneration which occurs in these intermediate devices when connected to their operational load impedances.

In the later sections an expression for the time domain transadmittance of a two-transducer structure is obtained, and an expression for the input admittance of a single transducer is obtained using the method of Auld and Kino[54], but recast in the present notation for use in later chapters. The last section of this chapter is devoted to a short discussion of the significance of the different factors in the derived formulae.

## 4.1 The Frequency Transadmittance $Y_{21}(\omega)$

The system for which an expression for the transadmittance is to be determined, is shown in Figure 4.1(a). The launching transducer $T_1$ is assumed to be of uniform width W while transducer $T_2$, of maximum width $\leqslant W$, may be apodized. To aid the calculation of the short-circuit output current $\dot{I}_2$ obtainable from transducer $T_2$ consequent upon the application of a voltage $\dot{V}_1$ to transducer $T_1$, the propagating surface-wave field will be represented as the sum of a set of orthogonal surface modes.

### 4.1.1 The Normal Mode Set

The calculation is facilitated by making the artificial assumption that the configuration is repeated periodically along the Y-axis with some large periodicity interval L; the principal effect of this assumption is the introduction of an artificial discrete set of normal modes. These modes are straight-crested surface-waves with

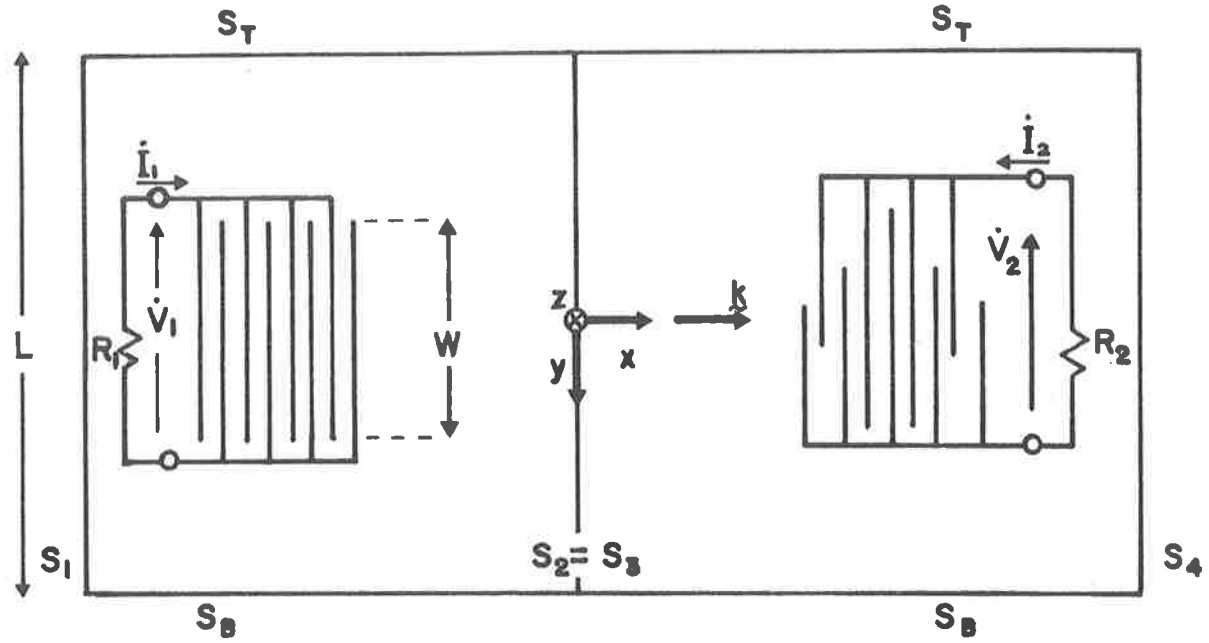


(a)

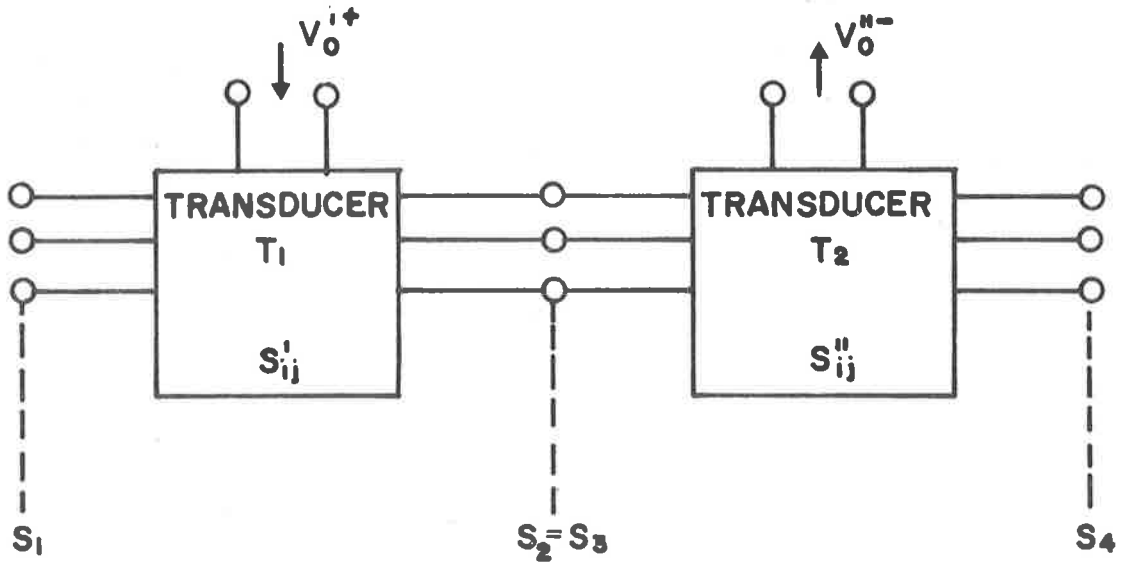


(b)

Figure 4.1 The two-transducer structure used in the trans-admittance derivation (a) schematic showing coordinate system and boundary surfaces referred to in text, (b) scattering matrix representation for the normal modes.

propagation vectors $\beta_m$ which satisfy the periodic boundary conditions at $y = \pm L/2$. In this way one obtains modal fields whose components are trigonometric functions of all the integer multiples of $2\pi y/L$, and at any particular frequency $\omega$ there will be a finite number $2N$ of such modes ($N=2$ integer $(\frac{L}{\lambda})$, where $\lambda$ is the free-surface wavelength).

For these modes we adopt the mode labelling scheme such that a mode with positive index m propagates to the right in Figure 4.1(a), while a mode with negative index -m propagates in the opposite direction*. The zero mode index is reserved for signals at the electrical ports of one or the other of the transducers.

If one assumes that the reference planes $S_1$, $S_2 = S_3$, and $S_4$, perpendicular to the X-axis in Figure 4.1(a), are sufficiently far from the transducers for the non-propagating modes to have decayed to negligible amplitude, then only the propagating modes need be considered. As a further consequence of the periodic boundary conditions it may be shown that the field vectors of the propagating acoustic surface-wave normal modes satisfy the orthogonality relations[51]

$$\int_S (-j\omega\phi_m \underset{\sim}{D}^*_n + j\omega \phi^*_n \underset{\sim}{D}_m - \underset{\sim}{v}_m \cdot \underset{\approx}{T}^*_n - \underset{\sim}{v}^*_n \cdot \underset{\approx}{T}_m) \cdot d\underset{\sim}{S}$$

$$= 0 \text{ when } m \neq n$$

$$= 4P_n \text{ when } m = n \qquad (4.1)$$

where $\phi_m(x,y,z)$, $\underset{\sim}{D}_m(x,y,z)$, $\underset{\sim}{v}_m(x,y,z)$ and $\underset{\approx}{T}_m(x,y,z)$ are complex phasors representing peak values of potential, electric displacement, particle velocity and stress tensor of normal mode m, and S is any one of the surfaces $S_1$, $S_2 = S_3$, or $S_4$ shown in Figure 4.1, and extending from $z = 0$ to $z \to \infty$ over the interval $-L/2 < y < L/2$. The power $P_m$ is the power carried to the right by normal mode m. In our mode labelling scheme where the propagation vector $\underset{\sim}{\beta}_m = -\underset{\sim}{\beta}_{-m}$, we have also $P_m = -P_{-m}$. Selecting a common value P for which $P_m = P$ for $m > 0$ and

---

* In this mode labelling scheme modes with equal x- and oppositely directed y- propagation constants are associated with different mode numbers.

$P_m = -P$ for $m < 0$, will normalize the fields $\phi_m$, $D_m$ etc. to definite values.

Since the nonpropagating modes are assumed to be of negligible amplitude at the reference plane $S_2 = S_3$ the fields at this point may be expressed as the linear sums,

$$\begin{aligned}
\phi &= \sum_{m=-1}^{-N} V_m^{(2)}\, \phi_m + \sum_{m=1}^{N} V_m^{(2)}\, \phi_m \\
\underset{\sim}{D} &= \sum_{m=-1}^{-N} V_m^{(2)}\, \underset{\sim}{D}_m + \sum_{m=1}^{N} V_m^{(2)}\, \underset{\sim}{D}_m \\
\underset{\approx}{T} &= \sum_{m=-1}^{-N} V_m^{(2)}\, \underset{\approx}{T}_m + \sum_{m=1}^{N} V_m^{(2)}\, \underset{\approx}{T}_m \\
\underset{\sim}{v} &= \sum_{m=-1}^{-N} V_m^{(2)}\, \underset{\sim}{v}_m + \sum_{m=1}^{N} V_m^{(2)}\, \underset{\sim}{v}_m
\end{aligned} \tag{4.2}$$

The coefficients $V_m^{(2)}$ may be regarded as complex generalized voltage amplitudes of forward and backward waves which enter ($m < 0$) or leave ($m > 0$) transducer $T_1$ through a series of N acoustic surface-wave ports which have a common reference plane $S_2$. Each transducer may now be represented as a passive junction with 2N acoustic ports and one electrical port.

### 4.1.2. The Scattering Matrices

If we assume that no signals enter $T_1$ across the plane $S_1$, and adopt the notation $V_0'^{+}$ and $V_0'^{-}$ for the input and output generalised voltage waves at the electrical port of $T_1$, we may write the scattering matrix equation

$$\begin{bmatrix} V_0'^{-} \\ V_1^{(2)} \\ V_2^{(2)} \\ \vdots \\ V_N^{(2)} \end{bmatrix} = \begin{bmatrix} S'_{00}, & S'_{0-1}, & S'_{0-2}, & \cdots\cdots & S'_{0-N} \\ S'_{10}, & S'_{1-1}, & \cdots\cdots\cdots\cdots & & S'_{1-N} \\ \vdots & & & & \vdots \\ S'_{NO} & \cdots\cdots\cdots\cdots\cdots\cdots & & & S'_{N-N} \end{bmatrix} \begin{bmatrix} V_0'^{+} \\ V_{-1}^{(2)} \\ V_{-2}^{(2)} \\ \vdots \\ V_{-N}^{(2)} \end{bmatrix} \tag{4.3}$$

in which the assignment of mode numbers has produced symmetry of the matrix in the form $S_{i0}' = S_{0-i}'$. A requirement for symmetry of the scattering matrix is that all generalized voltages are defined in a way that unit amplitude waves carry a common power P. This requirement has already been satisfied at the acoustic ports and to satisfy it at the electrical ports the normal transducer structures of $T_1$ and $T_2$ have been supplemented in Figure 4.1(a) by the parallel connected low value resistors $R_1$ and $R_2$, which are chosen to have resistance much less than the input impedances of $T_1$ and $T_2$, so that $T_1$ and $T_2$ can be regarded as matched when fed from transmission lines for which $R_1$ and $R_2$ are the respective characteristic impedances. A consequence of these restrictions is that the actual voltage $\dot{V}$ between the fingers of transducer $T_1$ will be related to the incident generalized voltage amplitude by

$$\dot{V}_1 = V_0''^{+}\sqrt{2PR_1} \tag{4.4}$$

It will be seen later, from Equation (4.25), that the transadmittance from $T_1$ to $T_2$ is independent of the choice of resistors $R_1$ and $R_2$.

The set of normal modes which communicate with transducer $T_2$, it being assumed that no signals enter $T_2$ from across $S_4$, are those which cross $S_3$. If these are assigned mode amplitudes $V_m^{(3)}$ ($m > 0$ for input modes and $m < 0$ for output modes), and the input and output waves at the electrical port have the respective amplitudes $V_0''^{+}$ and $V_0''^{-}$, the scattering matrix equation for $T_2$ takes the form

$$\begin{bmatrix} V_0''^{-} \\ V_{-1}^{(3)} \\ V_{-2}^{(3)} \\ V_{-3}^{(3)} \\ \vdots \\ V_{-N}^{(3)} \end{bmatrix} = \begin{bmatrix} S_{00}'', & S_{01}'', & S_{02}'' & \cdots & S_{0N}'' \\ S_{-10}'' & & & & S_{-1N}'' \\ S_{-20} & & & & \vdots \\ \vdots & & & & \vdots \\ \vdots & & & & \vdots \\ S_{-NO}'' & & & & S_{-NN}'' \end{bmatrix} \begin{bmatrix} V_0''^{+} \\ V_1^{(3)} \\ V_2^{(3)} \\ V_3^{(3)} \\ \vdots \\ V_N^{(3)} \end{bmatrix} \tag{4.5}$$

in which the assignment of mode numbers adopted has produced symmetry in the form $S''_{-io} = S''_{oi}$. It can be seen from Figure 4.1(b) that the output modes of $T_1$ become the input modes of $T_2$ and thus we obtain $V_m^{(2)} = V_m^{(3)}$ for all $m > 0$.

To proceed with the calculation of the transadmittance we assume that $T_1$ is excited with an incident voltage $V'_{0+}$ and that $T_2$ is terminated in a matched load $R_2$. The latter condition means $V'_{0+} = 0$ in Equation (4.5). If it can be assumed that the acoustic scattering $T_2$ is negligible when the electrical port is short-circuited or loaded with a low impedance*, then $V_{-m}^{(2)} = V_{-m}^{(3)} = 0$ in Equation (4.3) and (4.5). In this case it is possible to write

$$\frac{V''_{0-}}{V'_{0+}} = \sum_{i=1}^{N} S''_{0i} S'_{i0} = \sum_{i=1}^{N} S''_{-i0} S'_{i0} \qquad (4.6)$$

in which the symmetry of $\underset{\approx}{S}''$ has been used.

The short-circuit current $\dot{I}_2$ available from $T_2$ is related to the voltage $V''_{0-}$ by

$$\dot{I}_2 = -2 V''_{0-} \sqrt{\frac{2P}{R_2}} \qquad (4.7)$$

and by substitution from Equation (4.4) and (4.6) we may write for the transadmittance

$$Y_{21}(\omega) = \frac{\dot{I}_2(\omega)}{\dot{V}_1(\omega)} = \frac{-2}{\sqrt{R_1 R_2}} \sum_{i=0}^{N} S''_{0i} S'_{i0} \qquad (4.8)$$

For further progress explicit expressions for the scattering matrix elements are required.

---

* This approximation is not valid on strong-coupling substrates.

### 4.1.3. The Scattering Matrix Elements

The calculation of the amplitude of a normal mode field launched by a known source distribution on transducer $T_1$ proceeds from consideration of the complex reciprocity integral

$$\int_S \left(-j\omega\phi_s \underset{\sim}{D}_m^* + j\omega\phi_m^* \underset{\sim}{D}_s - \underset{\sim}{v}_s \cdot \underset{\approx}{T}_m^* - \underset{\sim}{v}_m^* \cdot \underset{\approx}{T}_s\right) \cdot d\underset{\sim}{S} = 0 \quad (4.9)$$

established by Auld[51] for a lossless piezoelectric medium in which no free charges or body forces are present. In the above integral $\phi_s$, $\underset{\sim}{D}_s$ etc. is the total field launched, at a frequency $\omega$, by a particular source distribution. $\phi_m$, $\underset{\sim}{D}_m$ etc. is the field of a normal mode at the same frequency $\omega$, and $d\underset{\sim}{S}$ is an element of area directed outward from a closed surface S which we will choose in the present case to consist of the propagation surface of the substrate, the boundary surfaces $S_1$, $S_2$, $S_T$ and $S_B$ in Figure 4.1(a), and a plane deep in the material. On the assumption that on planes $S_1$ and $S_2$ the propagating normal modes form a complete set for expansion of the fields $\phi_s$, $\underset{\sim}{D}_s$ etc. launched by the sources, and making use of the orthogonality relations (Equation (4.1)) we may derive the expression for the amplitude of normal mode m

$$V_m^{(2)} = \frac{-1}{4P} \int_{S'} \left[-j\omega\phi_s \underset{\sim}{D}_m^* + j\omega \underset{\sim}{D}_s \phi_m^*\right] \cdot d\underset{\sim}{S} \quad (4.10)$$

where the integration is over the surface $S'$ of transducer $T_1$, $d\underset{\sim}{S}$ is directed upward and mode m has $m > 0$. The displacement vectors for the source field and the Rayleigh normal mode field can be eliminated from this expression to obtain

$$V_m^{(2)} = \frac{j\omega}{4P} \int_{S'} \left[\varepsilon_0 \beta_m \phi_s + \sigma_s\right] \phi_m^* \, dS \quad (4.11)$$

where $\sigma_s$ is the charge density on the underside of a finger, $\phi_s$ is the electrostatic potential established at the substrate surface by the

source distribution, and we have used the fact that for a Rayleigh wave of propagation constant $\underset{\sim}{\beta}_m$, of magnitude $\beta_m$, the normal component of electric flux density is related to the potential by

$$\underset{\sim}{D}_m \cdot \underset{\sim}{dS} = \varepsilon_0 \beta_m \phi_m \, dS$$

for all propagation directions in the x-y plane. At this point it is assumed that the variation in propagation velocity with direction on the substrate can be neglected, and $\beta_m$ may be replaced by a constant value $\beta$.

Equation (4.11) can be condensed somewhat by the definition of a source function $f'(x,y)$ for a transducer pattern operated at a particular frequency, by the relation

$$\varepsilon_0 \dot{V} f'(x,y) = \sigma_s(x,y,o) + \varepsilon_0 \beta \phi_s(x,y,o) \qquad (4.12)$$

The amplitude of a normal mode m launched toward reference plane $S_2$ then becomes

$$V_m^{(2)} = \frac{j\omega\varepsilon_0 \dot{V}}{4P} \int_{S'} f'(x,y) \, \phi_m^*(x,y) \, dS \qquad (4.13)$$

If we make use of Equation (4.4) to eliminate $\dot{V}$ the result is the equation for the scattering matrix element

$$S'_{i0} = \frac{j \omega \varepsilon_0 \sqrt{2PR_1}}{4P} \int_{S'} f'(x,y) \, \phi_i^*(x,y) \, dS \qquad (4.14)$$

A similar equation may be deduced for $S''_{-i0}$, viz.

$$S_{-i0} = \frac{j \omega \varepsilon_0 \sqrt{2PR_2}}{4P} \int_{S''} f''(x,y) \, \phi_{-i}^*(x,y) \, dS \qquad (4.15)$$

The voltage ratio (Equation (4.6)) may now be written

$$\frac{V_0''^-}{V_0'^+} = \frac{-\omega^2 \varepsilon_0^2 \sqrt{R_1 R_2}}{8P} \sum_{i=1}^{N} \int_{S'} \phi_i^*(x,y) f'(x,y) dS \int_{S''} \phi_{-i}^*(x,y) f''(x,y) dS \qquad (4.16)$$

By making use of the result $\phi^{*}_{-i}(x,y) = \phi_i(x,y)$, which follows if we adopt (without loss of generality) the convention $\phi_i(0,0) = \phi^{*}_i(0,0)$ for all normal modes, it is possible to change the order of summing and forming the second projection to obtain

$$\frac{V_0^{''-}}{V_0^{'+}} = \frac{-\omega^2 \varepsilon_0{}^2 \sqrt{R_1 R_2}}{8P} \int_{S''} \left[ \sum_{i=1}^{N} \int_{S'} \phi^{*}_i(x,y) f'(x,y) dS \right] \phi_i(x,y) f''(x,y) dS \quad (4.17)$$

In view of the normal mode expansion (Equation (4.2)) and the expressions for normal mode amplitudes (Equation (4.13)), the coefficient of $f''(x,y)$ in the integral can be recognised (apart from a constant factor) as the total field, which we will call $\phi(x,y)$, radiated by transducer $T_1$ towards the region of transducer $T_2$. Thus

$$\frac{V_0^{''-}}{V_0^{'+}} = \frac{j \omega \varepsilon_0 \sqrt{2PR_2}}{4P} \int_{S''} \phi(x,y) f''(x,y) dS \quad (4.18)$$

and this expression allows for the effects of diffraction in the field launched by transducer $T_1$. At this point an expression for the potential $\phi(x,y)$ in terms of the source field of $T_1$ is required and this is obtained as follows.

We assume that at all frequencies of interest the width W of transducer $T_1$ is $>> \lambda$, so that its radiated field $\phi(x,y)$ in the vicinity of transducer $T_2$ is essentially the uniform plane wave

$$\phi(x,y) = \phi(0,0)\, e^{-j\beta x} \quad \text{for} \quad \frac{-W}{2} < y < \frac{W}{2} \quad (4.19)$$

where $\beta$ is the propagation vector at frequency $\omega$ in the x direction on the unperturbed substrate. The coefficient $\phi(0,0)$ can be related to the driving amplitude $V_0^{'+}$ by invoking conservation of power between the field $\phi(x,y)$ and the set of normal modes $\phi_i(x,y)$ into which it can be decomposed. The power $\Pi$ carried in width W by a uniform plane wave

is given in terms of the surface-wave potential $\phi$ and the commonly accepted measure $\Delta$, of piezoelectric coupling for surface-waves, by Ingebrigsten's[57] perturbation formula as

$$\Pi = -|\omega| W (\varepsilon_0 + \varepsilon_p) |\phi(0,0)|^2 / (4\Delta) \tag{4.20}$$

where $\varepsilon_p = (\varepsilon_{xx}\varepsilon_{zz} - \varepsilon_{xz}^2)^{\frac{1}{2}}$ is the effective permittivity of the substrate and $\Delta$ is the fractional change in surface-wave velocity between a free and a metallized propagating surface. The power $\Pi$ is also given in terms of the normal mode amplitudes by the equation

$$\Pi = P \sum_{i=1}^{N} V_i^{(2)} V_i^{(2)*} \tag{4.21}$$

which, after substitution for $V_i^{(2)}$ from Equation (4.13) and interchange of order of summation and integration becomes

$$\Pi = \frac{j \omega \varepsilon_0 V_0'^{+} \sqrt{2PR_1}}{4} \int_{S'} f'(x,y) \sum_{i=1}^{N} V_i^{(2)*} \phi_i^{*}(x,y)\, dS \tag{4.22}$$

$$= \frac{j \omega \varepsilon_0 V_0'^{+} \sqrt{2PR_1}}{4} \phi^{*}(0,0) \int_{S'} f'(x,y)\, e^{j\beta x}\, dS$$

Equating the two values of $\Pi$ obtained gives

$$\phi(0,0) = \frac{j \omega \Delta \varepsilon_0 V_0'^{+} \sqrt{2PR_1}}{|\omega| W (\varepsilon_0 + \varepsilon_p)} \int_{S'} f'(x,y)\, e^{j\beta x}\, dS \tag{4.23}$$

We may now substitute for $\phi(x,y) = \phi(0,0)\, e^{-j\beta x}$ in Equation (4.18) for the output of transducer $T_2$ and obtain

$$\frac{V_0''^{-}}{V'^{+}} = \frac{|\omega| \Delta \varepsilon_0^2 \sqrt{R_1 R_2}}{2 W(\varepsilon_0 + \varepsilon_p)} \int_{S'} f'(x,y)\, e^{j\beta x}\, dS \int_{S''} f''(x,y)\, e^{-j\beta x}\, dS \tag{4.24}$$

By substitution into Equation (4.8) the desired expression for the frequency transadmittance is obtained

$$Y_{21}(\omega) = \frac{-|\omega|\ \Delta\ \varepsilon_0^2}{W(\varepsilon_0 + \varepsilon_p)} \int_{S'} f'(x,y)\ e^{j\beta x}\ dS \int_{S''} f''(x,y)\ e^{-j\beta x} d\ S \tag{4.25}$$

Since the forward transadmittance between the transducers does not depend on the values of the parallel connected resistances $R_1$ and $R_2$ we may assume this expression applies also to the transducers in the normal situation in which they are absent.

For numerical evaluation of transadmittance functions by means of Equation (4.25) an expression for the source function $f(x,y)$ is required. In the weak-coupling approximation $f(x,y)$ may be obtained from the potential distribution $\phi_s$, and charge density $\sigma_s$ on the underside of a finger, which arises in the solution for the electrostatic field when the given finger pattern is placed on an equivalent non-piezoelectric substrate. Detailed expressions for the source function $f$, based on Engan's solution[80] for the field of a uniform transducer on a weak-coupling substrate, are obtained in Section 5.1 and 5.2 and a computer program which has been produced for the efficient computation of the transadmittance functions is also described.

## 4.2 The Time Domain Transadmittance $y_{21}(t)$

Since the main interest in this investigation is in the time domain description of coded delay lines, it is of some interest to seek an expression for the time domain transadmittance, or impulse response, of a two-transducer structure.

To simplify the discussion we consider the case of two acoustically coupled transducers having all their electrodes parallel to the Y-axis and of length W. The frequency transfer function is given by Equation (4.25) and may now be factorised as

$$Y_{21}(\omega) = K\,|\omega|\,F(\omega) \tag{4.26}$$

where

$$K = \frac{-W\,\Delta\,\varepsilon_0^{\,2}}{(\varepsilon_p + \varepsilon_0)} \tag{4.27}$$

$$F(\omega) = F_1(-\omega)\;F_2(\omega) \tag{4.28}$$

and

$$F_1(-\omega) = \int_{\ell_1}^{\ell_2} f'(x,o)\; e^{j\beta x}\; dx$$

$$F_2(\omega) = \int_{\ell_3}^{\ell_4} f''(x,o)\; e^{-j\beta x}\; dx$$

where $F_1(-\omega)$ and $F_2(\omega)$ are the Fourier transforms of the source functions* $f'(x,o)$ and $f''(x,o)$ respectively, $\ell_1, \ell_2$ and $\ell_3, \ell_4$ are limits containing the non-zero domains of the respective (non-overlapping) source functions, and $\beta=\omega/v$ where v is the constant surface-wave velocity. The Equation (4.26) may be rewritten in the form

$$Y_{21}(\omega) = K\,\{\,(j\omega)\;(-j\;\text{sign}\;(\omega)\;)\}\;F(\omega) \tag{4.29}$$

But it may be shown[84] that $\{(-j\;\text{sign}\;(\omega)\;F(\omega)\}$ is the Fourier transform of the inverse Hilbert transform of f(t) i.e.

$$Y_{21}(\omega) = K\;(j\omega)\;\;D\;(\omega) \tag{4.30}$$

where

$$d(t) \overset{FT}{\Leftrightarrow} D(\omega) \tag{4.31}$$

indicating that d(t) and D(ω) are Fourier transform related, and

$$d(t) = H_i'\{f(t)\} = \frac{1}{\Pi}\int_{-\infty}^{\infty} \frac{f(x)}{(t - x)}\; dx \tag{4.32}$$

is the definition of the inverse Hilbert transform[85]. The Equation (4.30) may be simplified still further by making use of the relationship

---

* It is shown in Section 5.2 that $f'(x,o)$ may, to a good approximation, be regarded as independent of β.

that multiplication by the factor $(j\omega)$ in the frequency domain is equivalent to differentiation in the time domain, to write

$$Y_{21}(\omega) = K \quad U(\omega) \tag{4.33}$$

where

$$u(t) \overset{FT}{\Leftrightarrow} U(\omega)$$

and

$$u(t) = \frac{d}{dt} [\ d(t)]$$

We are now able to take the Fourier transform of both sides of Equation (4.33) to obtain an expression for the time domain response,

$$\begin{aligned} y_{21}(t) &= K\ u(t) \\ &= K\ \frac{d}{dt} [\ d(t)] \\ &= K\ \frac{d}{dt} [H_i' \{f(t)\}] \end{aligned} \tag{4.34}$$

Referring to Equation (4.28) we may write f(t) in the form

$$\begin{aligned} f(t) &= f_1(-t) * f_2(t) \\ &= f_1(t) \text{ ¢ } f_2(t) \end{aligned} \tag{4.35}$$

where, for convenience the independent variable has been changed to $t = x/v$, and the operator ¢ indicates crosscorrelation. We may also represent the inverse Hilbert transform in the time domain as the convolution product[84] with the factor $(\frac{1}{\pi t})$ to obtain

$$y_{21}(t) = K\frac{d}{dt} [\ (\frac{1}{\pi t}) * \{f_1(t) \text{ ¢ } f_2(t)\}\ ] \tag{4.36}$$

or

$$y_{21}(t) = -\frac{K}{\pi} (\frac{1}{t^2}) * \{f_1(t) \text{ ¢ } f_2(t)\} \tag{4.37}$$

The restriction of the analysis to transducers with identical uniform overlap was introduced to simplify the algebra, and in fact this expression may be applied to cases with one apodized transducer where, as before, the maximum overlap of the apodized transducer does not exceed

the overlap length of the uniform transducer. It should also be noted that this analysis assumes transducer $T_2$ is to the right of $T_1$ on the X-axis: if $T_2$ is to the left of $T_1$ it is necessary to compute $\{f_2(t) \circledast f_1(t)\}$, and hence

$$y_{21}(t) = y_{12}(t) \tag{4.38}$$

as is expected.

## 4.3 The Frequency Input Admittance $Y_{11}(\omega)$

Auld and Kino[54] derived an expression for the input impedance of an acoustic surface-wave transducer by making use of a variational expression for the input impedance, involving an approximate estimate of the charge distribution on the fingers, amd adopting a representation of the acoustic field based on a set of open-circuited normal modes. They point out that the analogous variational expression making use of an approximate estimate of the potential distribution between the fingers may be used for the derivation of an expression for the input admittance, and give a general expression for $Y_{11}(\omega)$ derived using a normal mode expansion based on a set of short-circuited modes. Several algebraic errors however appear in their published derivation, and their principal result (Equation 77), and several of the preceding equations appear to be dimensionally incorrect.

In this section a corrected summary of their derivation is presented, which differs from their approach in notation and in the use of an expansion of the acoustic fields in terms of open-circuit normal modes. The variations have been introduced in order that the result so obtained will bear a more direct relation to Equation (4.25) and the latter change is a necessary consequence of the fact that the propagation of the surface-waves takes place on an unmetallized surface.

We take as a starting point their variational expression

(Equation (51), corrected and amended to conform to the present notation) for the input admittance of a transducer of uniform width W

$$Y_{11}(\omega) = \frac{j\omega W \int_{-\infty}^{\infty} \phi(x)\, \sigma(x)dx}{V^2} \tag{4.39}$$

where $\phi(x)$ is the potential distribution on and between the fingers, and $\sigma(x)$ is the total charge on the fingers resulting from an applied potential difference V at frequency $\omega$.

Defining $\Phi(\beta)$ and $S(\beta)$ to be Fourier transforms of $\phi(x)$ and $\sigma(x)$, and making use of the theorem that

$$\int_{-\infty}^{\infty} F(\beta)G^*(\beta)d\beta = 2\pi \int_{-\infty}^{\infty} f(x)g^*(x)dx \tag{4.40}$$

we may rewrite Equation (4.39) in the form

$$Y_{11}(\omega) = \frac{j\omega W}{2\pi V^2} \int_{-\infty}^{\infty} \Phi(\beta)S(-\beta)d\beta \tag{4.41}$$

The next step is to express the propagating potential field $\phi(x,y,z)$ excited under the transducer, by the charge distribution $S(\beta)$ at the surface, in terms of the original modes of the unperturbed system. This normal mode expansion may be written in the form

$$\phi(x,y,z) = \sum_m a_m \phi_m(z)\, e^{-j\beta_m x} \tag{4.42}$$

By means of the relation (which may be established from the complex reciprocity relation (Equation (4.9)) and the associated orthogonality condition (Equation (4.1)))between a sinusoidal charge distribution $\sigma(x,y,o) = \sigma_S\, e^{-j\beta x}$, at some frequency $\omega_0$ and wave number $\beta$ placed on the substrate surface, and the resulting potential $\phi(x,y,z) = \phi_S(y,z)e^{-j\beta x}$, of the same potential and wave number, the normal mode amplitudes may be determined as

$$a_m = \frac{-\omega_0\, \sigma_S\, \phi_x^*(0)}{4P_{mn}\, (\beta_n^* - \beta)} \tag{4.43}$$

where modes m and n are related by the condition $\beta_m = \beta_n^*$ and $P_{mn}$ is defined in Reference 54: for propagating modes $\beta_m$ and $\beta_n$ are real and $P_{mn} = P_{nn}$ becomes the power per unit width of the Y-axis carried in the direction of propagation.

In the further development the contribution to the potential from the non-propagating modes is neglected, on the assumption that this contribution relates only to the component of static transducer capacitance which can be calculated separately. The potential $\phi(x,y,o)$ of the propagating modes launched by a source varying as $e^{-j\beta x}$ is then

$$\phi(x,y,o) = \sum_n \frac{\omega_o \sigma_s}{(\beta - \beta_n)} \frac{\phi_n^*(0)\ \phi_n(0)}{4P_{nn}} e^{-j\beta x} \qquad (4.44)$$

where the sum is over all modes which propagate at frequency $\omega_o$. We now assume that relation between the amplitude $\sigma_s$ of a sinusoidal change distribution and the amplitude $\phi_s$ of the resulting potential can be extended to the spatial Fourier components $S(\beta)$ and $\Phi(\beta)$ of the charge distribution and potential on the transducer. Thus

$$\Phi(\beta) = \sum_n \frac{\omega_o S(\beta)}{(\beta - \beta_n)} \frac{\phi_n^*(0)\phi_n(0)}{4P_{nn}} \qquad (4.45)$$

Substitution of this result into the expression for the input admittance (Equation (4.41) gives the contribution $Y_p$ to $Y_{11}$ from the propagating waves in the form:-

$$Y_p(\omega_o) = \frac{j\omega_o^2 W}{2\pi V^2} \int_{-\infty}^{\infty} \sum_n \frac{S(\beta)S(-\beta)}{(\beta-\beta_n)} \frac{\phi_n^*(0)\phi_n(0)}{4P_{nn}} d\beta \qquad (4.46)$$

We now assume the propagating waves launched by the transducer consist of a single forward and a single backward surface-wave with propagation vectors $\beta_o$ and $-\beta_o$, determined by the frequency $\omega_o$. The

contributions in Equation (4.46) from these two waves may then be combined to give

$$Y_p(\omega_o) = \frac{j\omega_o^2 W}{2\pi V^2} \beta_o Z_o \int_{-\infty}^{\infty} \frac{S(\beta)S(-\beta)}{(\beta^2-\beta_o^2)} d\beta \qquad (4.47)$$

where $$Z_o = \frac{\phi_n^*(0)\phi_n(0)}{2P_{nn}} \qquad (\beta_n = \beta_o) \qquad (4.48)$$

defined as the normal mode impedance for the acoustic surface-wave, has been shown by Kino and Reeder[86] to be

$$Z_o = \frac{-2(\Delta v/v)}{|\omega_o|(\varepsilon_o+\varepsilon_p)} \qquad (4.49)$$

where $\varepsilon_p = (\varepsilon_{xx}\varepsilon_{zz} - \varepsilon_{xz}^2)^{\frac{1}{2}}$ is the effective permittivity of the medium.

Equation (4.47) contains the real and imaginary parts of the radiation admittance, but not in a form amenable to practical calculation. It may be observed that since the Fourier transform $S(\beta)$ of the real transducer charge distribution satisfies the condition $S(-\beta) = S^*(\beta)$, the contribution of the integral to the real part of Equation (4.47), over all the $\beta$ axis except for the small intervals near $\pm \beta_o$, is zero. Thus the real part of $Y_p(\omega) = G(\omega) + j\, B(\omega)$ is determined by the integral contributions surrounding the points $\pm \beta_o$, and these are readily shown (after introducing a small loss component[54] to the propagation constant $\beta_o$) to give

$$G(\omega) = \frac{-|\omega|W(\Delta v/v)}{(\varepsilon_o+\varepsilon_p)V^2} |S(\beta)|^2 \qquad (4.50)$$

where we now write $\omega$ and $\beta$ in place of $\omega_o$ and $\beta_o$. This result gives us $G(\omega)$ in terms of $S(\beta)$, the Fourier transform of the charge distribution $\sigma(x)$.

The imaginary part of the radiation admittance, $B(\omega)$, may

in principle be evaluated from Equation (4.47), if suitable precautions to preclude the contributions from the intervals near $\beta = \pm \beta_o$ are taken. However when using numerical integration a large amount of calculation is required, and it is computationally more efficient to make use of the relation pointed out by Nalamwar and Epstein[87]

$$B(\omega) = G_{Hi}(\omega) \tag{4.51}$$

where $G_{Hi}(\omega)$ is the Hilbert transform of $G(\omega)$. An efficient method for the computation of the Hilbert transform of a sampled function is described in Section 5.3.

To complete the evaluation of the input admittance $Y_{11}(\omega)$ it is necessary to include the contribution from the cutoff modes, more commonly described as the transducer static capacitance. The expression derived for this quantity by Engan[80] is

$$C_T = \tfrac{1}{2} W (\varepsilon_o + \varepsilon_p) \frac{K(\cos(\frac{\pi}{2} a))}{K(\sin(\frac{\pi}{2} a))} \tag{4.52}$$

in Farads/gap in the transducer, where K is the complete elliptic integral of the first kind[88], and a is defined in Figure 5.1.

The total input admittance of a single transducer is thus given by

$$Y_{11}(\omega) = G(\omega) + j (B(\omega) + \omega C_T) \tag{4.53}$$

and the individual terms may be evaluated by means of Equations (4.50), (4.51) and (4.52).

## 4.4 Discussion

A number of interesting features may be observed in the results obtained in the previous sections.

Equation (4.25) shows that the frequency domain performance of a two-transducer delay line is determined by the product of the

spatial Fourier transforms of the source functions of each transducer, a $|\omega|$ factor and a constant determined by the physical substrate properties.

The most interesting of these is the $|\omega|$ factor: at an early stage in this project a dimensional analysis of the simple $\delta$-function model showed that it did not scale correctly with frequency, but the analysis did not indicate how to rectify this. The subsequent appearance of the $|\omega|$ in the preceding derivation resolved this problem. This result can be compared with the impulse model development of Hartmann[69,89] in which it is shown, by a dimensional analysis approach, that transducers with log-tapered gaps must have the overlap lengths multiplied by $f^{-\frac{3}{2}}$ to achieve a flat frequency transfer function. Experimental confirmation of the effect of the $|\omega|$ factor is obtained in the observed rising frequency sensitivity of logarithmically frequency-chirped transducers reported in Chapter 6, and similar results have been published by Smith et al.[90]. The above analysis predicts that the $|\omega|$ factor applies to all interdigital transducers, including uniform gap-width devices, and the resulting tilting of the passband response and sidelobes of the delay line spectrum is discussed in Chapter 6.

Another point of interest is the fact that the real transfer admittance $Y_{21}(\omega)$ obtained when Equation (4.25) is applied to two identical transducers with zero relative displacement, is identical to the real part of the input admittance $Y_{11}(\omega)$ calculated by means of Equation (4.50) for one of the transducers, indicating that the two expressions for $Y_{21}(\omega)$ and $G(\omega)$, although reached by different approaches, are in fact consistent.* It is interesting to note also that Equations

---

* It is a straight-forward matter to show by deduction (from a consideration of the input admittance of two adjacent transducers, of length $\frac{L}{2}$ and spaced $\frac{L}{2}$ between centres, wired externally to function as a single transducer of length L ) that this relationship between the real part of the input admittance, and the transfer admittance between identical transducers, must hold.

(4.25) and (4.50) predict that the harmonics of the transducer fundamental response will also be weighted by the $|\omega|$ factor, and this is still awaiting experimental verification.

The time domain transfer admittance $y_{21}(t)$ of a two-transducer delay line is predicted by Equations (4.34) and (4.37). From Equation (4.34) this response may be interpreted as the derivative of the inverse Hilbert transform of the crosscorrelation product of the two source functions specified in the $(t=\frac{x}{v})$ domain. The equivalent expression, Equation (4.37), must be used with caution because the factor $(\frac{1}{t^2})$ is not a function in the normal sense and must be interpreted as a distribution[92]. The effect of this convolution is to sharpen up any peaks of the crosscorrelation product and smear the edges of the waveform slightly: these effects are discussed in the light of the experimental measurements and computer simulation studies in Chapter 6.

A further point of interest in the time domain response is the polarity of the output. The peak of the time domain response $y_{21}(t)$ in Equation (4.34) between two identical transducers is positive*, and on substitution into Equation (3.12), the first-order delay line impulse response will have a negative peak; in fact it will be a delayed and inverted replica of the real part of the input admittance g(t) of a single transducer ($Z_L$ being real), specified in the time domain. This inversion of the line output does not appear to have been acknowledged explicitly in the literature, presumably due to the fact that the conventional analysis techniques are concerned with single transducers in isolation. The effect is clearly demonstrated in the experimental results achieved in Chapter 6, and is also evident in the recently

---

* The crosscorrelation product f(t) becomes an autocorrelation function which must yield a positive peak, and the combined operations of differentiation and inverse Hilbert transformation may be shown to be noninverting.

published results of Sugiyama and Yoshikawa[91]. This question of output polarity is of importance in determining the relative phases of the interfering higher-order responses in coded delay lines, as discussed in Chapters 7,9 and 10.

It is relevant at this point to compare the frequency domain and time domain representations, of the off-diagonal or transadmittance elements of the general N-port admittance matrix, in terms of their relative computational efficiency. Examination of Equation (4.25) and (4.36) shows that the former involves the simple product of a constant and three functions of frequency while the latter involves the computation of a convolution and a correlation product. Since the product of two sample vectors of length N requires only N multiplications, while the convolution of two such vectors requires $N^2$ multiplications, it is obvious that the frequency domain transadmittance may be computed much more efficiently than the equivalent time domain response (provided efficient means are available to obtain the Fourier transform of a source function), and this is the approach followed in the development of the computer model in the next chapter.

# CHAPTER 5

# A COMPUTER MODEL FOR SURFACE-WAVE DEVICES

## 5.0 Introduction

One of the major aims in the project was to obtain a computer model capable of predicting the behaviour not just of single inter-digital transducers, but of complete (e.g. coded) surface-wave devices, when inserted into an operational system. It was felt that if a reasonably efficient model could be obtained it would provide a very attractive alternative to conducting time consuming and expensive laboratory testing of large batches of surface-wave delay lines, when evaluating complex systems employing such devices. With such a model available, the necessary experimentation is reduced to a small number of experiments, sufficient to evaluate the accuracy of the model itself, and then further studies of the various aspects of device behaviour may be investigated by computer simulation.

In Chapter 3 it was shown how a knowledge of the admittance matrix (specified throughout either the time or frequency domains)for an N-port surface-wave device, permits a complete determination of the device behaviour when connected into a practical circuit. In the last chapter approximate analytical expressions were derived for the individual elements in the admittance matrix for any N-port device on a weak-coupling substrate, and we look now at methods by which these expressions may be evaluated on a computer.

As explained in the last chapter, the single most important parameter is $Y_{21}(\omega)$, the transfer admittance between two acoustically-coupled transducers, and an approximate expression suitable for programming is derived in the next section. In Section 5.2 a method for high-speed integration is developed and in Section 5.3 the additional

expressions necessary for the computation of the complete transducer input admittance are derived.

The resulting expressions have been used in a series of computer programs developed for execution on a digital computer. The necessity for the use of a digital machine means that one is inevitably working with sampled representations of the continuous functions representing the device parameters. This factor brings its own problems, and these are outlined in Section 5.4.

## 5.1 Transadmittance Evaluation

An examination of Equation(4.25)giving the transadmittance between a pair of transducers reveals that the expression may be factorised into four parts, namely the material constants, the $|\omega|$ factor, and two integrals each containing the source function $f(x)$ of a single transducer. The most time consuming part of this calculation is the evaluation of the two-dimensional integrals, a process which must be repeated at every frequency of interest. In consequence of this, efforts were made to simplify the calculation procedure by using approximate expressions, and the first step is the reduction of the integration to a one-dimensional problem.

### 5.1.1 Problem Reduction to One Dimension

The first step in the reduction of the integrals in Equation(4.25) to a more tractable form is to eliminate the integration with respect to the width of the propagating wave. This may be achieved if we make use of what we shall call the 'independent-gap' approximation, where we assume that the source function in any particular 'gap' in the transducer is independent of the geometry of the adjacent gaps. This approximation will later be shown to introduce negligibly small errors in modelling transducers with slowly varying gap widths along their lengths.

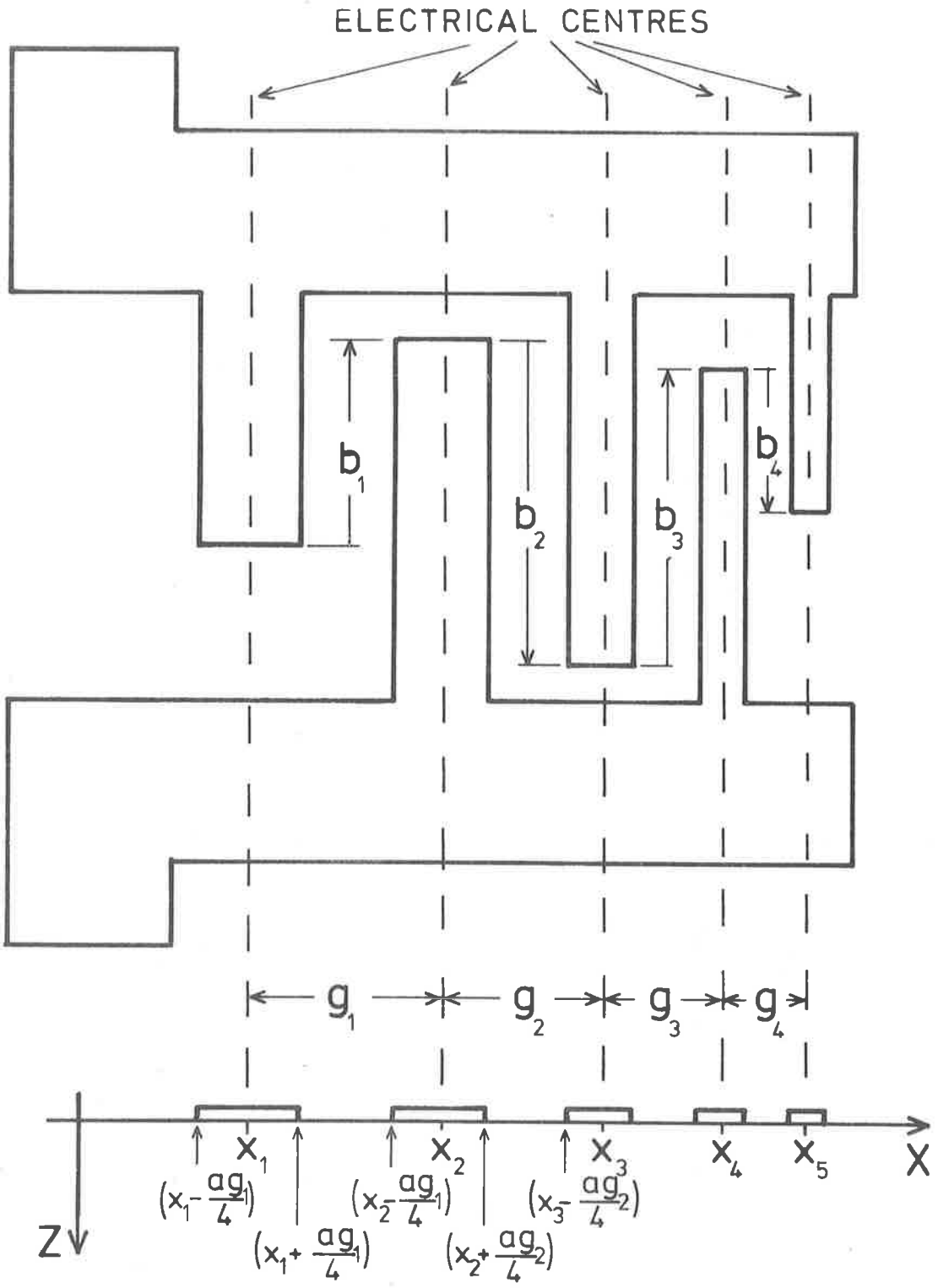


Figure 5.1 Sketch illustrating the definition of a transducer metallization pattern in terms of the 'electrical centres' $x_i$, gap widths $g_i$ and overlap lengths $b_i$. (Note overlap lengths are negative when measured in the downward direction.)

This source field representation necessitates the introduction of the concept of an 'electrical centre' for each electrode in the transducer, and the 'gap' between each pair of electrodes is then defined to be the region between the 'electrical centres'of adjacent electrodes, as illustrated in Figure 5.1. With the adoption of the independent-gap approximation we can assume that the source function in each gap, within the region of electrode overlap, is independent of the variable y (this is not normally the case with apodized transducers). We can thus evaluate the integrals as the sum of the contribution from each of the gaps, and if we refer to the restrictions applied in the derivation of the transadmittance formula, that the input transducer has uniform overlap W and may have variable gap widths, while the output transducer may have variation of both the electrode overlap length (<W) and the gap width, we can obtain by integrating with respect to y,

$$Y_{21}(\omega) = K \int_{L_1}^{L_2} \sum_{i=1}^{N} f'_i(x)\, e^{j\beta x}\, dx \int_{L_3}^{L_4} \sum_{j=1}^{M} b_j\, f''_j(x) e^{j\beta x} dx \qquad (5.1)$$

where

$$K = \frac{-|\omega| \Delta\varepsilon_o^{\,2}}{\varepsilon_o + \varepsilon_p} ,$$

$f'_i(x)$ = the source function i for the transmit transducer, which is understood to be zero everywhere except within gap i.

$f''_j(x)$ = the receive transducer source function j, with similar properties to $f'_i(x)$.

$b_j$ = the (signed) overlap length of gap j.

The parameter W does not appear in this expression and the restriction that the transmit transducer have uniform overlap was introduced in order to simplify the algebra. More correctly we must specify that all electrodes in the transmit transducer must be greater than or

equal to the longest overlap in the receiving transducer. In a practical circuit analysis the effect of varying the transmit transducer overlap lengths, while satisfying this restriction, is accommodated in the calculation of $Y_{11}(\omega)$.

Since the surface-wave devices are reciprocal, i.e. $Y_{21}(\omega) = Y_{12}(\omega)$, we can simply use the above formula to calculate $Y_{12}(\omega)$ if the input transducer is apodized and has a maximum overlap length less than that of the output transducer.

The situation where both transducers are apodized is much more difficult to represent analytically because the propagating surface-wave field onto which we must project the receiver source field is not independent of y, and the resulting expression for $Y_{21}(\omega)$ does not factorise into two separate integrals. The simplest practical solution in this case appears to be[66] to divide the propagation path into a number of parallel strips selected so that each strip intersects the launching and receiving transducers in such a way that the restriction, that at least one of the transducers may be considered to be unapodized across that beam width, is satisfied.

We now need convenient expressions for the source functions $f_i'(x)$ and $f_i''(x)$.

### 5.1.2 Source Function Generation

The source function $f(x)$ is related to the electric potential and charge distributions under the transducer electrodes by Equation (4.12) which is reproduced here,

$$f(x) = \frac{1}{\varepsilon_o \dot{V}} \left( \sigma_s(x) + \varepsilon_o \beta \phi_s(x) \right) \qquad (5.2)$$

Again invoking the weak-coupling approximation, we commence with the electrostatic field solution for an infinite uniform interdigital grid on a non-piezoelectric but anisotropic dielectric, which has been derived

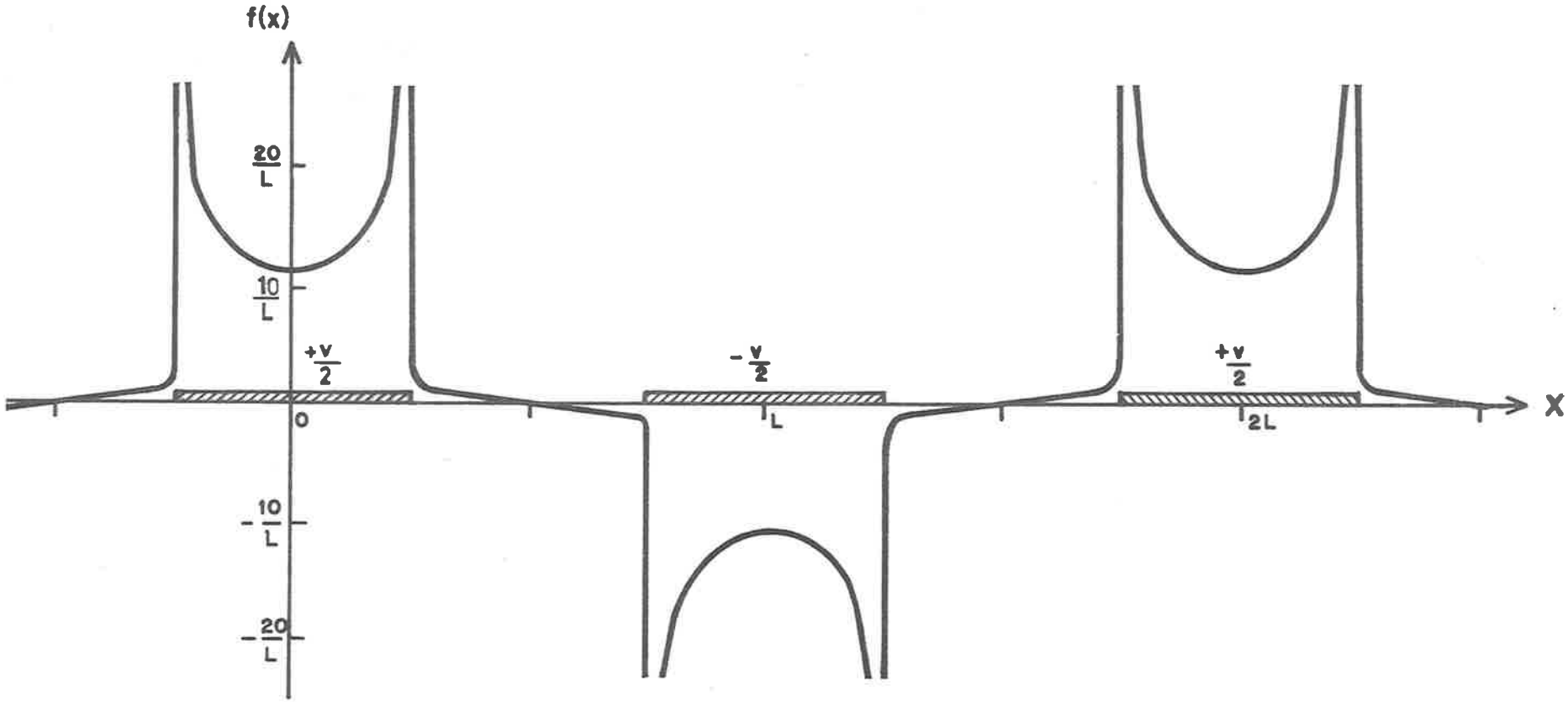


Figure 5.2 Source function $f(x)$ for a uniform interdigital transducer on YX-quartz, shown plotted in relation to the electrode metallization for the case a=½.

by Engan [80]. Shifting the origin as shown in Figure 5.2, and correcting an error of sign, we obtain his results in the form

$$E_x(x) = \sum_{n=o}^{\infty} \frac{\pi V \, P_n(\cos\pi a)}{L \, K(\cos(\frac{\pi a}{2}))} (-1)^n \sin(B_n x) \qquad (5.3)$$

and

$$D_z(x) = -\sum_{n=o}^{\infty} \frac{\varepsilon_p \, \pi V \, P_n(\cos(\pi a))}{L \quad K(\cos(\frac{\pi a}{2}))} (-1)^n \cos(B_n x) \qquad (5.4)$$

here

$P_n(\cos\pi a)$ = Legendre polynomial of the first kind.

$K(\cos\frac{\pi}{2}a)$ = the complete elliptic integral [88] of the first kind.

$\varepsilon_p = \{\varepsilon_{xx}\varepsilon_{zz} - \varepsilon_{xz}^2\}^{\frac{1}{2}}$ and, $B_n = (2n+1)\frac{\pi}{L}$

By making use of the relations

$$\sigma_s(x) = -D_z(x)\big|_{x_3=0} \qquad (5.5)$$

and

$$\phi(x) = -\int E_x \, dx \qquad (5.6)$$

we can obtain the following expression for the source function for an infinite uniform interdigital transducer

$$f(x) = \sum_{n=o}^{\infty} \left[\frac{\varepsilon_p}{\varepsilon_o} + \frac{\beta}{B_n}\right] \frac{\pi \quad P_n(\cos(\pi a))}{L \quad K(\cos(\frac{\pi a}{2}))} (-1)^n \cos(B_n x) \qquad (5.7)$$

This expression contains the result obtained by Engan, that in a uniform transducer, only odd harmonies will be generated, independently of the value of a, the fraction of the gap width which is metallized. In practice it is desirable to work with values of a between 0.25 and 0.75, and if we select the particular case a=0.5 (often called unity mark-space ratio) then the third harmonic will be zero, ensuring that the lowest harmonic which can interfere with the fundamental response of a wideband transducer becomes the fifth harmonic.

### 5.1.3. Variable Gap-Width Transducers

The expression for the source function given in Equation (5.7) is suitable for use with uniform transducers, if simply truncated to correspond to the number of fingers in the transducer. We still need an expression for the source functions in the individual gaps in variable gap-width transducers, as required in Equation (5.1).

The solution adopted here was to make further use of the independent-gap approximation, and simply use the series expansion in Equation (5.7) corresponding to a given gap width, in each gap of that width. The problem which arises in applying this method to the analysis of an existing transducer pattern is to find the location of the 'electrical centres' of the electrodes in order to ascertain the individual gap widths. The solution which has been adopted here, on an intuitive basis, is to divide the electrodes into left and right portions in direct proportion to the widths of the unmetallized regions to the left and right of the electrode.

The converse procedure, of producing the metallization pattern corresponding to a given set of electrical centres, is readily achieved by metallizing the regions $x_i < x < (x_i + g_i/4)$ and $(x_{i+1} - g_i/4) < x < x_{i+1}$, as shown in Figure 5.1. These two procedures are mutually inverse, and the errors involved in modelling devices not synthesised in this fashion will be small if the rate of variation in gap widths is small.

The resulting expression for the source function in the first integral in Equation (5.1) then becomes

$$f_i'(x) = \sum_{n=o}^{\infty} \left\{ \frac{\varepsilon\rho}{\varepsilon_o} + \frac{\beta}{B_n} \right\} \frac{(-1)^n \pi \, P_n(\cos(\pi a))}{(x_{i+1}-x_i)K(\cos(\frac{\pi a}{2}))} \cos B_n(x-x_i)$$

$$\text{for } x_i \leqslant x < x_{i+1}$$

$$= 0 \qquad \text{for} \qquad \begin{matrix} (x < x_i \\ ( \\ (x \geqslant x_{i+1} \end{matrix} \qquad (5.8)$$

In this approximation to the source function, no attempt has been made to allow for the fact that fringing fields will exist at the end electrodes and at other electrodes within apodized transducers. This point is discussed further in relation to the experimental results.

## 5.2 Transadmittance Evaluation

While seeking an efficient method for the computer evaluation of equation (5.1) it became apparent that the two integral expressions would be simple Fourier transforms, but for the presence of the term $\beta/B_n$ which appears in Equation (5.8). Examination of the significance of this term shows that on moderate to strong dielectric materials, its contribution relative to the term $\varepsilon_p/\varepsilon_o$ is small, and in the region of fundamental operation of the transducer will suppress the contributions from the harmonies of the spatial field. Thus if we assume that the transducer is to operate in fundamental mode over moderate bandwidths we may use only the first term in the series expansion for the spatial field in Equation (5.7), and we may, to a good approximation, replace the term $\beta/B_n$ with unity.* If we make the further assumption of unity mark-space ratio in each gap the source function becomes

$$f_i'(x) = \frac{\pi (\varepsilon_p + \varepsilon_o)}{1.854\ \varepsilon_o\ (x_{i+1} - x_i)} \cos\left(\frac{\pi}{L}(x - x_i)\right) \qquad (5.9)$$

$$x_i \leqslant x < x_{i-1}$$

$$= 0 \text{ for } \begin{cases} x < x_i \\ x \geqslant x_{i+1} \end{cases}$$

This expression is independent of the wave vector $\beta$, and the evaluation of the integrals in the transadmittance, Equation (5.1), now reduces to the evaluation of the familiar Fourier integrals.

---

* It may be observed here that the effect of this approximation is to make the admittance proportional to the total charge on the electrodes rather than the charge on the under surface, as assumed in the derivation of $Y_{21}(\omega)$.

### 5.2.1. The Discrete Fourier Transform

To evaluate the integrals in Equation (5.1) on a digital machine it is necessary to sample the functions, and the discrete Fourier transform (DFT) must be used. Initial attempts to use the conventional definition for this transform showed it to be inconvenient in use[93], and a version with modified scale factors was used to achieve a direct approximation to the continuous integrals in Equation (5.1). The definition for the DFT used throughout this work is,

$$X_n = \Delta y \sum_{m=o}^{N-1} Y_m \; e^{\frac{j(2\pi)\, nm}{N}} \qquad n=0,1,--,\ N-1 \tag{5.10}$$

and

$$Y_m = \Delta x \sum_{n=o}^{N-1} X_n \; e^{\frac{-j(2\pi)\, nm}{N}} \qquad m=0,1,---,\ N-1 \tag{5.11}$$

where

$X_n$ = correspond to samples in the time domain.

$\Delta_x$ = the uniform sampling interval in the time domain.

$Y_m$ = correspond to samples in the complex frequency domain.

$\Delta_y$ = the uniform sampling interval in the frequency domain.

N = the number of complex samples in both domains.

In this transform definition we have the implied constraint that for the transform and its inverse to be normalised, then

$$\Delta x \quad \Delta y = 1/N \tag{5.12}$$

### 5.2.2. The Fast-Fourier Algorithm

The efforts at the beginning of this section to manipulate the required integrals into Fourier integral form was motivated by an awareness of the availability of the fast-Fourier transform (FFT) algorithm. This algorithm was published by Cooley and Tukey in 1965[94], and makes use of the cyclic properties of the exponential term in the

integral definition to effect significant savings in computing time. The algorithm reduces the number of multiplications necessary to evaluate the DFT for N samples from $h_1 N^2$ to $h_2 N \log_2 N$, where $h_1$ and $h_2$ are constants of unit order and depend on the programming details.

For waveforms requiring several thousand samples, as found in the system studies in Chapter 9, a reduction in computing time of two orders in magnitude is achieved, and this significantly reduces the cost of the modelling techniques which are presented in this thesis.

A subroutine based on the version of the algorithm by Cooley Lewis and Welch[95] and optimised by Downing[96] for multiple calls, was modified to evaluate the DFT as defined in Equations 5.10 and 5.11, and extended to output the sample interval for the output vector. A listing for this subroutine, called BFAST is given in Appendix A1.3.

### 5.2.3. The Transadmittance Program

The basic program used for the evaluation of the transfer admittance between a pair of interdigital transducers is called SAWDLY 1, and a listing is presented in Appendix A1.4. The program is set up to evaluate logarithmically tapered transducers, tapered in both gap width and electrode overlap, uniform transducers simply being treated as the special case of zero taper. However, any other transducers may be investigated by inputting the relevant geometric description, in terms of the electrode electrical centres and the overlap lengths. The only additional required input data are the dielectric constants and the coupling factor $\Delta$, and if the latter is not already known it may be obtained for any crystal orientation by means of program SURF02, described in Chapter 2.

In addition to its use in evaluating the frequency transadmittance integrals, the subroutine BFAST is also used as a means for rapidly converting the initial program output vector to the time domain,

and the output is available in both the time and frequency domains. Examples of the plotted output may be seen with the results in Chapter 6.

## 5.3 Input Admittance Evaluation

The input admittance may be considered as containing two components; one is dependent upon the piezoelectric coupling, and the other is not. The radiation immittance is dependent upon the coupling factor and for computational convenience the real and imaginary parts will be considered separately. The coupling-independent component is the capacitive susceptance, which is also computed separately.

### 5.3.1. The Radiation Conductance

Reference to Equation(4.50) showsthat the real part of the radiation admittance may be calculated using the same program as used for the calculation of the transfer admittance. The same source function is used for both transducers and the transducer separation is put to zero. A more efficient method is to compute the first integral, and then the modulus-squared of the resulting values, and to omit second integration. This procedure is followed in a program written to evaluate the complete input admittance. A listing of this program, called INAD, is given in Appendix A1.5.

One restriction on the calculation of the input admittance by this method, is that the transducer should not be apodized, for the same reasons that prevent the calculation of the transadmittance between two apodized transducers. This limitation may sometimes be disregarded when the apodizing is not significant for the set of fingers operating at each particular frequency, as in the case of slowly tapered, frequency-chirped transducers. Otherwise, the only solution is to divide the propagation path into notional 'lanes', as described for the

transadmittance calculation, and evaluate the admittance contribution from each 'lane'.

### 5.3.2. The Radiation Susceptance

As explained in Section 4.3 the complex radiation immittance may be calculated from an evaluation of the integral expression in Equation (4.47). However, a computationally more efficient method is to evaluate the real part of the radiation immittance by the method of the previous section and then compute the complex part using the Hilbert transform relation given in Equation (4.51).

To do this we need an efficient means for computing the Hilbert transform. The method chosen here is to make use of the equivalent operation to the Hilbert transform in the Fourier transform domain[84]. The method is described by the following steps:-

(1) Take the real conductance $G(\omega)$.

(2) Take the Fourier transform $G(\omega) \Rightarrow g(t)$

(3) Multiply by the Fourier transform of the Hilbert operator

$$g(t) \times h(t) = g^1(t)$$

where

$$h(t) = \begin{cases} -j & \omega > 0 \\ 0 & \omega = 0 \\ j & \omega < 0 \end{cases}$$

(4) Take the inverse Fourier transform $B(\omega) \Leftarrow g^1(t)$

the radiation susceptance is given by the resulting real vector $B(\omega)$.

This apparently indirect method for the calculation of the Hilbert transform has been chosen because it is able to capitalise yet again on the efficiency of the FFT algorithm: it is still much faster to compute the FFT twice, than to attempt to evaluate the discrete Hilbert transform[97] directly.

The above procedure is followed in program INAD listed in Appendix A1.5.

### 5.3.3. The Static Capacitive Susceptance

The transducer capacitance is evaluated using the expression derived by Engan[80] and rewritten in the form

$$C = \tfrac{1}{2} \sum_{i=1}^{N} |b_i| (\varepsilon_o + \varepsilon_p) \frac{K(\cos\frac{\pi}{2}a_i)}{K(\sin\frac{\pi}{2}a_i)} \qquad (5.13)$$

where

$a_i$ = metallization ratio in gap i

$b_i$ = electrode overlap in gap i

If we specify a = 0.5, then this simplifies to,

$$C = \tfrac{1}{2} (\varepsilon_o + \varepsilon_p) \sum_{i=1}^{N} |b_i| \qquad (5.14)$$

which presents no problems in computation.

These formulae may be used for variable gap width and apodized transducers, provided we are able to neglect the effect of fringing fields at the ends of the grid and in the apodized regions.

### 5.3.4. The Input Admittance Program

To perform these calculations evaluating the various components of input admittance the program INAD was developed. A flow chart and listing is given in Appendix A1.5. The output may be obtained as either a print or a plot of the complex frequency components. Examples of the plotted output may be found with the experimental results in Chapter 6.

## 5.4 Accuracy of the Results

An important question with any computer model is the accuracy of the results which can be obtained. In this case we must look at two possible sources of error: the first is errors resulting from the finite accuracy of the machine used, and the second is errors resulting

from the use of sampled data to represent continuous functions. Any errors introduced from these sources will be superimposed on the inaccuracies resulting from the approximations made in the analysis.

### 5.4.1. Rounding Errors

Since the machine has a finite word length, small errors are introduced in the rounding of the results of the various arithmetic operations, at each stage of the computation.

If we assume the use of floating point arithmetic then Gentleman and Sande[98] have shown that the cumulative effect of rounding the resultant of each arithmetic operation, gives an output RMS noise-to-signal ratio proportional to $\log_2 N$ (where N is the number of samples) when using the FFT. Weinstein[99] has shown that this performance may be improved upon by the implementation of a randomised rounding process to yield an RMS noise-to-signal ratio proportional to $(\log_2 N)^{\frac{1}{2}}$. For comparison, the direct calculation of the DFT, with truncation, would give[98] an RMS noise-to-signal ratio proportional to N, and here we can see a further advantage in deliberately seeking to use the FFT algorithm for numerical integration.

In the experimental modelling studies a CDC 6400 computer with floating point arithmetic was used. This machine has a 45 bit mantissa giving approximately 15 decimal digit accuracy. Application of the above bound for the noise-to-signal level for rounded arithmetic, indicates that calculation of the FFT for $N = 2^{10}$ will result in a noise level only 10 times greater than the noise level for a 1-point transform. In more general terms, we will lose about 1 decimal digit in accuracy. The level of inaccuracy is trivial in relation to the errors discussed in the next section.

### 5.4.2 Aliasing Errors

The Sampling Theorem[100] states that for any given time waveform the original waveform may be faithfully reconstructed from a uniformly spaced set of samples of that waveform, by low pass filtering, provided the original waveform had no spectral components at frequencies greater than half the sampling frequency (F). If this restriction is not satisfied then the reconstructed waveform will be found to have errors in detail, and its complex spectrum will have corresponding errors which can be interpreted as the result of folding back the spectral components of the original waveform at frequencies higher than $\frac{F}{2}$, back into the frequency range 0 to $\frac{F}{2}$. This phenomenon, of errors resulting from undersampling (i.e. $\Delta T > \frac{1}{F}$), is known as aliasing.

When using the DFT we are operating with sampled representations of both the time and frequency waveforms, and aliasing may occur in either domain, if the (complex) waveforms are undersampled in the alternate domain. This can be seen to be related to the periodic properties of the DFT, and poses a basic problem, in any computer modelling exercise, in the choice of suitable sampling frequencies. Fourier theory asserts that a waveform which is of finite duration in one domain (e.g. the spatial distribution of the source function of a transducer) will have infinite duration in the Fourier transform (e.g. $\beta$) domain. Hence it is impossible to satisfy the Sampling Theorem simultaneously in both domains.

The solution in practice is to increase the relevant sampling frequency until the aliasing error has been reduced to an unimportant level. But one is always working under the constraint of finite computer memory capacity and this determines the practical maximum sampling frequency for waveforms with a fixed time-bandwidth product.

It is thus relevant to ask what is the relation between the actual spectrum level above the chosen folding frequency $F/_2$, and the resulting distortion in the computed spectrum.

The bounds on the apparent magnitude of a unit sinewave after the addition of another sinewave with the same frequency but unknown phase is plotted against the level of this interfering signal, in Figure 5.3. From this graph one can set an acceptable error level due to aliasing, and determine the corresponding maximum level for the out-of-band spectral components. For example to obtain an error tolerance of $\pm$0.5 dB the out-of-band spectrum must be more than 25 dB below all portions of the spectrum which are of interest.

Determination of the level of the neglected spectral components by careful empirical exploration is necessary if an analytic asymptote for the spectrum roll-off with frequency is not available. In the computing for the experiments , aliasing was encountered due to the high spatial frequency content of the postulated source function, arising from the discontinuities at the edges of the gaps, particularly at the ends of the transducer. The problem was minimised by increasing the sampling frequency. A more efficient solution is to use digital prefiltering[93] prior to evaluation of the DFT: time did not permit the incorporation of this technique into the existing programs. This is felt to be the only significant shortcoming in the present form of the computer programs for modelling the admittance coefficients of surface-wave devices.

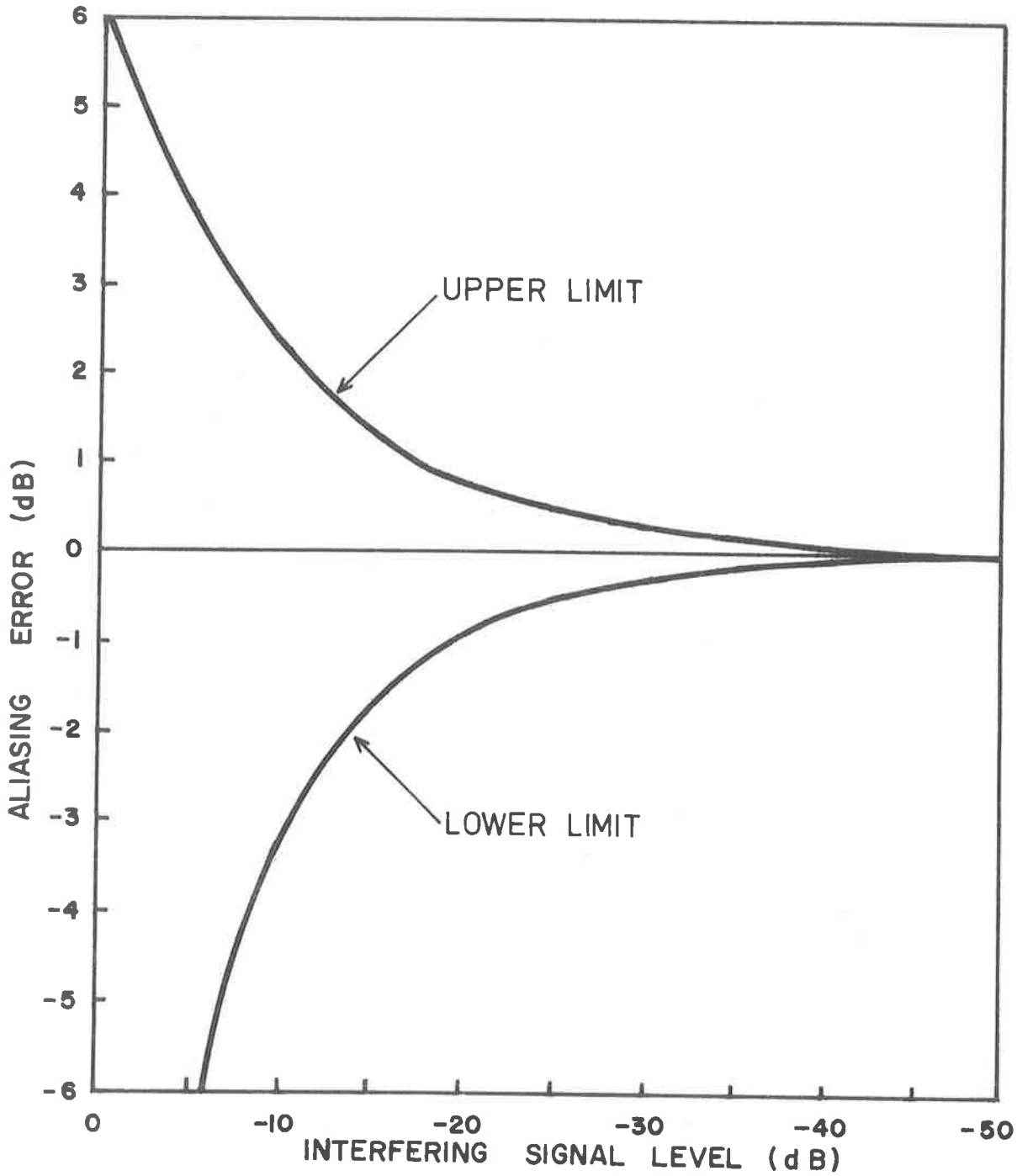


Figure 5.3 Upper and lower limits on the apparent magnitude of a unit amplitude sine-wave after the addition of a smaller sine-wave of the same frequency and unknown phase.

# CHAPTER 6

# EXPERIMENTAL AND COMPUTED RESULTS FOR TYPICAL TRANSDUCERS

## 6.0 Introduction

To test the validity of the admittance formulation and integral expressions derived in Chapter 4 for the characterisation of interdigital surface-wave transducers, a number of experiments were performed to provide practical data for comparison with the theory. The results are shown alongside the expected theoretical results computed using the best available knowledge of the effective circuit and stray electrical component values in the measurement configuration, for comparison. For convenience, the experiments reported in this chapter have been divided under the headings of uniform and non-uniform transducers: the particular type of non-uniform transducer examined is the logarithmically frequency-tapered transducer with uniform overlap.

### 6.0.1 Background to the Experiments

All the experiments were performed on substrates cut and polished from the piezoelectric single-crystal material α-quartz; both X-cut and Y-cut surfaces were used. Although the coupling factors for XY- and YX- propagation are very similar[20], the latter was preferred because the non-collinearity of the power-flow and wave vectors for XY-propagation[20] was found to be an impediment to the interpretation of experimental results.

The delay lines were fabricated in the laboratory using the facilities described in the next section and the individual transducers used in the experiments are described alongside the results. The use of quartz with its weak coupling in preference to the various strong-coupling crystals which have recently become

available[92-95], resulted in quite high insertion losses in some of the experiments (in the case of the impulse response measurements quite elaborate measurement techniques had to be devised), but had the advantage that the accuracy of measurement of the first-order delay line response was not affected by the presence of the second-order responses.

In many cases, more than one sample of each line was tested and it was found that the performance of the experimental lines was quite repeatable from one day to the next and from one sample to another to within experimental error. The delay lines were found to be quite robust: some were remounted and demounted in the various experimental jigs used up to 10 times without any apparent harm, and some were still operating after 2 or 3 years with only a small (2 dB) increase in insertion loss - apparently due to contamination on the propagating surface because the mounting jigs were not sealed. It was also found that the substrates could be reused without further repreparation apart from etching the electrodes from the surface.

## 6.1 Delay Line Fabrication

The manufacture of interdigital transducers requires the location of a grid of thin conducting electrodes, with suitable connections at the ends of the electrodes depending upon the grid phasing, on the polished surface of a piezoelectric substrate. The narrow electrode widths ranging from about a hundred microns down to fractions of a micron, preclude normal machining operations (although one such method of assembly, using a line-engraving machine, is reported by Viktorov and Talashev[96]) and photolithographic techniques borrowed from the technology of the printing and semi-conductor industries, are normally employed. The standard process involves the generation of a large scale drawing of the desired conductor pattern, its reduction in size using photographic techniques to produce a

mask made of either metal or photoresist, and then either the deposition of the metal conductor through a negative mask, or the etching of a continuous metal film on the crystal surface through a positive mask. The type of process is limited in resolution by optical diffraction of the light in the photographic steps[97] and to produce lines less than about one micron wide it is necessary to use electron beams to obtain the final masks, which are made using a suitable sensitized polymer material [98].

In this study the experiments were conducted in the 10 to 50 MHz frequency range (i.e. line widths from 16 to 80 microns) using aluminium metallization on α-quartz. The particular techniques used and the equipment developed during the project for the manufacture of the experimental delay lines, are described briefly in this chapter, and quantitative data on the actual procedures used may be found in Appendix A2.

A perpetual problem in high-resolution photographic and photoresist work is the degradation of the images due to the presence of dust in the working environment, and to prevent dust spots from rendering the resultant transducers unserviceable this work is normally carried out in clean conditions. The conventional dark-room in the Electrical Engineering Department was found to give unacceptably low image yields and it was necessary to construct a rudimentary clean-room with a filtered air supply and an airconditioning unit (for temperature stablization) to house the photoreduction equipment described below. Difficulty was still encountered with contamination in the photoresist images and it was found necessary to install a laminar-flow bench, suitably modified to prevent solvent vapours accumulating in the clean-room, to achieve an acceptable device yield.

### 6.1.1 Mask Generation

Simple patterns were cut directly onto Rubylith sheet by hand, by tracing original drawings produced on a basic drafting machine, to provide a transparency suitable for photography. For more complex transducer patterns, having non-uniform electrode overlap length or spacing, a computer program was written by the author to draw any desired interdigital electrode pattern on a CALCOMP 30 inch drum plotter, driven by the computer. The patterns were drawn using black ink on triacetate plastic sheet to produce a positive transparency suitable for mounting directly on the 30" x 40" copyboard. A listing of the basic plotting program used to draw the electrodes, PATBL, is included in Appendix A1.7. To minimise plotting time the contact pads in the pattern were added by hand using Rubylith at the first stage of reduction.

The photographic reduction was performed using an optical bench and copyboard, designed by the author and assembled in the Departmental workshops, which is shown in Figure 6.1. Two reduction cameras, were designed jointly by the author and Dr. P.H. Cole, and built in the workshop. The first-stage camera, shown in Figure 6.1, produced images on 10" x 8" film sheet and had an operating range of 2½x to 5x reduction. The second-stage camera, shown in Figure 6.2, produced images 2" x 2" high-resolution glass plate and had an operating range of 20x to 35x reduction. More information on the equipment and processes used can be found in Appendix A2.

### 6.1.2 Substrate Preparation

Single crystal α-quartz was selected for use in the experiments on the basis of its relatively low cost and ready availability. The attenuation rate for surface-waves on this

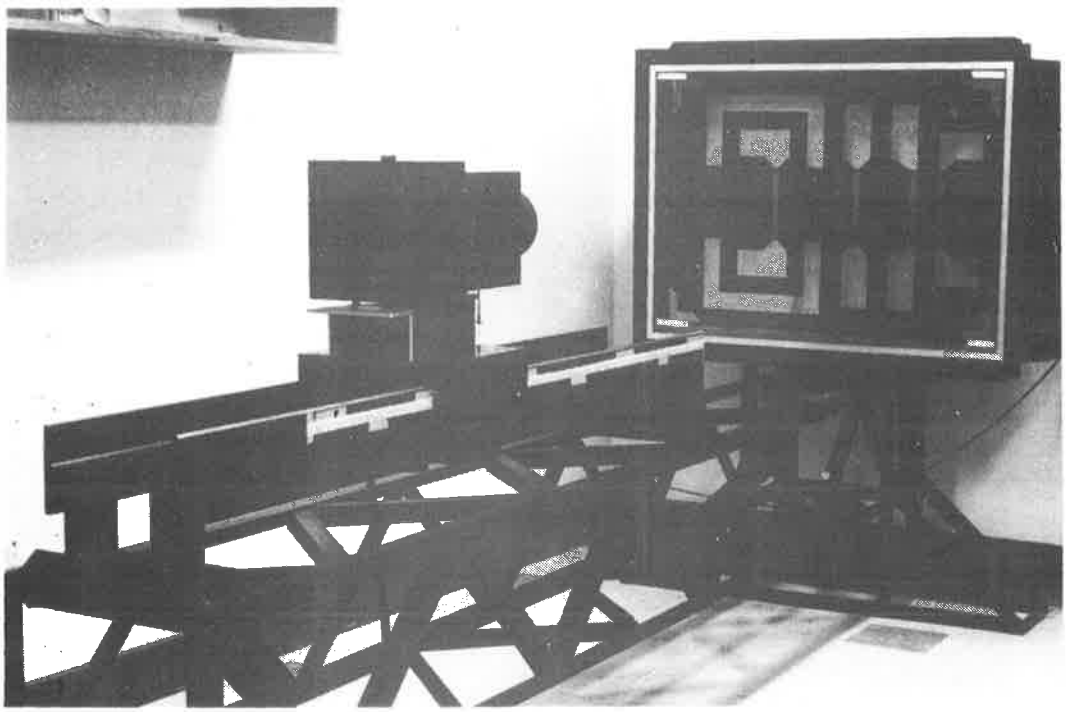

Figure 6.1 The optical bench and copyboard, shown with the first-stage reduction camera mounted on the carriage.

(a)

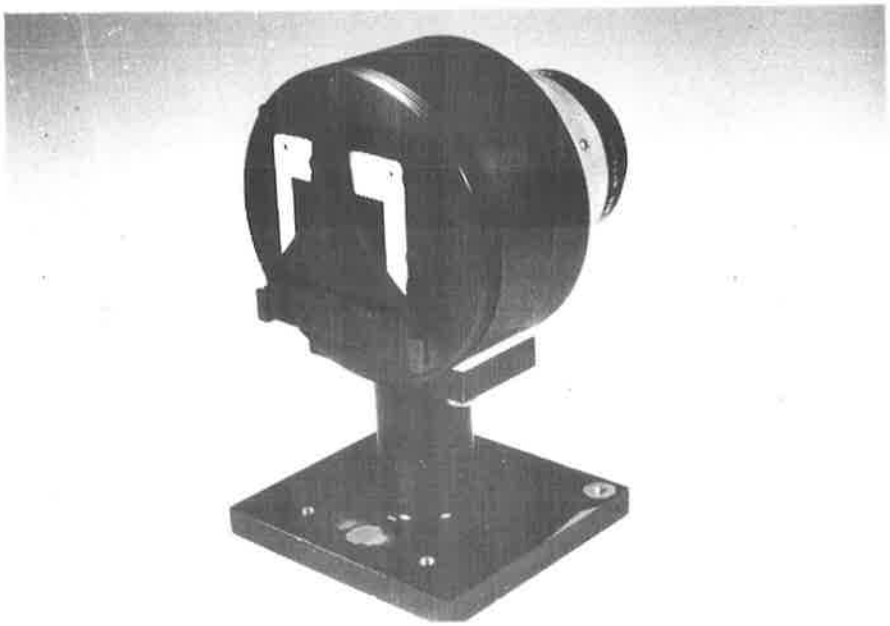

(b)

Figure 6.2 Second stage reduction camera (a) front view, and (b) rear view.

material is negligibly small at the frequencies of experimental interest and, although the piezoelectric coupling factor is considerably lower than that obtainable on some of the newer synthetic crystal materials, its choice did permit advantage to be taken of its relatively greater durability, with regard to physical, thermal and chemical damage, in the fabrication processes and the experiments.

The surface finish on the rectangular crystal blanks obtained from various suppliers was found to vary considerably and to provide a constant surface condition the working surface of each crystal was polished flat to within one wavelength of light by a specialist optical company, before use in the experiments. Such a finish is better than is required to minimise surface-wave propagation losses at the frequencies used: the flatness was specified in order to permit good contact with the glass-slide when contact-printing the photoresist.

In the early part of the experiments some difficulty was experienced in obtaining good adhesion of the aluminium metallization to the substrate surface. The problem was resolved with the introduction of more elaborate cleaning procedures and the introduction of substrate preheating prior to the metal deposition. The different steps used in the final cleaning procedure consisted of immersion in degreasing and detergent solutions in an ultrasonic bath, immersion in a vapour-reflux bath and finally, in the vacuum chamber, glow-discharge cleaning. The commercial ultrasonic bath, and the vapour bath assembled in the laboratory, can be seen in Figure 6.3.

The metallization of the substrate surface was achieved using the apparatus shown sketched in Figure 6.4, which was installed in a vacuum chamber loaned by the Material Science Department. The substrates were loaded onto the aluminium supporting jig before immersion in the

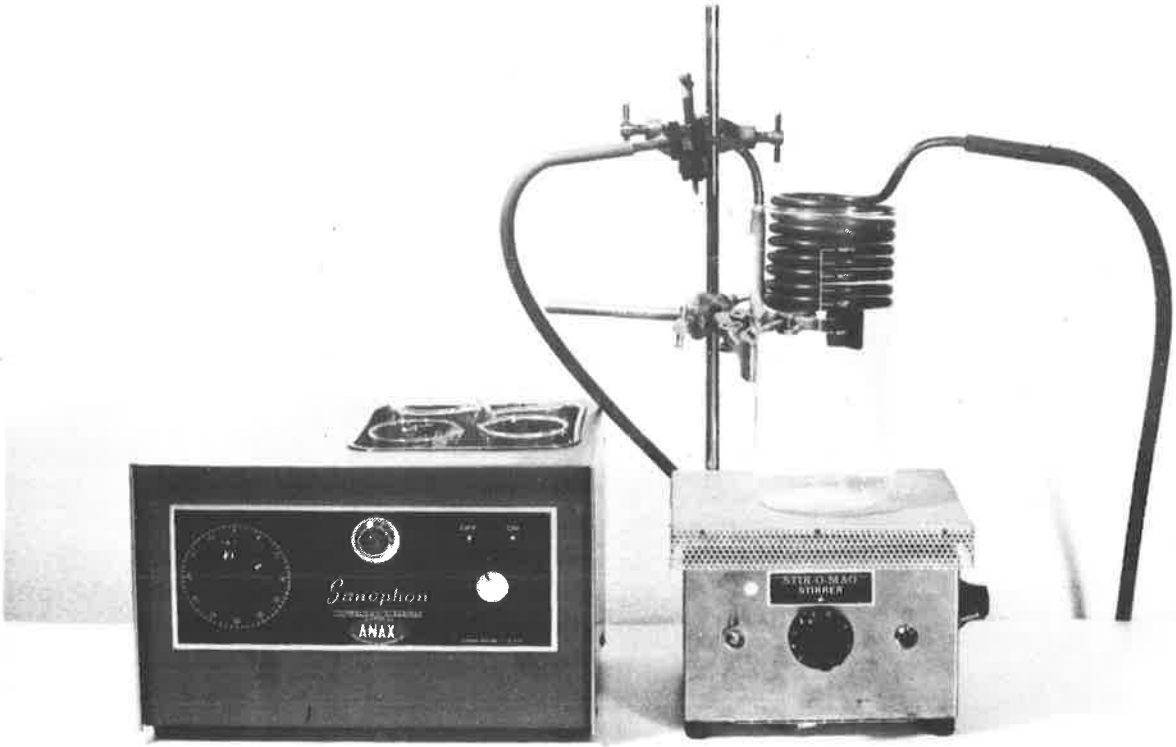


Figure 6.3 Substrate cleaning apparatus (a) the commercial ultrasonic bath at left, and (b) the vapour-reflux bath assembled in the laboratory, at right.

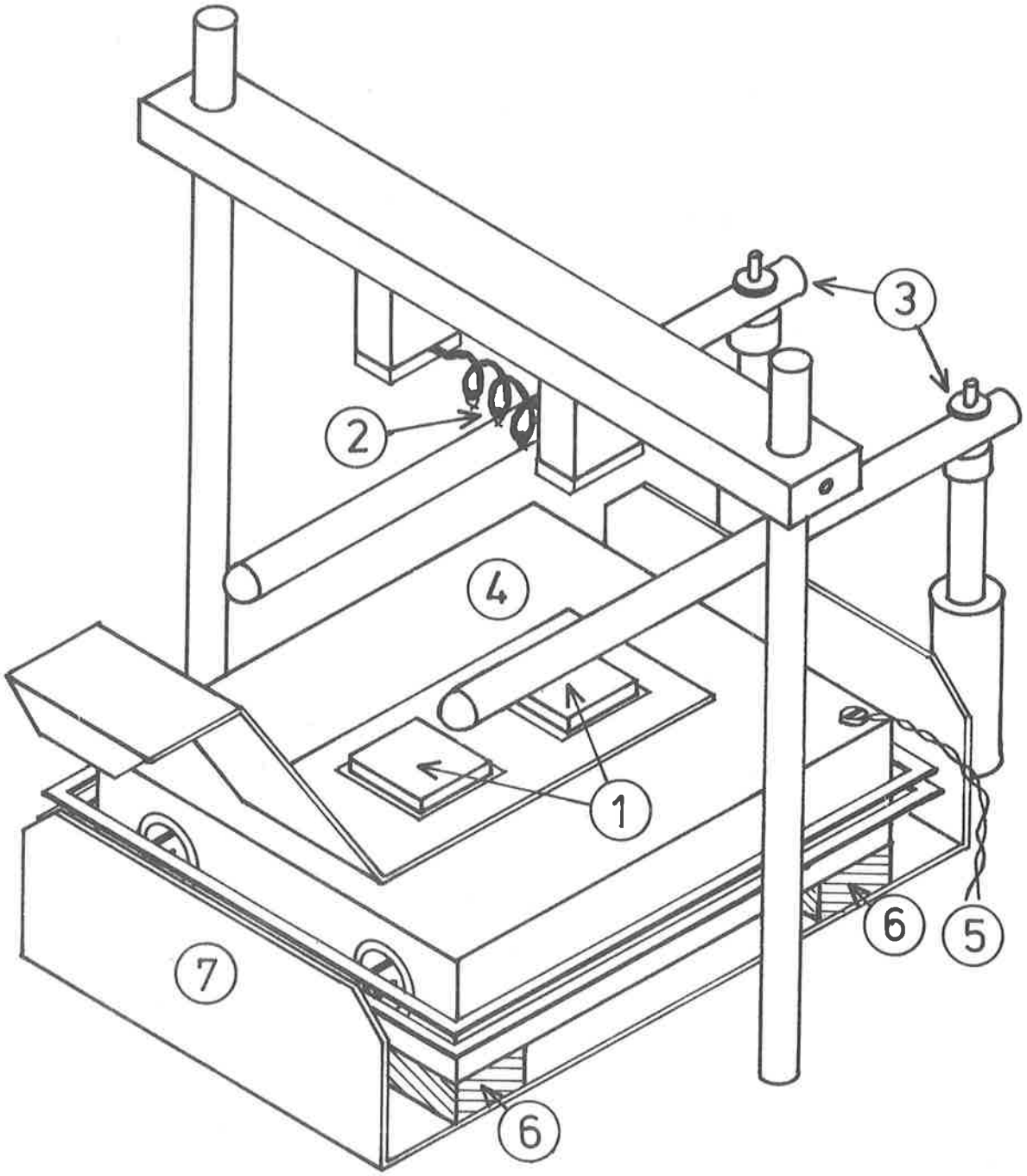


Figure 6.4 The metallization apparatus showing (1) crystals in aluminium supporting jig (2) tungsten filament loaded with aluminium loops (3) glow-discharge electrodes (4) substrate heater block (5) thermo-couple fitting (6) thermal insulators (glass), and (7) shield to contain thermal radiation from heater lamps.

vapour bath, and then transferred to the position shown for the coating process. The final cleaning of the substrate was performed using an ionic glow-discharge obtained by applying a high potential between the electrodes shown in the sketch, in a moderate vacuum. The substrate was then heated slowly to 200°C by means of the substrate heater* before the system was pumped right down and the aluminium evaporated onto the surface by passing a short pulse of current through the tungsten filament.

After the coating operation the substrates were cooled in still air before transfer to the laminar-flow bench for coating with photoresist.

### 6.1.3 Photo-etching

The method used to produce the electrode patterns on the substrates involved contact-printing a negative of the required image onto a thin film of negative-working photoresist spread over the metallized substrate, and then immersion of the developed resist image in a chemical etching solution to remove the undesired portions of the metal film. This work was carried out in the laminar-flow clean-cabinet shown in Figure 6.5(a) which was constructed by modifying a commercial instrument cabinet in the Departmental workshops under the supervision of the author and his supervisor. The alterations were necessary to provide an increased working area and to arrange for the exhaust from the cabinet to be vented outside to prevent solvent vapour accumulation in the clean-room.

Due to the high viscosity of the photoresist used (Kodak KTFR) it was found necessary to use both dilution and a high-speed spinner[108] to obtain resist films thin enough for good image resolution when producing 16μm wide electrodes. The KTFR resist was first diluted with KTFR

---

* Supplied by Dr. P.V.H. Sabine of the Department.

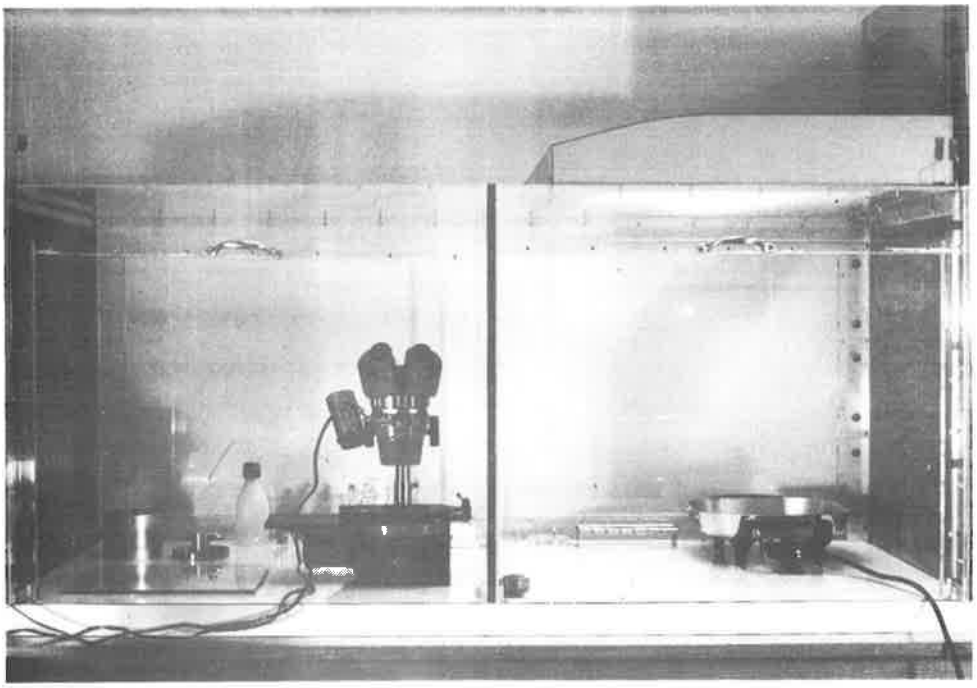

(a)

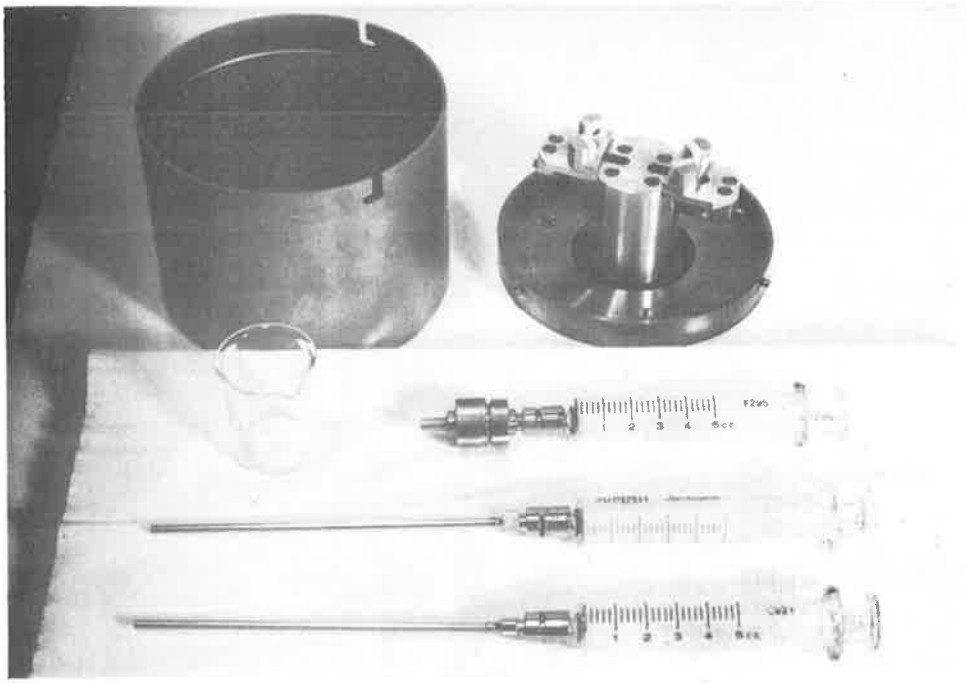

(b)

Figure 6.5 Photoresist processing equipment showing (a) the laminar-flow cabinet with inlet filter at right, outlet filter at left, safelight housing at top and alignment microscope with the contact printing jig in left foreground and (b) a closer view of the syringes and filter used for resist dilution and filtration, and the clamp and safety cover of the substrate spinner.

thinners and mixed thoroughly, passed through a set of submicron filters on the end of a syringe, and then applied directly to the surface of the stationary metallized substrate clamped to the spinner head. The measuring syringes, application syringe with filter-holder, and spinner head are shown in Figure 6.5(b). The spinner was designed by the author and comprises a 3000 R.P.M. induction motor, selected for its acceleration characteristics[108], directly coupled to the crossbar carrying the substrate, which was clamped mechanically, rather than by vacuum as used in semiconductor facilities. Both jaws of the clamp have freedom of rotation about vertical axes permitting rectangular as well as square substrates to be firmly held, and both jaws move on opposing threads when tightened to ensure that the substrates are always dynamically balanced, this allowing quite large (up to 7 cm. diagonally) and thick substrates to be spun as required. Consistently good resist films, approximately 5μm thick, were achieved with this apparatus, and after spinning the substrates were baked on a hotplate to remove all traces of solvent before the contact printing. The hotplate is a simple commercial unit, shown at right in Figure 6.5(a), with the thermostat deactivated and temperature control achieved by means of a preset mains autotransformer and a thermocouple probe to check any temperature drift.

The exposure jig used for contact printing is shown under the alignment microscope in Figure 6.5(a) and in more detail in Figure 6.6(a). The jig was loaded first with the 2" x 2" glass plate (emulsion side up) and then the resist-coated substrate placed face down onto the glass plate and aligned by means of orientation marks incorporated into the pattern on the plate, as viewed through the microscope at low magnification (for this purpose a wide-aperture transmitted-light source was built into a special base for the commercial

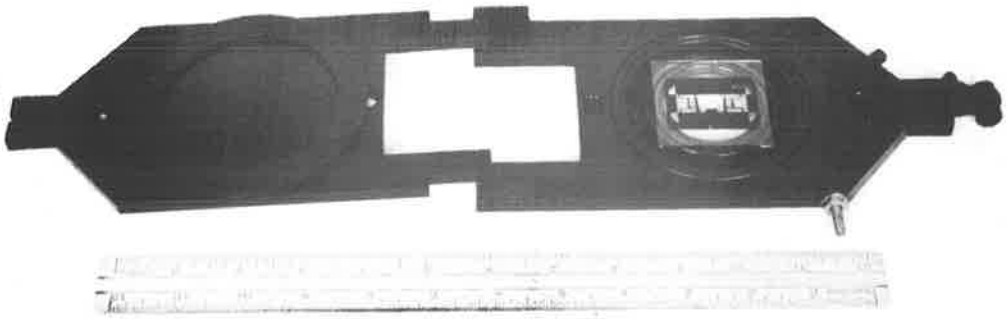

(a)

(b)

Figure 6.6 The contact printing apparatus designed by the author (a) the contact printing jig (in fully open position) and (b) the lamphouse containing the ultraviolet light source.

zoom microscope). With correct registration of the substrate achieved, the jig was closed and evacuated through a non-return valve and the resulting internal vacuum pulled down the neoprene diaphragm in the upper plate of the jig to envelope the substrate and clamp the substrate and plate together with approximately one atmosphere compression. This ensured good contact with the photoresist surface, and also resulted in a 70% reduction in exposure time necessary for polymerisation of the resist and similarly reduced substrate heating, apparently due to the removal of oxygen from the resist [109].

The resist was exposed to ultraviolet radiation through an aperture in the lower plate of the jig by placing the jig over a matching aperture in the top of the UV-lamphouse shown in Figure 6.6(b). The UV-lamphouse was designed by the author to complement the exposure jig and includes forced ventilation to permit continuous running as this was found to improve the thermal stability of the UV-lamp. After exposure the substrate was removed from the jig and allowed to cool before 'development' by immersion in KTFR developer to remove the unexposed resist, before flushing with KTFR rinse. The substrate was then baked on the hot-plate again before inspection under the microscope (at high magnification) for blemishes.

The substrate was then immersed in an aluminium etchant, with continuous agitation and removed as soon as etching was complete to prevent undercutting of the resist.

The final stage in device fabrication entailed the removal of the resist film without damaging the electrodes. This caused considerable difficulty in the early experiments and was finally achieved by use of a proprietary solvent obtained for the purpose. The substrate was then rinsed in distilled water and dried in the clean-cabinet.

More details of the chemicals, processing times and equipment used etc. may be found in Appendix A2.5.

### 6.1.4 Mounting Techniques

Various mounting schemes were used in the experiments and some are shown in Figure 6.7. The delay lines with large substrates used mechanical clamps and the smaller substrates were held down simply by placing them on a strip of double-sided adhesive tape (this latter method was found to give a very strong grip between the perfectly plane surfaces of the crystal and the base - in some cases sufficient to cause crystal damage when attempting to remove the crystal from the jig). The delay line performance parameter most affected by the wiring layout and mounting enclosure design was found to be the direct leakage of input signal from the input wiring to the output wiring by capacitive coupling. With high insertion-loss delay lines the undelayed signal was found to greatly exceed the delayed output signal, and this resulted in the adoption in later design of boxes with separate screened compartments for the input and output wiring with just a clearance hole in the dividing wall to accomodate the substrate.

A number of methods of making electrical contact to the transducer pads were used with success. Gold wire (.005 inch dia.) was used for the connecting leads to the transducer pads and was used with conducting silver paint, conducting silver epoxy, and pure indium, Both the paint and the epoxy required long curing times which was inconvenient for experimental work, but the epoxy did give a very strong connection. Pure indium, used as a solder with a low-temperature soldering iron and without flux was found to give very low resistance joints between the gold wire and aluminium bonding pads, although the bond strength was quite low( the indium could be pulled away by pulling

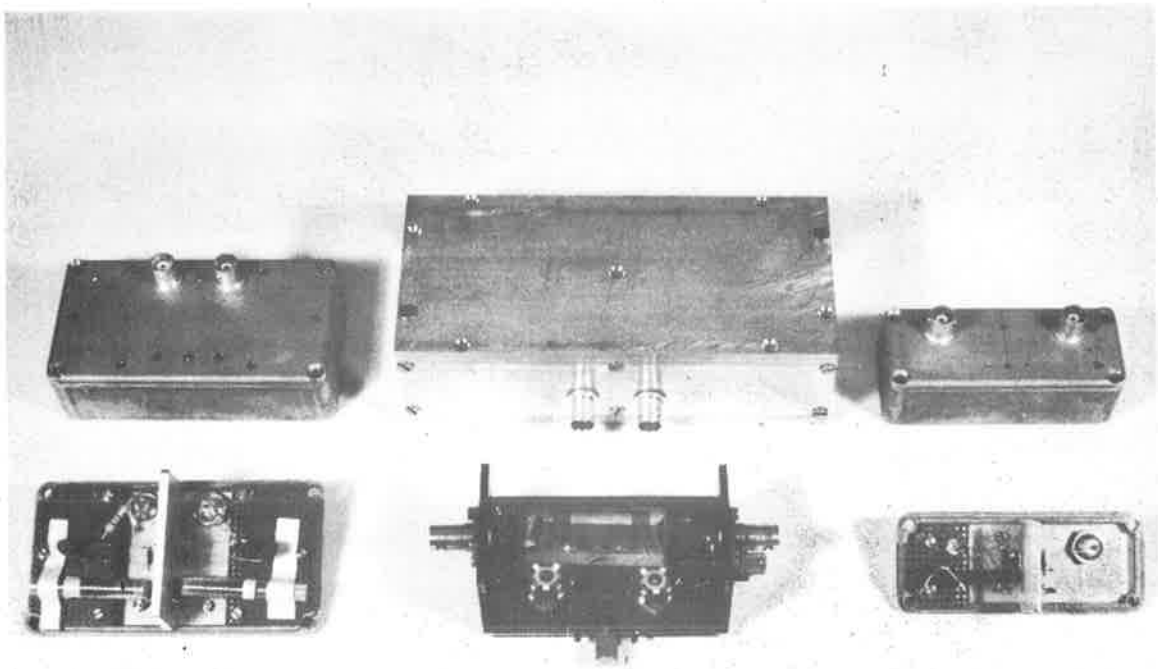

Figure 6.7 Some of the experimental mounting jigs used for measurement of the delay line responses in the laboratory.

on the wires without damaging the aluminium pads). This method was used almost exclusively in the experimental work because of the ease with which connections could be made and altered.

In many experiments involving long pulses or CW signals it is desirable to be able to absorb surface-waves without reflection to prevent interference effects arising, and a number of techniques were used to minimise reflection. It was found that edge reflections could be reduced by polishing a radius (large relative to the wavelength) on the edge concerned or by applying an absorber such as adhesive masking tape or black (apiezon W) wax. Temporary damping could be applied in exploratory work using a piece of rubber or a drop of a volatile solvent such as isopropyl alcohol. For more permanent assemblies black-wax applied by melting with the low-temperature soldering was considered the best.

## 6.2 Uniform Interdigital Transducer Measurements

The first series of experiments were conducted on elementary surface-wave delay lines, employing a pair of uniform interdigital transducers for the generation and reception of the surface-waves. The aim was to measure the admittance parameters of the lines and compare the results with the predictions of the computer model. The initial experiments were conducted on some transducers designed for use in the experimental one-port coding system, to be examined later, and the impedance levels of these transducers were rather high to permit accurate measurement of the input admittance. The transadmittance however, can be readily measured by inserting the high-impedance devices directly into a 50Ω measurement system. This is a further advantage of the admittance formalism, chosen originally for reasons of analytical convenience, as the transimpedance is much more difficult

to measure accurately when the device impedance levels are very much greater than the measurement system characteristic impedance level.

### 6.2.1. Frequency Domain Transadmittance $Y_{21}(\omega)$

The delay lines used for this measurement employed two 9-finger transducers, each 50 wavelengths wide at the synchronous frequency of 50 MHz, on Y-cut X-propagating synthetic quartz crystals. Aluminium metallization was used and the lines were fabricated using the processes described in the previous section. The lines were mounted in the die-cast metal box shown at bottom right in Figure 6.7.

The standard measurement network adopted for both CW and pulse measurements on two-port delay lines is shown in Figure 6.8, while the actual apparatus used in the laboratory is shown in the photograph Figure 6.9. The delay lines could be excited with variable length pulses from a 50Ω source impedance, and the output voltage was observed across the calibrated input impedance of the preamplifier, which was of the order of 50Ω. The entire system was calibrated by substituting a stepped 50Ω coaxial attenuator for the delay line and taking measurements at spot frequencies in the range of interest to permit calculation of the effective preamplifier voltage gain.

The results for above delay line are shown in Figure 6.10 where the measured and computed value of the voltage transfer ratio are shown for comparison. The voltage transfer ratio is simply computed from the relation

$$\frac{V_o}{V_I} = -Y_{21}(\omega) \quad Z_p \qquad (6.1)$$

(where $Z_p$ is the measured preamplifier input impedance) using the program SAWDLY1 described in Appendix A1.4.

Considerable difficulty was experienced with volume modes contributing to the line output at the higher sidelobe frequencies.

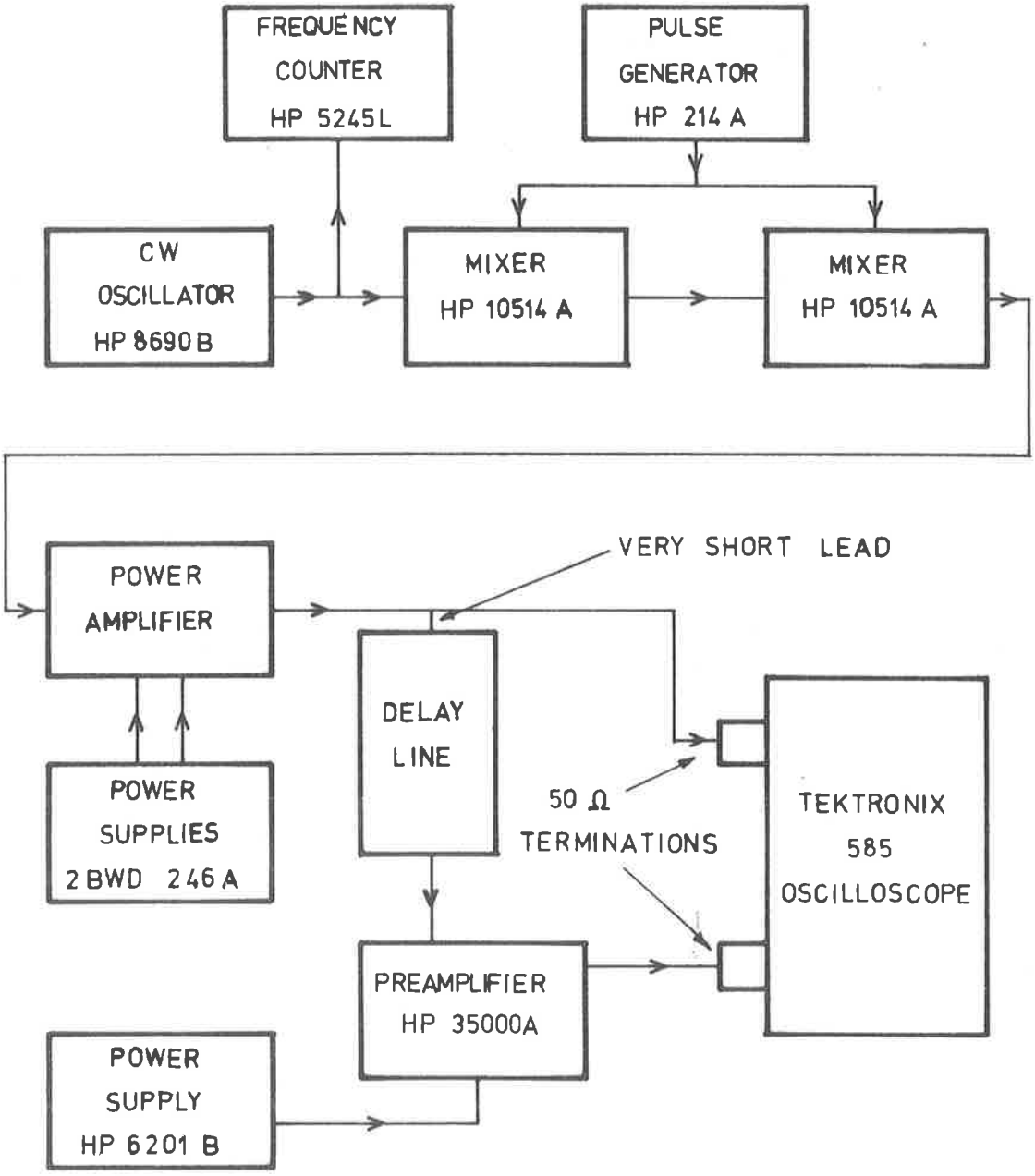


Figure 6.8 Equipment configuration for frequency response measurements using pulsed CW signals.

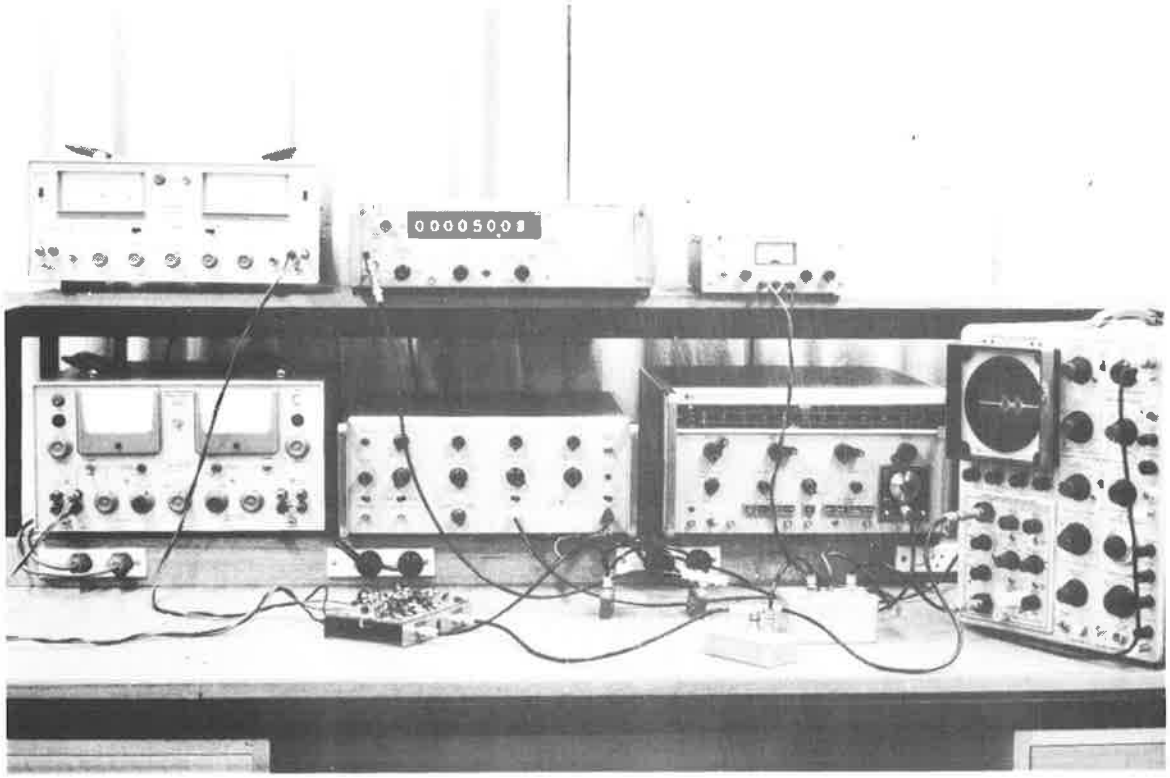

Figure 6.9 Experimental equipment used for CW and pulsed-CW measurements on both one-port and two-port delay lines.

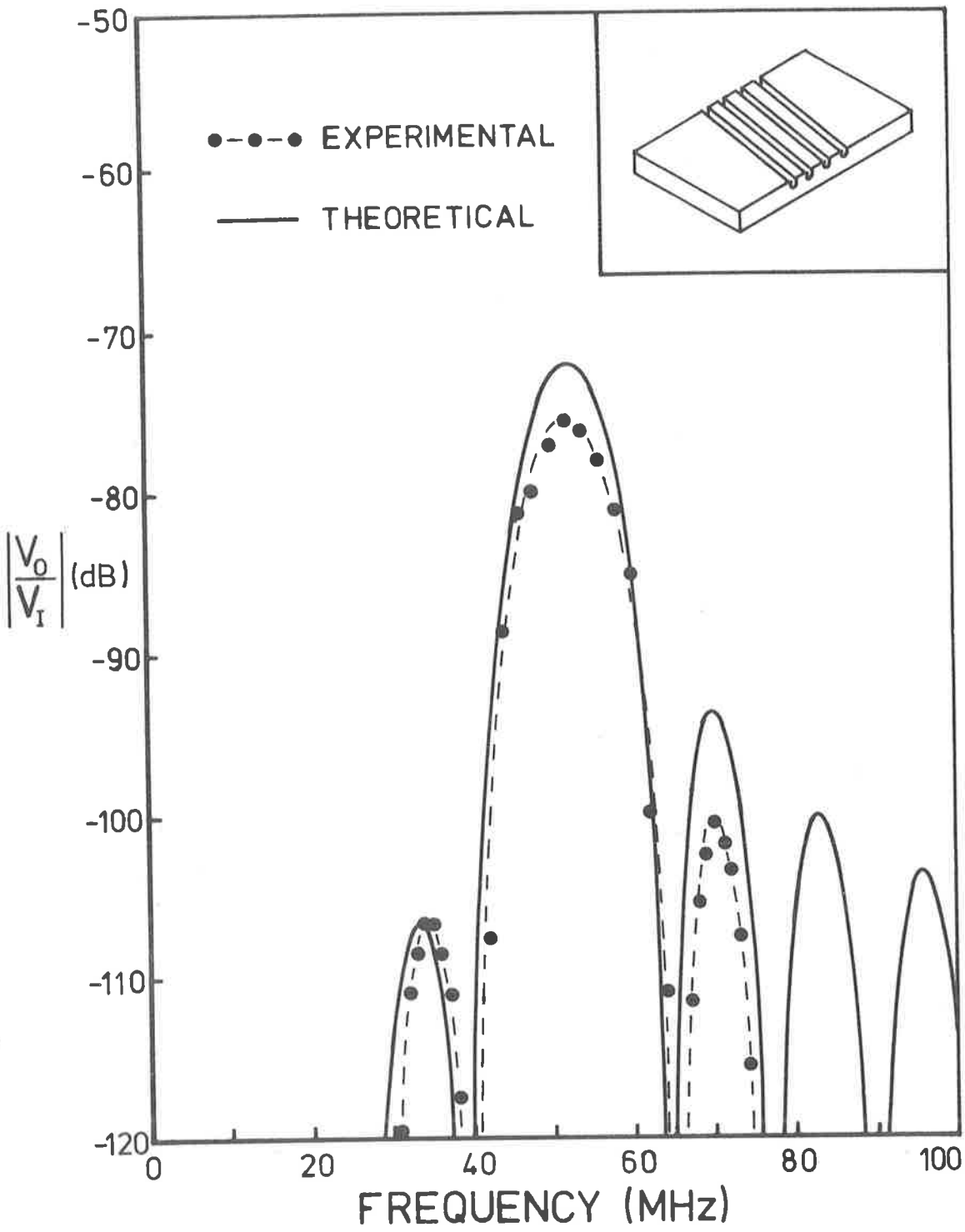


Figure 6.10 Measured and computed curves for the voltage transfer ratio ($Y_{21} Z_L$) for a delay line employing two 9-finger transducers on YX-quartz. Inset shows method of cutting slots in the lower surface of the crystal (which is shown inverted).

The presence of the undesired acoustic modes could be observed on the oscilloscope by using very short input pulses, and because the spurious modes were sometimes coincident with the desired output signal, readings were found to be very unreliable. Numerous techniques were tried to prevent the volume-modes reaching the output transducer, including the application of various acoustic absorbing materials to the underside of the crystal, and attempts to couple the volume-mode energy out through the base of the crystal. These were partially successful but the best results were obtained when it was decided to intercept the volume waves by cutting oblique slots 1mm deep across the bottom of the crystal in the region between the transducers, as shown in the insert in Figure 6.10. This treatment, in association with the liberal coating of the bottom and end surfaces with black wax, reduced the problem to a satisfactory level, although some interference was still experienced at the highest measurement frequencies.

The results show fair agreement with the expected curve, but several points of detail deserve comment. It will be observed that the centre frequency of the line is slightly higher than 50 MHz by about 4%. Examination of the electrode patterns on a travelling microscope revealed that, due to a slight inaccuracy in setting the photographic reduction ratio, the patterns were about 1% too small. The remainder of the centre frequency shift is considered to be due to two factors.

Firstly, the effect of the $|\omega|$-factor, predicted in the analysis, is to tilt the main lobe in the frequency response up a little on the high frequency side. Analysis shows that this shifts the frequency of most efficient transducer operation (to a first-order approximation)to,

$$\omega = \left(1 + \frac{1.5}{(N\pi)^2}\right) \omega_o \qquad (6.2)$$

where $\omega_o$ = the synchronous frequency

$N$ = length of the transducer in synchronous wavelengths.

For the present experiment N = 4 and we expect an upward shift of 1%.

The second source of discrepancy in the apparent centre frequency arises from the fact that the correct spectrum of a truncated sinewave (i.e the fundamental component of the source function) is not a simple (sin x)/x in form, but has the form

$$F(\omega) = \frac{\sin [K(\omega-\omega_o)]}{K(\omega-\omega_o)} + \frac{\sin[K(\omega+\omega_o)]}{K(\omega+\omega_o)} \qquad (6.3)$$

where

$$K = \frac{N\pi}{\omega_o}$$

The effect of the second function may be described as an interference effect between its sidelobes and the basic (sin x)/x response. For N integer, this interference gives rise to a further upward shift in the most efficient frequency of operation, given to first order, by

$$\omega = \omega_o \left(1 + \frac{1.5}{(N\pi)^2}\right) \qquad (6.4)$$

This expression is identical to Equation (6.2) but in this case the relation only holds for N integer. For N non-integer the magnitude, and direction, of peak frequency shift depend upon the actual magnitude of N. If N is an odd multiple of a half-wavelength this shift is negative and will completely cancel the effect of the $|\omega|$-factor.

For the experimental case N = 4 and Equation (6.4) predicts a further upward shift of 1%, giving a total expected displacement of approximately 3%, in fair agreement with the observed results.

It will also be oberved that the sidelobes in both responses in Figure 6.10 are not symmetric in amplitude about the main lobe,

although this is frequently assumed in the analysis of uniform transducers. The cause lies in the two factors cited above, namely the $|\omega|$-factor and the correct description of the frequency response. The latter effect is accentuated in this case because we are observing the product of the frequency response of two transducers. Whether the sidelobes are distorted up or down depends critically on the exact value of N, and the results are usually only qualitatively predictable.

The discrepancy in the relative magnitude of the calculated and measured sidelobes is considered to arise from the complete neglect of the fringing fields at the end electrodes in the model. These fields could readily be represented in the computer model if necessary.

These effects of apparent centre frequency shift, and asymmetric sidelobes, are only significant for relatively short transducers, as indicated by Equations (6.2) and (6.4).

The experimentally observed insertion loss is 3.5 dB greater than predicted at the centre frequency and this discrepancy is due to the fact that no attempt was made to incorporate the various loss mechanisms which affect practical delay lines into the model: these are discussed in detail in Section 6.4 and 6.5.

### 6.2.2 Time Domain Transadmittance $y_{21}(t)$

To validate the computer model predictions in the time domain, an experiment was set up using the same lines as in the above experiment, to obtain the impulse response. To obtain a good representation of the impulse response it is necessary to use very short input impulses (5 nsec) to excite the line and with only a limited voltage permitted across the transmitting transducer (see Section 6.4), the total energy input to the line was too small to give a useable output with the previous measurement apparatus.

To overcome this problem, the experiment shown diagrammatically in Figure 6.11 was devised. The total gain of the receiver chain, including the amplifiers in the XY-recorder was more than adequate to give full scale deflection of the pen trace. The signal however, was buried in the amplified noise from the pre-amplifier input stage added to the jitter from the oscilloscope sampling heads. This noise was reduced to an acceptable level by integrating the output signal from the oscilloscope, achieved by the 0.5Hz low-pass filter. This severe filtering drastically limited the rate at which the output from the oscilloscope could be permitted to vary, if gain and phase shift errors were not to be introduced into the output trace. This limitation was accepted and use made of the sampling oscilloscope facility to accept very low frequency horizontal drive signals from an external ramp generator. The operational procedure was to obtain the desired waveform on the oscilloscope screen, then obtain a permanent noise-free record on the plotter by adjusting the sweep parameters to satisfy the relation

$$V_p < [10 f_p]^{-1}$$

where

$V_p$ = horizontal pen speed in inches/sec.

$f_p$ = signal frequency in cycles/inch.

This ensured maximum gain and phase errors of - 0.17 dB and $11.5^{o}$ due to the integrating filter.

The apparatus was used to obtain the impulse waveform, which is the time domain equivalent of Figure 6.10, shown in Figure 6.12. The plot is an unsmoothed copy of the plotter output and shows the freedom from noise in the trace achieved by this experimental technique. The relevant parameters for the experiment are given below:

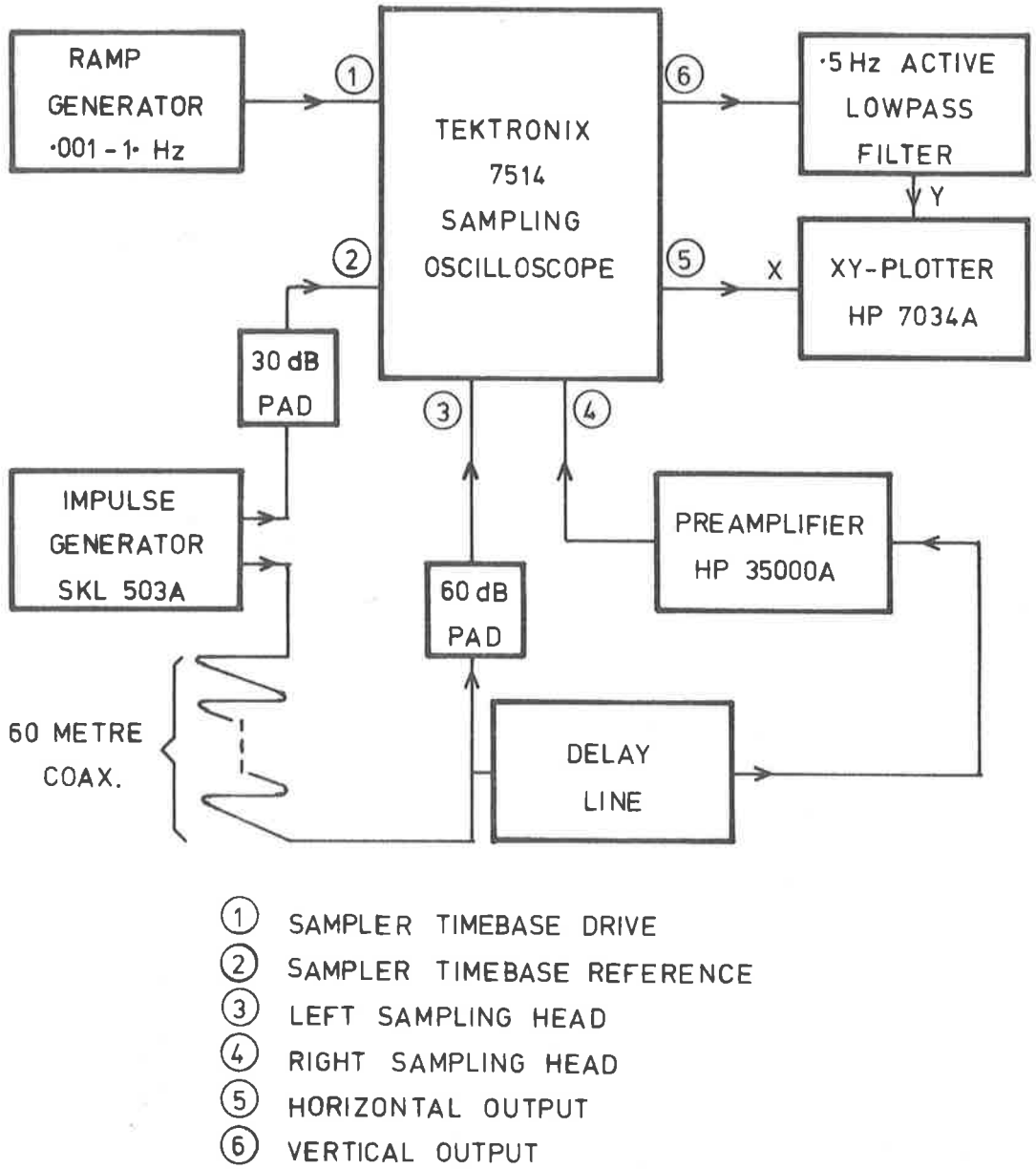


Figure 6.11 Equipment configuration for measurement of the impulse responses of surface-wave delay lines.

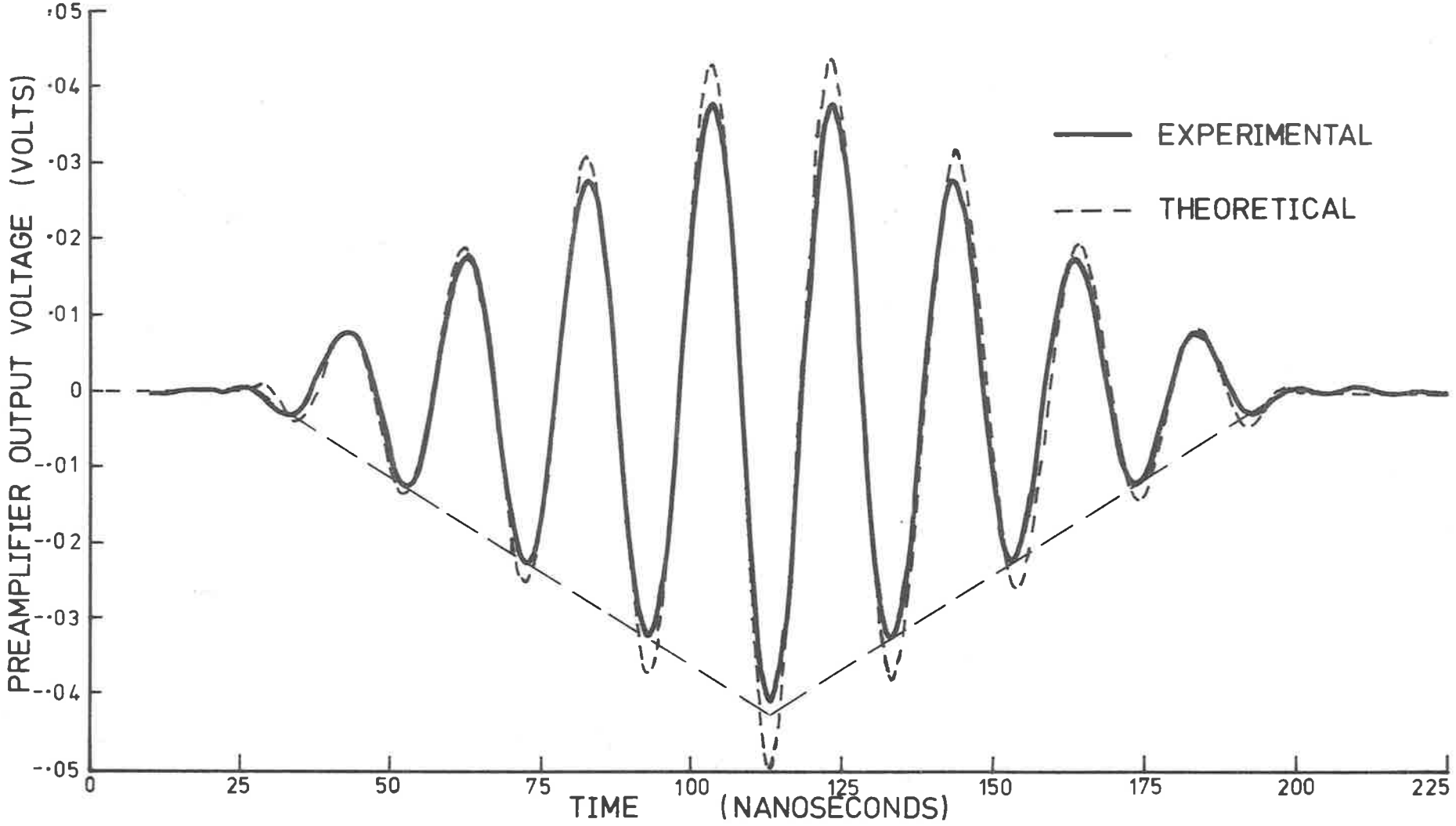


Figure 6.12 Measured and computed time domain responses for the delay line described in Section 6.2.1, following excitation by a 5 nsec voltage impulse at the input.

| | |
|---|---|
| Input pulse voltage | = 114V |
| Input pulse duration | = 5 nsec |
| Measurement bandwidth (3dB) | = 110 MHz |
| Vertical scale (referred to input) | = 630 μV/inch |
| Horizontal scale | = 25 nsec/inch |
| Plotter scan time | = 100 sec |
| Noise level (visual estimate - referred to input) | = 10 μV R.M.S. |

For comparison, the output from the computer model for the specified input voltage waveform is also shown in Figure 6.11. The graphs can be seen to be almost identical in shape, with only +2 dB discrepancy in the predicted amplitude. The envelope of the waveform has roughly the triangular form predicted by Krairoyananan and Redwood[73] in their impulse model for interdigital transducers, but closer examination shows that the actual envelope is not a simple triangle, as indicated by the dashed envelope in the Figure. The peak of the triangle is somewhat flattened and the tails of the triangle are extended as shown by both the model results and the experiment. Trial runs with the computer model have shown that this non-triangular envelope is the result of including the $|\omega|$-factor and the correct spectrum for the source function.

An important feature of Figure 6.11 is the fact that the largest peak is negative as predicted by the admittance model theory in Chapter 4. This phenomenon seems to have been overlooked in the literature, presumably due to the fact that it is customary to consider the operation of single transducers instead of the transfer function of coupled transducers. This inversion of the output waveform is apparent in the recently published experimental results of Sugiyama and Yashikawa[91] obtained with digitally coded interdigital transducers, and was also observed in impulse testing* of the frequency-chirped

---

* These particular results have been omitted from Section 6.3.

transducers to be described in Section 6.3, indicating the generality of this phenomenon.

These waveforms are not representative of the operational responses of practical delay lines where input signals of much greater duration are used, and this point will be examined in Chapter 10.

### 6.2.3 Frequency Domain Input Admittance $Y_{11}(\omega)$

The input admittance of an interdigital transducer is comprised of the static input susceptance and radiation admittance.

The static capacitance was measured on a low frequency impedance bridge using a 3-terminal measurement procedure. The transducer was a 41-electrode device with electrodes 9.7mm long and spaced 163μm on XY-cut quartz. The measured capacitance was 11.0pF, and the computed capacitance (assuming unity mark space ratio, based on a visual examination of the transducer) using the formula in Equation (5.14) gave 9.6pF. The larger experimental reading is thought to be due to the capacitance between the transducer bonding pads on the crystal surface and between the lead-in wires. In all the experiments it was noted that stray capacitances raised the effective transducer capacitance above the predicted value, usually by 1 or 2 pF, the precise amount being dependent upon the layout of the circuit wiring.

Since interdigital transducers with moderate numbers of fingers on quartz have a very high electrical Q-factor at the synchronous frequency, either a series or short equivalent circuit representation[47] may be used. In this case it was decided to assume the series representation, and measure the radiation resistance of one of the transducers used in Sections 6.2.1 and 6.2.2. The transducer was series-tuned to permit a better measurement of the real part of the radiation impedance: the total impedance was tuned to zero phase

and measured using a HP 4815A Vector Impedance Meter. To minimise strays the crystal was mounted in air on dielectric supports, and placed in a large earthed metal box to reduce RF interference. The Q of the transducer proved to be considerably higher than the best coils available at 50MHz, so the measurements were conducted by tuning the coil and taking a reading, then substituting an air-spaced variable capacitor for the line to determine what fraction of the series resistance could be attributed to the transducer. The resulting plot of series radiation resistance is given in Figure 6.13, and the computed components of the input admittance are given in Figure 6.14.

The experimental curve has the expected shape but is 80% low in amplitude. This is probably due to the stray capacitances mentioned above: the incorporation of 0.65pF strays in the position shown dashed in the equivalent circuit in Figure 6.13(a) would bring the experimental results into complete agreement with the theory.

The serious departure of the experimental results from the computed curve at frequencies above 59MHz demonstrates the limited usefulness of input impedance measurements for the prediction of surface-wave launching efficiency, for in this region the transducer is coupling more strongly to volume waves within the substrate. The input admittance also becomes quite complicated, again reducing its usefulness as a design aid, when a number of transducers are connected in parallel as in transversal filters and coded lines, as will be shown in Chapter 10.

No attempt was made to measure the imaginary part of the radiation admittance (or impedance) because with these transducers it is completely dominated by the static susceptance. In this situation the static susceptance and parasitic strays are of much greater concern to the device designer, and the radiation susceptance may be neglected.

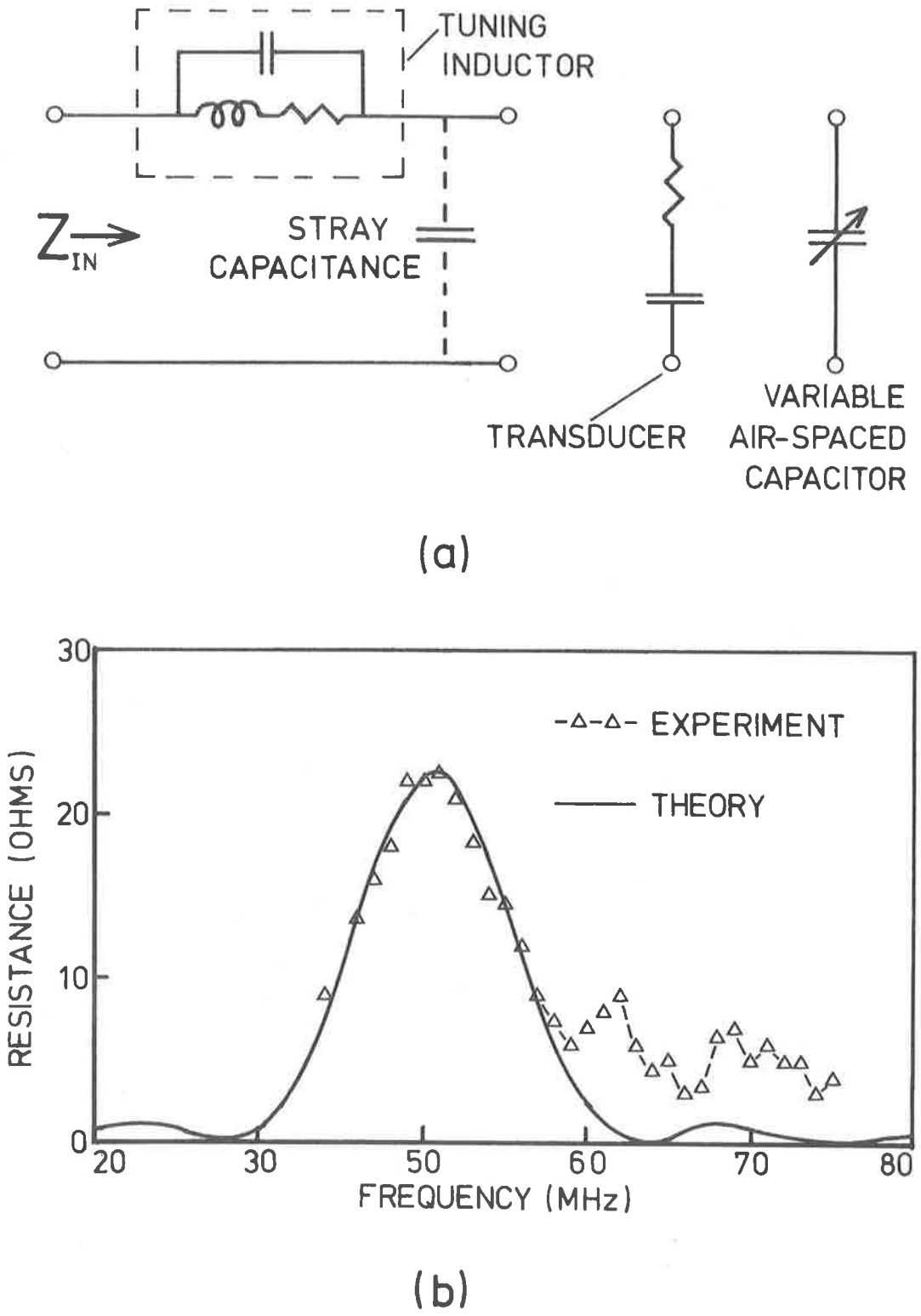


Figure 6.13 Measurement of the radiation resistance of a 9-finger (50λ aperture) 50 MHz transducer on YX-quartz. (a) measurement equivalent circuit, and (b) the experimental result. For comparison the computed series-radiation resistance is shown (normalised to the experimental curve amplitude).

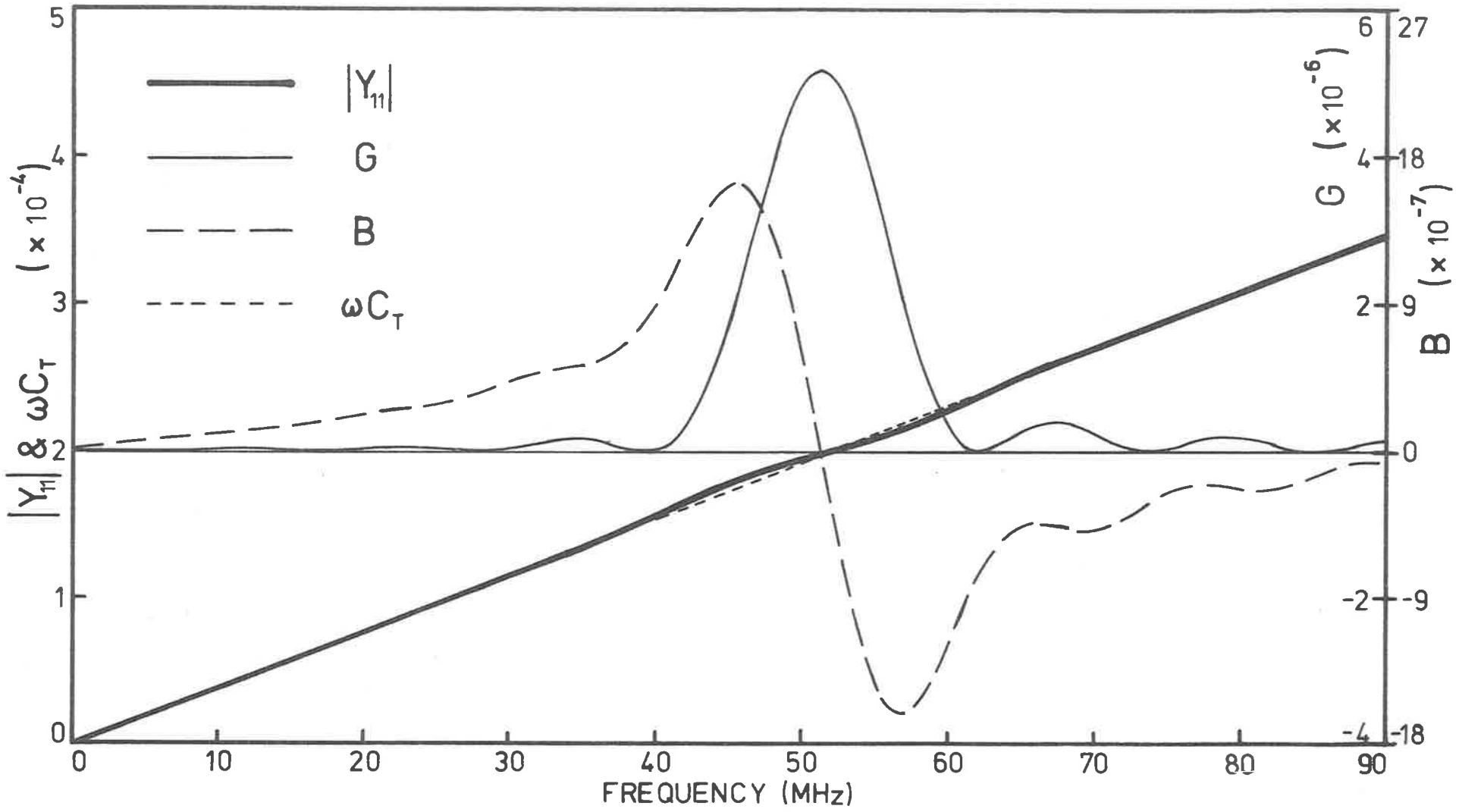


Figure 6.14 The computed admittance parameters for the transducer referred to in Figure 6.13.

However, to show the expected magnitude and characteristic variation of this parameter, it has been computed using the Hilbert transform technique described in Chapter 5, and is included in Figure 6.14. The plot of $|Y_{11}|$ shows the radiation susceptance B has little effect on the total input admittance.

These results for $Y_{21}(\omega)$, $y_{21}(t)$ and $Y_{11}(\omega)$ for uniform transducers show good agreement with the shapes of the respective functions generated by the computer model, but that the magnitude of the model predictions need to be adjusted slightly to include the effects of non-ideal behaviour in the delay lines. The major potential sources of these discrepancies are reviewed in Section 6.4.

## 6.3 Non-uniform Interdigital Transducer Measurements

Since the behaviour of uniform interdigital transducers may be deduced by approximate analytical means, the computer model does not necessarily represent the most efficient solution in this case, and in this section we now test the model on a more complicated structure. The device chosen had a pair of logarithmically chirped uniform overlap transducers deposited on YX-quartz, with both transducers chirped in the same direction to provide a non-dispersive structure. Each transducer had 41 electrodes and the ratio between successive gap widths was held constant at 0.972 , yielding a ratio between first and last gap widths of 3:1. The synchronous frequencies for the first and last gap widths were 15 and 45 MHz respectively and the overlap lengths were fixed at 4.7 mm corresponding to $50\lambda$ at 33.5MHz.

To produce this pattern experimentally the master artwork for the electrodes was drawn on a computer controlled XY-plotter, by using program PATBL as described in Section 6.1. The electrode widths in each gap were set equal to a quarter of the instantaneous gap width,

following the convention described in Section 5.1. The experimental devices were then fabricated using the procedures outlined in Section 6.1, and mounted in the metal box shown in the centre of Figure 6.8 to provide good shielding between input and output wiring. The electrode pattern of one of the transducers and mounting details are shown in Figure 6.15.

### 6.3.1 Frequency Domain Transadmittance $Y_{21}(\omega)$

The frequency transadmittance for this broadband delay line was measured by connecting it to the experimental equipment described in Figures 6.8 and 6.9. Again no attempt was made to either tune or match to the transducer impedance, in order that the approximations in Equation (3.12) would be valid.

The initial measurements showed a serious departure from the predicted response at frequencies above 38 MHz, and subsequent investigation using short pulses showed that volume modes were reaching the output transducer. The problem was reduced to an acceptable level by sawing diagonal slots into the base of the crystal, to a depth equal to a third of the crystal thickness using a 0.010" dia. wire saw, in the region between the transducers. The effectiveness of this treatment is shown in Figure 6.16 where the output of the delay line is shown before and after treatment, with input pulses of approximately 1 μsec duration at 50 MHz.

The experimental results, after correction for variation in the effective preamplifier gain and input impedance over the frequency range is shown in Figure 6.17 by the thin line joining the measurement points. The solid line is the output of the computer model (i.e. program SAWDLY 1) shown on the same scale for comparison.

The most significant feature of the experimental result is

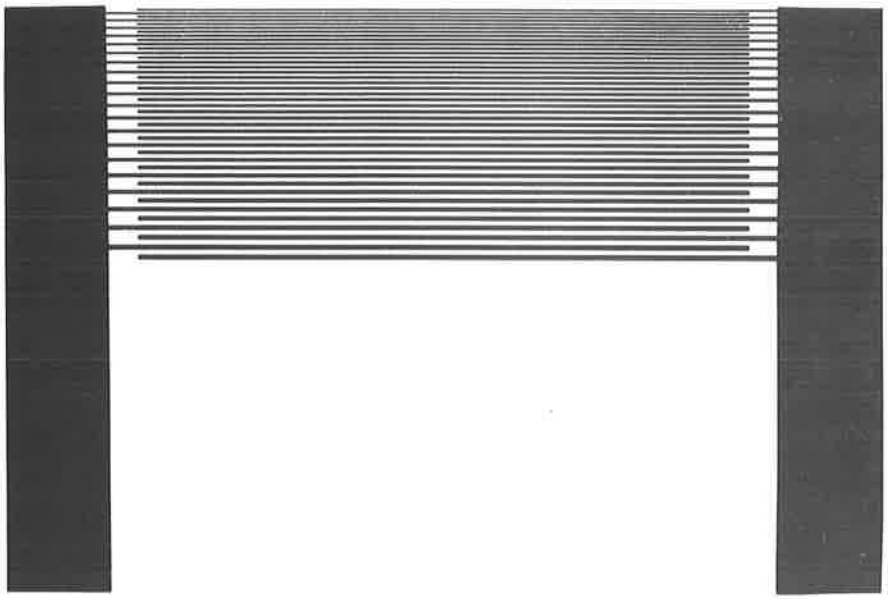

(a)

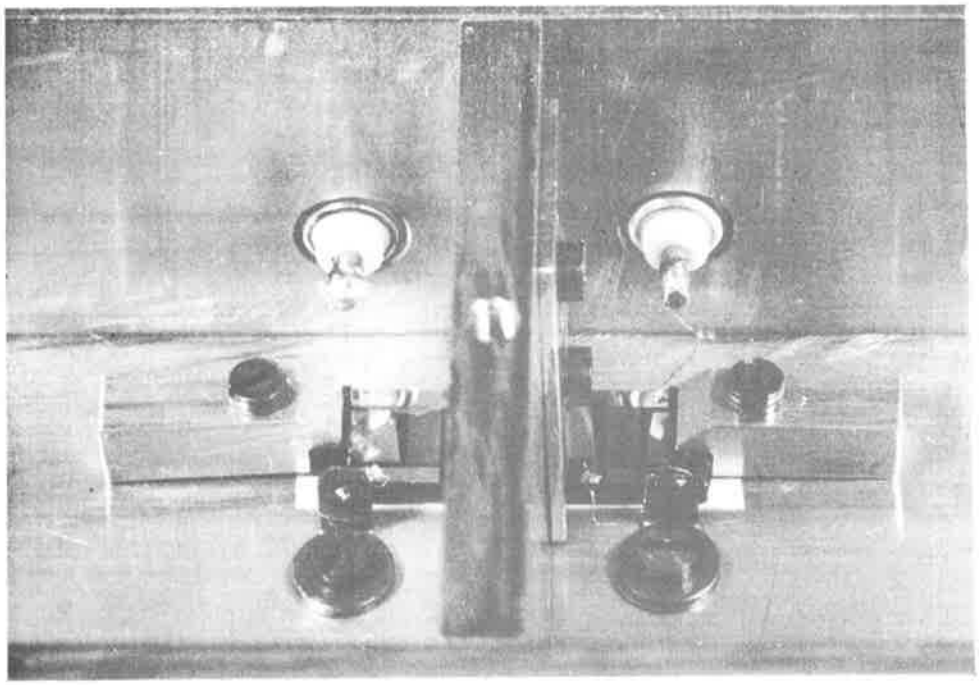

(b)

Figure 6.15 Broadband delay line (a) the dispersive log-chirped electrode pattern used for both transducers, and (b) details of the crystal mounting (note the electrostatic shield between the input and output wiring).

(a)

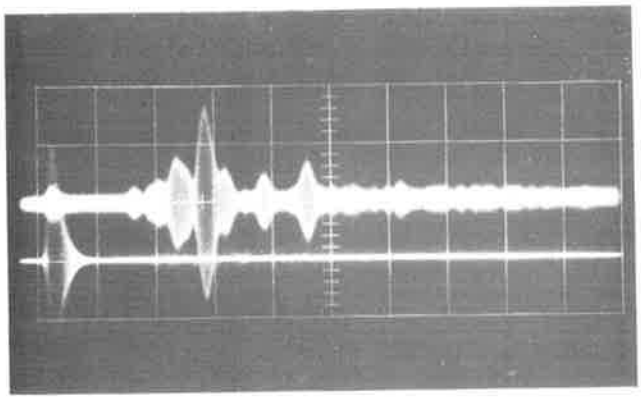

(b)

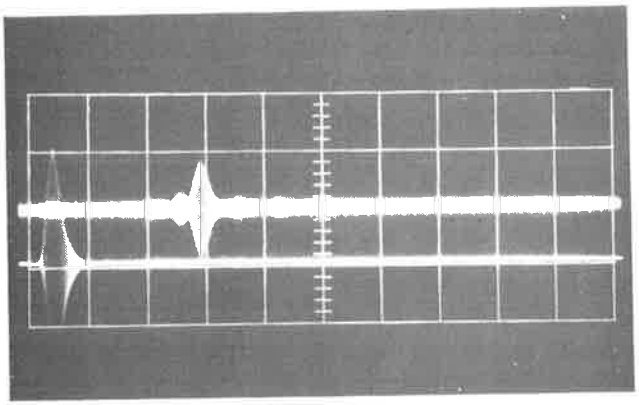

(c)

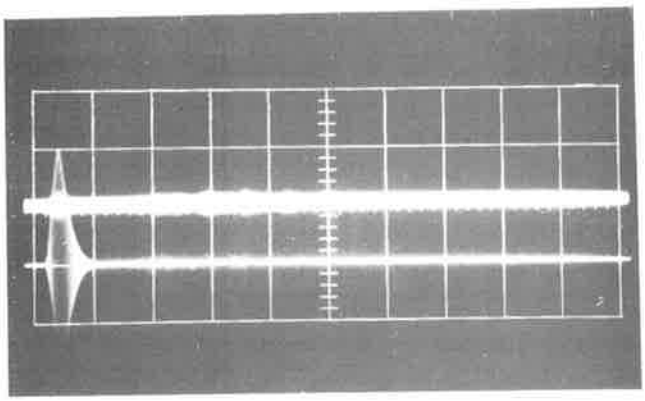

Figure 6.16 Impulse response testing of the broadband delay line. The lower traces show the 50 MHz input pulse and the upper traces show the delay line impulse response at the preamplifier output (a) before treatment to intercept the volume modes, (b) after treatment, and (c) with a surface-wave absorber (neoprene) between the transducers, verifying that the residual energy in (b) is in fact a surface-wave. Horizontal scale: 2 μsec/cm. Vertical scales: lower trace - 5V/cm and upper trace - 10 mV/cm.

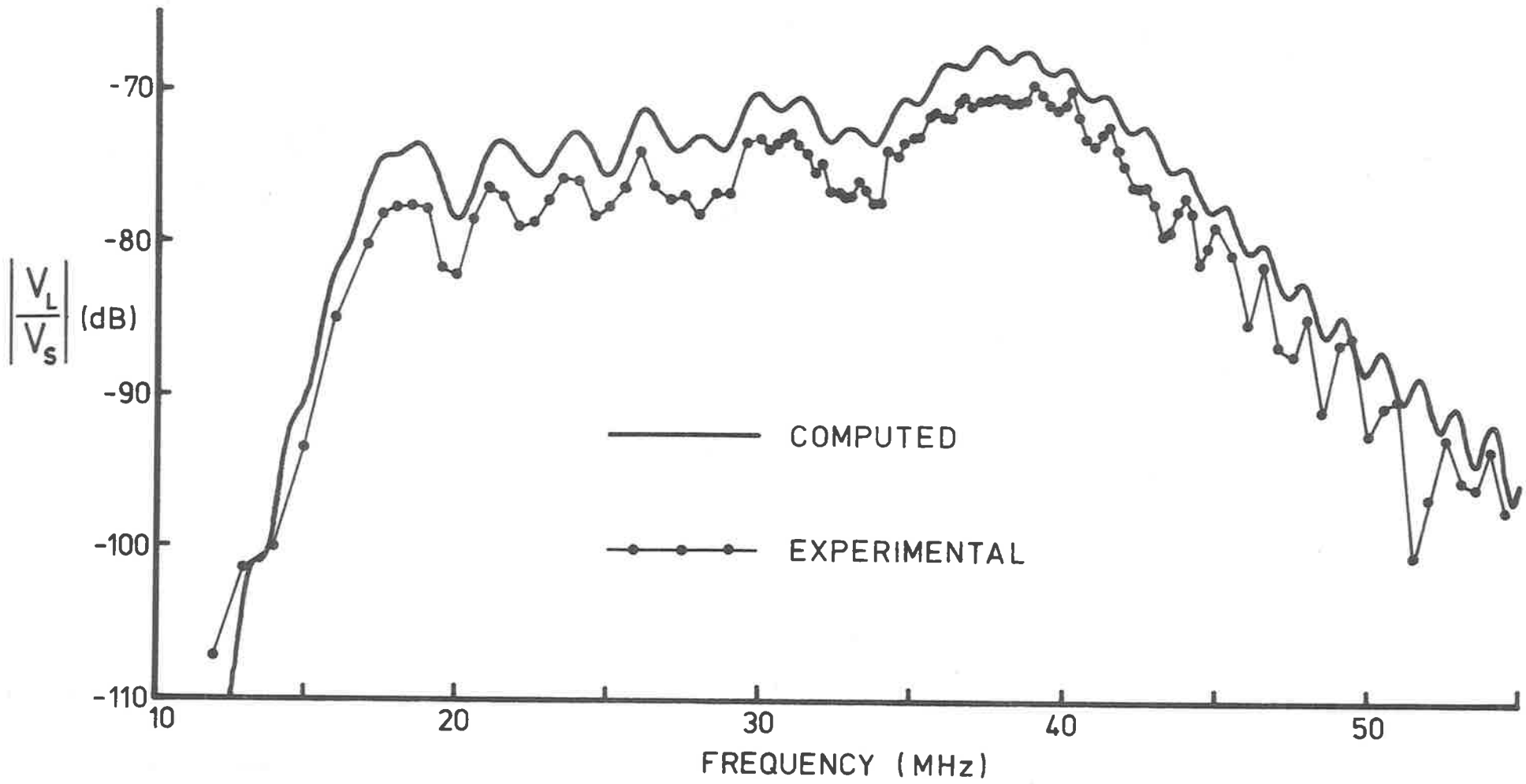


Figure 6.17 The measured and computed frequency responses of the broadband delay line employing unapodized logarithmically frequency-chirped transducers.

the mean slope of almost exactly 6dB/octave over the passband of the transducers. This provides a convincing justification for the $|\omega|$-factor predicted by the analysis in Chapter 4. Without this factor, the passband would be flat, as by making use of the stationary phase approximation[110] it may be shown that the Fourier transform of each of the individual source functions will have a flat frequency response. This result has been confirmed by the subsequent publication of very similar experimental results by Smith et al.[90].

By means of measurements at closely spaced frequencies, the fine ripple structure of the experimental curve has been resolved in some detail and it can be seen that the computer model, despite using only a simple representation for the transducer source functions, in fact gives a very good fit to the experimental response shape.

The only significant error in the output of the computer model is that the predicted insertion loss is on average 3dB less than measured. This is considered to arise mainly from the fact that loss-less propagation was assumed in the derivation of the device model, and in the next section we review the various ways in which practical delay lines may depart from this idealized behaviour.

## 6.4 Non-Ideal Behaviour in ASW Delay Lines

In this section the various sources of signal attenuation and distortion which are present in surface-wave delay lines, and which may affect the observable response characterised by the device transfer function, are reviewed. This summary will be used to aid the inter-pretation of the above experimental results, and also the coded devices to be described later.

### 6.4.1 Signal Loss Mechanisms

Under this heading we include all those mechanisms which

reduce either the energy density of the surface-wave reaching the receiving transducer, or which reduce the effective conversion efficiency of the transducers themselves, and the main sources of signal attenuation which have been identified to date are listed in Table 6.1. The first item is surface-wave attenuation which is dependent upon the substrate material and has also been shown to be frequency and temperature dependent[13-15,111-116*]. If the substrate surface is not perfectly smooth, the resultant scattering of the surface-wave energy will give an increase in attenuation and a change in velocity[117]. The magnitude of this attenuation is difficult to predict for other than periodic surfaces[118], and it would appear that apparently smooth surfaces frequently have concealed micro-cracks in the surface due to polishing damage during manufacture[119,120]. Loading of the propagation surface may occur from residual photoresist or metal remaining on the surface after manufacture, from the deliberate introduction of a metal film[121] (e.g. for electrostatic shielding), or simply from the presence of air above the surface[113,122,123].

Beamsteering, where the surface-wave energy does not propagate parallel to the wave-vector, was described in Chapter 2 and must be taken into account in any attempt to predict the diffraction pattern of a radiation transducer on an anisotropic substrate[113,114,124]. Diffraction can also be a severe problem in the case of apodized transducers which have been shown to suffer additional diffraction of the launched wavefronts due to the unequal propagation delays across different parts of the launching structure[125,126]. Apart from causing a significant amount of the radiated energy to bypass the receiving transducer, diffraction may also cause the surface-waves to have uneven amplitude or curved phase-fronts under the receiving grid,

---

* For a more complete picture of the available literature on the topics discussed in Section 6.4, the reader is referred to the bibliographies in the articles cited in this section.

TABLE 6.1

FACTORS CONTRIBUTING TO DELAY LINE INSERTION LOSS

I SURFACE-WAVE ATTENUATION

1. Thermal-phonon interaction
2. Scattering by surface roughness
3. Damping due to surface loading
4. Diffraction
5. Beam-steering

II TRANSDUCTION LOSSES

6. Transducer bi-directionality
7. Electrical dissipative losses
8. Electrical impedance mismatch
9. Parasitic susceptances
10. Bulk-wave coupling
11. Coupling-coefficient variation
12. Pattern misalignment and distortion

creating an additional source of insertion loss [127].

The loss mechanisms associated with the transducers are listed in the second part of Table 6.1. The bidirectional property of simple uniform transducers results in 3 dB insertion loss for each transducer, although this may be reduced by means of special directional transducers[32] in some applications. Electrical dissipative losses include losses due to the finite conductivity of the transducer electrodes, the resistance of the lead-in wires and bonds, and also any dissipation in any necessary tuning and impedance matching elements. Electrode dissipation becomes a problem at the higher frequencies as the metal thickness must be reduced in proportion to the device size and this results in an increasing resistance per square as the frequency of operation is increased.

Impedance mismatch is listed as a source of loss here because it is not always possible to match the source impedance to the radiation impedance of a given transducer and the device conversion efficiency will be reduced as a result. With simple indicator tuning it is only possible to match the source and load impedances at a single frequency, so that the insertion loss is always higher at other frequencies, and several workers[128-131] have shown that it is possible to produce matching networks to operate over moderate bandwidths, reducing this problem considerably. The problem of achieving efficient power transfer to (or from) the transducer is often made more difficult in practice by the presence in practical devices of undesired stray reactances and susceptances which can be minimised, but not eliminated completely, by careful attention to the physical layout as mentioned earlier. This problem of impedance matching is also complicated in broad-band devices by the coupling of the transducers to volume waves[132-134] at frequencies above the synchronous frequency for surface-waves, because this coupling

is reflected in a rise in the radiation conductance of the transducer at the frequencies concerned (as shown in Figure 6.13).

The effective coupling coefficient of the substrate employed determines the radiation conductance for a given transducer geometry, and any variation in this parameter could result in increased delay line insertion loss. It has been shown[135,136] that the piezoelectric properties of substrate materials can be modified by the microcracks and the fusion of the material[119] which takes place in the region near the surface in the mechanical polishing process, and the thickness of substrate material involved indicates that this effect could be significant at frequencies above a few hundred megahertz. It has also been shown[137] that the piezoelectric coefficients of quartz are temperature dependent, and this effect should be taken into account in devices operated at other than ambient temperatures.

The last factor in the list, transducer misalignment, may have several consequences: if the transmit transducer is not correctly aligned with respect to the crystal axes then undesired beam-steering may result, and the seriousness of this problem is indicated by the slope of the misalignment angle curve for that crystal cut[124], while misalignment or distortion of the received transducer relative to the received surface-wave will simply result in reduced transducer efficiency by an amount which may be calculated[127], provided the diffraction field of the transmit transducer is known.

### 6.4.2 Signal Distortion Mechanisms

In this section the main sources of distortion, or spurious responses, in the output waveform of a two-port delay line are summarized, and the topics to be discussed are shown in Table 6.2.

Regeneration was mentioned in Chapter 3 and the contribution to the output of a delay line from this effect may be predicted by means

TABLE 6.2

FACTORS CONTRIBUTING TO DELAY LINE OUTPUT SIGNAL DISTORTION

I TRANSDUCER SECOND-ORDER EFFECTS

1. Regeneration
2. Reflection

II SPURIOUS SIGNALS

3. Electromagnetic modes
4. Volume and quasi-surface modes
5. Acoustic reflections
6. Harmonic generation

III PROPAGATION VELOCITY VARIATIONS

7. Temperature dependence
8. Frequency dependence or dispersion

of the admittance model. Reflection is taken here to be the reflected signal from shorted transducers (not the total energy relaunched in the direction from which the incident wave arrived, as in the more conventional terminology), and is not included in the admittance model as it was assumed small enough to be neglected. These reflected signals may be regarded as being due to variations in the electromechanical impedance of the propagation path, presented to the surface-wave passing under the transducer, which may be due to either the mass-loading of the fingers or the localised electric field-shorting effect of each electrode [76,124,138]. Experimental observations of short-circuit reflection levels are reported in Chapter 10, and elsewhere[139], and shown to be smaller than the regenerated signals in most circumstances, but they may be estimated if necessary by determination of the impedance discontinuities involved [76].

The spurious signal contributions which may appear in the delay line output may usually be identified by means of impulse testing. In devices with no electrostatic shielding between the input and output wiring the directly radiated electromagnetic signal may be quite large and may be identified by the almost zero time delay. Volume and quasi-surface modes were mentioned in the experimental results and in Section 6.4.1, and may prove very troublesome if quasi-surface modes can be supported by the substrate within the pass-band of the delay line. Acoustic reflections, in Table 6.2, refers to undesired surface-wave energy appearing at the output transducer e.g. after reflection from the ends of crystal.

The next item, harmonic generation, differs from the previous three items in that it is dependent only upon the substrate material and the launched surface-wave intensity. Harmonic generation, the conversion of fundamental frequency surface-wave energy into the second

and higher harmonics, has been reported by several workers[140,141], and the only means of avoiding this problem is to limit the maximum surface-wave intensity in the delay line.

The last two items affect the surface-wave velocity and can result in distortions visible principally in the time domain. The velocity may shift as a function of temperature[142-145], or may become dispersive, i.e. a function of frequency. The propagating surface may become dispersive with the application of thin film materials perturbing either the mechanical[121,146,147] or electrical[21,138] properties of the surface. It is also possible for changes in composition of the substrate material in the region near the surface to affect the propagation velocity[120,148].

This brief survey indicates the nature of the more important factors which may serve to affect the output response of a simple one- or two-port delay line. The resultant of all these effects must be added to the simple first-order response calculated by means of the expressions derived in Chapter 3, and in the next section an assessment is made of the various factors contributing to the total insertion losses of the experimental delay lines described in Sections 6.2 and 6.3.

## 6.5 Discussion of the Results

The factors considered to have contributed to the difference in amplitude between the predicted and observed frequency responses of the uniform and chirped transducer delay lines shown in Figure 6.10 and 6.17, are listed in Table 6.3; the estimates are based on the best available data from the sources listed in the last section. The natural surface-wave attenuation can be seen to be negligible at these frequencies compared with the diffraction losses, which are greater on YX-quartz than expected in the equivalent isotropic case due to

TABLE 6.3: ESTIMATES OF THE ADDITIONAL SOURCES OF INSERTION LOSS IN THE EXPERIMENTS

| LOSS MECHANISM | INSERTION LOSS CONTRIBUTION | |
|---|---|---|
| | UNIFORM TRANSDUCERS | CHIRPED TRANSDUCERS |
| 1. Surface-wave attenuation | 0.02 dB | 0.01 dB |
| 2. Damping by air-loading | 0.03 dB | 0.02 dB |
| 3. Diffraction (anisotropic) | 0.7 dB | 0.8 dB |
| 4. Beam-steering ($1^{o}$ error) | 0.3 dB | 0.4 dB |
| 5. Electrical dissipation | 1.8 dB | 1.0 dB |
| 6. Pattern misalignment | - | 0.2 dB |
| TOTALS | 2.8 dB | 2.4 dB |
| Difference between theoretical and experimental results | 3.5 dB | 3.0 dB |

the shape of the velocity surface [124]. The beam-steering loss is computed assuming a total 1 degree misalignment of the transducer relative to the crystal axes, which is considered reasonable in view of the fact that the crystal orientations were not checked, and in view of the relatively simple fabrication procedures employed. The estimates of dissipation loss are based on measurements of the conductivity of the aluminium metallization using a 4-terminal measurement procedure (giving 0.6 ohms/square), and the figure for pattern misalignment is included because a slight misorientation of one of the chirped transducers was observed when the patterns were checked under a travelling microscope.

The cumulative errors in the various stages of equipment calibration and in the experimental readings themselves is estimated to be of the order of ± 1 dB total, and the cumulative error in the computation of the theoretical responses, due to the numerical approximations involved and the limited accuracy of the available materials data and the assumed transducer dimensions, is also estimated at ± 1 dB. This gives a total error tolerance on the observed differences between the predicted and measured insertion losses of ± 2 dB, and it can be seen that the actual discrepancy between the two figures at the bottom of each column in the table is well within the total experimental error. This result is particularly pleasing when it is realized that the first-order delay response has been calculated from first principles, and that the formulae evaluated in the computer model contain no empirically adjustable constants.

The good agreement achieved in the experiments can also be taken to provide empirical justification for the assumption of the weak-coupling approximation in the derivation of the admittance

coefficients. Although the only substrate material employed in the experiments was α-quartz, there appears to be no reason why this admittance representation cannot be applied to the characterisation of complete surface-wave devices on any weak-coupling substrate material.

The remainder of this thesis is concerned with an evaluation of acoustic surface-wave delay lines for the physical realization of coded one-port structures.

# CHAPTER 7

# ONE-PORT DEVICE ADMITTANCE MODEL

## 7.0 Introduction

In Chapter 1 attention was drawn to the fact that surface-wave delay lines appear to offer an attractive method for the realization of time domain pulse-coded one-port labels and we now look at coded one-port lines in more detail. In this chapter the various responses which can be exhibited by such a device are derived analytically in terms of the line admittance parameters and the external circuit impedances, using the method outlined in Chapter 4. The analysis is then applied to the particular case of a delay line with N equi-spaced, identical transducers, and an expression derived for the modulation of the response signal of such a device in terms of the individual transducer location. (i.e. delay line coding.) In later chapters these expressions are used in modelling the responses of a prototype coding system.

## 7.1 The Admittance Representation of a Parallel-Connected One-Port Delay Line

The input admittance of a parallel-connected one-port structure, of the type shown diagrammatically in Figure 3.2, may be obtained from the admittance matrix for the original N-port structure (Equation (3.1)) by employing the following relations: the one-port terminal voltage appears at all the individual transducer terminals i.e.

$$\dot{V}_i(\omega) = \dot{V}(\omega) , \qquad i = 1 \text{ to } N \tag{7.1}$$

(where the dot indicates phasor notation), and the current into the one-port is simply the sum of the currents into each of the individual transducers.

$$\dot{I}(\omega) = \sum_{i=1}^{N} \dot{I}_i(\omega) . \tag{7.2}$$

Then substituting for $\dot{I}$ and $\dot{V}$ we obtain for the input admittance

$$Y(\omega) = \frac{\dot{I}(\omega)}{\dot{V}(\omega)} = \sum_{i=1}^{N} \sum_{j=1}^{N} Y_{ij}(\omega) \qquad (7.3)$$

which is the result quoted previously in Chapter 3.

## 7.2 Practical Equivalent Circuit With Interdigital Transducers

In Chapter 3 the basic measurement circuit of Figure 3.3(a) was used, containing a single external circuit impedance. This circuit would be representative of the situation where the one-port line was interrogated over a propagation link, and the source impedance seen by the line would be that of the single receiving and retransmitting antenna. In practice it is convenient to separate the transmitter and receiver circuitry and we now introduce the equivalent circuit shown in Figure 7.1 with separate source and load impedances, for further investigation. This change is of no theoretical significance as the new circuit may be readily shown to have a Thevenin equivalent of the form of Figure 3.3(a) and is introduced simply to enable the analytical results obtained to be more readily compared with the experimental results.

We now require an expression for $Y(\omega)$, the one-port input admittance of a parallel-connected surface-wave delay line with N separate interdigital transducers. For simplicity we assume the individual transducers are identical, and are all placed somewhere along a single acoustic propagation path. The individual elements of the N-port admittance matrix are then obtained by means of the integral expressions obtained in Chapter 4 and will take the form

$$Y_{ii}(\omega) = \{G(\omega) + j(B(\omega) + \omega C_T)\} A_i^2, \quad i = 1 \text{ to } N \qquad (7.4)$$

$$Y_{ij}(\omega) = G(\omega) A_i A_j e^{-j\beta l_{ij}} \qquad \begin{matrix} i \neq 1 \text{ to } N \\ j = 1 \text{ to } N \end{matrix} \qquad (7.5)$$

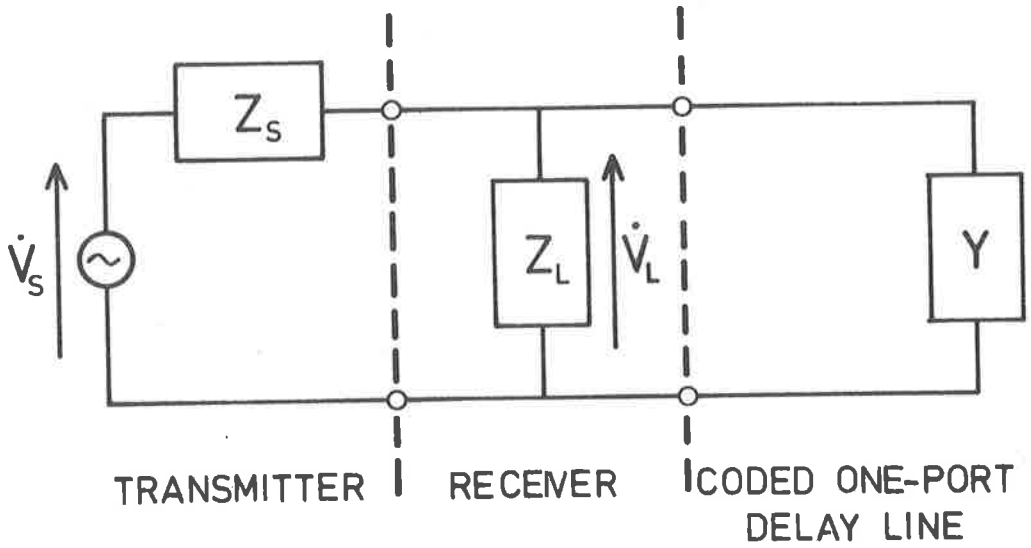


Figure 7.1 One-port delay line measurement equivalent circuit.

where

$G(\omega)$ = real part of the radiation admittance of a single transducer.

$B(\omega)$ = imaginary part of the radiation admittance of a single transducer.

$C_T$ = static transducer susceptance.

$\beta$ = $\omega/v$ = the wave vector.

$l_{ij}$ = the modulus of the distance between centres of transducers i and j.

$A_i$ = +1, -1, or 0 depending on whether transducer i is connected in phase with, in antiphase with, or is disconnected from the other transducers.

The terms $G(\omega)$, $B(\omega)$ and $C_T$ may all be evaluated for a single transducer using Equations (4.50), (4.51) and (4.52), derived in Chapter 4. Equation (7.5) exploits the similarity in form of the integral expressions for input admittance and transadmittance, to obtain an expression for the transadmittance between two identical transducers in terms of $G(\omega)$, the real part of the radiation admittance for one of the transducers.

By substituting for $Y_{ij}(\omega)$ in Equation (7.3) we obtain an expression for the one-port input admittance, and we will write this in the form,

$$Y(\omega) = Y_A(\omega) + j\, B_N(\omega) \qquad (7.6)$$

where

$$Y_A(\omega) = G(\omega) \sum_{i=1}^{N} \sum_{j=1}^{N} A_i\, A_j\, e^{-j\beta l_{ij}} \qquad (7.7)$$

and

$$B_N(\omega) = \left[ \sum_{i=1}^{N} |A_i| \right] \left[ B(\omega) + \omega C_T \right] \qquad (7.8)$$

In this expression $Y(\omega)$ has not been divided into real and complex parts, because $Y_A(\omega)$ is complex: this representation has been chosen because

it permits the placement of all information regarding the positioning of the transducers in $Y_A(\omega)$, and the simple form of the expression for $Y_A(\omega)$, is a consequence of the assumption of identical transducers and the similarity between Equations (4.25) and (4.50) for the input admittance and transadmittance.

## 7.3 Derivation of the Circuit Responses

We now seek to determine expressions for the various responses of the coded one-port delay line, using the expansion technique described in Chapter 4. If we assume the source impedance $Z_S$ is resistive, and that any tuning or matching components are incorporated in the load impedance $Z_L$, then the equivalent circuit becomes that shown in Figure 7.2 and the output voltage in response to an interrogation signal $\dot{V}_S(\omega)$ will be

$$\frac{\dot{V}_L}{\dot{V}_S} = \frac{Z_c}{R_S \left[ 1 + Z_c Y_A \right]} \tag{7.9}$$

where $Z_c$, which we call the "circuit impedance", is given by

$$Z_c = \left[ 1/R_S + 1/Z_L + jB_N \right]^{-1} \tag{7.10}$$

and can be seen to contain all the network elements other than the information bearing term $Y_A$. To be able to express the response as a series expansion in terms of $Y_A$ at all frequencies we must be able to assert that $|Z_c Y_A|<1$ at all frequencies. A further benefit of dividing the input admittance in Equation (7.6) now becomes apparent: by placing the one-port susceptance $B_N(\omega)$ in the circuit impedance, the remaining admittance $Y_A$ becomes bounded, and we can satisfy the inequality by suitable choice of source resistance and load impedance. We may then write

$$\dot{V}_L = \dot{V}_S \frac{Z_c}{R_S} \left[ 1 - (Z_c Y_A) + (Z_c Y_A)^2 - (Z_c Y_A)^3 + \ldots \right] \tag{7.11}$$

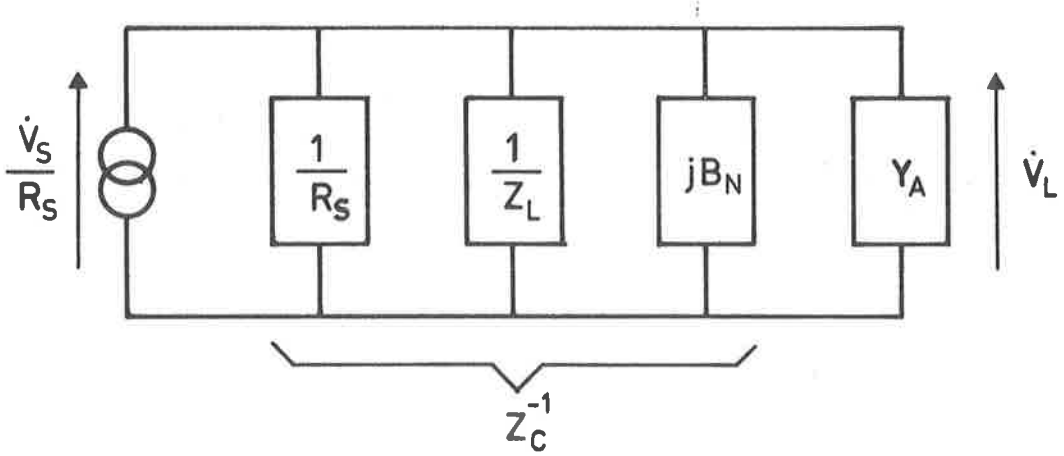


Figure 7.2 Equivalent circuit for coded delay line representation with element values expressed as admittances.

Since we are interested in time domain coding, it is more instructive to look at the time domain response, which may be obtained by taking the Fourier Transform of Equation (7.11) term by term, which is permissible since the expansion is valid at all frequencies. The time domain response is then given by

$$v_1(t) = v_0(t) + v_1(t) + v_2(t) + v_3(t) + \ldots \quad (7.12)$$

where the subscripts indicate the orders of the various responses in terms of the convolution products of $y_a(t)$, and the individual response terms are given by,

$$\begin{aligned}
&\text{Zero-order Response:} && v_0(t) = \frac{1}{R_S}\, v_s(t) * z_c(t) \\
&\text{Primary Response:} && v_1(t) = -\, v_0(t) * z_c(t) * y_a(t) \\
&\text{Secondary Response:} && v_2(t) = -\, v_1(t) * z_c(t) * y_a(t) \\
&\text{Tertiary Response:} && v_3(t) = -\, v_2(t) * z_c(t) * y_a(t) \\
&\text{Higher-order Responses:} && \text{etc.}
\end{aligned} \quad (7.13)$$

The zero-order response $v_0(t)$ can be identified as the voltage appearing at the one-port terminals as a result of the application of the source voltage $v_s(t)$ to the network. The primary response is the first set of delayed pulses to be returned by the line after the application of a pulse $v_0(t)$ to the one-port terminals and contains the reply code, in a practical device. Since this pulse train appears at the one-port terminals it contributes a secondary source voltage and each pulse in the primary response gives rise to another string of echo pulses. The sum of these regenerated signals is called the secondary response and is described by $v_2(t)$. The higher-order responses arise in similar fashion and are of little interest because in a practical situation, weak-coupling substrate materials are employed, and each successive convolution of the response with $z_c(t) * y_a(t)$ results in a significant reduction in the signal level. More will be said about interference from second-order responses in Chapter 10.

## 7.4 Definition of the Coding Factor k(t)

To see how the coded information is contained within the primary response we now look more closely at the transform admittance $y_a(t)$ which may be determined by taking the Fourier transform of the right-hand side of Equation (7.7) to give,

$$Y_a(t) = 2g(t)^* k(t) \tag{7.14}$$

where

$$k(t) = \tfrac{1}{2} \sum_{i=1}^{N} \sum_{j=1}^{N} A_i A_j \delta(t-\tau_{ij}) \tag{7.15}$$

$k(t)$ is defined to be the coding factor, $\delta(t)$ is the Dirac delta function, $\tau_{ij} = l_{ij}/v$ is the propagation delay between transducers i and j, and v is the surface-wave velocity.

The complete primary response may now be factorised as

$$v_1(t) = -\frac{2}{R_S} \underbrace{v_s(t)^*}_{\text{Input Signal}} \underbrace{z_c(t)^* g(t)^* z_c(t)^*}_{\text{Pulse-spreading factor}} \underbrace{k(t)}_{\text{Coding factor}} \tag{7.16}$$

This expression indicates that the primary response waveform from a coded one-port delay line will consist of a sequence of identical and possibly overlapping pulses whose shapes are given by the convolution of the input signal and the pulse-spreading factor for the line, and whose amplitudes and time positions are specified by the coding factor $k(t)$. The interrelation between these various factors is examined in more detail in Chapter 10.

In practice it is desirable to use lines with constant transducer spacing to permit ready interpretation of the line response and in this case the coding factor becomes

$$k(t) = \tfrac{1}{2} \sum_{i=1}^{N} \sum_{j=1}^{N} A_i A_j \delta(t - |j - i|\tau) \tag{7.17}$$

where $\tau$ is the propagation between adjacent transducer positions. This

may be simplified to

$$k(t) = \sum_{n=0}^{N-1} K_n \, \delta(t-n\tau) \qquad (7.18)$$

where,

$$\left.\begin{aligned} K_0 &= \tfrac{1}{2} \sum_{i=1}^{N} A_i^2 \\ K_n &= \sum_{i=1}^{N-n} A_i \, A_{i+n} \end{aligned}\right\} \qquad (7.19)$$

By choosing to use delay lines with constant transducer spacing we have reduced the number of possible output pulses separable in the time domain, from $\frac{N}{2}(N-1)+1$ to N, and obtained the simple relation in Equation (7.19) between the N amplitude coefficients $A_i$ for the equi-spaced transducers, and the N amplitude coefficients $K_i$ of the equi-spaced pulses in the primary response.

## 7.5 The Primary Response of a Tuned N-Transducer Line

In practical N-transducer delay lines (one-port or two-port) it is customary to use some sort of tuning or matching between the source (or receiver) and the transducer in an attempt to minimise the effect of the impedance mismatch caused by the transducer static capacitance. By resonating the capacitance with a shunt (or series) tuning inductor it is possible for the transducer capacitance to be made to appear to be zero at the transducer electrical terminals, or one specific frequency, which is normally chosen to be the synchronous frequency when wiring uniform interdigital transducers. The Q-factor of this tuned circuit is determined by the source resistance and transducer radiation impedance, and must be adjusted in the delay line design to give an operating bandwidth compatible with the design bandwidth of the transducers. The relation between transducer insertion loss, electrical Q-factor and the substrate parameters is discussed in Chapter 10.

In this section we will assume that a simple inductor has been placed in parallel with the receiver input resistance (i.e. $Z_L = R_L + j\omega L$) to tune the total capacitance presented by all the transducers in the delay line. We also assume that the source and load resistances are equal and together will give the desired electrical Q-factor with the resonance at the synchronous transducer frequency. (In practice it may be necessary to employ impedance transformers to achieve this.) Since the total capacitance depends upon the number of transducers M in use on any particular delay line, the factors which determine the output waveform will vary with M, and we now derive an expression for the primary response in terms of M, the selected Q-factor, and the characteristics g(t) and $C_T$ for a single transducer.

We have already assumed the weak-coupling approximation and invoking it again, we can approximate for $B_N$ in Equation (7.8) to get

$$B_N = M \omega C_T \tag{7.20}$$

where

$$M = \sum_{i=1}^{N} |A_i| \tag{7.21}$$

The appropriate values of tuning inductor and source resistance are then given by

$$\left.\begin{aligned} L &= \frac{1}{M\omega_0^2 C_T} \\ R_S &= \frac{2Q}{M\omega_0 C_T} \end{aligned}\right\} \tag{7.22}$$

where $\omega_0$ is the chosen resonant frequency. The circuit impedance $Z_c$ can now be written as,

$$Z_c = M^{-1}[\omega_0 C_T \left(\frac{1}{Q} + j\left(\frac{\omega}{\omega_0} - \frac{\omega_0}{\omega}\right)\right)]^{-1} \tag{7.23}$$

i.e.

$$Z_c = M^{-1} Z_{c1} \tag{7.24}$$

where $Z_{c1}$ is the tuned circuit impedance for a delay line with a single transducer with static capacitance $C_T$. We can now find the required expression for the primary response in terms of the single-transducer characteristics $C_T$, $G(\omega)$ and the impedance $Z_{c1}$ by substituting from Equations (7.22) and (7.24) into Equation (7.16) to obtain,

$$v_1(t) = \frac{-\omega_0 C_T}{MQ} \; v_s(t)^* \; z_{c1}(t)^* \; g(t)^* \; z_{c1}(t)^* \; k(t) \qquad (7.25)$$

This Equation predicts that the pulse shape is independent of M, and that the insertion loss of the device is proportional to M, the number of active transducers on the line. This expression is used as the basis for the waveform modelling undertaken in Chapters 9 and 10.

## 7.6 The Secondary Response of a Tuned N-Transducer Line

It is convenient at this point to extend the above analysis to the representation of the secondary response of a coded one-port delay line. Making use of Equations (7.14), (7.24)and (7.25) and substituting into Equation (7.13) we obtain,

$$v_2(t) = \frac{2\omega_0 C_T}{M^2 Q} \; v_s(t)^* \; z_{c1}(t)^* \; g(t)^* \; z_{c1}(t)^* \; g(t)^* \; z_{c1}(t)^* \; k(t)^* \; k(t) \qquad (7.26)$$

This expression shows that the envelope of the secondary response is in fact considerably more complicated than that of the primary response being in fact determined by the autoconvolution of the coding factor $k(t)$. Under certain circumstances peaks of this response may fall in time positions where there is a 'zero' in the primary response, to cause a decoding error; this problem is investigated in more detail in Chapter 10.

# CHAPTER 8

# PROPERTIES OF ONE-PORT CODES

## 8.0 Introduction

The previous chapter outlined an analytical approach which permits the separate identification of the various component waveforms which sum to make up the observable voltage between the terminals of a time-coded one-port surface-wave delay line, both during and after the excitation signal. The relation between the transducer pattern and the time domain primary response of a coded one-port delay line was shown to be not a simple one, and we now turn our attention to an investigation of the types of coding which will be most efficient for use with these devices.

In Equation (7.5) the concept of a set of amplitude coefficients $A_i$ describing the presence (or absence) and phase of each transducer in the delay line was introduced. For convenience we shall use the convention that any particular delay line may be identified by the values of the coefficients written in a serial string i.e. for a line with the coefficients $A_1, A_2, \ldots, A_8 = 1,0,0,1,1,0,1,1$ we will simply refer to the pattern 10011011. Similarly the response envelope for a line with equispaced identical transducers may be described by the relative peak heights given by the response coefficients $K_i$ (i=1, N-1) defined in Equation (7.19); for the example referred to above we would expect the response 2132011. It should be noted that $K_o$ is omitted from this string because the first pulse in the primary response is always obscured by the zero-order response which is much larger and which is usually approximately coincident in time.

## 8.1 General Properties of One-Port Codes

It is now necessary to pose the questions, are there any general constraints on the types of patterns which may be used for one-port coded devices, and do the responses of any particular coding scheme have any general properties of which the system designer should be aware? Probably the most important question is, does every source pattern give a unique response, i.e. one which cannot be obtained from any other source pattern? The answer to this last question is in the negative for any but very restricted sets of code patterns, and we will now investigate this problem of 'ambiguity' in the response codes in more detail.

### 8.1.1 Definition of a Useful Response

We look first at the requirements for a delay line to produce an acceptable output response. If we take the set of available patterns to be given by all the possible combinations of $A_i$=0 or 1 (i = 1,N) for example, it is clear that the particular pattern 0000 (N=4) will give no output and the patterns 1000, 0100, 0010 and 0001 will have $K_o$ as the only non-zero term in the output response. As suggested in the introduction, this response is of no use because it cannot be distinguished from the zero-order response. Thus in the rest of this work we shall omit $K_o$ from consideration of the output response, and make the stipulation that only patterns with $M \geqslant 2$ will be considered, where,as before, M is the number of active transducers on the line.

### 8.1.2 Ambiguity in the Response Codes

An examination of any reasonably large set of coding patterns reveals that response ambiguity is fairly common, and looking more closely at the relation between the pattern coefficients

$A_i$ and response coefficients $K_i$, we can deduce some general transformations on the pattern coefficients which have the property that the response coefficients are invariant with respect to the transformations, without making any assumptions about the coefficients $A_i$ other than that they are real. We proceed by defining the 'pattern function'

$$a(t) = \sum_{i=1}^{N} A_i \delta(t-i\tau) \tag{8.1}$$

which is a sequence of weighted delta functions representing the centres of the transducers on a coded one-port line. Corresponding to this pattern function the resulting 'response function'

$$k(t) = \sum_{i=1}^{N-1} K_i \delta(t-i\tau) \tag{8.2}$$

is obtained by substituting for a(t) in Equation (4.25) and making use of the fact that $\beta$ is negative for surface-waves travelling from right to left. It can also be shown that

$$k(t) = \int_{-\infty}^{\infty} a(x)\, a(x+t)dx = a(x) \mathbin{\text{€}} a(x), \; t > \frac{\tau}{2} \tag{8.3}$$

(where € indicates correlation) and the relation holds for positive values of t chosen so as not to include the undelayed component of the primary response.

The known properties of the autocorrelation function may now be used to deduce the transformations on a(t) which will leave k(t) invariant. If we have a pattern function a(t) which yields a response function k(t), then by substitution in Equation (8.3) we can verify that an alternative pattern function b(t) will give the same response function if b(t) satisfies the following relations,

Ambiguity Relations

(a) Sign Reversal i.e. $b(t) = -a(t)$

(b) Time Reversal i.e. $b(t) = a((N+1)\tau - t)$

(c) Translation i.e. $b(t) = a(t-T)$

(d) Any combination of (a) (b) and (c).

The significance of these ambiguity relations will depend upon the particular set of line codes chosen in any particular system e.g. relation (a) will not be relevant in a set of codes constructed using the values $A_i$= 0 or 1, but relations (b), (c) and (d) will still apply, and will have the effect of reducing the available set of transducer patterns giving distinct output responses. Relation (c) needs careful interpretation; it only applies in coding systems which permit $A_i$ to take the value zero. In this case some patterns utilize less than the full length of the delay line and will give an ambiguous response if the same string of non-zero coefficients $A_i$ occurs in another pattern in the available set of transducer patterns i.e the pattern 101100, 010110 and 001011 will all give the same output response.

The question as to whether this set of ambiguity relations covers all possible sources of ambiguity in the response codes is an important one. Extensive empirical investigations on the coding schemes discussed later in this chapter have shown that it is possible for two transducer patterns, not related by the above transformations, to produce identical output responses. Because of this the analytic expressions derived later (based on the 4 ambiguity relations), for the numbers of unique response codes available for a given number of transducer positions N in each coding system, may only be regarded as upper-bounds on the actual number of codes available. The actual incidence of these exceptional patterns is extremely small and the topic is discussed further in Section 8.6.3.

## 8.2 Classification of Coding and Decoding Procedures

The response code of a one-port coded delay line differs from the source pattern or code, and two separate tasks may be identified in the design of a system using such devices. The first is the selection

of a suitable set of transducer patterns which will give unambiguous responses, and this will be called the 'coding' operation. The second is that of identifying the coded line response, obtained after detection at the receiver, with the appropriate pattern or code and this will be called the 'decoding' operation. The conventions used in the remainder of this work are summarized in the following section.

### 8.2.1 Pattern Generation or Coding

If we accept the constraint introduced in Chapter 7, that the individual transducer weighting coefficients $A_i$ be limited to the range of values -1, 0 or +1, chosen to simplify the delay line fabrication by permitting the use of identical transducers, then we may identify the following classes of transducer patterns.

(a) Binary Coded : $A_i = 0$ or 1

(b) Biphase Coded : $A_i = +1$ or $-1$

(c) Ternary Coded : $A_i = +1$, 0 or $-1$

It is apparent that the sets of codes available in the Binary and Biphase categories will be subsets of the Ternary case. The other possible distinct subset of the Ternary case is the case $A_i = 0$ or $-1$, and is omitted because by the first ambiguity relation (Section 8.1.2) such patterns would produce responses identical to those of the Binary Codes.

### 8.2.2 Response Identification or Decoding

When using a one-port coded delay line system it is desirable to be able to relate the received response code with either the pattern which produced it, or use it directly as an identifier to access stored information on the object which is known to be carrying that particular label. Both approaches encounter difficulties. In the first case, it does not appear to be possible to find an efficient algorithm which

will efficiently perform the deconvolution of the response code to give the source pattern code, for large values of N. This approach appears to be practicable only in the particular cases where the code has been selected to have a simple relationship between the pattern and response (e.g. delayed binary codes to be discussed later). In general this approach is not very attractive for the further reason that even if one could deduce the transducer patterns from their responses, they would not form monotonic binary or ternary sequences anyway, and one is faced with the problem of using an effectively random code as the identifier of each particular label.

This is similar to the difficulties which occur with the second approach i.e. attempting to use the response itself as an address variable to access the name etc. of the labelled object. The difficulty arises in that the individual response coefficients $K_1$ to $K_9$ may take any values from -9 to +9 for a 10 bit ternary pattern, i.e. we have a 9-dimensional quantity to use as our address number. In this example the receiver computer would have to correlate the received 9 digit string with all of the possible responses, sequentially, to verify that a valid response had been received, and determine which label had responded. This procedure would be very time-consuming for any reasonable value of N, and the solution which is proposed here is to produce an algorithm which will operate on the response coefficients for any response waveform detected by the receiver, and produce a single numerical value. This procedure has been labelled decoding, and the numerical value may be used as the external name of each label, within the system.

The simplest algorithm used in the examples to follow, evaluates the response code as a number to base $\alpha$, and gives the value as a decimal number, i.e.

$$K(\text{base ten}) = \sum_{n=1}^{N-1} K_n \alpha^{(n-1)} \qquad (8.4)$$

where $\alpha$ is chosen to be as small as possible but not less than the maximum value of $\{2|K_n| + 1\}$. In other cases it is convenient for practical reasons, to pass the reply response through a limiter before decoding, and this has the effect of reducing $\alpha$, and produces another potential source of ambiguity in the output responses, as two different responses may look identical after limiting.

In the examples which follow, the various decoders investigated have been divided into the following categories

(a) Binary Decoder: the decoder assigns a binary 1 when a pulse, greater in magnitude than some threshold value, is present in a given time slot (regardless of phase), and a binary 0 otherwise. The decoder then converts the binary number to a decimal number, assuming the first bit received is the least significant bit.

(b) Ternary Decoder: the synchronous detector assigns a +1 or -1 if the pulse is positive or negative respectively (regardless of amplitude), and a zero if it is smaller in magnitude than some threshold value. The decoder then converts this response to an integer modulo 3 by substituting the value 2 for each occurrence of -1 in the output, and then converts the result to a decimal number, again assuming least significant bit first.

(c) Multilevel Decoding: the synchronous detector produces zero, and positive and negative outputs of varying amplitudes which are quantized to N levels (N>3), assigned integer values 0, 1, ---, N-1, and the resulting string considered an integer modulo N.

In the following sections we examine in detail the performance

of Binary, Biphase and Ternary codes in conjunction with the appropriate decoding procedures.

## 8.3 Binary Coding Systems

In binary coding schemes the pattern coefficients $A_i$ are restricted to the values 0 and 1, and the responses to codes of this type consist of a series of pulses, with integer relative amplitudes, uniformly spaced in the time domain. We will consider several classes of binary codes, all with the basic binary decoder; the use of a synchronous detector might confer some improvement in the received signal-to-noise ratio in practice, but would not affect the number of unique output codes available.

### 8.3.1 Binary Codes

Binary codes are of interest because of their ease of fabrication, simply requiring up to N identical transducers connected in phase and in parallel, on a single substrate. The binary decoder which is used with these codes is also very attractive in practical applications for, apart from being easy to construct, it avoids the difficulties inherent in trying to detect multilevel codes over a propagation link with variable insertion loss.

A complete set of code patterns and responses available for N=6, is shown in Table 8.1, and an examination of this Table will highlight several features of one-port coding systems. The first, which will be seen by looking at column 1, is that not all the possible binary patterns for N<7 can be used: some are rendered ineffective by the ambiguity relations listed in Section 8.1, and a further number are eliminated after clipping to unit amplitude in the decoding process. The results in Table 8.1 were generated by a computer program which exhaustively set up all the possible transducer

TABLE 8.1: BINARY CODING AND BINARY DECODER

Primary responses, after clipping, from lines with six transducer positions.

| TRANSDUCER PATTERN | MULTILEVEL RESPONSE | CLIPPED RESPONSE | DECIMAL EQUIV. |
|---|---|---|---|
| 1 1 0 0 0 0 | 1 0 0 0 0 | 1 0 0 0 0 | 1 |
| 1 0 1 0 0 0 | 0 1 0 0 0 | 0 1 0 0 0 | 2 |
| 1 1 1 0 0 0 | 2 1 0 0 0 | 1 1 0 0 0 | 3 |
| 1 0 0 1 0 0 | 0 0 1 0 0 | 0 0 1 0 0 | 4 |
| 1 1 0 1 0 0 | 1 1 1 0 0 | 1 1 1 0 0 | 7 |
| 1 0 0 0 1 0 | 0 0 0 1 0 | 0 0 0 1 0 | 8 |
| 1 1 0 0 1 0 | 1 0 1 1 0 | 1 0 1 1 0 | 13 |
| 1 0 1 0 1 0 | 0 2 0 1 0 | 0 1 0 1 0 | 10 |
| 1 1 1 0 1 0 | 2 2 1 1 0 | 1 1 1 1 0 | 15 |
| 1 0 0 0 0 1 | 0 0 0 0 1 | 0 0 0 0 1 | 16 |
| 1 1 0 0 0 1 | 1 0 0 1 1 | 1 0 0 1 1 | 25 |
| 1 0 1 0 0 1 | 0 1 1 0 1 | 0 1 1 0 1 | 22 |
| 1 1 1 0 0 1 | 2 1 1 1 1 | 1 1 1 1 1 | 31 |
| 1 0 1 1 0 1 | 1 2 2 0 1 | 1 1 1 0 1 | 23 |
| 1 1 0 0 1 1 | 2 0 1 2 1 | 1 0 1 1 1 | 29 |

patterns, computed the response code and decoded it for each pattern, checked to see if that particular decoded value had been obtained before, and if so, discarded it. By this means a set of patterns giving the set of unique responses listed in Table 8.1 was obtained. It is apparent that this set of transducer patterns is only one of many such sets which could be obtained by searching through the set of possible transducer patterns in a different order. For reference, a computer program to perform these operations on binary codes with a binary decoder is described in Appendix A1.6.

The second general feature of one-port code responses with single-output decoders of the type described earlier, is that the decoded output values are not monotonic and are 'sparse' in the decimal domain. Looking at column 4 of Table 8.1, we can see that the numbers 5,6,9,11,12,14 etc. are missing, and by making use of the way in which the program is arranged (i.e. considering all patterns of length 2, then all patterns of length 3, etc. up to N=6) it can be shown that these numbers can not be generated by any possible binary transducer pattern, in conjunction with a binary decoder. This result appears to be quite general for all the types of codes examined; if clipping is omitted and a multilevel decoder used the number of unique output responses increases but the domain of the output responses also increases and the responses remain sparse.

It should be mentioned here that the method selected for searching through the transducer patterns is quite important in a practical situation, because two patterns giving the same decoded response may have quite different second-order responses. The second-order responses for the patterns in Table 8.1 are shown in Table 8.2 and it is obvious that a large second-order pulse could

TABLE 8.2: SECOND-ORDER RESPONSES FOR BINARY CODES AND BINARY DECODER

For lines with six transducer positions
Second-order responses falling on primary response zeros are underlined

| TRANSDUCER PATTERN | CLIPPED RESPONSE | SECONDARY* RESPONSE |
|---|---|---|
| 1 1 0 0 0 0 | 1 0 0 0 0 | 2 1 0 0 0 |
| 1 0 1 0 0 0 | 0 1 0 0 0 | 0 2 0 1 0 |
| 1 1 1 0 0 0 | 1 1 0 0 0 | 6 7 4 1 0 |
| 1 0 0 1 0 0 | 0 0 1 0 0 | 0 0 2 0 0 |
| 1 1 0 1 0 0 | 1 1 1 0 0 | 3 4 5 3 2 |
| 1 0 0 0 1 0 | 0 0 0 1 0 | 0 0 0 2 0 |
| 1 1 0 0 1 0 | 1 0 1 1 0 | 3 1 3 5 2 |
| 1 0 1 0 1 0 | 0 1 0 1 0 | 0 6 0 7 0 |
| 1 1 1 0 1 0 | 1 1 1 1 0 | 8 12 12 12 8 |
| 1 0 0 0 0 1 | 0 0 0 0 1 | 0 0 0 0 2 |
| 1 1 0 0 0 1 | 1 0 0 1 1 | 3 1 0 3 5 |
| 1 0 1 0 0 1 | 0 1 1 0 1 | 0 3 3 1 5 |
| 1 1 1 0 0 1 | 1 1 1 1 1 | 8 8 8 9 10 |
| 1 0 1 1 0 1 | 1 1 1 0 1 | 4 9 12 8 12 |
| 1 1 0 0 1 1 | 1 0 1 1 1 | 8 4 4 12 12 |

* only the first five echos are listed here.

result in a zero in the primary response being decoded as a one under unfavourable conditions, as illustrated by the 4th time position for pattern 101101. The second-order responses have been calculated alongside the primary responses in the computer programs, using the relationship derived in Equation (7.26) i.e.

$$\text{Second-Order Response } s(t) = k(t) * k(t) \qquad (8.5)$$

In the computer programs used to produce the results given in this Chapter, no check was made to ensure that the second-order responses s(t) were in fact minimised in each of the zero locations in the primary response, for each code produced by more than one pattern. The procedure adopted was to examine the patterns with the least number of transducers first, based on the general principle that the magnitude of the larger coefficients of s(t) is approximately proportional to $M^2$, where M is the number of active transducers on the delay line, and hence by using the patterns with minimum M we can minimise the peak levels of the interfering second-order signal. The general problem of controlling second-order responses is examined further in Chapter 10.

For practical application subgroups of the binary transducer patterns may be usefully distinguished, and some of these are discussed briefly below.

### 8.3.2 Natural Binary Codes

Looking at column 2 of Table 8.1, it can be seen that certain patterns yield responses which do not require clipping before decoding. These responses will be termed 'natural binary', and are of practical interest because they eliminate the problem of trying to detect a zero immediately following a pulse which has(prior to clipping) an integer relative amplitude much greater than unity.

The relative frequency of this type of pattern can be seen to be significantly less than the straight binary patterns, and a comparison of the relative frequencies is drawn in Section 8.6.

### 8.3.3 Delayed Binary Codes

As stated earlier, the simple binary coding procedure, with binary decoding results in responses which are sparse and are not monotonic. One coding scheme which does provide a uniform monotonic sequence of decoded values is one which employs patterns, of length $N \geqslant 2L$, of the form $100\ldots.0A_{N-L+1}\ A_{N-L+2}\cdot\ldots.A_N$. The reply pulse train from a pattern of this form consists of a sequence of (N-(L+1)) multilevel responses followed by a natural binary sequence of L pulses with amplitudes proportional to $A_{N-L+1}, A_{N-L+2}, \ldots, A_N$ as illustrated in Table 8.3, which gives the delayed binary codes for N=6 and L=3. It can be seen that if the decoder examines only the last L pulse positions, the result is a 1:1 correspondence between the transducer pattern and the response. With this type of coding one can obtain binary reply codes which represent, without gaps, all integer numbers from 1 to$(2^L-1)$, by appropriate manipulation of the pattern coefficients $A_{N-L+1}$ to $A_N$. This facilitates direct use of the response as an address to the relevant stored data for each label, without the need to first match the decoded number to a table of response values.

This type of coding has an additional practical advantage in that the portion of the response which is considered to contain the reply code, as well as being natural binary, is separated from the zero-order response by a large time interval. The importance of this feature is brought out in Chapter 10.

TABLE 8.3: DELAYED BINARY CODES

For lines with six transducer locations

| TRANSDUCER PATTERN | PRIMARY RESPONSE |
|---|---|
| 1 0 0 0 0 1 | 0 0 0 0 1 * |
| 1 0 0 0 1 0 | 0 0 0 1 0 * |
| 1 0 0 0 1 1 | 1 0 0 1 1 |
| 1 0 0 1 0 0 | 0 0 1 0 0 * |
| 1 0 0 1 0 1 | 0 1 1 0 1 |
| 1 0 0 1 1 0 | 1 0 1 1 0 |
| 1 0 0 1 1 1 | 2 1 1 1 1 |

Significant part of the response.

### 8.3.4 Constant Capacity Delayed Binary Codes

In Chapter 7 it was pointed out that it is desirable to tune the static capacitance of the transducers with an inductor, to reduce the insertion loss. In practical applications it is desirable that the required tuning and loading elements be independent of the particular code pattern employed: this condition can be satisfied if we employ a constant number M of transducers on the delay line. This restriction can be applied to any system of coding, and further reduces the available number of reply codes corresponding to a given N. If we apply this restriction to a delayed binary code set where N=2L, then the maximum number of available output responses occurs for $M = \frac{L}{2} + 1$ if L is even and $M = \frac{L+1}{2}$ when L is odd. The constant capacity delayed binary patterns for the case N=6, L=3, M=2 are indicated by asterisks in Table 8.3, and expressions for the total number of patterns available for any given N,L,M are given in Section 8.6.

## 8.4 Biphase Coding Systems

In this type of coding system, the pattern coefficients $A_i$ are assigned values of either +1 or -1, by selecting the appropriate phasing of the transducer connections and leaving no transducer position unoccupied. The response of such a delay line with N transducers, is a sequence of N-1 pulses, whose amplitudes can take positive, zero or negative integer values, and which will give different results using binary or ternary decoding.

### 8.4.1 Binary Decoder

The set of all the possible output responses for biphase codes of length N=6, with a binary decoder, is given in Table 8.4,

TABLE 8.4: BIPHASE CODING AND BINARY DECODER

Primary responses, after clipping, from lines with six transducers present.

| TRANSDUCER PATTERN | PRIMARY RESPONSE | CLIPPED RESPONSE | DECIMAL EQUIV. |
|---|---|---|---|
| 1 -1 -1 -1 -1 -1 | 3 2 1 0 -1 | 1 1 1 0 1 | 23 |
| 1 1 -1 -1 -1 -1 | 3 0 -1 -2 -1 | 1 0 1 1 1 | 29 |
| 1 -1 1 -1 1 -1 | -5 4 -3 2 -1 | 1 1 1 1 1 | 31 |

and, as can be seen, very few codes produce distinct outputs. This may be regarded as a result of the mismatch between the encoding and decoding processes used, and relates to the infrequent occurrence of zeros, which can only occur as a result of cancellation of positive and negative contributions to the autocorrelation function of the transducer pattern, at a particular time slot.

Checking, by means of an appropriate computer program, has verified that for the case N=6 there are in fact no natural binary output codes. This is not true for all N, but in all the cases examined(N=1 to 13) the number of natural binary output codes did not exceed 1. These results indicate that biphase codes with a binary decoder are not likely to be of any practical use.

### 8.4.2 Ternary Decoder

The performance of this coding scheme in conjunction with a ternary decoder of the type described in Section 8.2 is illustrated in Table 8.5 for biphase codes with N=6. This scheme shows a significant increase in the number of transducer patterns providing unique output codes when compared with Table 8.4. The responses, however, remain sparse in the decimal domain because of the increased radix.

Again the available number of natural binary output codes is zero for N=6, although 1 or 2 such responses have been observed for other values of N.

The more complicated multilevel decoding schemes have not been examined in detail as the practical application of one-port delay devices commonly lies in situations where communication is over channels of variable or uncertain passband characteristics, and the determination of the multilevel amplitude information, in the presence of the consequent waveform distortion, is difficult

TABLE 8.5: BIPHASE CODING AND TERNARY DECODER

Primary responses, after clipping, from lines with six transducers present.

| TRANSDUCER PATTERN | MULTILEVEL RESPONSE | CLIPPED RESPONSE | DECIMAL EQUIV. |
|---|---|---|---|
| 1 -1 -1 -1 -1 -1 | 3 2 1 0 -1 | 1 1 1 0 -1 | 175 |
| 1 1 -1 -1 -1 -1 | 3 0 -1 -2 -1 | 1 0 -1 -1 -1 | 235 |
| 1 -1 1 -1 -1 -1 | -1 2 -1 0 -1 | -1 1 -1 0 -1 | 185 |
| 1 -1 -1 1 -1 -1 | -1 -2 3 0 -1 | -1 -1 1 0 -1 | 179 |
| 1 1 -1 1 -1 -1 | -1 0 1 -2 -1 | -1 0 1 -1 -1 | 227 |
| 1 -1 -1 -1 1 -1 | -1 0 -1 2 -1 | -1 0 -1 1 -1 | 209 |
| 1 -1 1 -1 1 -1 | -5 4 -3 2 -1 | -1 1 -1 1 -1 | 212 |
| 1 -1 -1 1 1 -1 | -1 -4 1 2 -1 | -1 -1 1 1 -1 | 206 |
| 1 -1 -1 -1 -1 1 | 1 0 -1 -2 1 | 1 0 -1 -1 1 | 154 |
| 1 1 -1 -1 -1 1 | 1 -2 -3 0 1 | 1 -1 -1 0 1 | 106 |
| 1 -1 1 -1 -1 1 | -3 0 1 -2 1 | -1 0 1 -1 1 | 146 |
| 1 1 -1 1 -1 1 | -3 2 -1 0 1 | -1 1 -1 0 1 | 104 |
| 1 1 1 1 -1 1 | 1 2 1 0 1 | 1 1 1 0 1 | 94 |
| 1 1 -1 -1 1 1 | 1 -4 -1 2 1 | 1 -1 -1 1 1 | 133 |
| 1 1 1 -1 1 1 | 1 0 1 2 1 | 1 0 1 1 1 | 118 |
| 1 1 1 1 1 1 | 5 4 3 2 1 | 1 1 1 1 1 | 121 |

to ensure. Furthermore, the results in Section 8.6 indicate that only a moderate number of additional codes would be made available at the expense of a considerable increase in the complexity of the decoding system.

## 8.5 Ternary Coding Systems

Ternary coding is the most general case permitted under the constraints adopted in Section 8.2: in this case the pattern coefficients are permuted through the values $A_i$ = 0, +1 and -1, and the patterns resulting contain, as subsets, all of those which have been discussed previously.

### 8.5.1 Binary Decoder

The performance of this coding scheme with a binary decoder is illustrated in Table 8.6. In contrast with its action on the biphase codes in the previous section, the binary decoder does in this case give a useful set of output codes. For a given value of N these patterns give more useable responses than the simple binary codes, (which is why the Table 8.6 has been limited to N=5) as could be expected. A further significant difference between binary and ternary codes is that patterns which include negative coefficients frequently have lower second-order response levels, a factor which could be significant in some applications.

Close examination of Table 8.6 shows that natural binary (i.e. $|k_i|=1$) responses appear quite frequently, and as shown in Section 8.6, occur somewhat more frequently than the natural binary responses of binary codes.

### 8.5.2 Ternary Decoder

As could be expected, the ternary decoder is more

TABLE 8.6: TERNARY CODING AND BINARY DECODER

Primary responses, after clipping, from lines with five transducer positions.

| TRANSDUCER PATTERN | MULTILEVEL RESPONSES | CLIPPED RESPONSE | DECIMAL EQUIV. |
|---|---|---|---|
| 1 1 0 0 0 | 1 0 0 0 | 1 0 0 0 | 1 |
| 0 1 0 0 | 0 1 0 0 | 0 1 0 0 | 2 |
| 1 1 1 0 0 | 2 1 0 0 | 1 1 0 0 | 3 |
| 1 0 0 1 0 | 0 0 1 0 | 0 0 1 0 | 4 |
| 1 1 0 1 0 | 1 1 1 0 | 1 1 1 0 | 7 |
| 1 -1 1 1 0 | -1 0 1 0 | 1 0 1 0 | 5 |
| 1 0 0 0 1 | 0 0 0 1 | 0 0 0 1 | 8 |
| 1 1 0 0 1 | 1 0 1 1 | 1 0 1 1 | 13 |
| 1 0 1 0 1 | 0 2 0 1 | 0 1 0 1 | 10 |
| 1 1 1 0 1 | 2 2 1 1 | 1 1 1 1 | 15 |
| 1 1 -1 0 1 | 0 -2 1 1 | 0 1 1 1 | 14 |
| 1 1 -1 0 -1 | 0 0 -1 -1 | 0 0 1 1 | 12 |
| 1 1 1 1 -1 | 2 1 0 -1 | 1 1 0 1 | 11 |

efficient than the binary decoder, in that it rejects fewer of the transducer patterns as duplicating previously obtained responses. A typical code set for the case N=4 is presented in Table 8.7, and close examination reveals that a useful proportion of the codes are in fact natural ternary codes.

Again since only a fairly small proportion of codes are rejected by the ternary decoder, there seems to be little advantage in going to the complexity of a multilevel decoding scheme.

## 8.6 Relative Coding Efficiencies

The relative coding efficiency for any particular coder and decoder combination is measured by the total number of useful output responses available for a given number of transducer positions available in the one-port delay line. For convenience the results are shown graphically and classified according to the type of coding used.

### 8.6.1 Binary Codes

The performances of the various types of binary coding are shown plotted over an extended range of N in Figure 8.1. The results were obtained by using a digital computer to explore the responses of all possible patterns for different values of N, and record only the unique responses and the first occurrence of the duplicated ones.

The graph for multilevel responses is computed to represent the perfect decoder, i.e. one which does not reject any distinct multilevel response, and is included as it represents an upper-bound on the performance with simpler decoders. For this case it is possible to derive an analytic expression for the number of distinct responses, using the ambiguity relations listed in Section 8.1, and we obtain

TABLE 8.7: TERNARY CODING AND TERNARY DECODER

Primary responses, after clipping, from lines with four transducer positions

| TRANSDUCER PATTERN | MULTILEVEL RESPONSE | CLIPPED RESPONSE | DECIMAL EQUIV. |
|---|---|---|---|
| 1 1 0 0 | 1 0 0 | 1 0 0 | 1 |
| 1 -1 0 0 | -1 0 0 | -1 0 0 | 2 |
| 1 0 1 0 | 0 1 0 | 0 1 0 | 3 |
| 1 1 1 0 | 2 1 0 | 1 1 0 | 4 |
| 1 -1 1 0 | -2 1 0 | -1 1 0 | 5 |
| 1 0 -1 0 | 0 -1 0 | 0 -1 0 | 6 |
| 1 0 0 1 | 0 0 1 | 0 0 1 | 9 |
| 1 1 0 1 | 1 1 1 | 1 1 1 | 13 |
| 1 -1 0 1 | -1 -1 1 | -1 -1 1 | 17 |
| 1 -1 1 1 | -1 0 1 | -1 0 1 | 11 |
| 1 0 0 -1 | 0 0 -1 | 0 0 -1 | 18 |
| 1 1 0 -1 | 1 -1 -1 | 1 -1 -1 | 25 |
| 1 -1 0 -1 | -1 1 -1 | -1 1 -1 | 23 |
| 1 1 1 -1 | 1 0 -1 | 1 0 -1 | 19 |

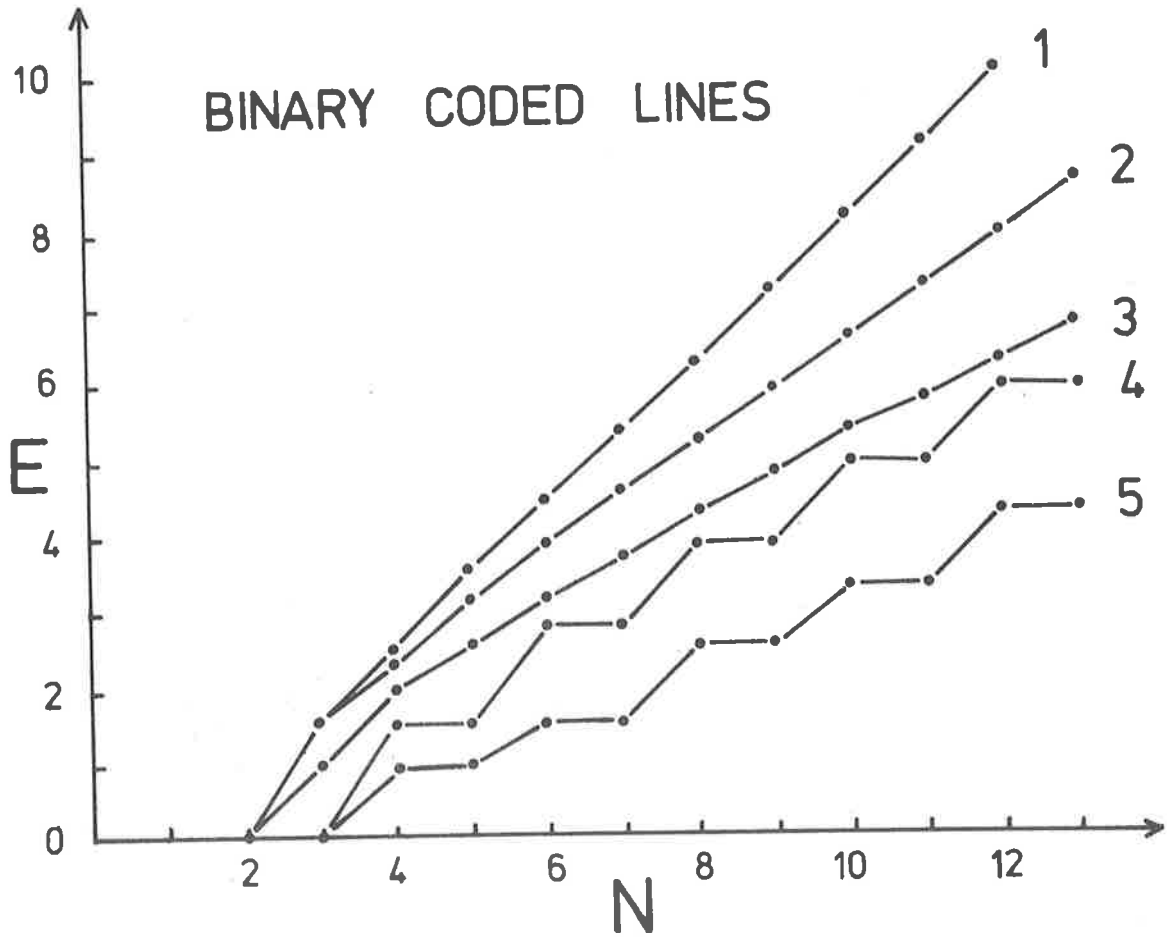


Figure 8.1 Relative coding efficiencies of binary coded lines of length N positions for various decoders i.e. (1) multilevel , (2) clipped binary, (3) natural binary, (4) delayed binary, and (5) constant capacity delayed binary, decoders.

$$C = \begin{cases} 2^{\frac{N}{2}} + 2^{N-2} - 2 & N \text{ even} \\ 3.2^{\frac{N-3}{2}} + 2^{N-2} - 2 & N \text{ odd} \end{cases} \qquad (8.6)$$

which checks against the computer output.

It is a straightforward matter to determine a general expression for the delayed-binary codes, which is

$$C = 2^{L-1} \qquad (8.7)$$

where

$$L = \begin{cases} \frac{N}{2} & N \text{ even} \\ \frac{N-1}{2} & N \text{ odd} \end{cases}$$

and for the constant capacity delayed-binary codes we derive

$$C = C_J^L = \frac{L!}{J!(L-J)!} \qquad (8.8)$$

where L is defined in Equation (8.8), and

$$J = \begin{cases} \frac{L}{2} & L \text{ even} \\ \frac{L-1}{2} & L \text{ odd} \end{cases}$$

The graphs are plotted on a logarithmic vertical scale to bring out the exponential nature of the numbers of codes, and by linearising the points, to permit extrapolation. The ordinate is in fact the variable E, where

$$E = \log_2 C \qquad (8.9)$$

The discrete points on the graphs have been linked to identify the different coding systems.

### 8.6.2 Biphase Codes

The numbers of codes available from biphase codes, with various decoders are shown in Figure 8.2, plotted against N. It might be noted that a biphase code of length N has N active transducers whereas for a binary or ternary code of length N the number of active

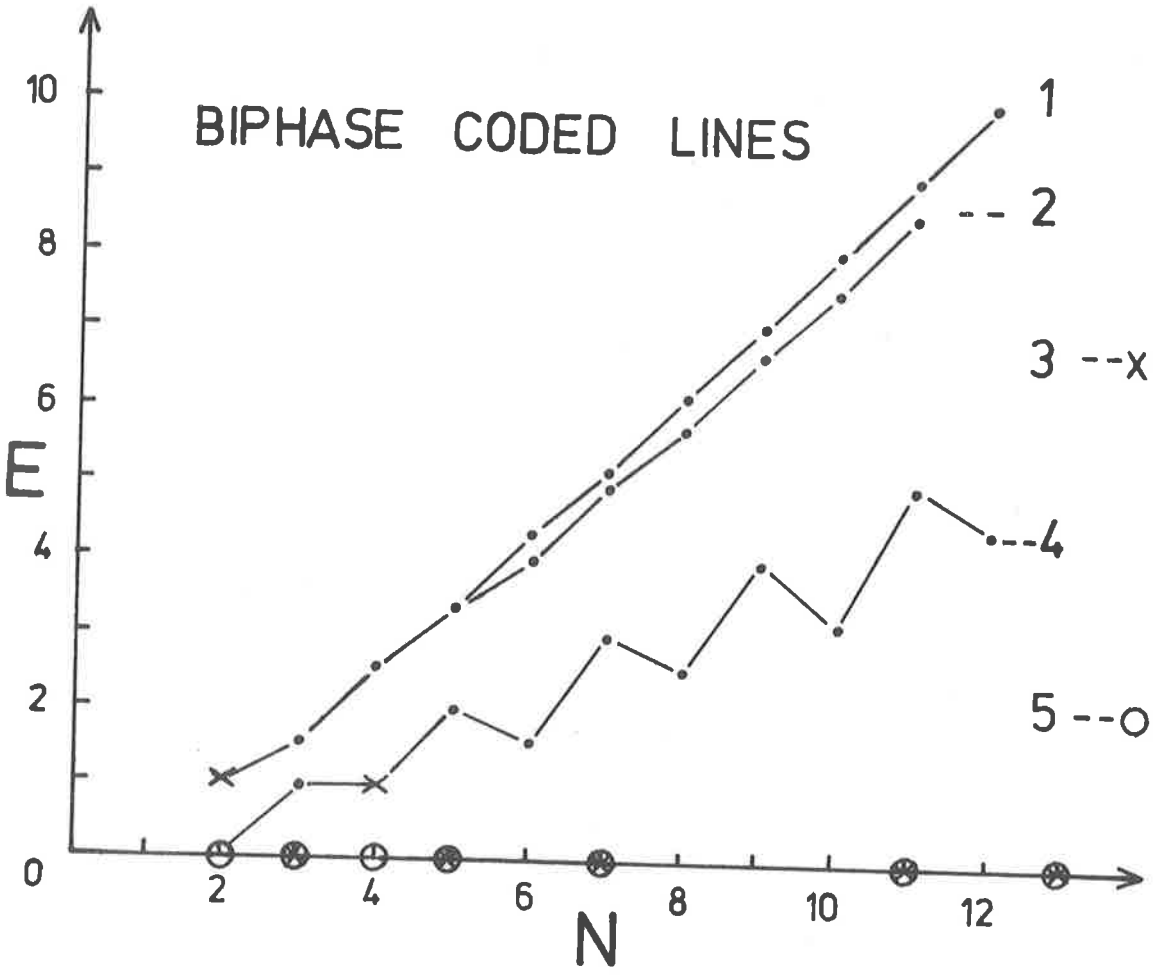


Figure 8.2 Relative coding efficiences for biphase coded lines of length N transducers with various decoders, i.e. (1) multilevel, (2) clipped ternary, (3) natural ternary (4) clipped binary, and (5) natural binary, decoders.

transducers may vary anywhere from 2 to N. This means that the procedure used for the determination of the total number of responses with a given N is slightly different; the total number of biphase codes of length N does not include the codes of length (N-1) or less, but binary or ternary codes of length N, include all codes of length (N-1), which include all codes of length (N-2), etc..

The curve for multilevel unclipped codes, representing the perfect decoder, is again included to serve as an upper-bound for the performance of simpler decoders. The general expression for the number of patterns available in this case is derived using similar methods to those used in the previous case, to obtain

$$C = \begin{cases} 2^{\frac{N}{2}-1} + 2^{N-2} & N \text{ even} \\ 2^{\frac{N-3}{2}} + 2^{N-2} & N \text{ odd} \end{cases} \qquad (8.10)$$

The extreme paucity of natural codes, using either binary or ternary decoders, is notable in these graphs. Another point of interest is to note how closely the curve for the ternary decoder approaches the performance of the perfect detector. This small margin for improvement supports the earlier assertion that there seems little advantage in going to more complex decoders.

### 8.6.3 Ternary Codes

The results for ternary codes, with binary and ternary decoders, are recorded in Figure 8.3, using a logarithmic scale to base two for comparison with the earlier results, although the use of logarithms to base three would be more natural.

An upper-bound for decoder performance with ternary codes has been derived as

$$C = \begin{cases} \frac{5}{2}.3^{\frac{N}{2}-1} + \frac{1}{2}.3^{N-1} - 2 & N \text{ even} \\ \frac{1}{2}.3^{\frac{N+1}{2}} + \frac{1}{2}.3^{N-1} - 2 & N \text{ odd} \end{cases} \qquad (8.11)$$

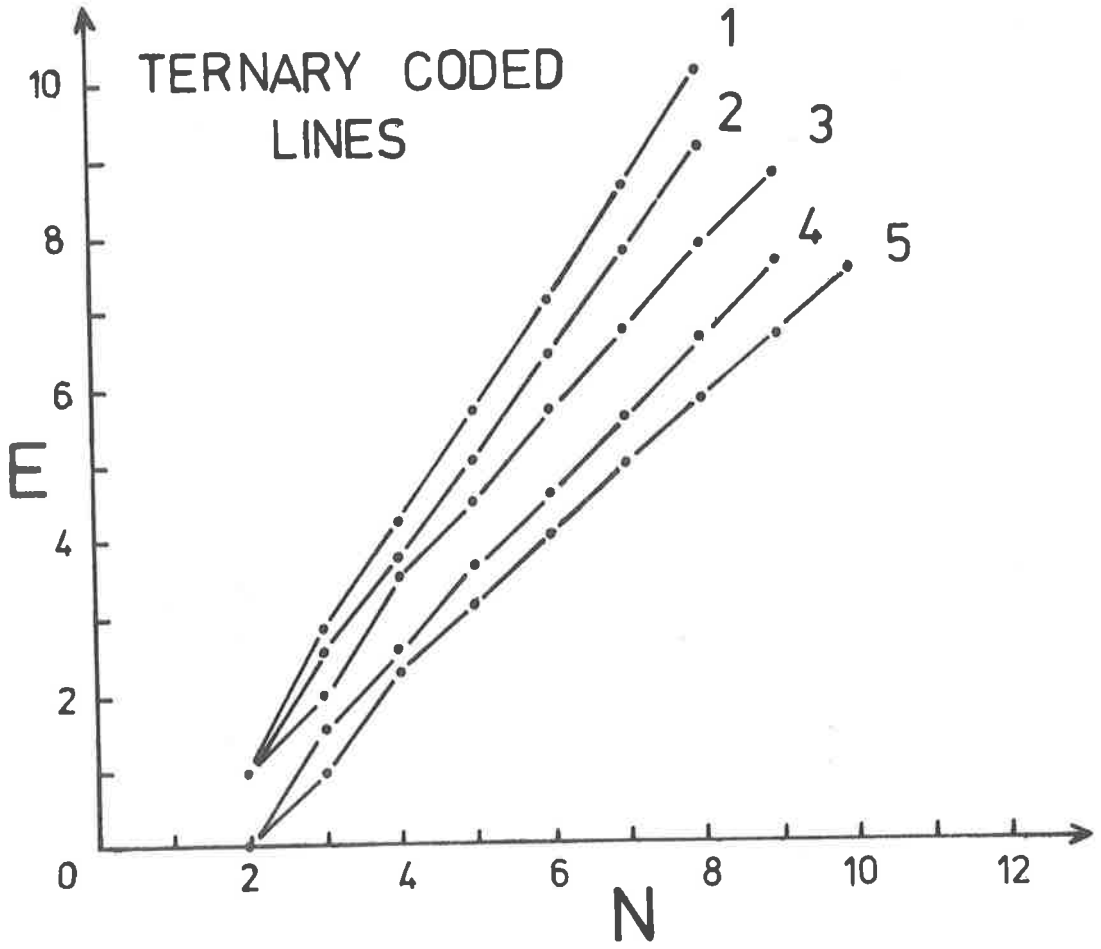


Figure 8.3 Relative coding efficiencies for ternary coded lines of length N positions with various decoders, i.e. (1) multilevel, (2) clipped ternary, (3) natural ternary, (4) clipped binary, and (5) natural binary, decoders.

by making use of the ambiguity relations from Section 8.1.2, as before. However, in this case comparison of the number of unique multilevel responses identified by the appropriate pattern-testing computer program with the numbers of codes predicted by Equation (8.11) showed small discrepancies for certain values of N. Further investigation showed that it is possible for certain pairs of ternary codes, not related by the ambiguity relations, to generate identical output responses e.g. the codes 1 0 -1 -1 0 1 and 1 -1 -1 0 1 1 which both generate the primary response 1 -2 -2 0 1. The discovery of these additional ambiguous pattern-pairs showed that the ambiguity relations obtained in Section 8.1.2 do not in fact describe all possible sources of ambiguity for any arbitrary coding scheme, and that other forms of ambiguity may be possible, dependent upon the nature of the coding scheme chosen.

In the present example of ternary coding the incidence of these additional ambiguities is quite small (only 6 pairs occur in the 242 possible code patterns with N=6) and it is considered that Equation (8.11) still describes a useful upper-bound on the efficiency of ternary decoders.

### 8.6.4 Conclusions

The results shown in Figures 8.1 to 8.3 display some not unexpected features. For example, the more restrictions applied in the coding rules, or the simpler the decoding operation, the fewer the distinct responses which can be obtained. Also as expected, the ternary codes exhibit a higher slope than the binary and biphase codes, approximately in the ratio log3/log2, in consequence of the larger range of codes available to be explored for any given N.

Two further conclusions of practical importance may be drawn: the first is that if binary codes are to be used, and natural

binary responses are desired, then there is little reduction in the overall coding efficiency if delayed binary coding is adopted, instead of natural binary coding. The second is that if ternary coding can be implemented, then even with a binary detector, the number of natural binary codes available increases approximately fourfold (for N=10) relative to the number of codes available with binary coding. The introduction of synchronous detection in a ternary decoder for natural ternary decoding, would increase the coding efficiency still further.

A rather fortunate property of all the curves is that they become essentially straight for values of N greater than five, permitting extrapolation for larger values of N, with some confidence. Looking at the general formulae obtained for the cases of the perfect detectors it is apparent that for large N, the factor with the largest exponent will dominate in each formula, and in the case of binary codes and biphase codes E will be asymptotic to [N-2], and for ternary codes E will be asymptotic to $[(\log_2 3).(N-1) - 1]$. The asymptotic slopes for the simpler decoders can be readily determined from the graphs.

# CHAPTER 9

# EXPERIMENTAL ONE-PORT CODING SYSTEM

## 9.0 Introduction

In Chapter 7 it was shown how the time domain response of a time domain coded one-port delay line structure may be described in terms of the admittance parameters of the appropriate basic N-port structure. In the subsequent chapter it was assumed that the individual reply pulses in the echo-train from the one-port would be clearly distinguishable, and the relation between the pattern coding and device responses was explored in some depth. We now return to look in more detail at the types of waveshapes which can be expected in the responses from practical delay lines.

The one-port delay line responses are dependent upon the nature of the input signal, the type of transducers employed and the nature of any associated circuitry. To simplify the interpretation of the results we shall first look at the behaviour of simple tuned delay lines, before moving on to look at the responses of a simple one-port structure, and finally to the evaluation of a more complex prototype labelling system. Frequent use is made of the one-port theory developed in Chapter 7, and the results of the computer modelling are compared with experimental results to establish the accuracy of the model.

The investigation was limited to binary coded lines using a set of identical equispaced interdigital transducers on a single propagation path, on a YX-quartz blank. 9-finger transducers with a $50\lambda$ aperture were employed with a uniform spacing unit between centres of $10\lambda$, corresponding to 200 nsec at the centre frequency of 50 MHz. The metallization pattern for a typical one-port delay

line structure is shown in Figure 9.1 for a line with the pattern code 10011011. The experimental lines used were up to 17 units long and were fabricated using the apparatus described in Chapter 6.

## 9.1 Multiple Transducer Delay Line Performance

It is instructive to compare the relative merits of characterisation of the more complex N-port structures in both the time and frequency domains. We commence with the time domain response which is of primary interest because it will eventually incorporate the required coding.

### 9.1.1 Output Pulse Shapes

The response of a one-port structure may be predicted in the time domain by means of Equation (7.25). This equation shows that the output response consists of a sequence of pulses of variable amplitude and spacing but identical shape i.e.

$$v_1(t) \quad \alpha \quad v_s(t) \quad * \quad z_{c1}(t) * g(t) * z_{c1}(t) \qquad (9.1)$$

The shape can be seen to depend on the source voltage $v_s(t)$, the tuned circuit impedance $z_c(t)$ (twice) and the real part of the transducer radiation conductance $g(t)$.

Typical calculated waveforms for these variables are shown in Figure 9.2. The input signal $v_s(t)$ is taken to be a burst of 5 cycles of an RF signal at the synchronous frequency. The tuned circuit impulse response has been computed using Equations (7.23) and (7.24) and an assumed Q of 10, and the radiation conductance $g(t)$ has been computed using program INAD, described previously. This waveform for $g(t)$ is impossible to measure experimentally but is known from Chapter 4 to be equal to the time domain transadmittance between two identical transducers with zero spacing. This impulse transadmittance

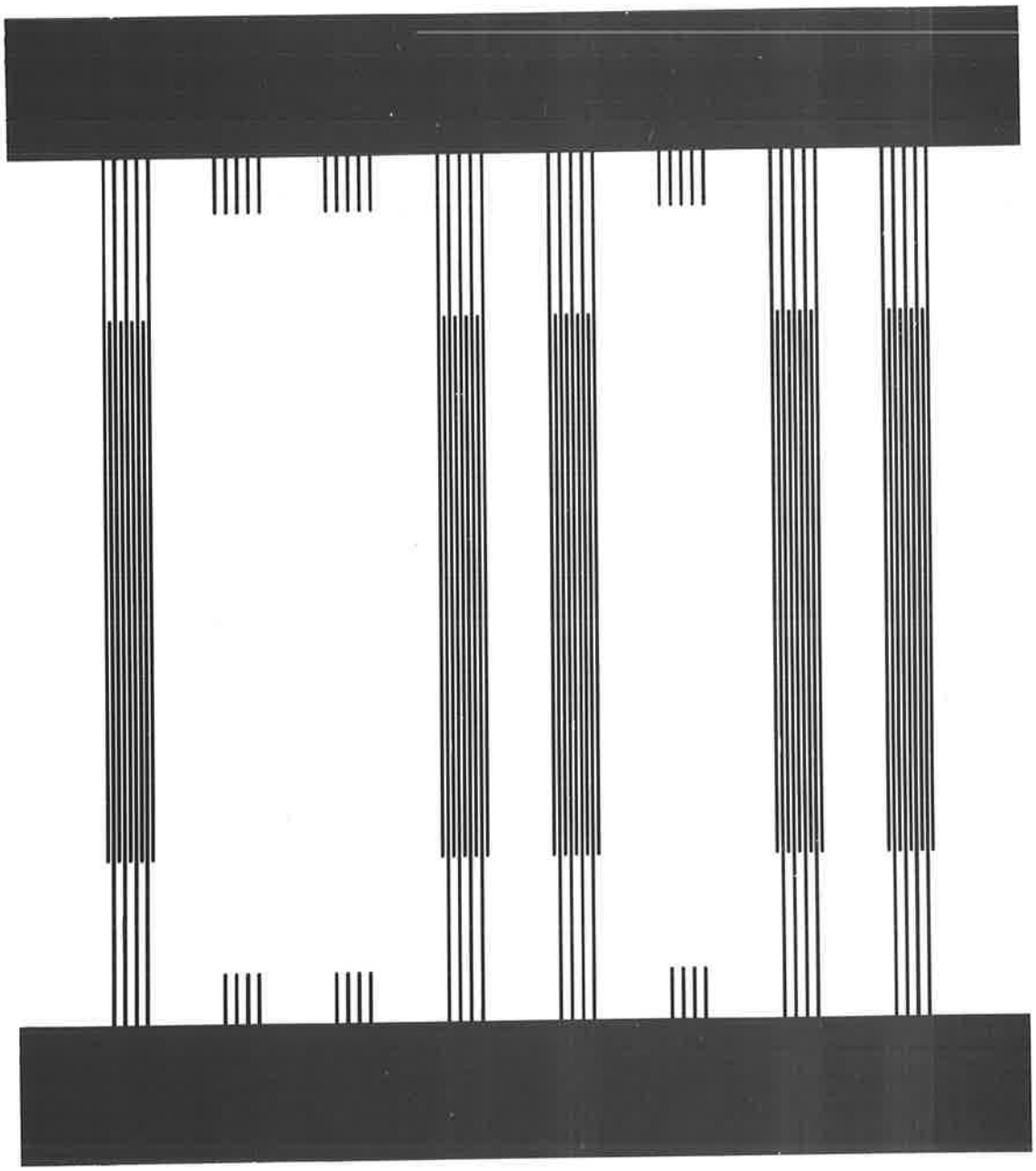

Figure 9.1 The metallization pattern for a typical one-port device with the pattern 10011011. The transducers have 9 fingers, 50λ aperture and 10λ spacing between centres.

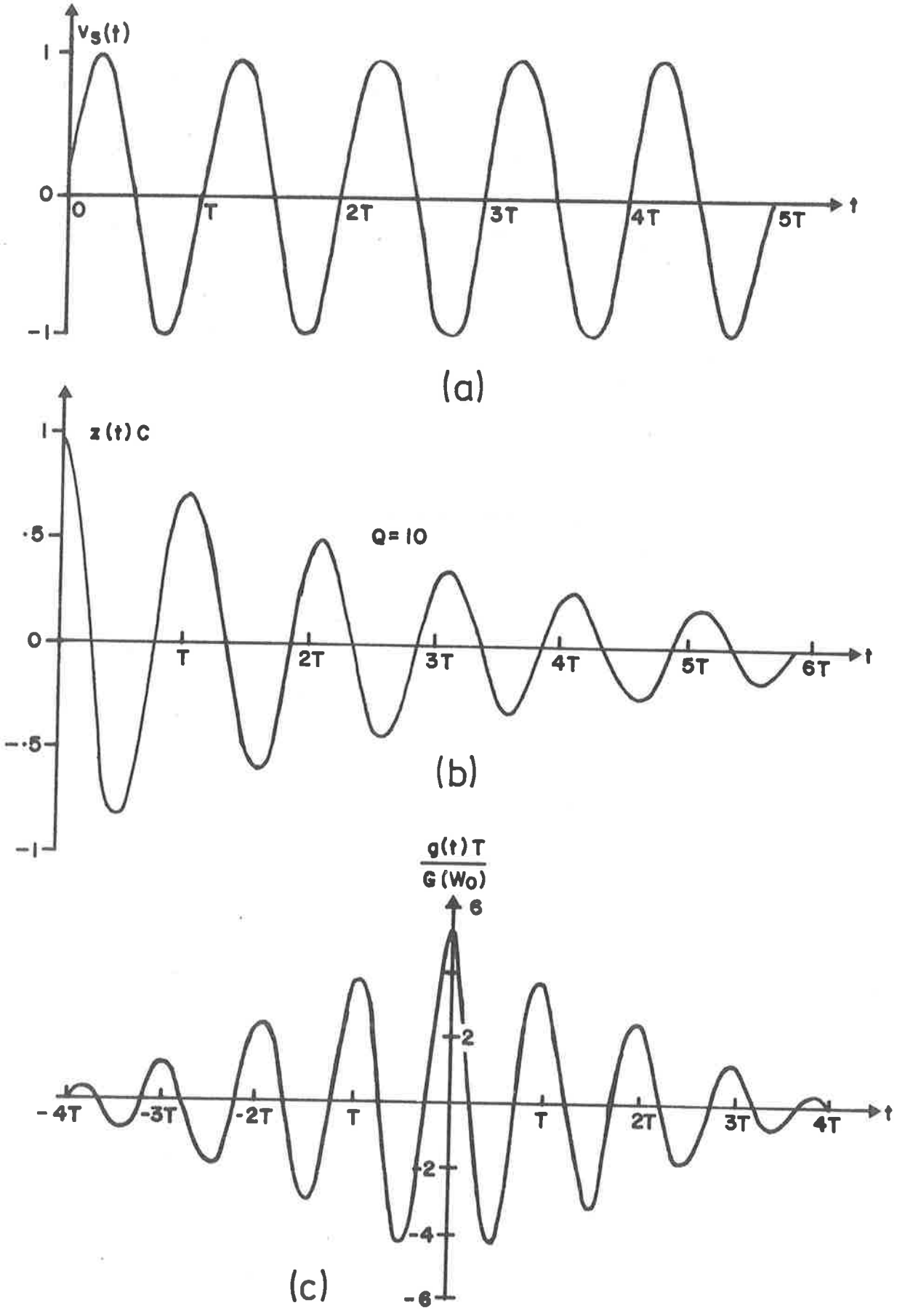


Figure 9.2 Typical waveforms for (a) the source voltage $v_s(t)$, (b) the circuit impulse response z(t), and (c) the impulse conductance for a transducer.

between two such transducers has already been measured (Figure 6.12), and confirmed the accuracy of the computer model which is being employed here.

The predicted zero- and first-order responses from a one-port device with these parameters has been computed by means of Equations (7.12) and (7.13), and the envelope of the 50MHz waveform is shown in Figure (9.3). The relative amplitudes and different shapes of the zero- and first-order responses are clearly shown. The first pulse of the primary response is completely obscured by the larger zero-order response, and the opposite phase of the zero- and first-order signals results in the cancellation null at 20T.

The large relative amplitude of the zero-order response, makes it experimentally difficult to observe the primary response of a one-port without a time-gated receiver to protect the receiving apparatus from severe overload at high gain settings, and initial investigations were conducted using two-port devices. The output pulse shapes from such devices are representative of the one-port case as described by Equation (9.1), provided both input and output circuits are tuned to the correct Q value.

A typical result for a one-port delay line with the pattern 1000000011111111, connected as a two-port, is shown in Figure 9.4. The first transducer has been isolated from the remainder and used as the transmitter, and the device operates as a conventional transversal filter. The photograph was obtained using a test jig which was employed for proving the delay lines manufactured for the coding system in Section 9.3, by means of these simple two-port measurements. The line shows excellent agreement with the predicted pulse shape in Figure 9.3, (the experimental pulses have slightly shorter tails because only the output transducers were tuned), and demonstrates the low attenuation

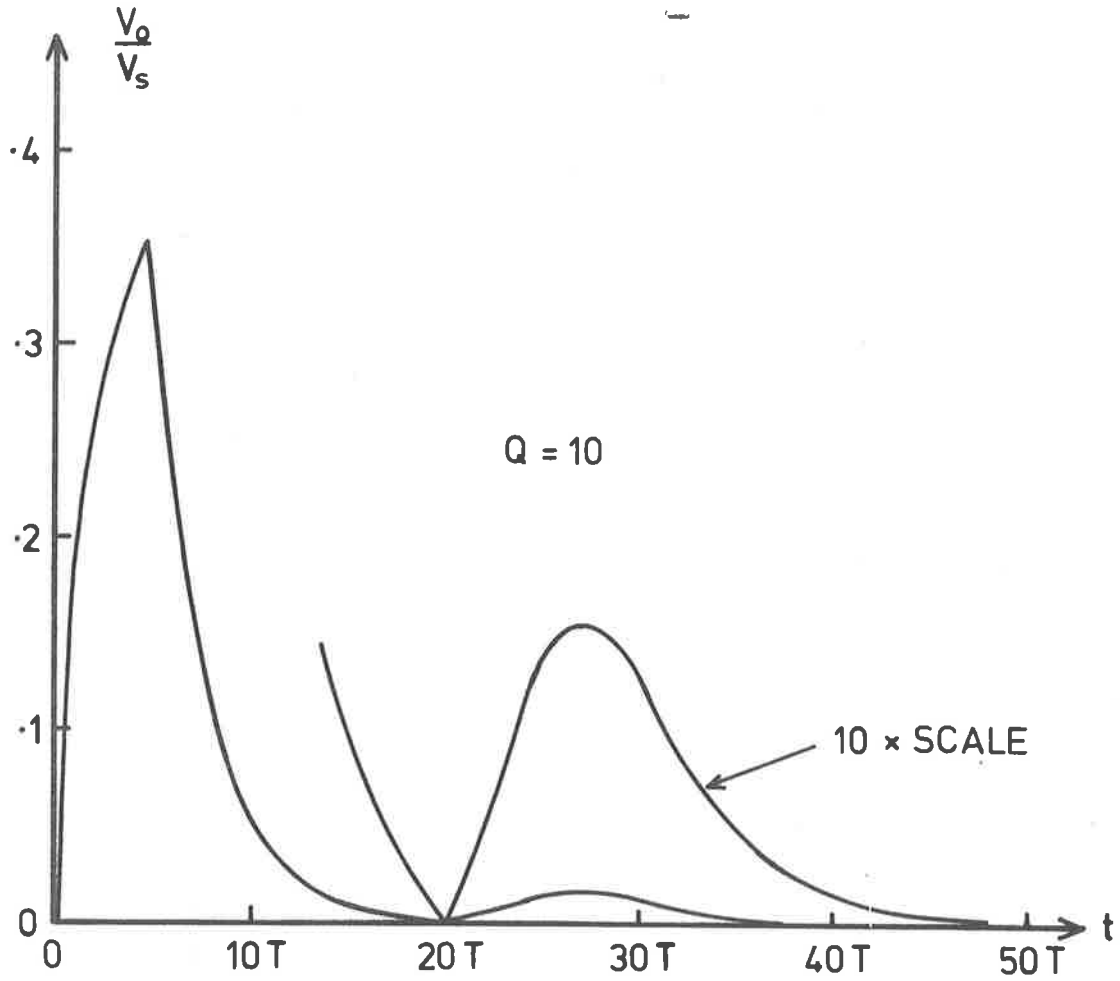


Figure 9.3 The zero and primary response envelopes for a 2-transducer one-port structure tuned for Q=10.

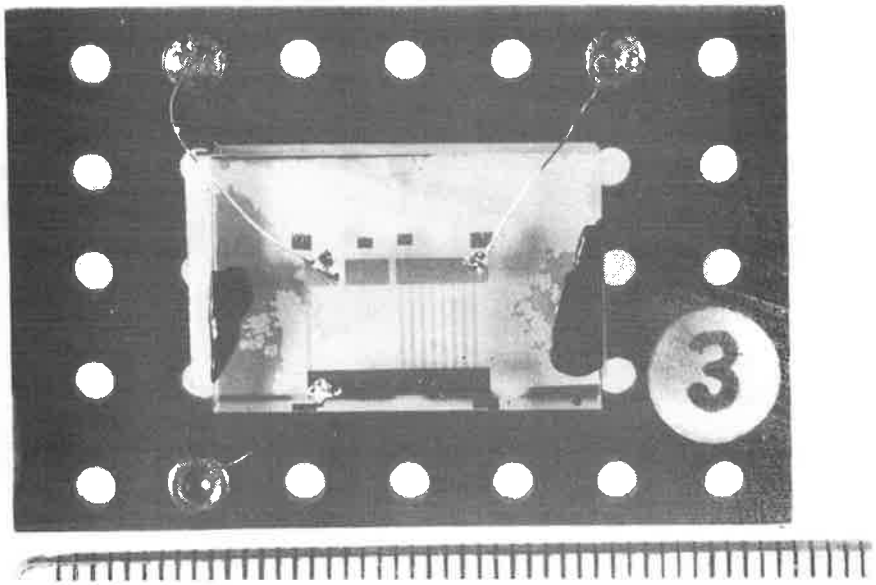


(a)

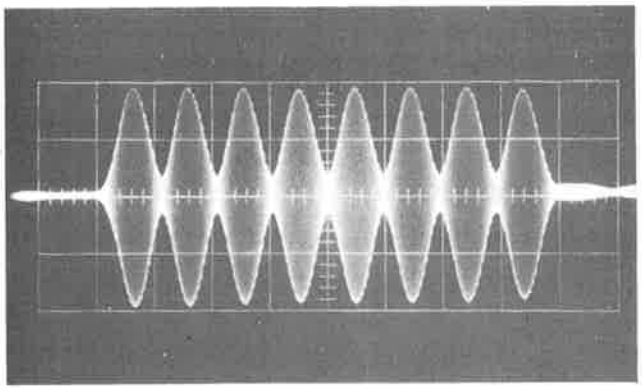

(b)

Figure 9.4 (a) An experimental 50 MHz delay line on YX-quartz, connected as a two-port device (the included scale is graduated in millimetres) and (b) the output of this line on a two-port test jig when excited with 5 cycles of a 50 MHz sine-wave. The input transducer was untuned and the output transducers tuned and damped to Q=5.

of the surface-waves which can be achieved on quartz when using weak-coupling transducers.

### 9.1.2 Frequency Domain Input Admittance

In the previous section it was asserted that the real part of the radiation conductance of a transducer is identical to the trans-admittance between two such transducers, apart from a phase factor in the latter case. Since this assumption, based on the admittance formulae derived in Chapter 4, plays an important part in the development of the theoretical one-port device model, an experiment was proposed in an attempt to verify the relationship.

Simplification of Equation (7.7) for a two transducer one-port delay line yields

$$Y_A(\omega) = 2G(\omega) \quad (1 + e^{-j\beta\ell}) \tag{9.2}$$

where $\ell$ is the transducer separation. The real part of the input admittance, given by the real part of $Y_A(\omega)$, is then

$$G_{IN}(\omega) = 2G(\omega) \quad (1 + \cos\frac{j\omega\ell}{v}) \tag{9.3}$$

In other words, the radiation conductance for a pair of acoustically and electrically coupled transducers will have peaks of four times the single transducer value, with complete nulls in between.

The real part of the input impedance for a pair of identical 9-finger transducers separated by $30\lambda$, was measured using the resonance and substitution technique described in Chapter 6, and the result is shown in Figure 9.5. For comparison, the expected result given by the computer model for the same device is shown in Figure 9.6. The anticipated nulls appear in the theoretical response as expected, at frequencies spaced by $f_o/30$ Hz, and the experimental result is observed to have the same general shape.

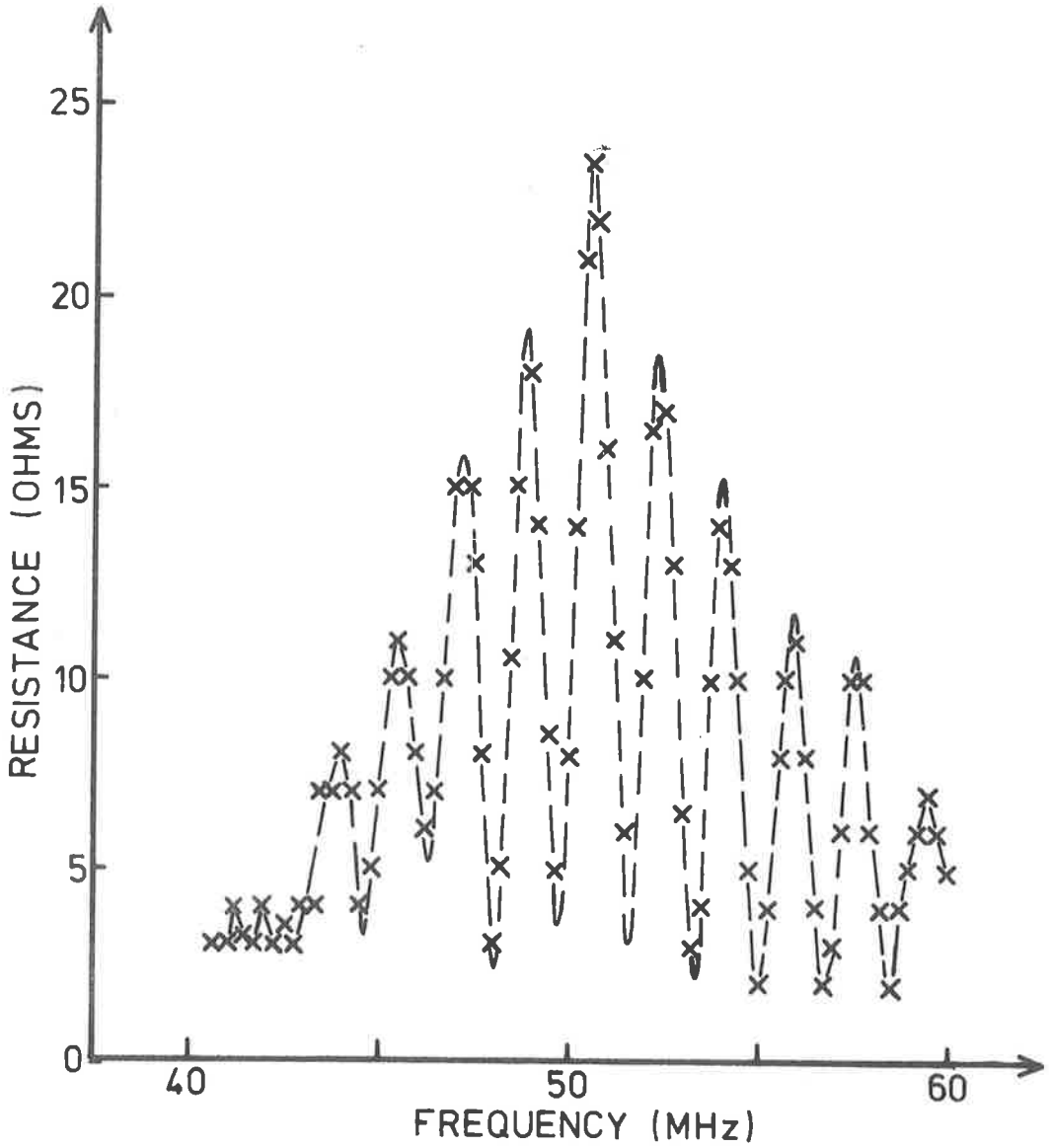


Figure 9.5 Measured series radiation resistance of a pair of parallel connected 9-finger transducers spaced 30λ apart on YX-quartz.

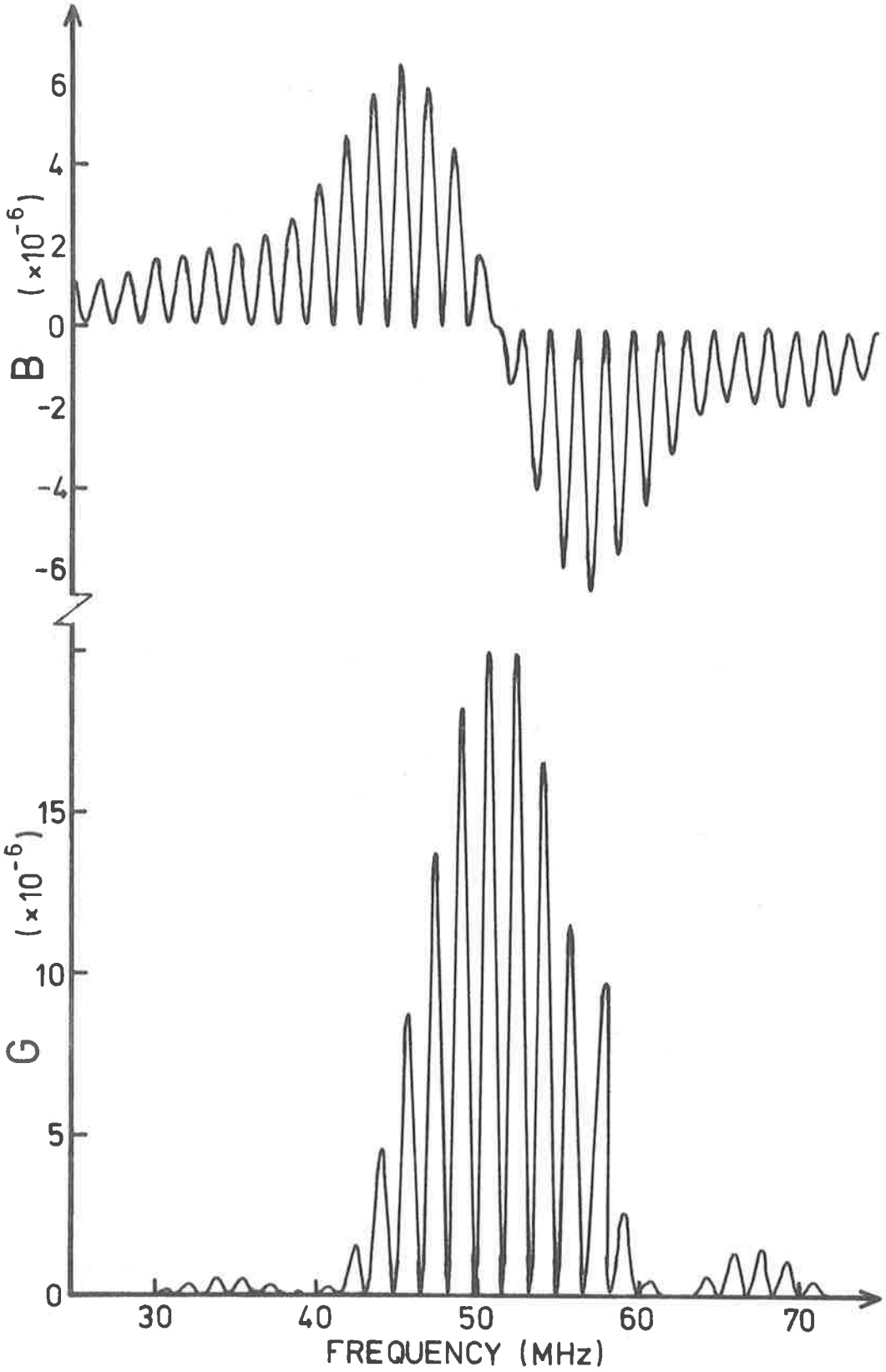


Figure 9.6 Computed input admittance parameters for a pair of parallel-connected 9-finger transducers spaced 30λ apart on YX-quartz.

The minima in the experimental curve do not go down to zero, indicating that the magnitude of the parameters $G_{ii}(\omega)$ and $G_{ij}(\omega)$ are not in fact identical. The non-zero relative heights of these minima indicate that the transadmittance signal is lower than the self-conductance, which may be accounted for by the surface-wave attenuation and transduction losses between the two transducers under test, as described in Section 6.4. The absolute accuracy of these resistance measurements is uncertain because the desired values are obtained by subtraction from coil losses of up to several hundred ohms. The measurements at these relatively high Q values are also very susceptible to stray capacitance and lead inductance: in fact the measurements may be modified to give the expected value by postulating a total stray capacitance across both transducers and their connecting conductors of 1.3 pF. In the light of experience in tuning other experimental lines this does not appear to be an unreasonable figure for the stray capacitance.

This experiment thus produced results which had the expected form of the theoretical predictions, within experimental error. The experiment is interesting because, being in the frequency domain, it does permit the primary response (Equation(3.7))to be observed in its entirety, which is not possible in the time domain. The results are also indicative of the complexity which can be expected in the frequency domain input immittance for multitransducer structures. This is a further argument in favour of the introduction of deliberate impedance mismatching to the transducers in transversal filters and coded one-port devices.

## 9.2 Binary Coded One-Port Delay Line

To observe the response of a simple binary coded one-port

delay line, the line code 10011011 was selected from the computer coding programs used in Chapter 8 as being a typical code which would produce a multilevel response. The same transducer geometry and spacing was used as above, and the desired pattern obtained by carefully severing the ends of the electrodes of the unwanted transducers, on a delay line like that shown in Figure 9.4 (this procedure will be justified in the next chapter).

### 9.2.1 Experimental Results

The equivalent circuit for the measurement apparatus is shown in Figure 9.7: the 50 Ω source and receiver circuits (shown in Figures 6.8 and 6.9) were connected to the tuned one-port device by resistors R, representing two long communication links. The total capacitance of the 5 transducers plus strays, represented by C, was tuned empirically with a variable inductor L to resonance. In this circuit the two resistors R determine the effective Q of the one-port resonance and also isolate the receiver from the full transmitter voltage.

The output waveform obtained on the oscilloscope with this circuit is shown in Figure 9.8, for R=5kΩ giving an approximate Q factor of 5.

### 9.2.2 The Model Prediction

For comparison with the experiment, the computer program, which obtained the constituent waveforms shown in Figure 9.2, was extended to compute the expected response for the above delay line, and the result is shown plotted in Figure 9.9.

The expected response code for this particular structure, taken from the coding programs, is 2132011 (where the zero time response is ignored), and this is easily seen in the predicted primary waveform although some pulse overlap has occurred. The

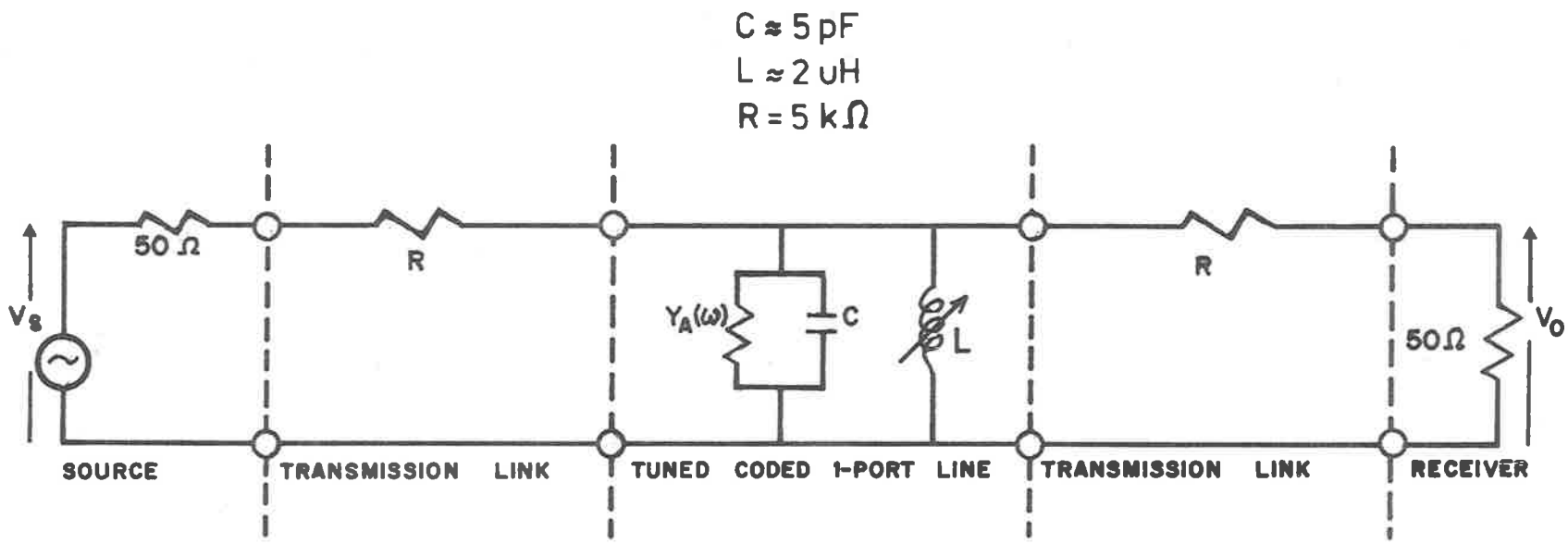


Figure 9.7 Measurement circuit for the observation of the response of an inductively tuned one-port surface-wave delay line.

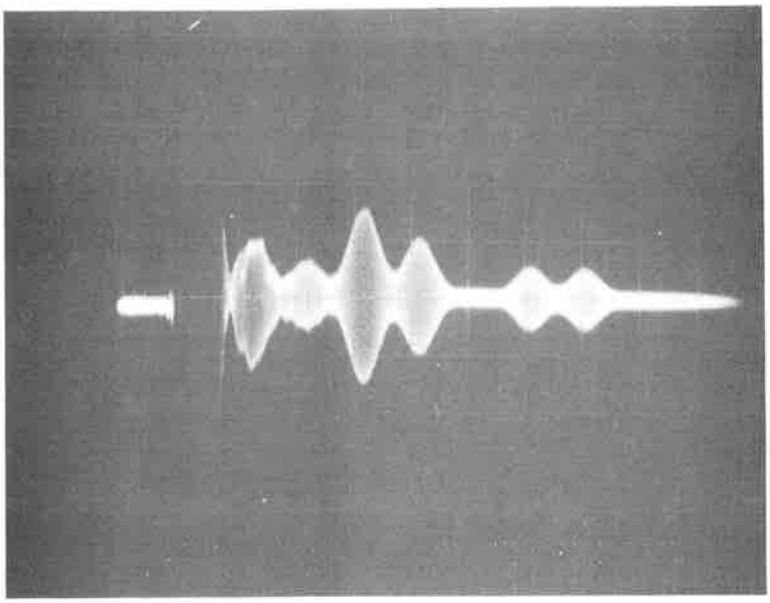

Figure 9.8 The multilevel response waveform from a simple binary coded one-port line with the pattern 10011011. The excitation signal is 5 cycles at 50 MHz, and the device is tuned to Q=5.

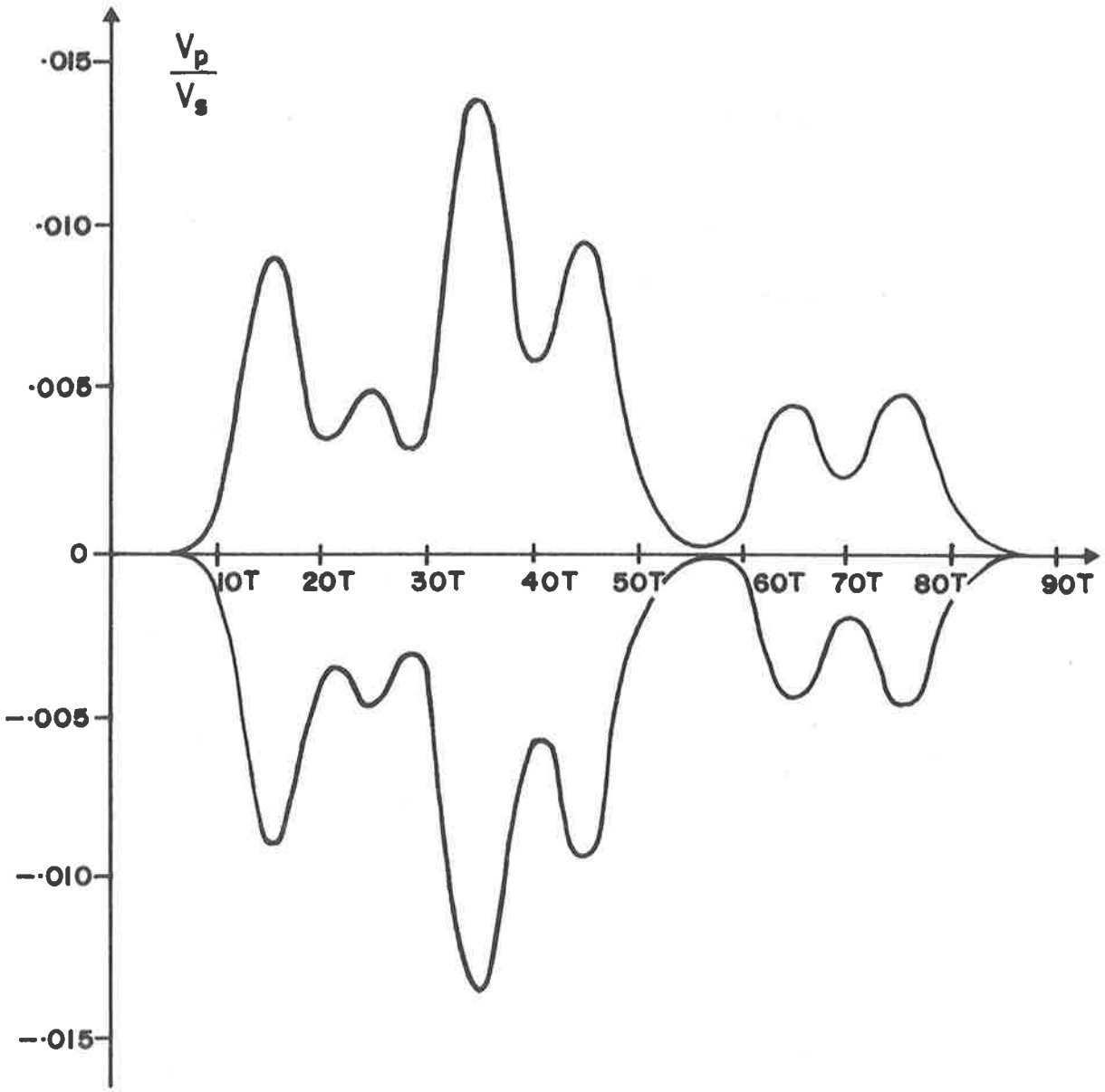


Figure 9.9 The primary response envelope predicted by the computer model for the binary coded one-port line 10011011, tuned to Q=5.

same waveform may be clearly seen in the experimental response (the blur on the trace is due to the preamplifier noise becoming obvious at the low signal level necessary to avoid overloading the pre-amplifier output with the zero-order response) but the zero and first bit positions in the primary response are overlapped by the offscale zero-order response, as predicted in Figure 9.3. The null at the trailing edge of the zero-order response predicted by Figure 9.3 is also visible in the experimental waveform, and is due to the essentially $180^{o}$ difference in phase of the zero- and first-order responses which occurs when the transducers are spaced by an integer number of wavelengths at the centre frequency.

### 9.2.3 Conclusions

From these simple experiments a number of conclusions were able to be drawn. Firstly, despite the approximations made in the analysis in Chapters 4 and 5, the computer model gives very good agreement with the observed waveforms obtained from coded two-port and one-port delay lines employing interdigital transducers. The only significant source of discrepancy with the observed results is in the predicted magnitude of the output responses, and these small differences arise from the lack of a sufficiently accurate determination of the sources of loss in the experimental devices, which consequently are omitted from the model.

The computing techniques developed are very economical: the complete response of a multitransducer structure is obtainable by simple arithmetic operations on the three basic waveforms, typified by those shown in Figure 9.2. Complete responses may thus be computed to any desired order of accuracy, in a few seconds e.g. total computing time to evaluate the basic waveforms and then the desired result in Figure 9.9 was 16 seconds CP time on a CDC 6400 machine.

The original proposal, that a one-port device with a pulse-modulated time domain response might be achieved using a surface-wave delay line, has been successfully demonstrated. However, the devices examined above could not seriously be proposed as approaching a working system. The most serious problem is the very large difference in level of the zero-order and first-order responses, which is inevitable using weakly-coupled transducers, and which creates problems at the receiver when attempting to observe the primary response code. We now attempt to evaluate the potential usefulness of one-port coded lines through the investigation of a complete prototype system designed with the aim of overcoming this and associated problems.

## 9.3 Prototype One-Port Coding System

The essential components of any delay line labelling system are shown diagrammatically in Figure 9.10(a), and consist of a pulsed transmitter and antenna, a coded one-port delay line coupled to a transponding antenna, and a suitable receiver also connected to the transmitting antenna to detect the coded string of reply pulses. To protect the sensitive receiver input circuitry from the full transmitter voltage, suitable switching equipment is necessary to isolate the receiver for the duration of the transmitter pulse.

### 9.3.1 System Design Considerations

The general form of the system described in Figure 9.10(a) resembles closely that of a conventional radar system, and an examination of the similarities and differences of the two types of systems will enable some useful insights to be gained regarding the questions of selection of good transmitter waveforms, and the optimum receiver design. The present example of a one-port system employing

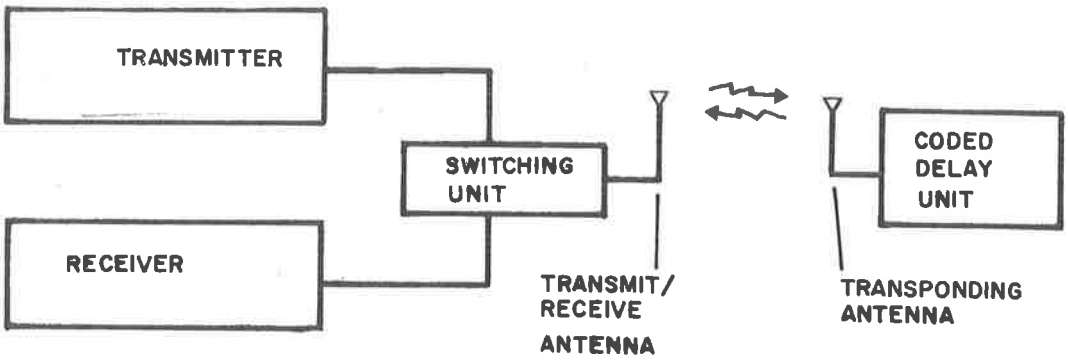


(a)

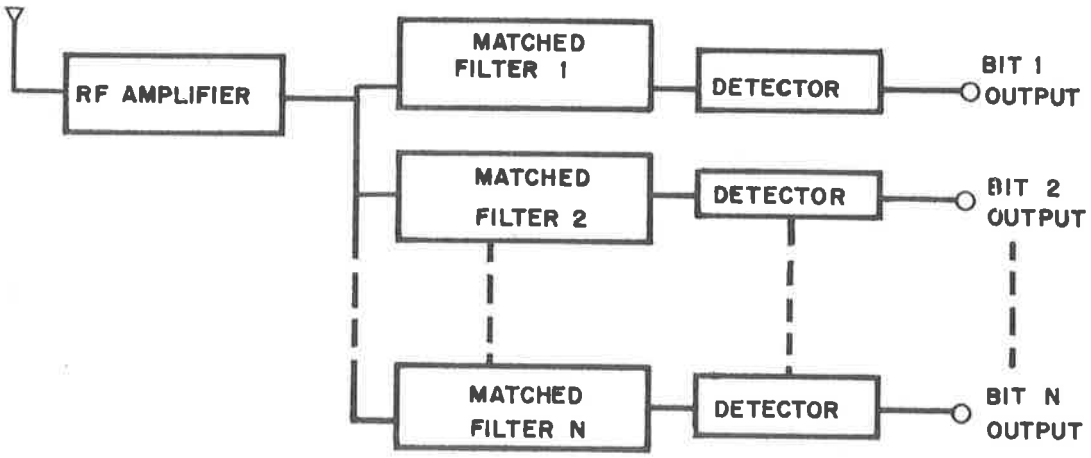


(b)

Figure 9.10 Schematics of (a) a basic coded line interrogation system, and (b) the optimum receiver configuration.

time-delayed pulse coding corresponds directly to a conventional pulsed radar seeking a number of targets at predetermined ranges. Interrogation of a number of coded one-port devices on different channels would correspond to a radar observing targets on different bearings: for simplicity only single-channel interrogation will be considered here.

From signal processing theory for radar receivers it is now well known that to maximise the signal-to-noise ratio at the receiver output, a matched filter[149] should be employed, and the general format of an optimum receiver for the detection of N separate reply pulses is shown in Figure 9.10(b). A separate matched filter must be designed for each echo pulse, and the specification for a matched filter is that the frequency transfer function should be equal to the conjugate spectrum of the known input signal (plus a simple time delay to permit physical realization of the filter). This knowledge of the desired receiver characteristics imposes an indirect constraint on the transmitter waveform, as it is obvious that little advantage will be derived by going to more complex transmitter waveforms if the appropriate matched filter response is not readily realizable.

Having maximised the available signal-to-noise ratio at some instant in time, relative to the transmitter pulse, for each reply pulse it is necessary to sample the matched filter output, make a decision as to whether a pulse has been received, and store the result for subsequent use (and also possibly for integration over several interrogation cycles). For this purpose a detector is shown after the matched filters for each reply pulse. The operational constraints on the detector will differ considerably from the typical radar situation, where the emphasis is usually on minimising

the false-alarm rate for target echos obscured in noise. For a labelling system to be of any use it must achieve reliable detection of each pulse in the reply code and this will necessitate working with good signal-to-noise ratios at the receiver output. A further difference to be reflected in the detector design is that not only false-alarms but missed-detections also must be held below an acceptable level.

To investigate the behaviour and limitations of coded one-port surface-wave delay lines when subject to the constraints imposed when operating in a practical interrogation system, the prototype system described in the following sections was simulated in the laboratory.

### 9.3.2 Selection of the Coding Method

The first decision required in the design of any labelling system is the type of line coding to be adopted, and in this case delayed binary coding was chosen, for the following reasons. It was commented previously that the large difference in amplitude between the zero-order and primary responses resulted in the overlap of the early reply pulses by the tail of the zero-order response. In the practical situation shown in Figure 9.10(a) this problem is aggravated by the additional attenuation of the primary response by twice the one-way propagation loss, and the problem becomes serious. To avoid the need to go to a large individual transducer spacing in an effort to prevent overlap of the zero-order response, it was considered that more efficient use of the substrate area would be achieved if close transducer spacing was retained and the first few reply pulses ignored by the decoder. This led naturally to a consideration of the delayed binary codes described in Chapter 8. These codes were also considered attractive because they provide a natural binary output which simplifies the detector design, and because of the availability of a set of monotonic

binary output codes which is attractive from the system designer's point of view.

Delayed binary codes are not the most efficient codes available in terms of the number of discrete codes available with N-transducers, and the possibility of using the more efficient ternary codes in a delayed ternary format was also considered. However the use of biphase and ternary codes requires an accurate phase-reference at the receiver relative to the reply code, and since a one-way propagation path length change of only 1.5 metres would result in $180^{o}$ phase shift of the carrier frequency at 50 MHz, the use of these coding systems would require accurate location of the transponding label before interrogation, and they were not considered further.

### 9.3.3 Description of the Prototype System*

The integrated transmitter-receiver system used for the experimental interrogation of the one-port delay lines is shown in Figure 9.11, and its operation may be understood by reference to the waveforms in Figure 9.12. The system is designed to operate with 17-bit length delayed binary one-port lines using the transducer geometry described in Section 9.1, and the maximum primary response envelope from a line with all 9 transducers present is indicated by the waveform in Figure 9.12(c).

The system operation is controlled by the timing unit which is synchronized with the 50 MHz master oscillator and an interrogation cycle is initiated with a short pulse T1 which gates a burst of 5

---

* The prototype system described in this section was designed by the author in collaboration with his supervisor, Dr. P.H. Cole, of the University of Adelaide and Dr. R. Vaughan of the University of New South Wales. The preliminary system concept was tested with a computer model developed by the author and, following successful results in the feasibility study, an experimental transmitter and receiver was designed and built by Dr.s Cole and Vaughan. This receiver system was made available to the author for validation of the computer system model, and was used to obtain the experimental results presented in Sections 9.3.5. and 9.3.6. and the reflection measurements in Section 10.3.3.

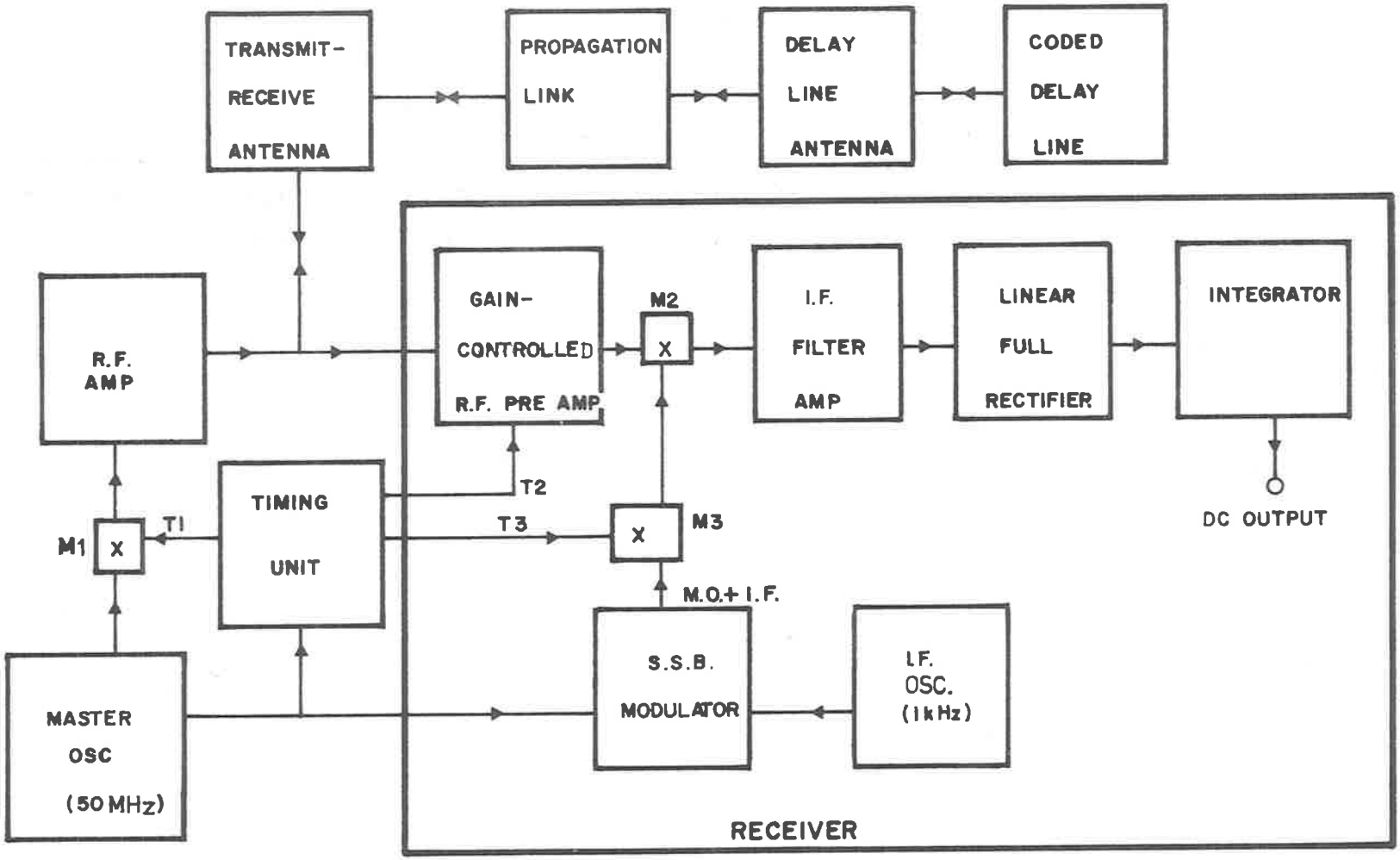


Figure 9.11 Schematic of the complete coded line interrogation system.

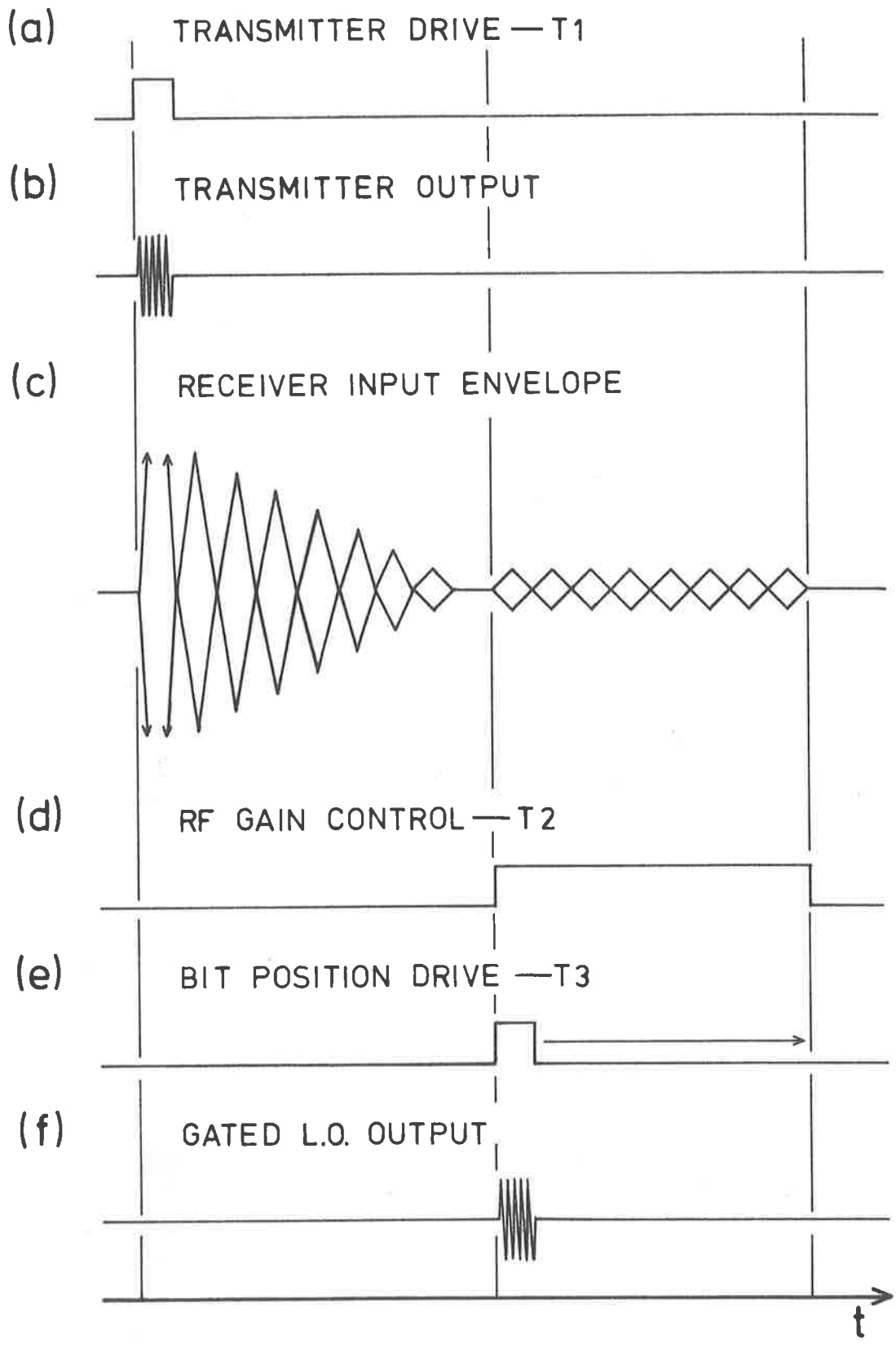


Figure 9.12 Waveforms present in different locations in the prototype interrogation system described in Figure 9.11.

cycles through mixer M1 to the RF amplifier (to improve the on-off ratio the amplifier is just biased into class C mode), and a pulse is launched into the simulated antenna and propagation link, and the delay line. The receiver preamplifier is held off by the timing signal T2 (waveform (d)) until the reply-code interval to allow time for the ringing in the antenna circuits to decay. The subsequent stages of the receiver simulate a matched filtering action.

The optimum filter for a single pulse, as mentioned before, has a transfer function equal to the conjugate spectrum of the pulse. It is more enlightening to describe the matched filter in the time domain, as one whose impulse response is simply a time reversed version of the signal pulse. Hence matched filtering is equivalent to convolution with a time-reversed replica of the signal i.e. it is equivalent to a correlation detector. In this case a matched filter is simulated by multiplying the RF waveform (c) with a short 10 cycle burst of local oscillator signal gated through mixer M3, in mixer M2. The correlation process is then completed by the integration effect of the narrow bandpass IF filter.

This is not a very accurate simulation of a matched filter response, because we are correlating the received signal pulse with a pulse with a rectangular envelope, not a replica of the input pulse. The resulting degradation in signal-to-noise ratio is about 1.0 dB,[150] which is considered acceptable in an experimental system. Another simplication, which will have been observed by the reader, is that only one matched filter is shown in Figure 9.11. The individual reply pulses are observed in the experiments by manually altering the time position of the timing signal T3, in order to examine the system response to each pulse.

The addition of an audio frequency offset to the master

oscillator frequency achieves two things: it enables the single mixer M2 to substitute for a full quadrature mixer (albeit at a 3 dB loss in signal-to-noise ratio) and it permits AC instead of DC post-mixer amplification thus minimising drift problems in the circuit design. The final stage prior to detector operation is the rectification and filtering of the audio signal to DC. The transmitter is in fact pulsed at a PRF of 100 kHz, and this final low-pass filter performs the additional function of integrating the system output to improve the output signal-to-noise ratio still further.

The detector shown in Figure 9.10(b) was not realized experimentally, this function being performed by the operator observing the DC output as a function of the bit position drive signal T3.

### 9.3.4 The Computer Simulation

The main interest in the investigation of this experimental one-port coding system was in determining the effect of the antennas, line tuning and receiver circuitry on the detectability of the output code, particularly in the case of moderate to severe pass-band distortion in the communication channel. Apart from degradation of the signal-to-noise ratio, waveform distortion will also result in intersymbol interference between the output pulses.

A computer simulation was set up to calculate first the complete primary response waveform at the input to the mixer M2, then the operation of the matched filter was simulated to derive a plot of the receiver output versus the matched filter delay. The frequency dependent circuit elements, external to the source and receiver, in the experimental system simulation are shown in Figure 9.13, and the individual segments were modelled in program INTER. It will be noted that an inductive loop antenna is assumed for the transponding

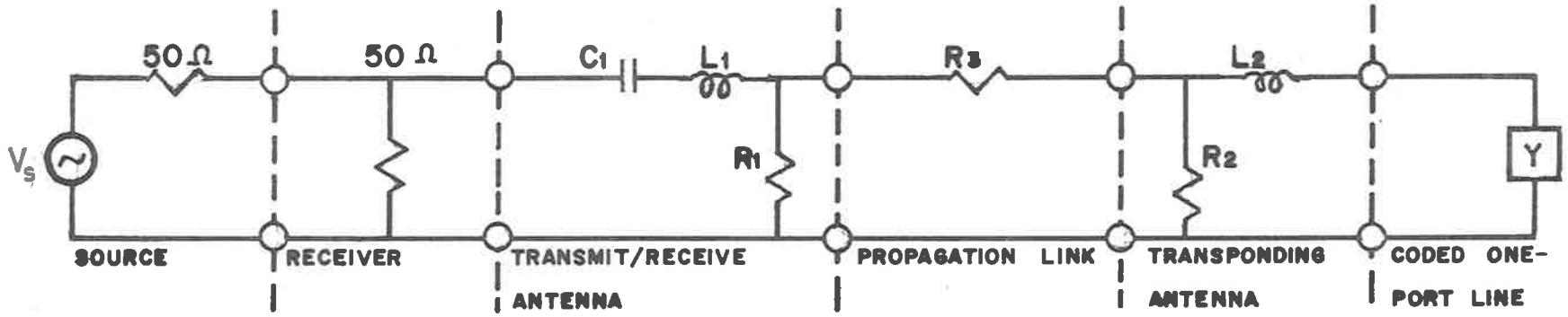


$R_1 = 25\ \Omega$ $R_3 = 470\ \Omega$ $R_2 = 110\ \Omega$
$C_1 = 13{\cdot}5\ pF$ $C_2 = 6{\cdot}0\ pF$
$L_1 = {\cdot}84\ \mu H$ $L_2 = 1{\cdot}7\ \mu H$

Figure 9.13 Equivalent circuit used to represent the propagation link in the prototype one-port coding system.

antenna and that the self inductance is used to resonate the static delay line capacitance. The source was assumed to deliver exactly five cycles of a perfect sine wave, and the receiver RF circuits were considered to be sufficiently broadband to have negligible effect on the RF waveform except for the high and low-pass filters associated with the RF gates between stages, and these were included in the program in case the side-band phase shifts proved significant. The program uses the FFT algorithm to transform between the time and frequency domains, to permit the most efficient computation of the operation of each system element, and a flow chart and listing of the program may be found in Appendix A1.8.

To match the transducer bandwidths all the antenna circuits were assumed to be effectively tuned then damped, if necessary, to a Q value of 5 in each case at 50 MHz. The predicted waveform at the mixer input in the receiver is shown in Figure 9.14. This plot clearly shows the expected delayed binary code of 11010011, but the pulses have spread in time due to the restriction of the signal bandwidth by the various tuned circuits.

The action of a quadrature multiplier was then simulated in the succeeding section of the program, and a plot of the output versus various time positions of the gating signal T3, obtained. The result for the typical RF waveform shown in Figure 9.14, is shown in Figure 9.15. The presentation of the results in this form was found to be useful for diagnostic purposes, but the interpretation of results needs care as the curve is not a function of time in the normal sense. The curve represents the output of an infinite number of matched filters with varying delays, and in a practical system only eight matched filters would be used, one for each expected reply pulse. The correct delays for these filters are indicated by the vertical bars in the figure.

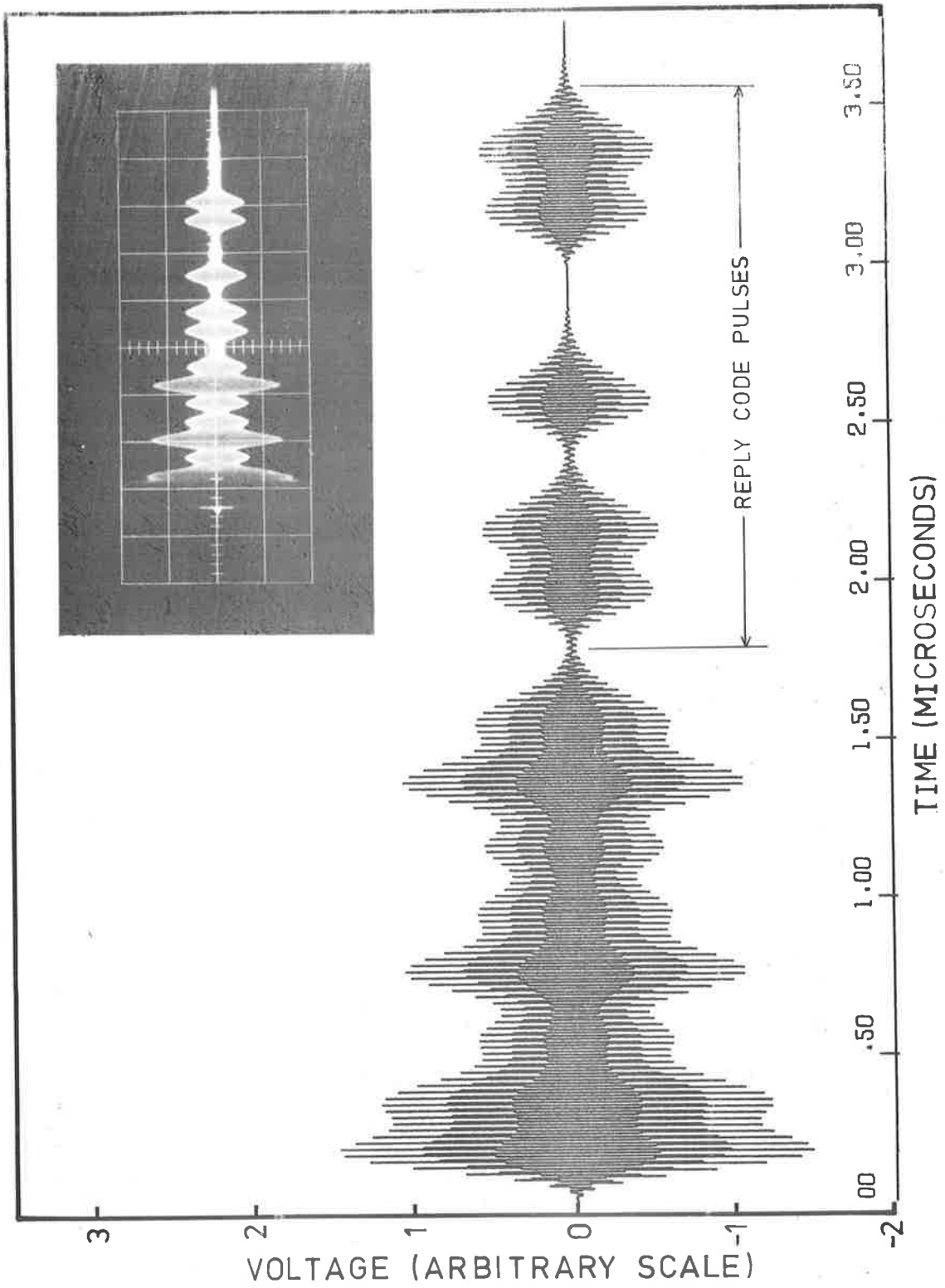


Figure 9.14 The input waveform to the detection mixer as predicted by the system simulation program. All antenna circuits are tuned to Q=5 at 50 MHz and the expected reply code is 11010011. The inset photograph shows the corresponding experimental waveform, observed at the receiver input, for comparison.

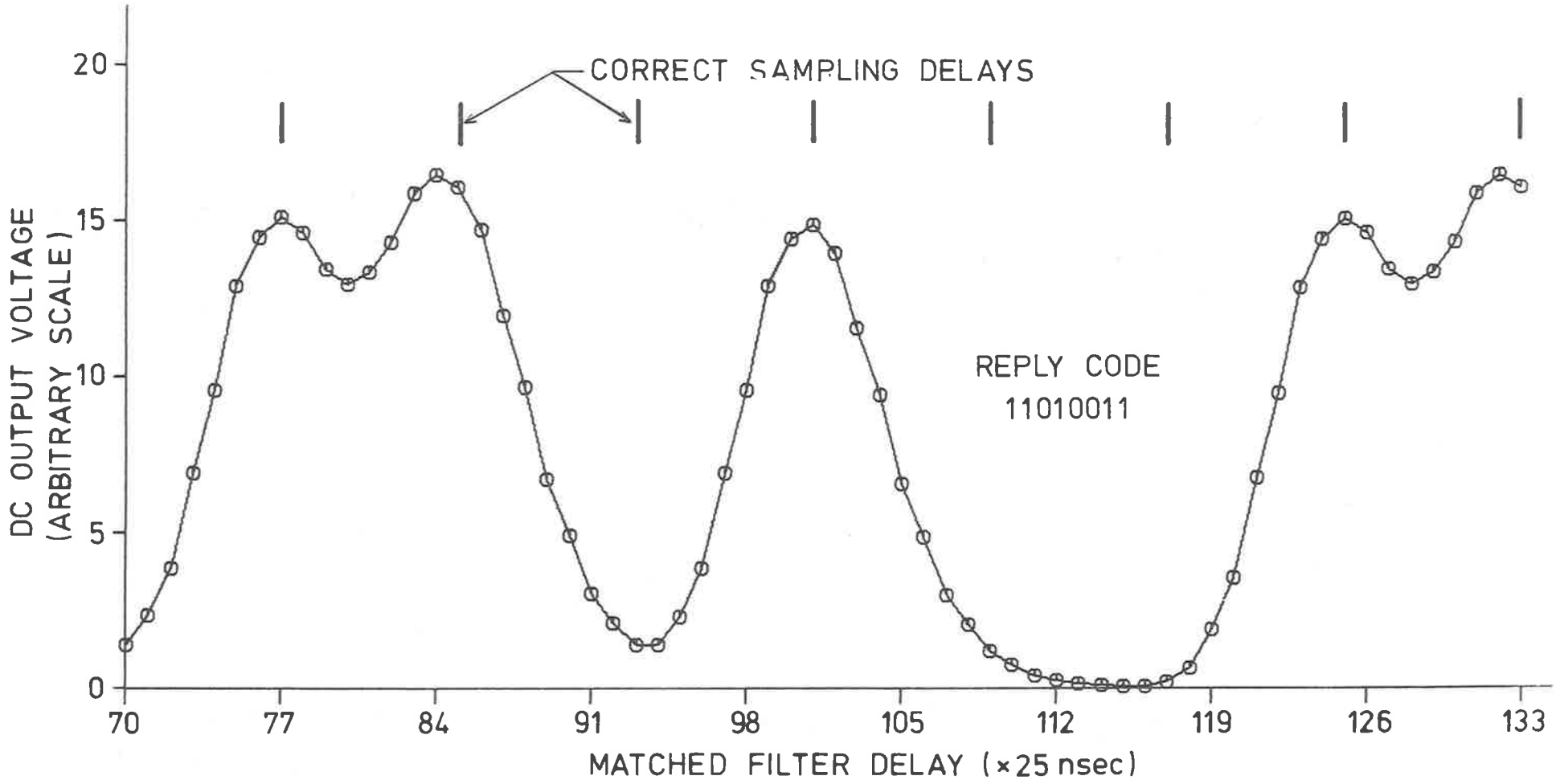


Figure 9.15 Computed receiver output plotted against matched filter delay (measured relative to the transmitter pulse) for the waveform shown in Figure 9.14.

The presence of pulse-overlap can be observed in this curve: the output has not fallen to zero at the second marker due to the tail of the first pulse, and the output for pulse four is greater than pulse one, due to the overlap from pulse three (pulse one avoids this problem only because it has been deliberately preceded by a blank in the disregarded part of the response code - as shown in Figure 9.14.)

### 9.3.5 Experimental Results

The experimental results were obtained using a laboratory prototype* of the receiver system in Figure 9.11, using the circuit components shown in Figure 9.13 to represent the antennas and propagation link. The delay line was manufactured on Y-cut quartz using the techniques described in Chapter 6. The ends of the crystal were coated with black wax to reduce the reflections from the crystal edges, but no treatment for volume modes was considered necessary. A typical delay line with all transducers present is shown in Figure 9.4(a). One advantage inherent in one-port devices which is obvious from the photograph of the mounted crystal, is the absence of any necessity to attempt to shield any of the transducers from one another - one of the most persistent problems in two-port device mounting.

A standard transducer pattern was modified by severing the fingers of selected transducers to produce the effective pattern of 10000000011010011. This pattern was arbitrarily selected as being a fairly representative response which would illustrate the effect of pulse-spreading on both succeeding '1's and '0's.

The DC output response obtained using this system by varying the effective matched filter delay setting is shown in Figure 9.16. The results show good agreement with the curve predicted in Figure 9.15 with very similar degrees of pulse overlap. The curve does not

---

* See footnote in Section 9.3.3.

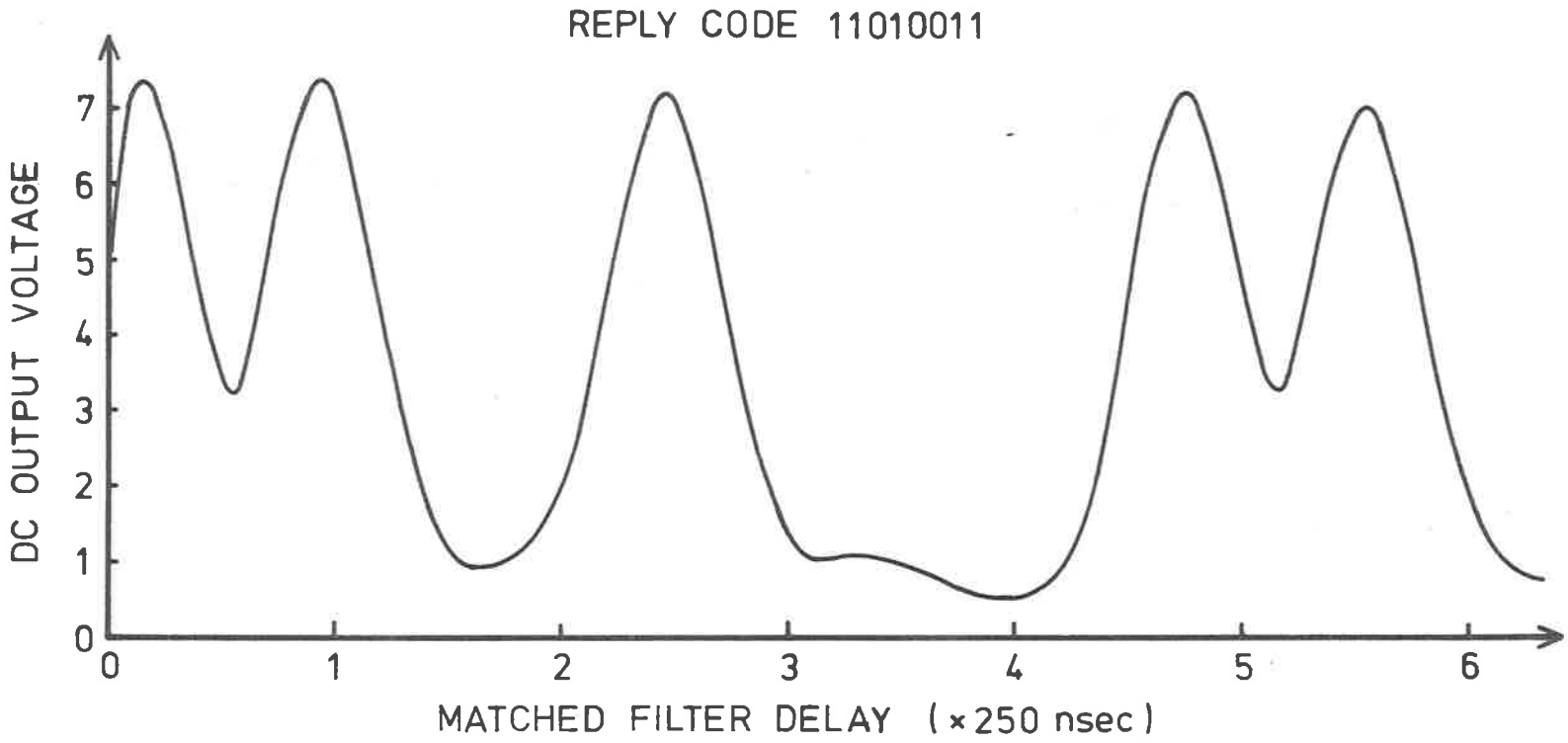


Figure 9.16 Experimental output curve obtained with the prototype receiver system operating under the same conditions as assumed for Figure 9.15.

immediately fall to zero following a pulse due to the exponential decay following excitation of the tuned circuits, and this limits the minimum acceptable pulse spacing as will be discussed in the next chapter. The greater irregularity in the observed peak heights (allowing for the overlap of successive '1's) in comparison with the theoretical result is apparently due to the presence of second-order effects in the practical devices. Volume waves were discounted because impulse-tests on several lines, using the equipment in Figures 6.11 showed no sign of volume wave energy reaching the output in two-port configuration, except for a small amount at third harmonic frequency which would be rejected by the matched filter in the experimental receiver. The significance of second-order effects is discussed further in the next chapter.

### 9.3.6 Performance Under Adverse Conditions

These experimental results show that clearly detectable coded responses can be obtained from one-port delay lines over a simulated propagation link of moderate insertion loss under ideal conditions. An important question in evaluating the potential utility of a system such as this is the extent to which the coded receiver input is affected by additional distortion in the propagation link to the label.

The source of variation in the system behaviour considered to be most likely is variation in the antenna patterns due to the incursion of foreign objects into the near-field of either the transmitting or transponding antennas. This is considered highly probable if the coded line is used as a transferable label to be fixed to various objects as required. Apart from any screening of the energy propagating to and from the label, the close proximity of a conducting object would result in severe detuning of the simple inductive loop antenna

which is assumed in the system simulation above.

A series of runs were conducted using the computer model to study the effect of variation of the effective Q-factor and resonant frequency of the antenna tuning circuits and a typical system output for a run with the transponding antenna detuned to resonate at 40 MHz as shown in Figure 9.17, instead of 50 MHz (still Q=5) is shown in Figure 9.18. The relative system output is reduced by 13 dB as could be expected, but less expected is the fact that the intersymbol interference is also noticeably reduced as indicated by the narrower peaks in the curve. The general conclusion of this study was that, for any variation in the reactive antenna equivalent circuit values, the insertion loss of the line increased and the pulse overlap reduced. The explanation appears to lie in the fact that in any detuning, the centre frequency shift is more important than the slight change in Q-factor of that particular resonant circuit. The only way the pulse overlap, and hence the code detectability could be made worse was by increasing the Q-factor of one of the tuned circuits without changing the resonant frequency, which is considered unlikely to occur due to external interference.

The general trend of these conclusions was verified by some representative experimental runs on the laboratory bench. The experimental output obtained under the same conditions as assumed for Figure 9.18 is shown in Figure 9.19 and apart from different scales good agreement can be seen.

A further point revealed by the computer studies is that the group delay in signal transmission through the resonant circuits varies when the equivalent circuit parameters are altered. This result is observed as a relative horizontal shift of the output response curve. The effective envelope delay per resonant circuit

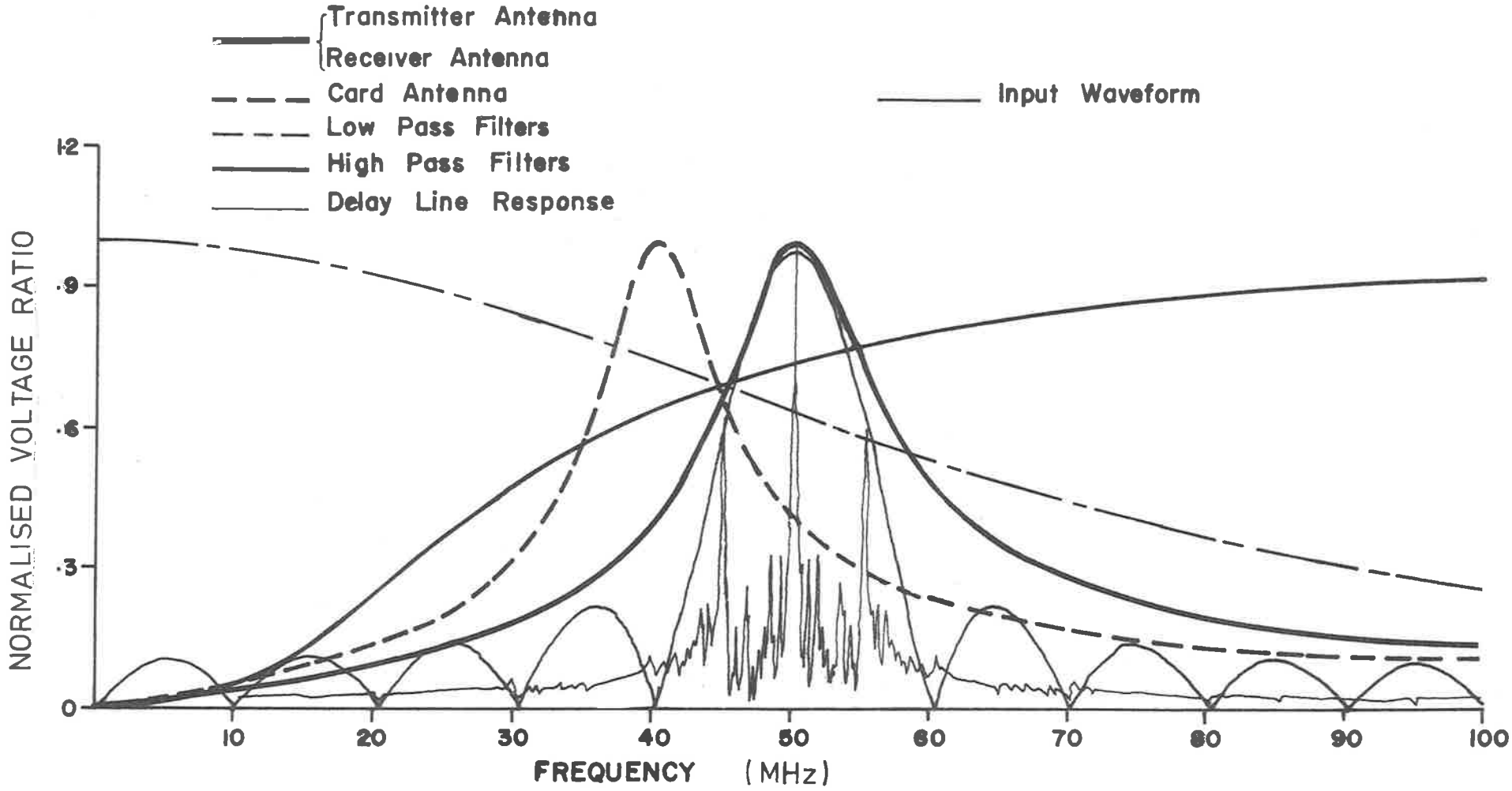


Figure 9.17 The frequency functions generated in the system simulation program INTER in the simulation run which produced the output curve in Figure 9.18. Note the detuning of the delay line antenna to 40 MHz.

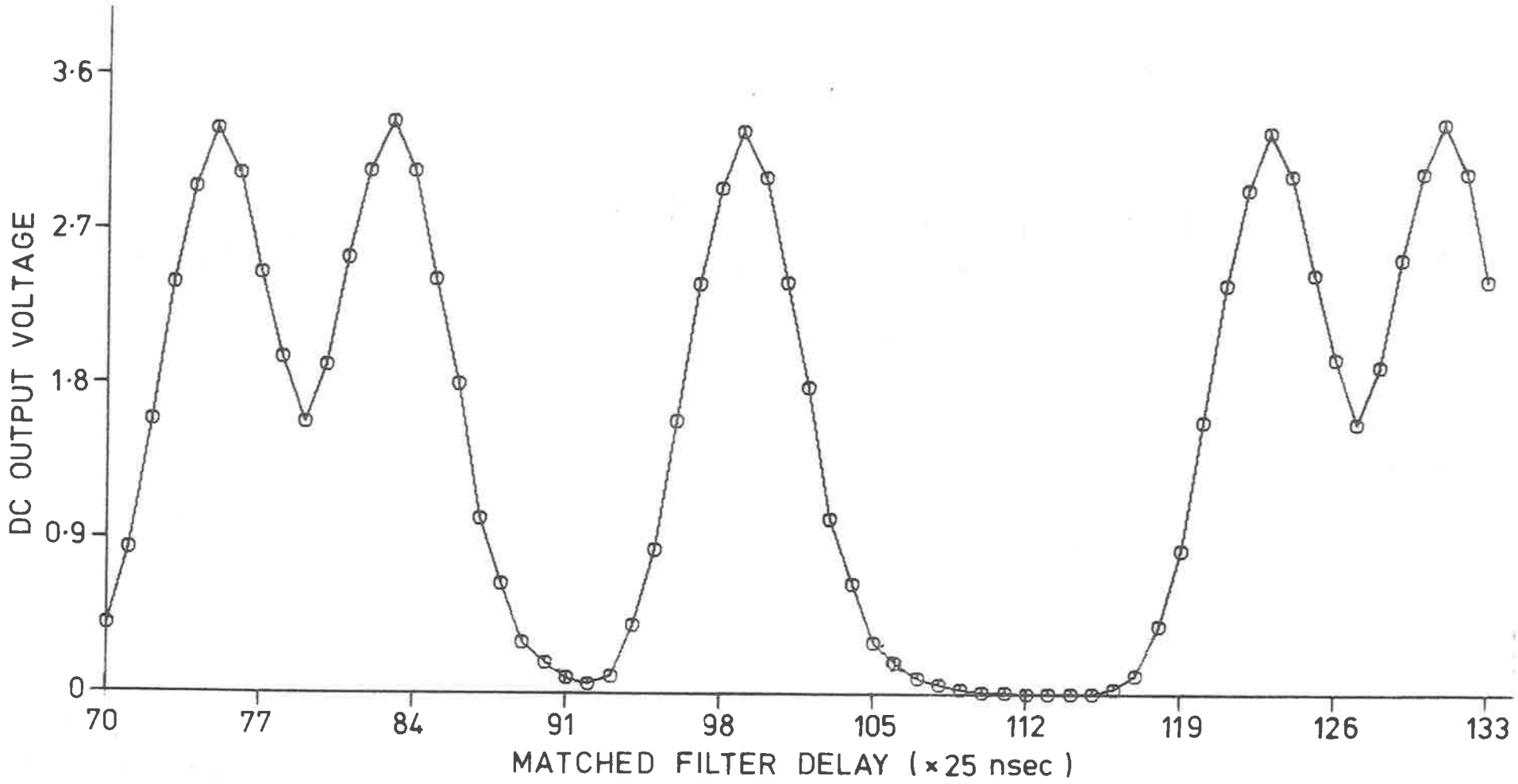


Figure 9.18 Computed system output for the same delay line as in Figure 9.16, but with the mistuned delay line antenna shown in Figure 9.17. The output voltage is referred to the same reference level as Figure 9.15.

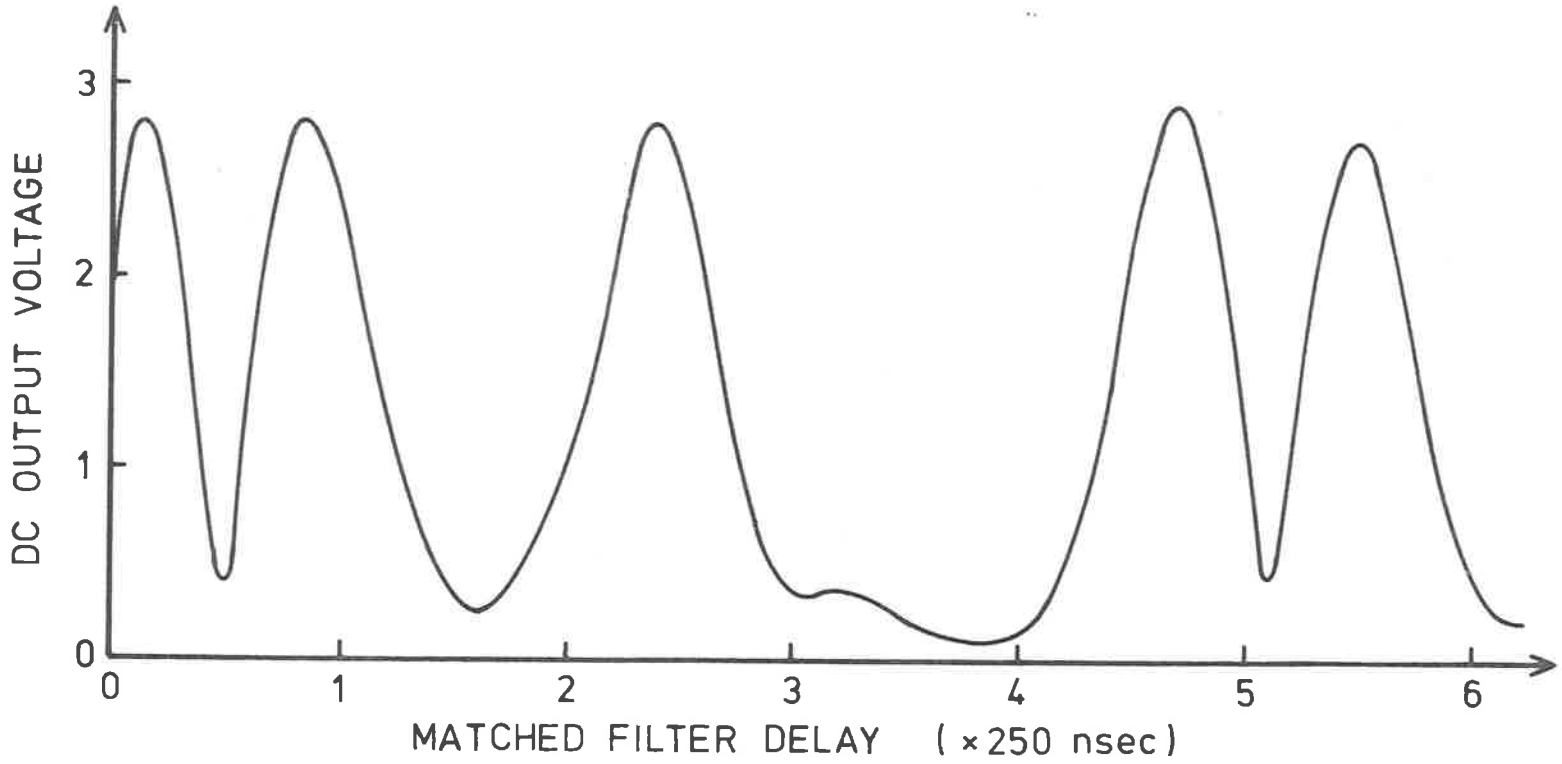


Figure 9.19 Experimental output curve obtained with a simulated mistuned delay line antenna as described in Figure 9.17. The output voltage is referred to the same reference level as in Figure 9.16.

was determined from computer studies to be approximately 24 nsec which agrees well with the figure of $Q/(4f_o)$ = 25 nsec obtained by the author from the theory of simple resonant circuits. Since the received signal passes through each resonant circuit twice the delay variation due to any detuning can be quite significant and creates a problem in determining the correct delays for the matched filters. Extending the general conclusion reached above, it appears that the group delay is never increased due to antenna detuning, and in a practical system design it would seem sensible to anticipate some detuning and set the matched filter delays slightly ahead of the optimum position to minimise the effects of detuning.

### 9.3.7 Conclusions

In this chapter the behaviour of simple delay lines connected as one-port devices has been shown to be adequately described by the theory of Chapters 3,4 and 7. A simple prototype delay line interrogation system was simulated both on a computer and in the laboratory; the resulting output waveforms of this system demonstrate the feasibility of using surface-wave devices with inter-digital transducers to generate identifiable digitally coded time domain responses.

The paramaters of this experimental system, such as the number of transducer fingers and the antenna bandwidth etc., were selected largely on the basis of intuition, and the results achieved were quite gratifying. An obvious question is what parameters determine the minimum acceptable transducer spacing i.e. what is the maximum bit density we can achieve on the substrate for a given available operating bandwidth? The lines observed had a maximum of 9 transducers spread over 17 possible locations on the substrate: another important question is what determines the upper limit on the

number of transducers which may be employed i.e. the maximum number of bits in the code? These and related questions are addressed in the next chapter.

# CHAPTER 10

# LIMITATIONS OF TIME DOMAIN CODED SYSTEMS

## 10.0 Introduction

In any practical delay line labelling scheme where the label is to be attached to diverse objects physically remote from the interrogation unit, a large variation in the received signal strength can be expected. This makes the problem of reliable decoding of the received signal considerably more difficult.

When the received signal is very weak, our ability to decode it will be limited by the ambient or receiver self-noise. This was the situation assumed to exist in the last chapter, because the requirement to detect weak signals in noise will dominate the form the receiver will take. The actual signal-to-noise ratios achieved in practice, and hence the minimum possible error rate, will be determined by the exigencies of the particular application in hand. In this study the form of the receiver is considered to be of interest only for the way in which it affects our ability to decode the waveforms generated by the interdigital transducers employed on the surface-wave delay lines.

When a strong response is applied to the input of the receiver, the decoding is not limited by noise, but by the appearance of undesired energy in the zero positions in the code. The major sources of trouble are the overlap of the individual reply pulses, and the regeneration and reflection of signals within the delay line, giving rise to spurious output pulses. These phenomena impose limitations on the closeness of the transducer spacing and the number, and timing, of the transducers which can be employed in practice, and an investigation of these limitations is reported in this chapter.

## 10.1 Output Pulse Spreading

The presence of narrow band-pass filters in the signal path means that each individual reply pulse will have a tail, which decays exponentially with time. At high signal levels this relatively small tail will exceed the receiver threshold and result in an automated detector recording '1's in all following bit positions regardless of the actual code present. The most obvious solution is to use an automatic gain control, actuated by the largest received pulse, to reduce the receiver gain. However, the presence of the pulse tail will still raise the effective noise level in the '0' positions, requiring adjustment of the detector threshold and increasing the error-rate of the detector.

This problem becomes quite severe when the transducers must be spaced as closely as possible, and we now look at the basic factors contributing to the duration of the pulses reaching the receiver.

### 10.1.1 Receiver Input Waveform

The output waveform of a tuned one-port device (neglecting for the moment the transmitter antenna) is given by Equation(9.1),and typical component waveforms are shown in Figure 9.2. The significant feature to be observed here is that the transmitter pulse and radiation conductance waveforms may be regarded as being effectively of finite duration*, whereas the circuit response extends to infinity.

If the transmitter pulse has duration T and the time conductance g(t) has duration 2T, then 3T after its commencement the output response will be determined solely by the tuned circuit decay. The relative decay rates for different circuit Q values have been computed using the waveforms in Figure 9.2, by means of Equation(9.1),and the results are shown in Figure 10.1. The response for Q=1 shows the

---

* The presence of the $|\omega|$-factor in the conductance formula means that this is not strictly true, but the rate of decay of the tails is sufficient to justify this approximation.

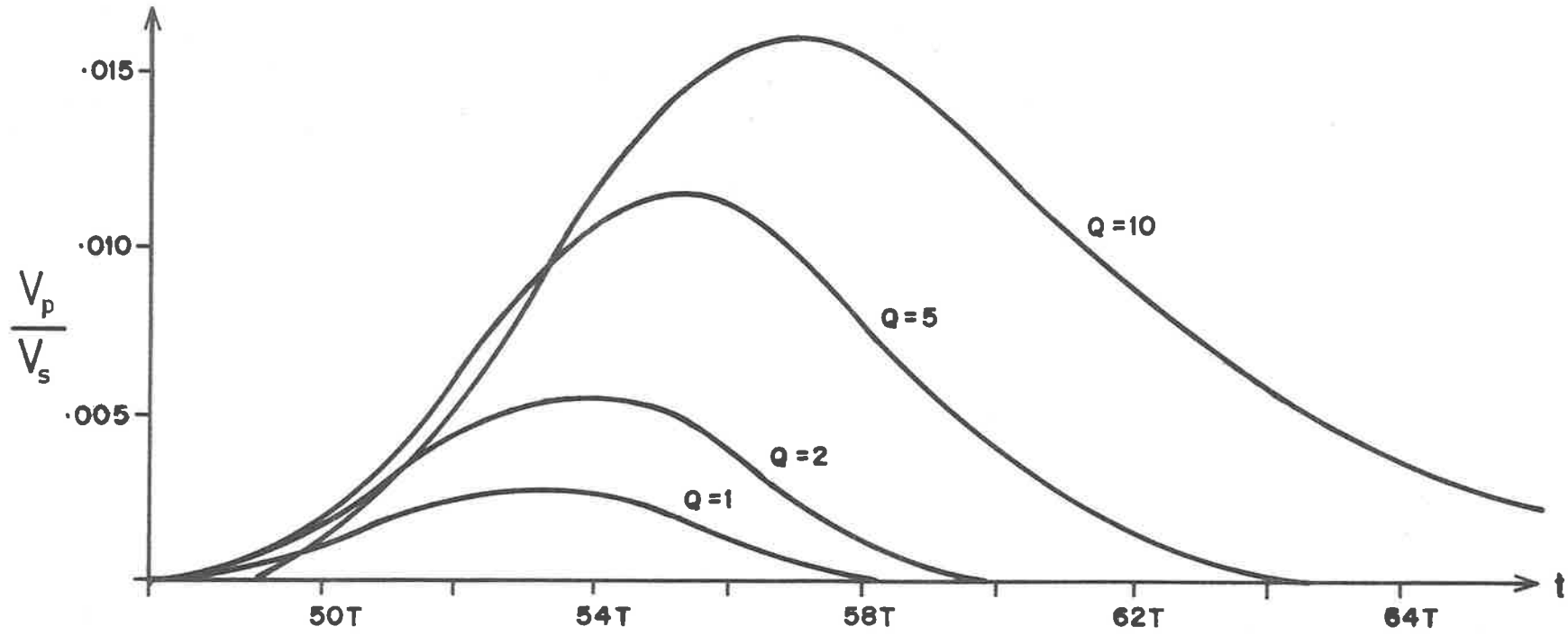


Figure 10.1 Primary response pulse envelopes predicted by the computer model for different Q-values in the transducer tuning. The transducer separation is 50 wavelengths at the synchronous frequency.

basic line response, determined by the convolution of the input voltage and the 2-transducer impulse response. The effect of increasing the Q of the circuit tuning the transducer static capacitance is clearly demonstrated: the insertion loss is reduced, but the overall pulse-width, and the envelope delay increase markedly.

An experimental two-port device with tuned input and output circuits to simulate a one-port structure (as described in Section 9.2.1)was used to obtain the waveforms shown in Figure 10.2, using the apparatus in Figure 6.9. Only the envelope of the output waveform is shown because the gating signal determining the transmitter pulse-length was not phase-synchronised with the RF carrier frequency. The waveform shown corresponds to an 01010 response code for transducers with dimensions and spacing identical to those used in the prototype system in Section 9.3. The detector would examine the signal level at the mid-point of the horizontal graticule to determine the presence or absence of the middle bit in this reply code, and it is apparent that the signal level at this position, resulting from overlap by the preceding pulse, rises significantly as the circuit Q-value is increased.

The good agreement between these results and the computer predictions gives reason for confidence in the latter, and in the next section the computer model is used to explore the dependence of pulse length upon the relevant parameters.

### 10.1.2 Discrimination Ratio

Since it is difficult to justify the selection of any particular level of pulse overlap as being universally acceptable, the computer model was employed to generate a set of curves describing the degree of overlap for various combinations of system parameters.

The results are expressed in terms of the discrimination

(a)

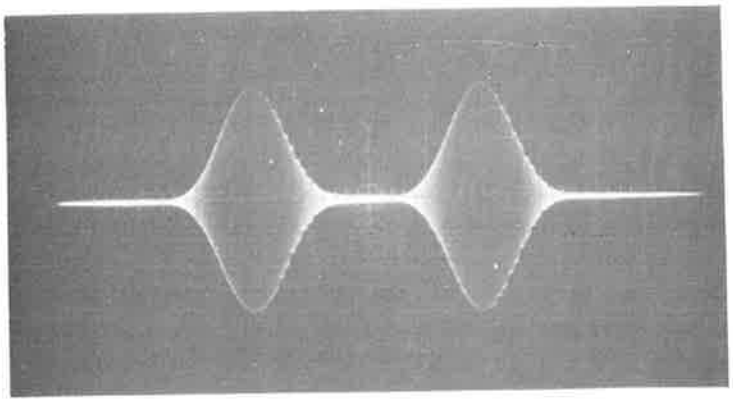

(b)

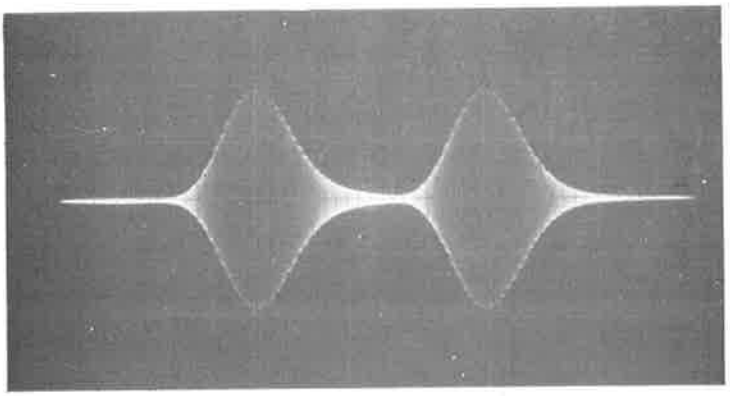

(c)

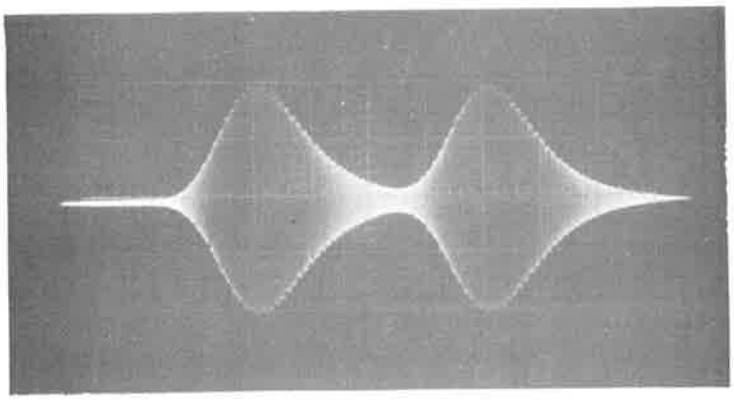

**Figure 10.2** Experimentally observed wave-forms corresponding to a one-port device with output response code 01010, and with tuned circuit parameters (a) Q=2, (b) Q=5, and (c) Q=10. Horizontal scale 100 μsec/cm; vertical amplitudes not to scale - pulses normalised to 4 cm peak to peak.

ratio D, which is defined as,

$$D = \frac{\text{Height of a single pulse}}{\text{Height of same pulse at next bit position}} \qquad (10.1)$$

To reduce the number of variables to be considered the results have been plotted in terms of the convenient dimensionless ratios,

$$T_L = \frac{\text{Pulse Length (cycles)}}{N} \qquad (10.2)$$

$$T_S = \frac{\text{Transducer Spacing (wavelengths)}}{N} \qquad (10.3)$$

$$T_Q = \frac{\text{Tuned Circuit Q-factor}}{N} \qquad (10.4)$$

where N is the transducer length in wavelengths at the synchronous frequency. This particular choice of ratios permits the designer to select his transducer length, after consideration of the required insertion loss (to be discussed in the next section) and the available bandwidth (which will be determined by the available spectrum allocation), and then select the system parameters necessary to achieve the required discrimination ratio.

The resulting curves, for different values of transmitter pulse-length $T_L$, are given in Figures 10.3, 10.4 and 10.5. The effect of increasing $T_L$ is roughly to shift the curves to the right, indicating a need for greater transducer spacing as could be expected. In the top right area of the graphs the curves for constant $T_Q$ become asymptotic to straight lines, verifying the previous assertion that the exponential decay term dominates for large transducer spacing.

The discrimination ratio D increases slightly as $T_L$ is reduced, but for values of $T_L < 1.0$ the 2-transducer insertion loss goes up rapidly, so it would seem logical to operate with $T_L = 1.0$. In the present study a discrimination ratio of 20 dB was considered desirable, and this would mean working on a horizontal operating locus in Figure 10.4. The minimum acceptable $T_Q$ value will be determined by insertion loss considerations, and the minimum possible transducer

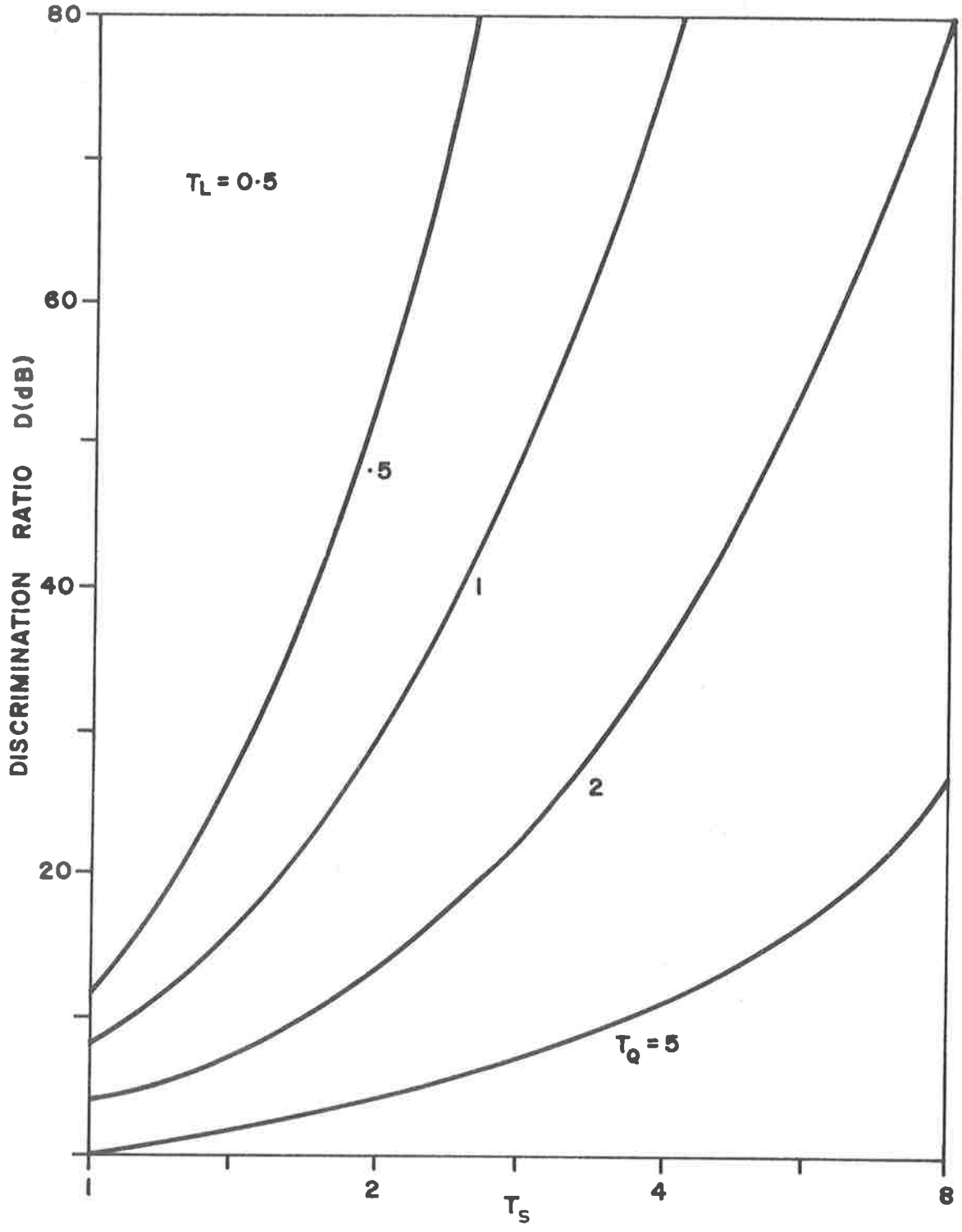


Figure 10.3 Computed contours showing the dependence of the discrimination ratio D on the parameter $T_Q$ and $T_S$ for $T_L = 0.5$. (The parameters are defined in the text.)

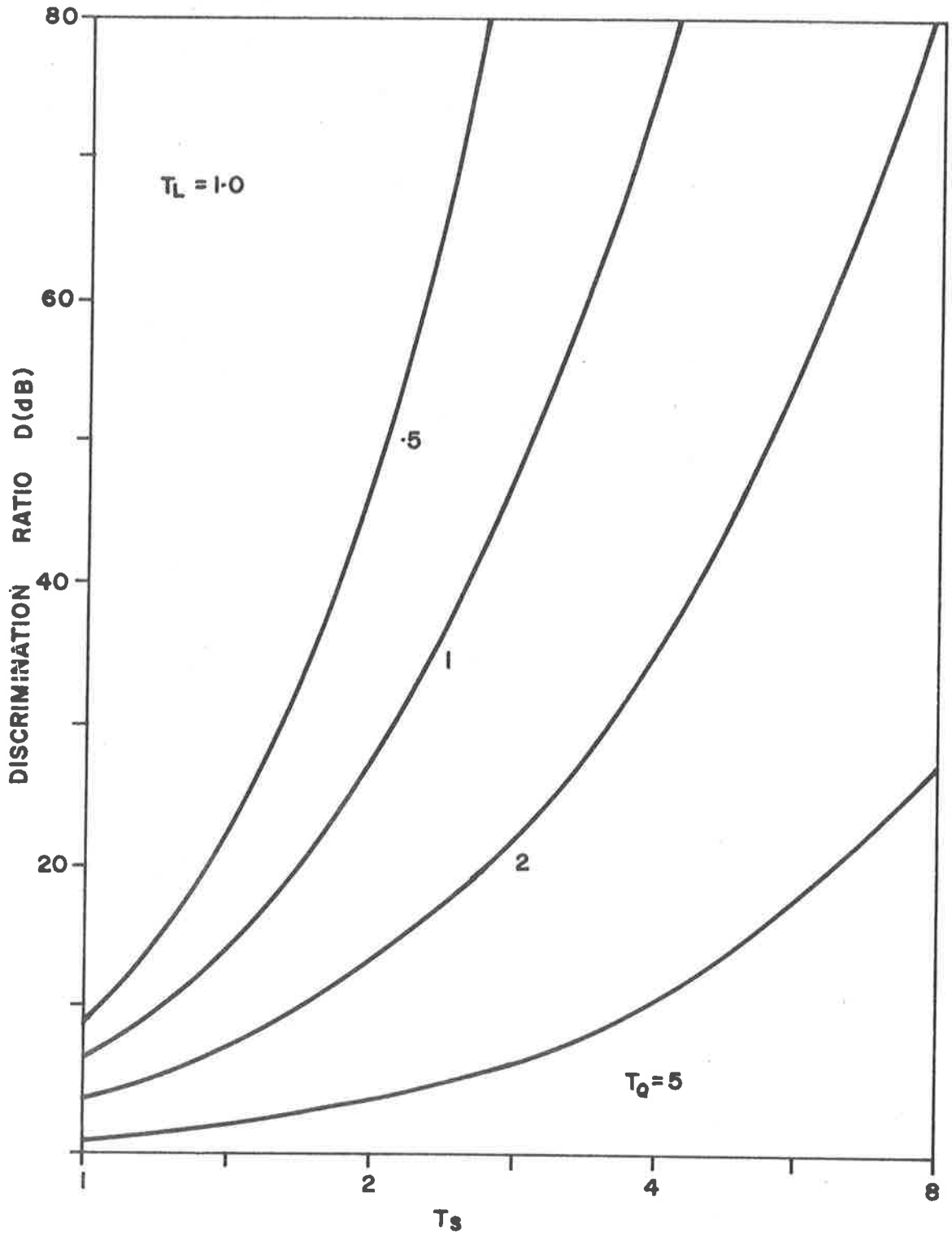


Figure 10.4 Contours showing the dependence of the discrimination ratio D on the parameters $T_Q$ and $T_S$ for $T_L$ = 1.0.

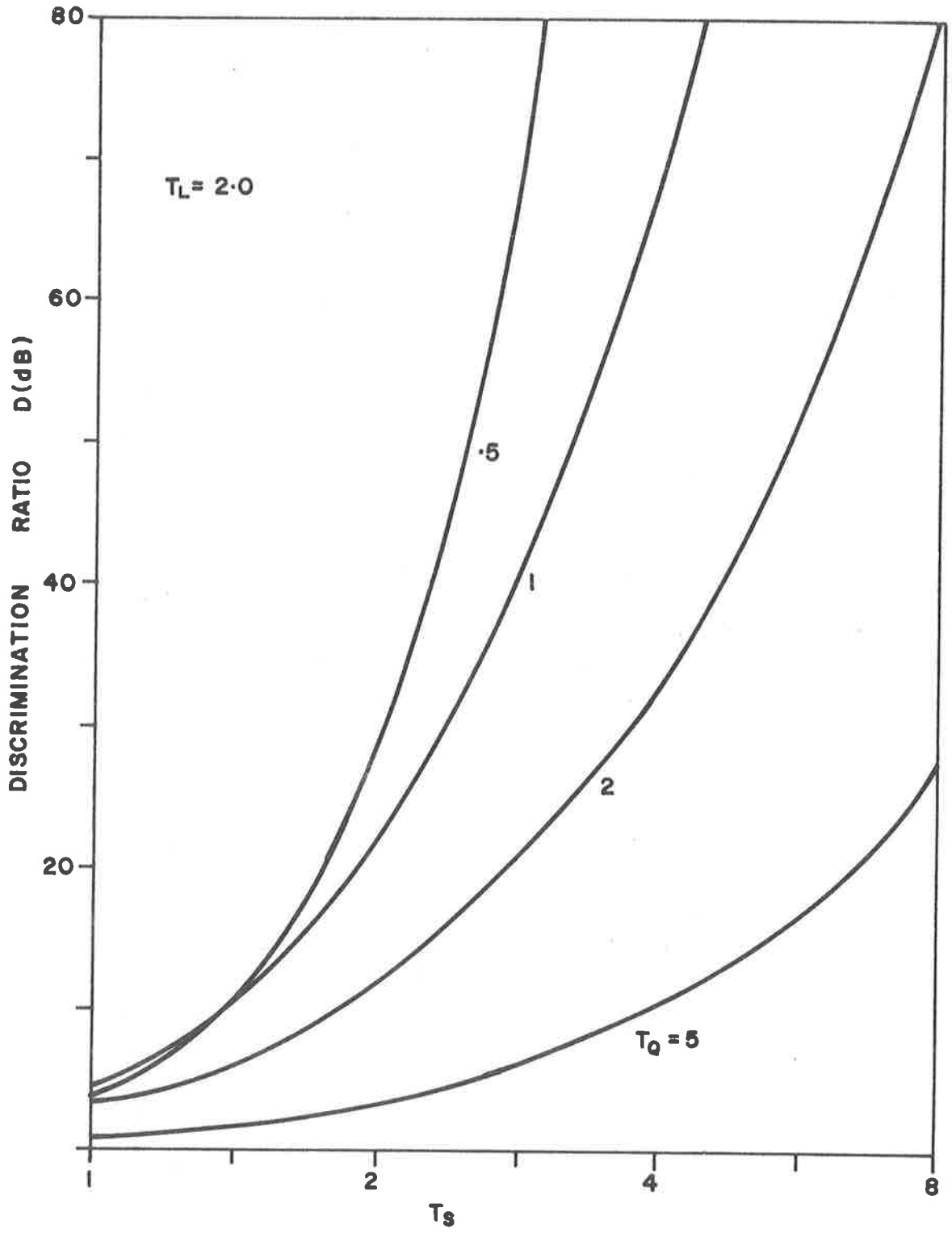


Figure 10.5 Contours showing the dependence of the discrimination ratio D on the parameters $T_Q$ and $T_S$ for $T_L$ = 2.0.

spacing can then be determined from the graph.

For example, the prototype system described in the last chapter (designed before these curves were available) had the parameter values $T_L = 1.25$, $T_S = 2.5$ and $T_Q = 1.25$, yielding an interpolated value of the discrimination ratio of 27 dB, which is in substantial agreement with the observed behaviour, when allowance is made for the action of the coherent detector.

It should be noted here that the effect of envelope delay variation with variation in the tuned circuit Q-factor has been neglected. The distance between successive bits remains unaltered, and it is assumed that the detector output for the single reference pulse has been adjusted for the maximum.

### 10.1.3 Insertion Loss

In the previous section reference was made to the relation between the number of transducer fingers and the insertion loss of the coded delay line. The actual insertion loss of any practical device in a particular circuit may be computed accurately using the computer model of Chapter 5, but this requires a complete specification of the transducer geometry. For preliminary discussions of various coding systems, it was considered desirable to obtain a graphical representation of the relationship between transducer length, the material constants and the tuned circuit Q-factor for use in conjunction with the discrimination ratio curves. The required curves were derived as follows.

Following the approach of Smith et al.[47,48] in regarding the interdigital transducer as a lossless 3-port device with one electrical and two acoustic ports, we may, by appropriate choice of impedance levels and reference planes, represent this device by the equivalent circuit shown in Figure 10.6. (This equivalent circuit is only valid for a single frequency - chosen here to be the synchronous

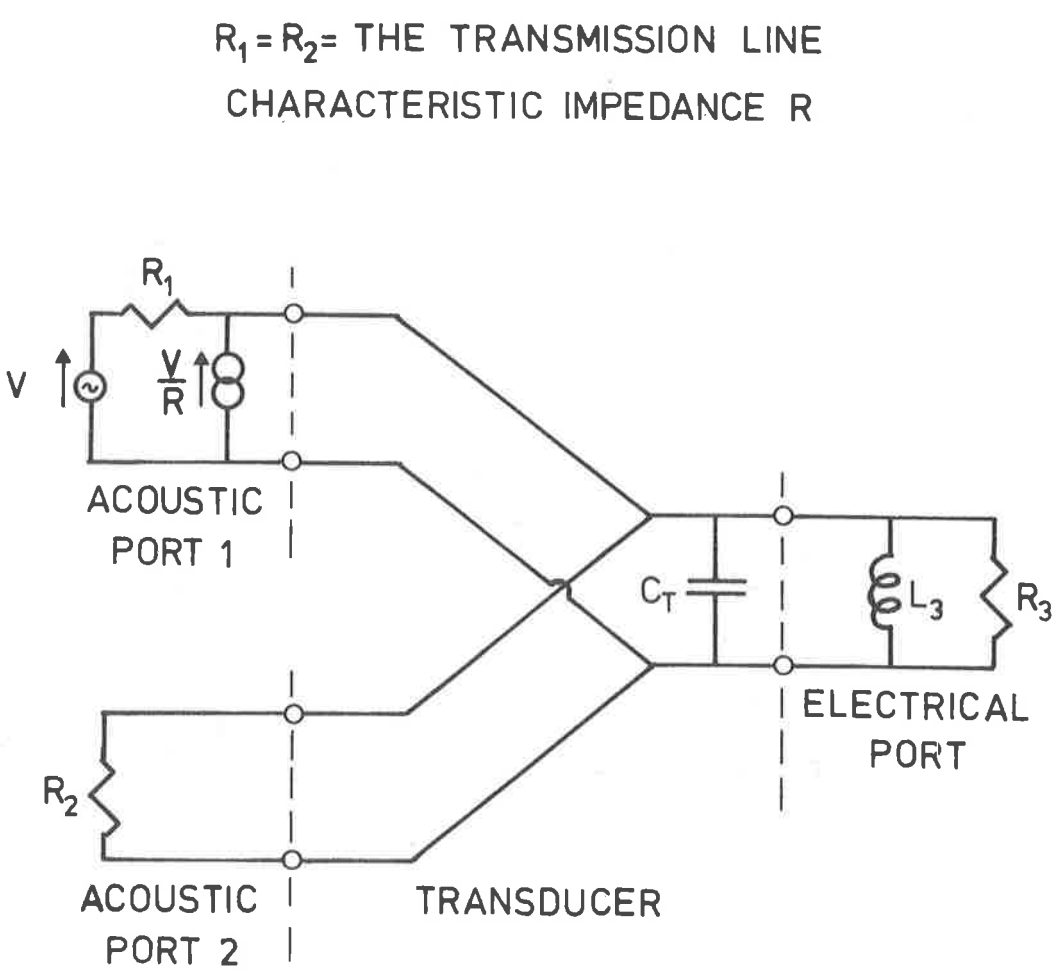


Figure 10.6 Single-frequency equivalent circuit for a passive lossless three-port transducer with external tuning and damping elements $L_3$ and $R_3$, and excitation at acoustic port 1.

frequency - and for lossless operation of the device i.e. when uncoupled to any other acoustic modes.) The transducer is shown with a shunt tuning inductor L chosen to resonate the static capacitance $C_T$, and with an external load resistance $R_L$. The device is assumed to be excited by an incident CW signal of amplitude V at acoustic port 1, and we wish to determine the relative fractions of the incident power P which are reflected back from port 1, $P_1$, transmitted through port 2, $P_2$, and delivered to $R_L$ at port 3, $P_3$.

The relative power levels are given by the powers dissipated in the resistors $R_1$, $R_2$ and $R_3$ respectively, and we obtain

Reflected Power

$$P_1 = \frac{T^2}{(1+T)^2} \tag{10.5}$$

Transmitted Power

$$P_2 = \frac{1}{(1+T)^2} \tag{10.6}$$

Converted Power

$$P_3 = \frac{2T}{(1+T)^2} \tag{10.7}$$

where

$$T = \frac{T_Q}{T_m^2} \tag{10.8}$$

$T_Q$ is the dimensionless transducer electrical Q-factor as defined previously, and $T_M$ is the dimensionless material coupling factor

$$T_M = \frac{Q_m}{N} \tag{10.9}$$

where $Q_m$ is the material coupling Q-factor[48]. Since the passive three-port structure is reciprocal, the conversion loss for a signal passing through a two-port delay line employing two identical transducers, both tuned to the same value of $T_Q$, is simply double that predicted by Equation (10.7). This expression is shown plotted on a log. scale against $T_M$, for various values of $T_Q$, in Figure 10.7.

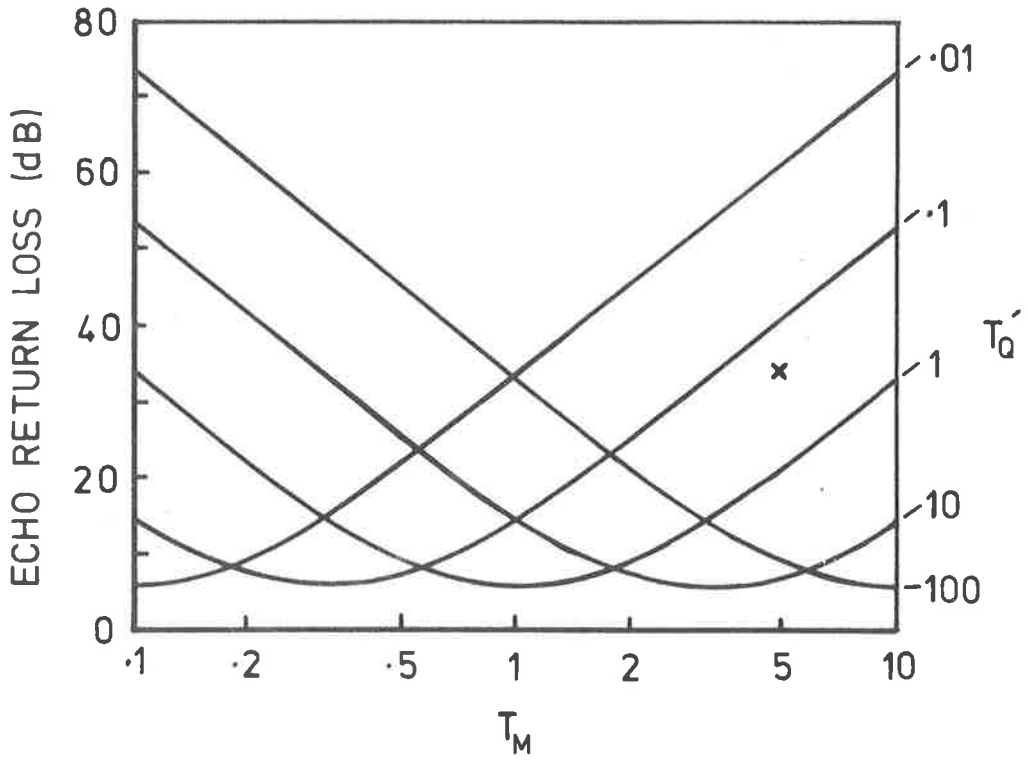


Figure 10.7 Graph showing the single-pass insertion loss of a two transducer delay line as a function of the dimensionless coupling factor $T_M$ and the dimensionless circuit tuning factor $T_Q$.

For this graph to be of any use we must be able to relate the single-pass insertion loss to the situation where each transducer is shunted by (M-1) other transducers, and also by a non-negligible amount of stray capacitance $C_S = SC_T$. In this case the return loss is given by Figure 10.7, if we use the modified parameter

$$T'_Q = \frac{2}{(M+S)} \quad T_Q \quad . \tag{10.10}$$

To illustrate the use of this graph, in the experimental coding system we had the parameter values $Q_m$ = 20, N=4, M=9, S=3, yielding values of $T_M$ = 5 and $T'_Q$ = 0.2 and we can interpolate from the graph to obtain the return loss figure of 35 dB.

These expressions have been derived assuming operation at a single frequency, and really only apply when the pulse length is much greater than the propagation time across the transducers. However they have the merit that they can provide approximate initial estimates of the return loss for moderate length pulses, in any proposed system, without the need for detailed analysis.

### 10.1.4 Receiver Output Waveform

In the preceding sections the degree of pulse overlap was estimated for the primary response of a tuned one-port delay line. This waveform would be relevant to a simple system with a broadband transmit-receive antenna, and a simple envelope detector in the receiver. For more elaborate types of receiver, additional pulse-spreading may occur as a result of the receiver action.

In the case of a matched filter receiver the output as a function of filter delay $\tau$, for an input waveform $v_1(t)$, is given by

$$v_f(\tau) = \int_o^T v_1(t) v_1(t + \tau - T)\, dt \qquad 0<\tau<2T \tag{10.11}$$

where T is selected to satisfy

$$v_1(t) \approx 0 \qquad \begin{cases} t \leqslant 0 \\ t \geqslant T \end{cases}$$

This output will have twice the duration of the input signal, with a maximum at $\tau=T$, resulting in a significant increase in overlap of the coded pulses. It is also interesting to note that this output pulse shape $v_f(\tau)$ is symmetric with respect to the peak, so that the pulse tails will overlap both leading and trailing zeros in the code.

The gated coherent detector used in the prototype system has slightly better performance than the matched filter in this respect. By correlating the input waveform with a shorter rectangular function, the pulse-spreading is reduced and the overlap of leading pulses is not present: this improvement, however, is associated with a slight drop in the signal-to-noise ratio observed at the receiver output [150].

### 10.1.5 Optimum Waveform Selection

This discussion of pulse shapes leads naturally to the question, what transducer geometry will minimise the transducer spacing? There is no general answer to this question because as has already been shown, the output response waveform depends upon all the components in the coding system. However a few general conclusions may be obtained if we restrict the discussion to systems using tuned one-port delay lines with uniform interdigital transducers, of the type employed in this study.

The first conclusion is that the transducer geometry has only a minor effect upon the final pulse shape, as by the Central-limit Theorem as applied to Fourier theory[151], a waveform derived by the convolution of multiple waveforms tends to Gaussian in shape*. In our practical system, the output waveform is derived from the convolution of the transmitter pulse with the antenna impulse response (twice), with the delay line tuning impulse response (twice) and with the single transducer sensitivity function (twice). And if the receiver uses

---

* The theorem is stated for non-negative waveforms. Here we are dealing with narrow-band functions with an envelope which is essentially non-negative.

matched filtering this output is also effectively correlated with a single reversed output pulse. The rapid convergence of the output waveform to the Gaussian shape is clearly demonstrated by the experimental waveforms in Figure 10.2 *.

This is a rather fortunate result as we know from the Uncertainty Principle[152] that for pulses whose spectra are restricted to a fixed half-power bandwidth, the pulse with the shortest width in the time domain is one having a Gaussian shape (in both time and frequency domains). So if the measure of pulse and spectrum width used in the derivation of the Uncertainty Principle (Equation(10.12)) is accepted, the system we have been observing will produce optimally short time domain pulses for the available bandwidth.

This leads to the well known radar designers' maxim, that to minimise the time domain pulse length, one must use pulses with the greatest possible bandwidth. Since both the uniform interdigital transducers and the tuned circuits suffer an increase in insertion loss when the bandwidth must be increased, it is a relatively simple matter to show that the system design is optimum when the time domain dispersion of each system component is made equal to a constant $\sigma_\tau^2$. The overall time domain dispersion is then given by

$$\sigma^2 = n\sigma_\tau^2$$

where the dispersion of a time waveform k is defined as

$$\sigma_k^2 = \int_{-\infty}^{\infty} (t - \eta_k)^2 f_k(t)\, dt \quad , \tag{10.12}$$

$\eta_k$ is the waveform mean, given by

$$\eta_k = \int_{-\infty}^{\infty} t\, f_k(t)\, dt, \tag{10.13}$$

and n is the number of component stages in the system.

## 10.2 Regeneration

Another phenomenon which can result in errors in decoding the

---

* For high-Q circuits the casual form of the Central-limit Theorem is more accurate - Ref. 85, page 234.

received waveform is the appearance of regenerated or second-order pulses in the line response. These were predicted by the theory in Chapter 7 and under certain conditions may approach the primary response in amplitude.

A related phenomemon, to be discussed in the next section, is that of reflection from interdigital transducers, and in an effort to avoid the ambiguity currently associated with the usage of these terms in the literature, the terms will be defined here as follows. Regeneration is here taken to describe the reconversion of energy from electrical to acoustic form, following the conversion from acoustic to electric form on detection of a surface wave by a transducer. Thus regeneration will take place at the receiving transducer and any other parallel-connected transducers.

The term reflection is reserved for the reflection of surface-wave energy by a transducer due to the electrical and mechanical discontinuities created by the presence of the electrodes on the surface i.e. the reflection coefficient of a transducer under this definition is independent of the electrical loading of that transducer. These somewhat unconventional definitions were adopted to avoid a number of paradoxes unique to the discussion of one-port devices, and conform naturally with the admittance matrix analysis of these devices.

The peak second-order signal levels are dependent upon both the insertion loss of the transducers, and the code pattern of the transducers present, and these aspects will be discussed separately.

### 10.2.1 Regenerated Pulse Waveform

An expression for the complete second-order response of a coded one-port structure was derived in terms of the single transducer impedances in Chapter 7, and the result is reproduced here for convenience,

$$v_{(t)} = \frac{2\omega_o C_T}{M^2 Q} \; v_s(t) * z_{c1}(t) * g(t) * z_{c1}(t) * g(t) * z_{c1}(t) * k(t) * k(t) \quad (10.14)$$

The shape of the individual pulses will be approximately Gaussian for the reasons outlined above, but the time dispersion of the pulses will be nearly double that of the primary response pulses described previously.

### 10.2.2 Regenerated Pulse Code

The second-order response, characterised by Equation (10.14), may be interpreted in the same manner as the primary response, in that it will consist of a sequence of pulses of identical shape and with amplitudes determined in magnitude and delay by the convolution product

$$\begin{aligned} s(t) &= k(t) * k(t) \\ &= \int_{-\infty}^{\infty} \sum_{i=0}^{N-1} K_i \, \delta(x - i\tau) \sum_{j=0}^{N-1} K_j \delta(t-x-j\tau) \, dx \\ &= \sum_{n=0}^{2(N-1)} S_n \delta(t - n\tau) \end{aligned} \qquad (10.15)$$

where

$$S_n = \begin{cases} \sum_{i=0}^{n} K_i \, K_{n-i} & 0 \leqslant n \leqslant N-1 \\ \sum_{i=n-(N-1)}^{N-1} K_i \, K_{n-i} & N \leqslant n \leqslant 2(N-1) \end{cases} \qquad (10.16)$$

We shall call s(t) the regenerated code, and it consists of the sequence of equi-spaced δ-functions with amplitudes $S_n$.

The response $v_2(t)$ is superimposed on the desired code in $v_1(t)$ and may result in a detector error if a regenerated pulse of significant amplitude takes the place of a '0' in the primary response. This process is aggravated by the fact that $v_1(t)$ and $v_2(t)$ are in antiphase (Equation 10.17) because this means regenerated pulses added to adjacent primary code '1's diminish the amplitude of these pulses, reducing the discrimination ratio still further.

An example of this type of interference has been selected from the code generating program for simple binary codes (which identifies the location of zero-fill occurrences) for the purpose of illustration.

The transducer pattern in this case is 101101 and the responses are

| TIME POSITION | 0 | 1 | 2 | 3 | 4 | 5 | 6 | 7 | 8 | 9 | 10 |
|---|---|---|---|---|---|---|---|---|---|---|---|
| PRIMARY RESPONSE | 2 | 1 | 2 | 2 | 0 | 1 | - | - | - | - | - |
| SECONDARY RESPONSE | 4 | 4 | 9 | 12 | 8 | 12 | 6 | 4 | 4 | 0 | 1 |

The useful part of the primary response code is 12201 and it can be seen that there is a regenerated pulse with 8-units of amplitude in time position 4, while the immediately adjacent pulses will be reduced in amplitude by 12-unit regenerated pulses.

### 10.2.3 Relative Amplitude of the Regenerated Response

It is obvious in the above example that the relative levels of the primary and secondary responses will determine whether this interference is going to be significant, and we can rewrite Equation (10.14) to give the secondary response in terms of the primary response,

$$v_2(t) = -\frac{2}{M} \; v_1(t) * z_{c1}(t) * g(t) * k(t) \qquad (10.17)$$

The relative amplitude of $v_2(t)$ depends upon g(t), the circuit tuning factor Q, and the number of operating transducers M on the delay line.

The Q-dependence is obtained in the term $z_{c_1}(t)$, as at the centre frequency $Z_{c1}(\omega_o) = Q/\omega_o C_T$, from Equation (7.23). Hence attempts to increase the tuned-circuit Q-factor, in order to decrease the delay line return loss, will result in an increase in the level of the regenerated response relative to the primary response.

The dependence of the relative regenerated signal level upon the number of transducers in a particular code pattern is quite complicated, but bounds may be found for the signal levels as follows. The weakest response which one would wish to detect as a '1' in the primary code is a pulse with unit amplitude, and we would like an estimate of the maximum possible secondary response level, relative to this pulse height. The actual maximum secondary code level is

dependent on both M the number of transducers in use, and the particular code pattern in use. The maximum possible secondary response level, for codes of length N, will be generated by the pattern $A_1 = A_2 = \text{---} = A_N = 1$; this pattern does not generate any '0's in the reply code, but will still suffer from some degree of primary pulse cancellation. The results we obtain with this code will serve as an upper bound for the secondary pulse levels to be expected from more sparse patterns of length N.

By means of Equation (7.18) we find that the reply code coefficients will have the form

$$K_i = \begin{cases} \frac{N}{2} & i=0 \\ N-i & 1 \leqslant i \leqslant N-1 \end{cases} \qquad (10.18)$$

and on substituting in Equation (10.16) we obtain for the secondary response coefficients

$$S_n = \frac{n}{6}(n^2 - 6N_n + 6N^2 - 1), \quad 0 \leqslant n \leqslant N-1 \qquad (10.19)$$

The secondary code differs from the primary code in being an auto-convolution product, instead of being dependent on an autocorrelation function. In consequence of this the code coefficients do not normally form a symmetric set about $S_{N-1}$, and the position of the maximum value of $S_i$ is dependent upon the code coefficients $A_i$. For the particular case in hand it is apparent that the maximum value will occur for $n<N-1$, and a solution by approximate methods shows that for large values of N (>10 say) the value of i corresponding to the maximum coefficient is the nearest integer value to

$$i = (2-\sqrt{2})N \qquad (10.20)$$

The corresponding peak value of the secondary response, for increasing values of N, is asymptotic to

$$S_{max.} = \frac{2}{3}(\sqrt{2} - 1)N^3 \qquad (10.21)$$

The significance of this result is seen on substitution back into Equation (10.17) where we see that in the upper limit, for fixed transducer geometry and choice of substrate,

$$[v_2(t)]_{max} \quad \alpha \quad N^2 Qv_1(t) \tag{10.22}$$

The lower limit is obtained from consideration of the simplest possible one-port structure of length N, i.e. when $A_1 = A_N = 1$ and $A_i = 0$, $1<i<N$, when we find

$$[v_2(t)]_{max} \quad \alpha \quad Qv_1(t) \tag{10.23}$$

All simple binary coded lines will give responses falling between these limits, but Equation (10.22) makes it clear that in practice the interference level due to second-order or regenerated pulses will become significant in delay lines employing large numbers of transducers.

For the purpose of illustration the second-order responses for the delayed binary codes used in the experimental coding system, have been computed for the particular cases where only one zero appears in the reply code, and the results are given in Table 10.1. The worst case of zero-fill is in the last example where the zero in time position 16 is overlaid with a second-order pulse of 42-unit amplitude. Thus the second-order pulse height will equal or exceed the primary unit-pulse height if the delay line primary return loss is less than or equal to 32.5 dB at the synchronous frequency. As pointed out previously, the problem is somewhat worse than this in practice as the adjacent ones in the primary response will be reduced by the addition of the antiphase secondary pulses, reducing the discrimination ratio even further.

## 10.3 Reflection

In conventional usage the term reflection describes the total signal energy propagating back down the input signal transmission

TABLE 10.1: COMPUTED PRIMARY AND SECONDARY RESPONSES

FOR 8-BIT DELAYED BINARY CODES WITH ONE ZERO

TIME POSITIONS

| | 0 | 1 | 2 | 3 | 4 | 5 | 6 | 7 | 8 | 9 | 10 | 11 | 12 | 13 | 14 | 15 | 16 |
|---|---|---|---|---|---|---|---|---|---|---|---|---|---|---|---|---|---|
| A = | 1 | 0 | 0 | 0 | 0 | 0 | 0 | 0 | 0 | 0 | 1 | 1 | 1 | 1 | 1 | 1 | 1 |
| B = | 4 | 6 | 5 | 4 | 3 | 2 | 1 | 0 | 0 | 0 | 1 | 1 | 1 | 1 | 1 | 1 | 1 |
| C = | 16 | 48 | 76 | 92 | 97 | 92 | 78 | 56 | 35 | 20 | 18 | 24 | 31 | 38 | 44 | 48 | 50 |
| A = | 1 | 0 | 0 | 0 | 0 | 0 | 0 | 0 | 0 | 1 | 0 | 1 | 1 | 1 | 1 | 1 | 1 |
| B = | 4 | 5 | 5 | 4 | 3 | 2 | 1 | 1 | 0 | 1 | 0 | 1 | 1 | 1 | 1 | 1 | 1 |
| C = | 16 | 40 | 65 | 82 | 89 | 86 | 74 | 62 | 45 | 38 | 28 | 28 | 31 | 36 | 41 | 44 | 48 |
| A = | 1 | 0 | 0 | 0 | 0 | 0 | 0 | 0 | 0 | 1 | 1 | 0 | 1 | 1 | 1 | 1 | 1 |
| B = | 4 | 5 | 4 | 4 | 3 | 2 | 2 | 1 | 0 | 1 | 1 | 0 | 1 | 1 | 1 | 1 | 1 |
| C = | 16 | 40 | 57 | 72 | 80 | 78 | 76 | 68 | 51 | 44 | 42 | 32 | 32 | 36 | 37 | 42 | 46 |
| A = | 1 | 0 | 0 | 0 | 0 | 0 | 0 | 0 | 0 | 1 | 1 | 1 | 0 | 1 | 1 | 1 | 1 |
| B = | 4 | 5 | 4 | 3 | 3 | 3 | 2 | 1 | 0 | 1 | 1 | 1 | 0 | 1 | 1 | 1 | 1 |
| C = | 16 | 40 | 57 | 64 | 70 | 78 | 79 | 70 | 53 | 46 | 45 | 44 | 34 | 32 | 37 | 42 | 44 |
| A = | 1 | 0 | 0 | 0 | 0 | 0 | 0 | 0 | 0 | 1 | 1 | 1 | 1 | 0 | 1 | 1 | 1 |
| B = | 4 | 5 | 4 | 3 | 3 | 3 | 2 | 1 | 0 | 1 | 1 | 1 | 1 | 0 | 1 | 1 | 1 |
| C = | 16 | 40 | 57 | 64 | 70 | 78 | 79 | 70 | 53 | 46 | 45 | 44 | 42 | 34 | 35 | 40 | 44 |
| A = | 1 | 0 | 0 | 0 | 0 | 0 | 0 | 0 | 0 | 1 | 1 | 1 | 1 | 1 | 0 | 1 | 1 |
| B = | 4 | 5 | 4 | 4 | 3 | 2 | 2 | 1 | 0 | 1 | 1 | 1 | 1 | 1 | 0 | 1 | 1 |
| C = | 16 | 40 | 57 | 72 | 80 | 78 | 76 | 68 | 51 | 44 | 42 | 40 | 42 | 44 | 37 | 38 | 42 |
| A = | 1 | 0 | 0 | 0 | 0 | 0 | 0 | 0 | 0 | 1 | 1 | 1 | 1 | 1 | 1 | 0 | 1 |
| B = | 4 | 5 | 5 | 4 | 3 | 2 | 1 | 1 | 0 | 1 | 1 | 1 | 1 | 1 | 1 | 0 | 1 |
| C = | 16 | 40 | 65 | 82 | 89 | 86 | 74 | 62 | 45 | 38 | 36 | 38 | 41 | 44 | 47 | 40 | 40 |
| A = | 1 | 0 | 0 | 0 | 0 | 0 | 0 | 0 | 0 | 1 | 1 | 1 | 1 | 1 | 1 | 1 | 0 |
| B = | 4 | 6 | 5 | 4 | 3 | 2 | 1 | 0 | 0 | 1 | 1 | 1 | 1 | 1 | 1 | 1 | 0 |
| C = | 16 | 48 | 76 | 92 | 97 | 92 | 78 | 56 | 35 | 28 | 30 | 34 | 39 | 44 | 48 | 50 | 42 |

A = Transducer Pattern

B = Primary Response

C = Secondary Response

path, relative to the input signal level to the device in question, at a single frequency. As mentioned above, it was found more convenient in this study to separate the fractions of this reversed energy flow into the component dependent upon the transducer loading, described above, and the components which are independent of the transducer loading. The latter are referred to here as reflected signals.

This particular usage has two main advantages. It avoids the situation where identical signals re-radiated by the transducers of a one-port structure are described variously as reflected or regenerated depending on which particular transducer received the acoustic energy, and it permits ready allowance for the fact that the components of the conventional reflected signal yield differing output codes.

It was seen above that signal regeneration is predicted in the admittance analysis of one-port structures. The reflections which we now wish to quantify are not accounted for in the above theory, because in the derivation of the transadmittance formulae the reflection from a short-circuited transducer was assumed to be zero. We now examine the validity of that assumption.

### 10.3.1 Reflected Pulse Waveform

In this case (in contrast to regeneration) the reflected signal may be obtained by the summation of the individual reflections from each of the electrodes in the transducer. We assume that for a uniform width transducer the electrodes may be represented by an infinitely thin reflector at the centre of each electrode, i, with an amplitude sensitivity coefficient $D_i$ at $x_i$, which we assume is frequency independent over the passband of the system. The waveform of a once-reflected output signal will then take the form*

$$v_r(t) = v_1(t) * d'(t) \qquad (10.24)$$

---

* Since the propagation changes direction, this expression is only valid for symmetric transducers. If the transducers are asymmetric g(t) must be calculated using $f_2(x) = f_1(-x)$ in Equation (4.25).

where d'(t) is related to the spatial reflection function d(x) by the relation d'(t) = d(½t) and changing the variable to x = vt,

$$d(x) = \sum_{i=1}^{N} D_i \, \delta(x-x_i) \qquad (10.25)$$

For uniform transducers d(t) will consist of a series of equal positive δ-functions (regardless of the transducer-connection phasing) spaced one period apart, and having a duration equal to twice the propagation time across the transducer.

The main differences between this waveform and the regenerated pulse shape predicted in Equation (10.17), is the absence of the sign reversal (depending upon the sign of $D_i$) and the fact that convolution with z(t) and g(t) has been replaced by convolution with a pulse having a rectangular envelope. However, invoking the Central-limit Theorem again, we can predict that the resulting pulses will have an approximately Gaussian pulse shape.

### 10.3.2 Reflected Pulse Code

As in the case for the regenerated signals, the reflections between the transducers in a multi-transducer structure will accumulate to give a sequence of pulses of identical shape, variable amplitude and uniform spacing, and which may be described by a code function. In this case the reflected signal code (ignoring reflections within a launching transducer) is given by

$$r(t) = \sum_{i=2}^{2(N-1)} R_i \, \delta(t - i\tau) \qquad (10.26)$$

where τ as before is the transducer separation, and the amplitude coefficients $R_i$ are given by,

$$R_i = \sum_{j=1}^{\ell_1} \sum_{k=\ell_2}^{\ell_3} A_j |A_{j+k}| A_{j+2k-i} + A_{N-(1+j)} |A_{N-(1+j+k)}| A_{N-(1+j+2k-i)} \qquad (10.27)$$

where

$\ell_1$ = Min {N-2, 2(N-1) - i}

$\ell_2$ = Max {1, Integer $[\frac{i-j+1}{2}]$ }

$\ell_3$ = Min {N-(1+j), i-1}

$A_i$ = amplitude coefficient of transducer i(+1,0 or -1).

This expression does not lend itself to any useful generalisations, but for examination of particular cases, may be easily evaluated on a digital computer.

### 10.3.3 Reflected Pulse Amplitude

Since the admittance analysis developed in Chapter 4 makes the basic assumption that the reflection from a short-circuited transducer may be neglected, efforts were made to check the validity of this assumption in the prototype delay lines.

An experiment was conducted using a four transducer structure, of the type shown in Figure 10.8, fabricated on YX-quartz. The first transducer (on the right)was used to launch surface-waves toward the electrostatic shield shown to its left. The incident and reflected signals from the reflector grid (third from right) were monitored at the second transducer, while the transmitted signal could be monitored by the fourth transducer. The transducer dimensions were the same as those used in the experiments conducted in Chapter 9, and the measurements were performed using the time-gated synchronous detector from the prototype receiver system.

To avoid exacerbating the electrostatic coupling problems no tuning was employed with the input and monitor transducers, and undersurface treatment to suppress volume modes was found necessary to permit unobscured identification of the reflected pulses when the reflecting grid was untuned. Long crystal blanks were used to avoid

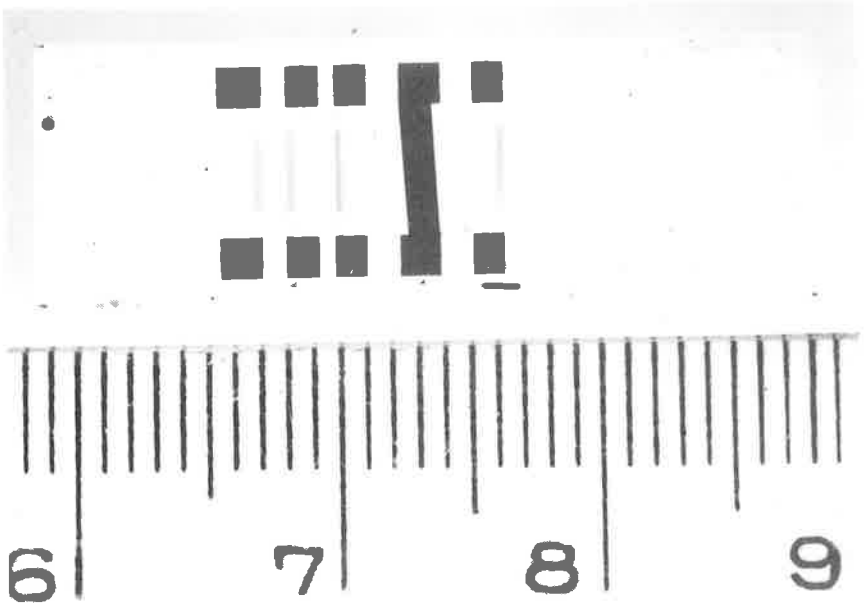


Figure 10.8 One of the quartz delay lines used in the reflection measurements at 50 MHz. The transmitting transducer is at right and the reflecting grid is second from left. (The scale graduations shown are millimetres.)

end reflections obscuring the very weak signals being sought, and a screened box with the crystal projecting through a tight-fitting internal metal screen was used, in addition to the grounded electrostatic screen shown in Figure 10.8, to minimise direct coupling of the input signal to the monitor transducer wiring.

By simply recording the peak pulse levels the following results were obtained. The reflection loss measured

| TRANSDUCER LOADING | REFLECTION FACTOR (dB) |
|---|---|
| Tuned Q=5 | -32 |
| Short circuit | -44 |
| Open circuit (free fingers) | -53 |

for the tuned transducer is dominated by the regenerated signal and is included here for comparison with the reflections from a short-circuited transducer. As can be seen, the original assumption that transducer reflections may be neglected in comparison with the regeneration which takes place at transducers with moderate insertion loss has been substantially vindicated.

It is of some interest to investigate the origin of this short-circuit reflection with a view to minimising it further if necessary. It is known that reflection may be due to the mass-loading or stiffness of the metal used for the fingers, or the localised electrical field shorting under each electrode. This problem has been investigated by Skeie[76], and Auld[51] by means of perturbation theory. Auld's formulation (Equation (80)) permits a ready estimation of the contributions to the scattering coefficient of a single electrode from each of the basic mechanisms. By substituting for the surface-wave particle velocities from the computer generated field plots given in Chapter 3, we obtain the result that the mass loading reflection factor is -80 dB, for the stiffness effect

it is negligible, and for the field shorting it is -61 dB. For our particular case with 9-finger transducers, the reflection factors at the synchronous frequency will be -61 dB for the mass-loading, and -42 dB for the field shorting. The figure of -42 dB is in very good agreement with the measured figure of -44 dB for a short-circuited transducer when allowance is made for the fact that measurements were made on a pulse basis, and we may conclude that with the thin aluminium films used (1500Å), the mass-loading provided by the fingers is not significant.

The other result presented is for the particular case of free floating fingers. It is known that the reflection coefficient of an open-circuit transducer is less than that of a short circuit transducer[125,139], as one might expect since the electrical boundary conditions of charge conservation on the electrodes will provide less of a perturbation on the CW propagating field than the requirement of effectively zero potential for the short circuit case. Measurements were made on both simple open circuit transducers, and then transducers with the pads disconnected leaving the fingers floating electrically isolated, and the results for the former case differed only slightly from the figure of 53 dB shown.

## 10.4 Discussion

From these results a number of significant differences between the regenerated and reflected responses of a one-port device may be drawn. Firstly, unless very weakly coupled transducers are used the regenerated signals will dominate, and the reflections between transducers may safely be neglected.

Inherent in this statement is the assumption that the rate of accumulation of the reflected pulse code will be less than

that of the regenerated pulse code for increasing values of N. This may be proved for the particular situation where the transducer coefficients $A_i$ are always positive by manipulation of Equations (10.16) and (10.27), and it would seem reasonable to generalise this result.

Associated with this result is the important factor that the reflection from disconnected electrodes is negligible compared with the regenerated pulses. This has an important practical application in one-port devices because it means it is acceptable to fabricate all the required delay lines with the full N transducers present, and then code them after manufacture by severing the electrodes of those transducers not required in each particular code. This procedure was used in some of the experimental lines. One consequence of this result is that on lines with many zeros in the code there may be many more inoperative than operative electrodes, and hence it is important that the reflection levels be even lower than for shorted transducers. Fortunately this appears to be the case in practice.

# CHAPTER 11

# FUTURE DEVELOPMENT OF THE SYSTEM

## 11.0 Introduction

In the last few years there has been a rapid growth in the technology for the manufacture of surface-wave devices and increasing sophistication is becoming evident in the solutions now being devised to overcome many of the defects of surface-wave devices for specific applications. In this section comment will be made on how some of these advances might be incorporated into a practical one-port labelling system.

## 11.1 Delay Line Manufacture

One of the basic limitations of any large labelling scheme will be the cost of producing and then encoding the delay lines. The recent development of manufacturing techniques for the production of surface-wave transducers by depositing piezoelectric thin film materials like zinc oxide[153,154] and cadmium sulphide[155] onto non-piezoelectric substrates creates the possibility of delay lines on cheap materials such as isopaustic glass [156]. As it has been shown that quite low transducer-coupling factors are required to minimise the second-order response levels, it should be practical to use very thin layers of piezoelectric over the transducer metallization, thus minimising the problem of frequency dispersion commonly associated with laminar structures.

It is also apparent that the cost of producing individual masks for the photolithography, for each transducer code, would be prohibitive using conventional high-resolution glass plates. This problem could be solved either by using a single mask in conjunction with an automated device for making or severing connections to specified

transducers on each line, or, more elegantly, by the use of a computer-controlled electron beam unit to draw the required transducer code directly onto the photoresist for each line.

## 11.2 Pulse Overlap Reduction

The arguments presented in Section 10.1.5 indicate that the time-spreading of each separate received pulse is inversely proportional to the bandwidth of the overall system, and in consequence must be considered unavoidable. It is perhaps worth mentioning that the use of large time-bandwidth product waveforms so popular in radar system designs offer no advantage here: the final pulse length after matched filtering is still determined by the reciprocal of the effective bandwidth (the main advantages of large time-bandwidth signals are improved doppler sensitivity, and improved signal-to-noise ratio at the receiver output due to the greater signal energy).

However having detected a reply pulse, an information theoretic approach tells us that with this knowledge, plus a knowledge of the expected pulse waveform, we should be able to compensate for the presence of a long pulse tail when making decisions on the presence or absence of pulses in succeeding bit positions. This type of processing is quite feasible but would require the addition of logic circuitry in the receiver.

A simpler solution in delay lines, such as the delayed binary system, which enjoy a simple correspondence between the transducer pattern and the reply code, is to incorporate into every zero position immediately following a one position a short antiphase transducer whose response, when added to the previous bit pulse and processed by the receiver, would give a zero resultant at the detector output. This technique would only require phase coherence over several tens of wavelengths on the substrate, and could be readily incorporated into patterns drawn with a

computer-controlled light pen or electron beam, of the type suggested earlier.

## 11.3 Regenerated Signal Minimisation

It was shown in Section 10.2 that the peak second-order response levels tend to rise relative to the primary response for increasing numbers of transducers on the line. The obvious solution is to increase the insertion loss of the individual transducers on the line, but this will increase the return loss of the primary response of the line, and in systems employing propagation to communicate with the labels, this will result in a serious decrease in the operating range from the interrogation unit. It is apparent that a reduction of the regenerated signal levels will be necessary before the development of more elaborate systems can occur.

The simplest approach is simply to delete those codes with unacceptably high second-order response levels from the code set, which could be readily achieved using a code selection program of the type developed in Chapter 8. It would also be worthwhile to set up the program to make use of the ambiguities in the patterns, i.e. where a number of transducer patterns produce the same response after decoding, to select the one producing the lowest peak second-order pulse level.

This procedure would be improved significantly if the selection of the codes was based on ternary patterns instead of binary patterns, because many ternary patterns produce identical codes to the binary patterns ( with a binary decoder) but have markedly reduced second-order response levels due to the cancellation between positive and negative coefficients.

However this does not produce any improvement for existing transducer patterns with high second-order response levels, such as the delayed binary patterns shown in Table 10.1. The most promising approach

here appears to be to vary the transducer spacing slightly, in either regular or random fashion. The idea is to produce destructive interference in the accumulated second-order response peaks by this 'phase-staggering' of the transducer pattern. In lines with natural binary outputs the effect on the primary response will be to vary the position of the pulse peaks by a maximum of plus or minus a half-period at the carrier frequency, which should not present any problems for the detector.

## 11.4 Reflected Signal Minimisation

For the prototype system, measurements indicated that reflection from the transducers could be neglected in comparison with the regeneration. However in a line with more transducers, and hence employing weaker coupling, reflection could become significant. This is also true at higher frequencies as relatively thicker metal films (in terms of acoustic wavelengths) are needed for the electrodes to maintain resistive losses at an acceptable level.

Some work has been reported in the literature on the reduction of triple-transit reflections in two-port lines and the reduction of the reflection from taps in matched filter type correlators, and these techniques can be applied here. One of the most promising is the use of split fingers (i.e. two electrodes $\lambda/8$ wide spaced $\lambda/4$ between centres instead of a single electrode $\lambda/4$ wide) as proposed by Carr [139]. This technique can reduce all the components of the reflected signal but not the regenerated signals which appear with a finite source impedance. The penalty in this technique is the requirement for doubled optical resolution in the line fabrication.

An alternative technique which does not appear to have been explored, is to make use of the fact that the mass-loading and field shorting produce reflection coefficients (Auld[51] Equation (80)) which can have opposite sign. It thus appears possible under some circum-

tances to select the metal electrode thickness to cancel the field-shorting reflections.

Other ingenious means for reducing transducer reflections have been proposed [157,158], including the skewing or slight rotation of the receiving transducer so that the reflected wavefronts do not intercept the transmitting transducer. However, in a one-port structure we cannot differentiate between transmitting and receiving transducers, and most proposals of this type may be viewed as means for increasing the single-pass insertion loss of the line.

## 11.5 Prototype System Improvements

The prototype labelling system simulated in the experiments in Chapter 9, was not expected to be optimum, but rather to function as a convenient vehicle for the examination of the general behaviour of one-port surface-wave delay lines. In the light of experience gained with this system, a number of improvements which could be incorporated into a practical system can be identified.

### 11.5.1 Signal-to-Noise Ratio

The most pressing practical problem is likely to be the achievement of an adequate signal-to-noise ratio at the receiver output to permit sufficiently reliable code detection. For example, if the acceptable error rate for individual reply code pulse detection is set at 1 in $10^{-8}$ then a signal-to-noise ratio of 18.5 dB is required at the detector input [159]. Using only a simple loop antenna on the delay line the two way propagation loss, under worst case conditions of antenna detuning and shielding by the tagged object, may exceed 100 dB. When this figure is added to the delay line insertion loss (which cannot be reduced because of the second-order response problem) we obtain a typical figure of 135 dB insertion loss, and the magnitude of the problem becomes apparent.

One method of improving the system performance is by averaging successive receiver outputs to suppress the noise. The transmitter pulse repetition frequency(limited by the delay line length to approximately 100 KHz) and the natural integration of the narrow-band IF filter, already supply significant integration, but this may be supplemented by a longer time-constant integrator before the detector. This technique was used for the reflection measurements in Section 10.3.2 where an 8 second integrater was used to achieve reliable measurements of reflected signals 130 dB down on the peak transmitter output level. The introduction of long integration times makes it essential that the code bits be decoded in parallel, not serially as in the experimental set-up.

### 11.5.2 Transmitter Pulse Energy

It is considered here that integration times longer than a few seconds are likely to be inconvenient in practice, and an alternative approach would be preferable. From detection theory it is known that the signal-to-noise ratio (power) at the matched filter output is given by[160]

$$SNR_{max} = \frac{2E}{N_o} \qquad (11.1)$$

where E is the total energy in the signal pulse, and $N_o$ is the noise power spectral density, both measured at the receiver input. The only way to boost this ratio, assuming the receiver noise factor is as good as possible, is to increase the total energy in the transmitter pulse. The simplest method here is to increase the transmitter power output level, but this process cannot be pushed very far before the problems of transmitter cost, operator safety and voltage breakdown of the interdigital transducers begin to appear.

The total signal energy may also be increased by extending the duration of the transmitted pulse, as is frequently done in peak-

power limited radar systems. This can be achieved without increasing the time-dispersion of the output code pulses, if the bandwidth of the transmitted signal is held constant, and the appropriate matched filter is used in the receiver. A simple method of extending the duration of the transmitted signal, retaining the same bandwidth, is to transmit a string of pulses with polarities varied in a pseudo-random fashion. Waveforms of the type which produce a single large-peak, and uniform unit amplitude time sidelobes at the matched filter output, are known as Barker coded [161].

### 11.5.3 Surface-Wave Matched Filters

The major problem in the realization of systems such as this, is in the construction of an effective matched filter, for the so-called biphase coded waveforms. Surface-wave correlators appear to offer the best solution to this problem, and a number of investigations of Barker code matched filters, for use in radar systems, have appeared in the literature [78,162-164]. It would appear to be only fitting, in the context of the present study, to suggest that biphase coding with a surface-wave matched filter could be used to improve the detection performance of the interrogation unit.

One restriction which should be borne in mind, is that the occurrence of the finite time sidelobes of compressed large time-bandwidth signals may limit this approach to coded one-port devices with natural binary output codes.

We return now to consideration of the basic system with a simple tone-burst transmitter pulse. The ideal receiver shown in Figure 9.10 can also be considerably simplified by the introduction of surface-wave matched filters. The requirement for a quadrature multiplier in the coherent detector arises because the phase of the received signal is not exactly known, and this complex circuit component

can be replaced by a surface-wave matched filter, which in this case would be simply a two-transducer delay line with a truncated Gaussian impulse response.

The simplicity of this approach means that the assembly of the whole bank of matched filters, one to each code pulse, could be quite inexpensive. Furthermore, the delays in these matched filters could be arranged to complement the code pulse delays so that all the filter outputs could be sampled simultaneously at the commencement of the following interrogation cycle, eliminating the need for almost all the complex timing circuitry which would be needed in a parallel version of the prototype system.

A sketch of such a system is given in Figure 11.1, and it is plain that this system configuration would also cope with the large time-bandwidth signals mentioned above, simply by inserting the appropriate matched filter delay lines.

### 11.5.4 Antenna Configurations

A topic which has not been broached in the previous discussions is the impact of the antenna selection on receiver design.

A fundamental problem in the search for an ideal label is that it is impossible to produce an omnidirectional transponding antenna for connection to the delay line. The simple inductive loop antenna assumed in the system simulation gives fairly good performance in this respect, but has a null plane, in the plane of the loop, for coupling to magnetic fields. The only way to overcome this difficulty is to use space diversity with two, or at worst three, transmitting antennas.

Having introduced the possibility of multiple antennas into the picture, we are now in a position to comtemplate using separate transmitter and receiver antennas and switching between the available

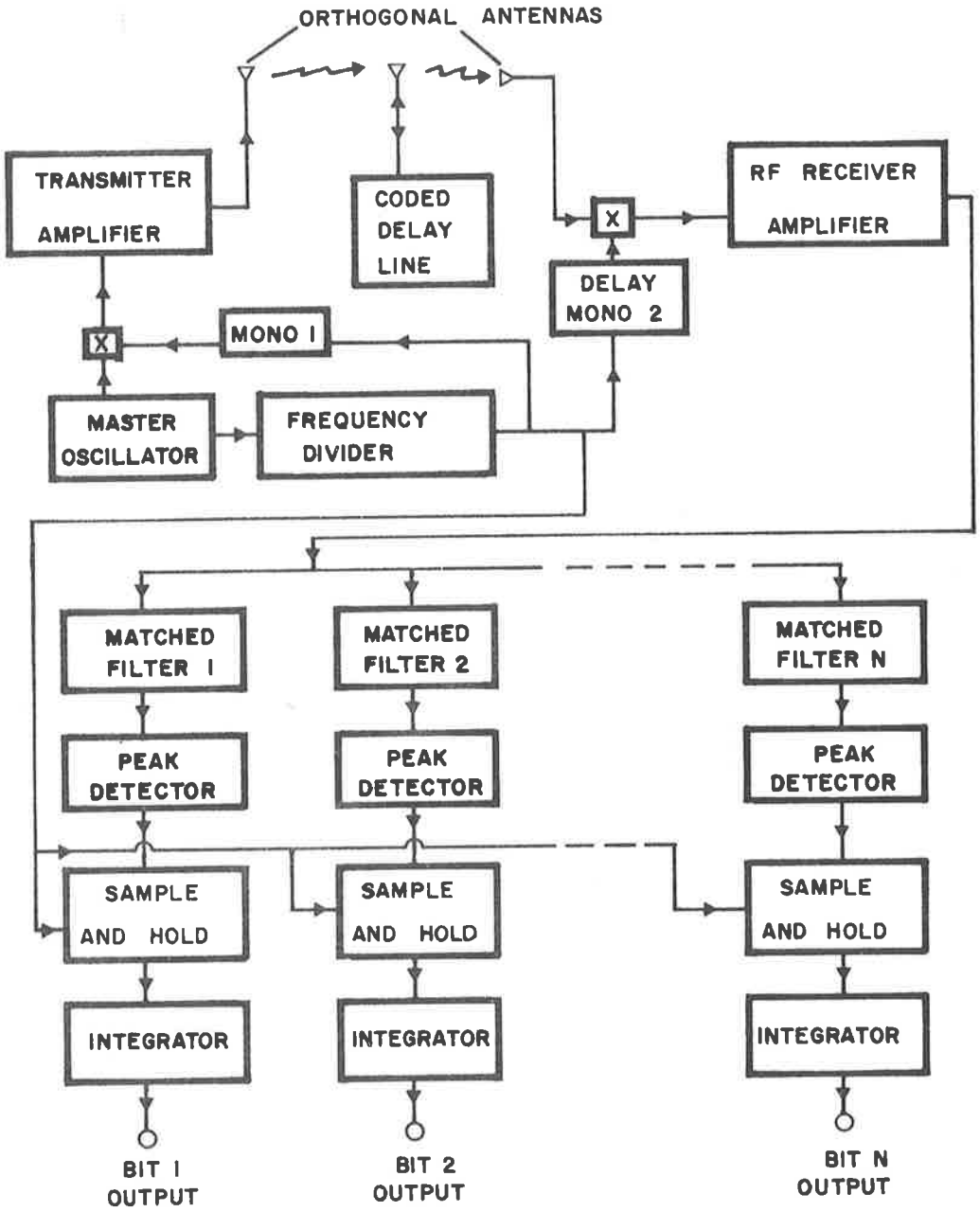


Figure 11.1 Schematic of a simplified system with parallel outputs for the interrogation of coded one-port delay lines. The matched filter delays complement the code-bit delays so that all bits may be read simultaneously, and the only timing circuitry necessary is a frequency divider and two monostables.

permutations for transmitting and receiving. This should effectively overcome the problem of the null plane and at the same time permits us a further improvement in system design. If we select transmit and receive antennas with zero mutual coupling, (achieved either by selection of radiation patterns or cross-polarising) we no longer expose the receiver input to the transmitter pulse, a factor which eases the receiver design considerably in view of the very large dynamic range to be covered.

# CHAPTER 12

# SUMMARY AND CONCLUSIONS

## 12.1 Summary of Results

This investigation into the practical utility of acoustic surface-wave delay lines for the realization of passive read-only information stores, suitable for remote interrogation, was conducted in several phases.

The first was concerned with gaining an appreciation of the general characteristics of surface-wave propagation on anisotropic piezoelectric single-crystal materials, and in the course of this work a computer program to seek surface-wave solutions on arbitrary piezoelectric materials was developed. This program enables the ready examination of the propagating acoustic and electric fields of the surface-wave on a surface covered with a shorting layer at a specified height, and supplied accurate data on the surface-wave velocity, piezoelectric coupling factor and misalignment angle for the particular crystal cuts of $\alpha$-quartz used in the experiments.

The next sections describe the development of a convenient and accurate model for surface-wave devices, suitable for use in the investigation of the proposed one-port delay line structures. The assumption of parallel, rather than series, transducer connection leads naturally to the choice of a device representation in admittance terms, and it is shown how the external behaviour of both one-port and two-port devices on weak-coupling substrates may be expressed as a series expansion in terms of the admittance coefficients of the equivalent N-port surface-wave structure. An important property of this expansion technique is that the individual terms in the expanded output response may be identified with different physical paths for energy passing through the surface-wave device, and that the individual contributions

from these higher-order (regenerated) signals may be estimated separately. It is apparent that second-order responses should be taken into account if accurately prescribed performance is required in either one-port or two-port devices, and these effects can be much more important than the frequently mentioned triple-transit-signal which is only a third-order response. By summing as many terms as required in the output response expansion, a surface-wave device may be analysed to any required degree of accuracy, subject only to the limiting assumptions involved in the calculation of the admittance coefficients.

The analysis of surface-wave devices in terms of the externally observable voltage parameters leads to a shift in emphasis from the more usual attempts to interpret device behaviour in terms of the efficiency of individual transducers. It becomes apparent that the most important parameter in device characterisation is the transadmittance between each coupled pair of transducers, not the input admittances of the individual transducers as are more commonly calculated.

To expedite this approach a general expression for the frequency transadmittance between two acoustically coupled surface-wave transducers is required. This is obtained, starting from first principles, by means of the normal mode expansion techniques pioneered by Auld[51] and Kino[54]. The resulting expression* predicts a number of previously unknown features of coupled-transducers as being quite general, namely the presence of the $|\omega|$-weighting factor in the frequency domain, and the sign reversal of the output voltage in the time domain. These features are subsequently verified experimentally. This general expression for the transadmittance may be readily related to the intuitively derived simple $\delta$-function models and the resulting equivalent circuits[167], thus placing these on a better footing.

---

* A similar expression for the transadmittance between an acoustically-coupled pair of interdigital transducers has recently been published by Ganguly and Vassell [165,166], and differs from this work in that it includes the effect of substrate piezoelectricity in determining the transducer source functions.

To permit convenient analysis of the surface-wave devices under study, the transadmittance expression has been modified to obtain it in a form suitable for programming on a digital computer. In the computer program, advantage is taken of the availability of the fast-Fourier transform algorithm, for the evaluation of the integrals in the formulae. The resulting computer model is quite efficient and would appear to be both simpler to use, and faster, than programs based on the empirical three-port model of Smith et al.[47], in the case of devices on weak-coupling substrates.

To test the validity of the transadmittance computer model the necessary facilities were developed in the laboratory to permit the fabrication of some experimental surface-wave delay lines. Measurements made in the laboratory, on devices produced using this apparatus, are described, and the results are found to give good agreement with the predictions of the computer model, to within experimental error. With this pleasing confirmation of the admittance formulation established, the computer model is then used in an investigation of the proposed one-port coded surface-wave delay lines.

By exploiting the similarities between the normal-mode derived expressions for the input and transfer admittances, the basic relation between the pattern of the transducers and the response code of a one-port delay line is obtained. This theoretical representation is then used to examine the properties of transducer patterns employing binary, biphase and ternary coding. It is shown that while not all the possible transducer patterns in any general coding scheme will produce unique response codes, it is usually possible to select a useful set of transducer patterns with unambiguous responses, by means of computer simulation studies.

The last part of this study involves an examination of the

problems involved in the detection and decoding of the responses from practical one-port coded delay lines in a prototype remote interrogation system. The output pulse shape from such a system may bear little resemblance to the excitation waveform, and the transfer functions of the various system components are included in a computer model to enable prediction of the complete system response. After the successful verification of the computer model, by comparison with representative experimental results, it is used to generate design curves relating the normalised system parameters to the discrimination ratio between successive pulses. This computer model of the complete prototype receiver system is also used to investigate the vulnerability of the received waveform to various forms of frequency passband distortion in the signal path, yielding the rather unexpected result that in general, while the output signal is decreased, our ability to identify the individual pulses is improved, provided the signals are still above the noise level.

The next section is concerned with the non-ideal aspects of surface-wave delay line behaviour which limit the total coding capacity of the one-port lines. The two major factors here are the occurrence of regenerated output pulses, which arise due to the fact that the device's input and output terminals may be considered as connected in parallel, and the reflections from the transducer electrodes due to the mechanical and electrical perturbations which they present to the propagating surface-waves. It is found, in the prototype system which was investigated here, that the regenerated and reflected pulses are spread to almost twice the duration of the primary pulses, and that the reflected pulse levels are not significant relative to the regenerated pulse levels. A general tendency is also identified for the peak secondary response levels to rise towards the primary response levels when the number of

active transducers on the line is increased.

The final chapter includes a short summary of techniques identified in the course of this work by which the prototype system, which was used as the test bench for the experimental coded surface-wave lines, might be improved upon in the development of a practical system.

## 12.2 Conclusions

The use of an acoustic surface-wave delay line in the realization of a passive one-port structure capable of producing a coded pulse train in the time domain following a brief excitation signal, has been successfully demonstrated. Due to the relatively narrow passband frequency characteristics of the interdigital transducer structures, the reply pulse train is of the form of a double-sideband suppressed carrier amplitude modulated waveform.

The adoption of equi-spaced identical interdigital transducers results in echo trains in which the amplitude modulated pulses are quantized in both amplitude and spacing. This type of output coding is considered most suitable for interfacing with digital logic as would be required in a practical label-sorting operation.

The output code from a one-port delay line is related to the transducer coefficients by a modified autocorrelation function, and due to the symmetry properties of this function, it is possible for different sets of transducer coefficients to produce the same output code. This means the number of different output codes is always less than the maximum number of permutations of the transducer coefficients in any given coding scheme. The introduction of a decoding procedure for the reply codes results in a simplification of the identification procedure and a further reduction in the number of unique output codes

available from a given number of transducers. To achieve a usefully large set of codes it is necessary that the coding and the decoder be carefully matched. Coding with non-identical transducers and non-uniform spacing merits further investigation as it may be possible by these means to increase the number of output codes which can be generated by lines of a given length.

It has been shown that the minimum useful transducer spacing is determined by the overall system bandwidth. Where the available fractional bandwidth is not restricted by external considerations, it would be tempting to contemplate very wideband systems. However, relative bandwidths of greater than 15 to 20% would probably be undesirable due to the rapid increase in the coupling efficiency of interdigital transducer structures to volume waves and quasi-surface-waves at frequencies about 10% above the synchronous frequency, resulting in serious interference to the time domain code.

From a knowledge of the interdependences of the system parameters identified in this study, a logical approach to one-port coding system design can be deduced. Given the required number of discrete output codes, and after adopting coding and decoding procedures appropriate to the application, the total number of transducer locations, the code set itself and the peak second-order response levels can be determined, by computer simulation if necessary. The peak second-order response level will determine the minimum useable insertion loss, and from an estimate of the likely amount of transducer 'passenger capacitance', the insertion loss figure for each individual transducer may be determined. If the system bandwidth is specified by external considerations, such as antenna design or the spectrum allocation we may calculate the appropriate length for a uniform transducer.

We now find that both the insertion loss and bandwidth for the

transducers has been specified. Smith et al.[47,48] have shown that uniform interdigital transducers have a maximum insertion gain-bandwidth product, determined by the material coupling efficiency. The optimum procedure here is to select a substrate with a gain-bandwidth product matched to the system requirements. Selection of a material with a stronger coupling factor will mean deliberate transducer mismatching will be required to achieve the desired level of insertion loss, and could lead to trouble with increased reflections from the transducers due to the stronger field shorting effect, while selection of a material with a weaker coupling factor will result in greater than necessary insertion loss.

The transmitter pulse length is then made equal to the surface-wave transit time across a transducer, and from the dimensionless design curves we can obtain the required transducer separation (the circuit tuning factors are determined by the bandwidth requirement). At this point the delay line configuration is completely determined. The operating range, if the system is to act as a remote reading device, will now be dictated by the difference between the dynamic range of the interrogation unit and the return loss of the label.

# APPENDIX A1

## COMPUTER PROGRAM LISTINGS

### A1.0 General

The computer programs listed here are written in FORTRAN IV, and are compatible with the Control Data Corporation 6400 computer installation at the University of Adelaide. With the exception of a number of subroutines (BFAST, POLYR, PHCDET and BCONTR) which were obtained elsewhere and modified by the author, all programs and subroutines were written by the author.

Each listing describes a typical working program deck and includes all necessary subroutines, and a typical set of data cards where applicable. Flow Charts are included as an aid to interpretation of the listings.

## A1.1 Program SURF02 - Surface Wave Solution

### A1.1.1 Flow Chart

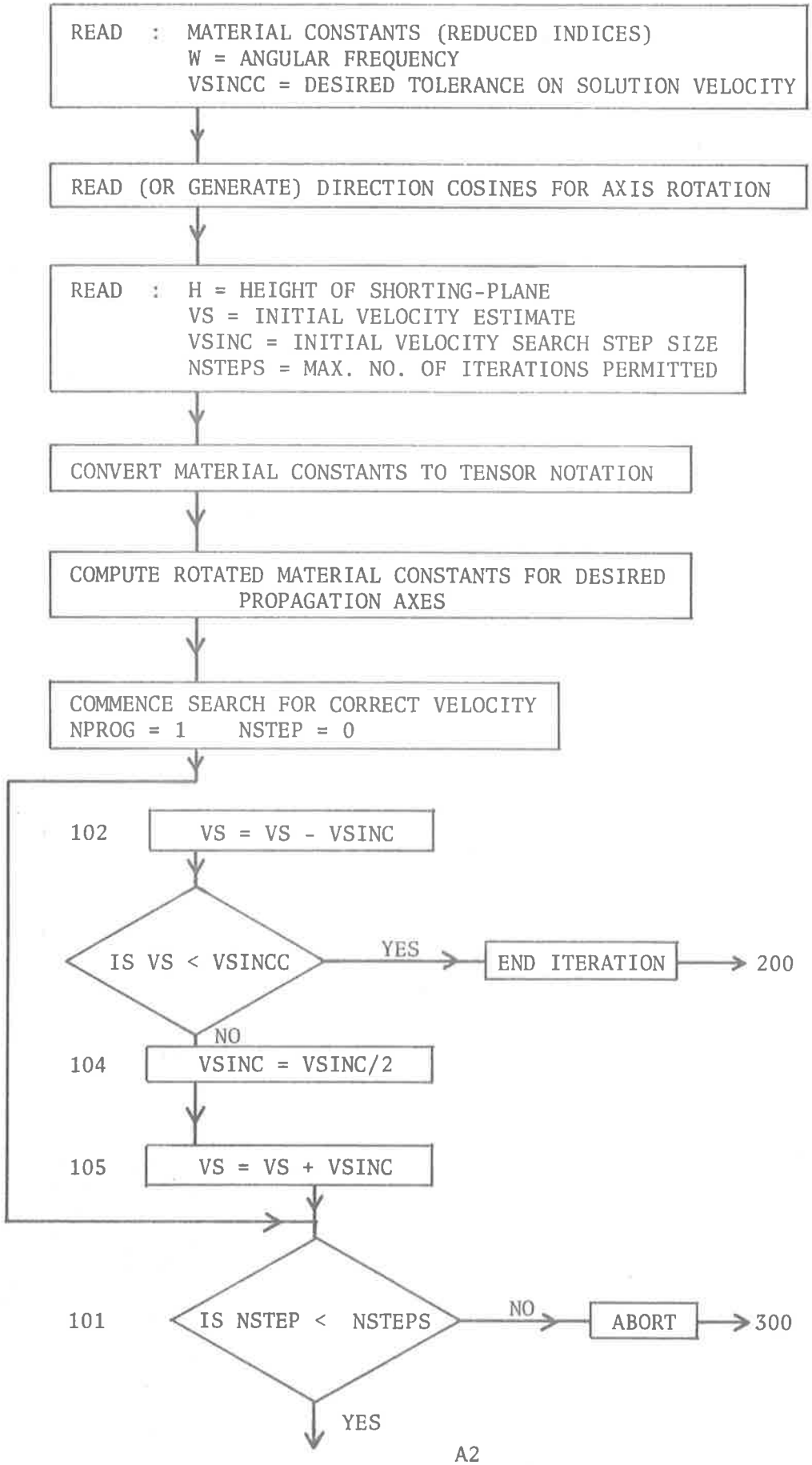

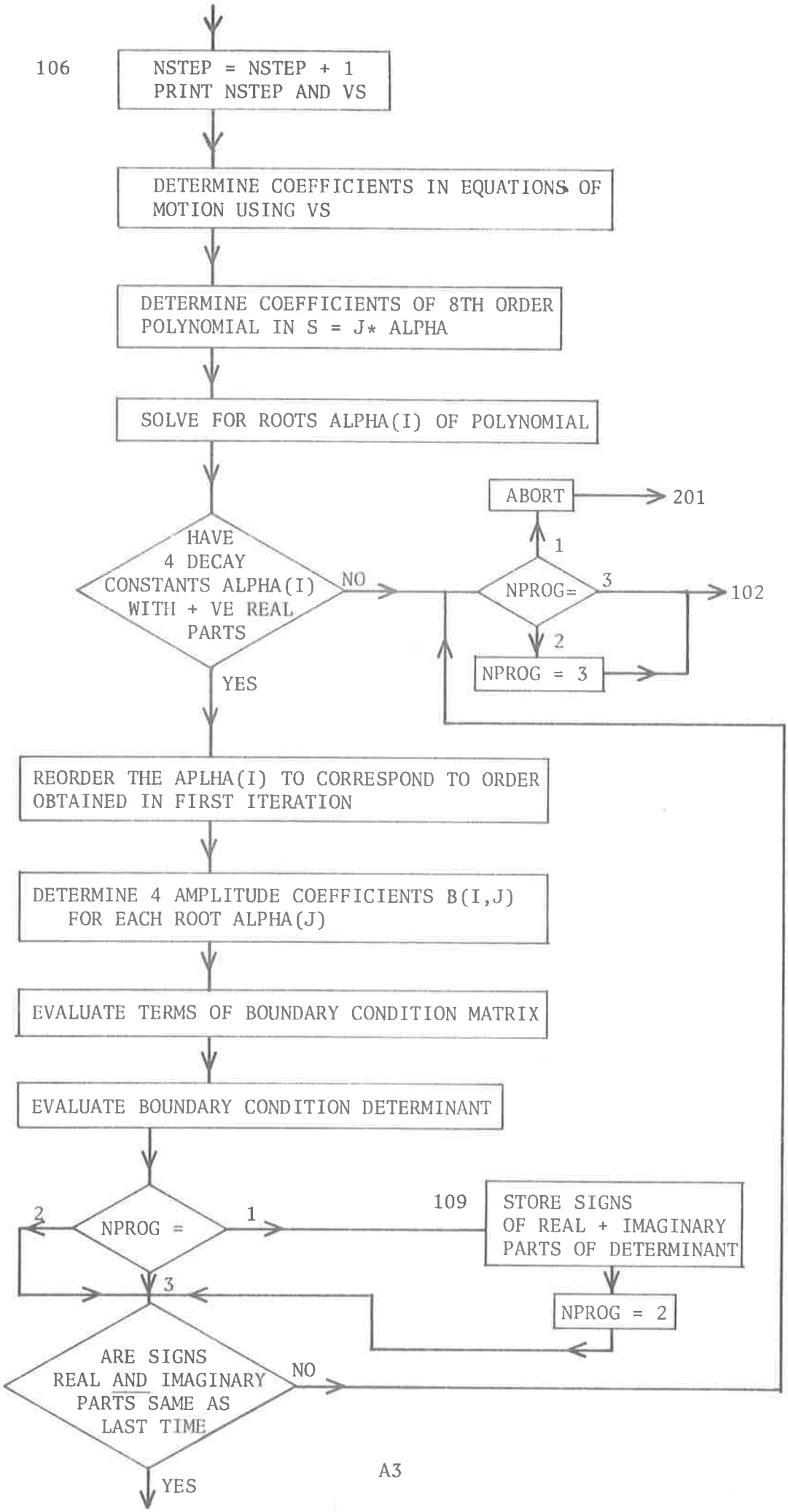
106
NSTEP = NSTEP + 1
PRINT NSTEP AND VS
DETERMINE COEFFICIENTS IN EQUATIONS OF MOTION USING VS
DETERMINE COEFFICIENTS OF 8TH ORDER POLYNOMIAL IN S = J* ALPHA
SOLVE FOR ROOTS ALPHA(I) OF POLYNOMIAL
ABORT
201
1
HAVE 4 DECAY CONSTANTS ALPHA(I) WITH + VE REAL PARTS
NO
NPROG=
3
102
2
NPROG = 3
YES
REORDER THE APLHA(I) TO CORRESPOND TO ORDER OBTAINED IN FIRST ITERATION
DETERMINE 4 AMPLITUDE COEFFICIENTS B(I,J) FOR EACH ROOT ALPHA(J)
EVALUATE TERMS OF BOUNDARY CONDITION MATRIX
EVALUATE BOUNDARY CONDITION DETERMINANT
109
STORE SIGNS OF REAL + IMAGINARY PARTS OF DETERMINANT
2
NPROG =
1
3
NPROG = 2
ARE SIGNS REAL AND IMAGINARY PARTS SAME AS LAST TIME
NO
YES

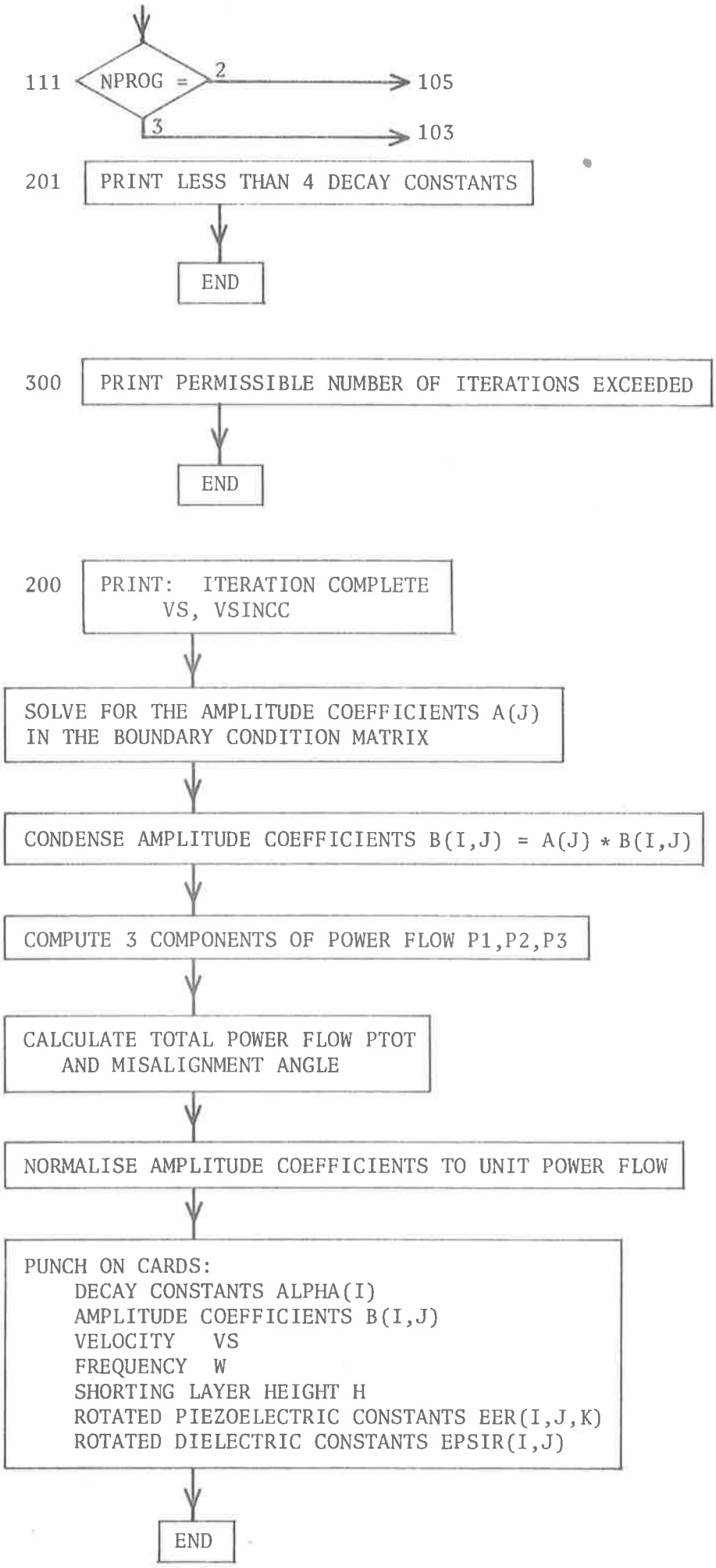
111
NPROG =
2
105
3
103
201
PRINT LESS THAN 4 DECAY CONSTANTS
END
300
PRINT PERMISSIBLE NUMBER OF ITERATIONS EXCEEDED
END
200
PRINT: ITERATION COMPLETE
VS, VSINCC
SOLVE FOR THE AMPLITUDE COEFFICIENTS A(J)
IN THE BOUNDARY CONDITION MATRIX
CONDENSE AMPLITUDE COEFFICIENTS B(I,J) = A(J) * B(I,J)
COMPUTE 3 COMPONENTS OF POWER FLOW P1,P2,P3
CALCULATE TOTAL POWER FLOW PTOT
AND MISALIGNMENT ANGLE
NORMALISE AMPLITUDE COEFFICIENTS TO UNIT POWER FLOW
PUNCH ON CARDS:
DECAY CONSTANTS ALPHA(I)
AMPLITUDE COEFFICIENTS B(I,J)
VELOCITY VS
FREQUENCY W
SHORTING LAYER HEIGHT H
ROTATED PIEZOELECTRIC CONSTANTS EER(I,J,K)
ROTATED DIELECTRIC CONSTANTS EPSIR(I,J)
END

## A1.1.2 Program Listing

```
      PROGRAM SURF02(INPUT,OUTPUT,PUNCH)
C
C     THIS PROGRAM DETERMINES THE SURFACE WAVE VELOCITY AND DECAY
C     CONSTANTS ON A PIEZOELECTRIC CRYSTAL
C     PROPAGATION IS IN THE X1 DIRECTION
C     SURFACE NORMAL IS ASSUMED TO BE PARALLEL TO -X3
C     READ IN MATERIAL CONSTANTS RELATIVE TO FREE XYZ AXES
C     DIRECTION COSINES ARE GIVEN BY V(I,J)
C     DIRECTION COSINES ROTATE AXES SO THAT (X1,X2,X3)=(V)(X,Y,Z)
C
C     DATA NEEDED (IN ORDER)
C        C(I,J)= 18 ELASTIC CONSTANTS
C        E(I,J)= 9 PIEZOELECTRIC CONSTANTS
C        EPSIO = DIELECTRIC CONSTANT OF FREE SPACE
C        EPSI(I,J) = 9 DIELECTRIC CONSTANTS
C        W=ANGULAR FREQUENCY (IN RADS/SEC)
C        RHO = MATERIAL DENSITY
C        VSINCC = SMALLEST STEP SIZE USED IN SEEKING VELOCITY (M/SEC)
C        THETA = ROTATION ABOUT X1 AXIS (DEGREES)
C        PSI = ROTATION ABOUT X2 AXIS (DEGREES)
C         GAMMA = MISALIGNMENT ANGLE (DEGREES )
C        H= HEIGHT OF CONDUCTING LAYER ABOVE SURFACE (IN METRES)
C        VS - STARTING VELOCITY
C        VSINC = INITIAL VELOCITY INCREMENT
C        NSTEPS = MAX NUMBER OF ITERATIONS OF VELOCITY PERMITTED
C
C

      COMPLEX S(8),ACOM(4,4),CCOM,AC(4,4),B(4,4),BETA(4),ALPHA(4)
      COMPLEX AMP(4),ALPHAC(4),BC(4,4)
      COMPLEX BTEMP,XTEMP
      COMPLEX P1,P2,P3
      COMPLEX JAY,CZERO
      COMPLEX BT1,BT2,BT3
      COMPLEX T(4)
      REAL C(6,6),E(6,6),EPSI(3,3),V(3,3)
      REAL C1(3,3,3),C2(3,3,3),C3(3,3,3),EE(3,3,3)
      REAL C1R(3,3,3),C2R(3,3,3),C3R(3,3,3),EER(3,3,3)
      REAL EPSIR(3,3),A(4,4,3)
      REAL RHO,VS,VSINC,COEFF(10)
      PI=3.14159265358979
      CZERO=CMPLX(0.,0.)
      JAY=CMPLX(0.,1.)
      CALL STIME
C        READ IN THE ELASTIC CONSTANTS (IN NEWTONS/METRE-SQUARED)
      READ 1,((C(I,J),J=I,6,1),I=1,6,1)
    1 FORMAT(E10.3)
      PRINT 5
    5 FORMAT (/*1ELASTIC CONSTANTS  (IN NEWTONS/METRE SQUARED)*/)
      DO 2 I=1,6
      DO 2 J=I,6,1
      PRINT 4,I,J,C(I,J)
    4 FORMAT (* C(*I1*,*I1*)= *E10.3)
    2 CONTINUE
C        READ IN PIEZOELECTRIC STRESS CONSTANTS (IN COULOMB/METRE-SQUARED)
      PRINT 9
    9 FORMAT(/* PIEZOELECTRIC STRESS CONSTANTS (IN COULOMB/METRE-SQUARED
     1)*/)
      DO 6 I=1,3
      DO 6 J=1,6
      READ 8,E(I,J)
    8 FORMAT(E10.3)
      PRINT 10,I,J,E(I,J)
   10 FORMAT(* E(*I1*,*I1*)=  *E10.3)
    6 CONTINUE
      PRINT 11
   11 FORMAT(/* DIELECTRIC CONSTANTS (IN FARADS/METRE)*/)
C        READ DIELECTRIC PERMITTIVITY (IN FARADS/METRE)
      READ 7, EPSIO
    7 FORMAT(E10.3)
      PRINT 13,EPSIO
   13 FORMAT (*-EPSIO=*E10.3/)
      DO 12 I=1,3
      DO 12J=1,3
      READ 14,EPSI(I,J)
   14 FORMAT(E10.3)
      PRINT 15,I,J,EPSI(I,J)
   15 FORMAT(* EPSI(*I1*,*I1*)= *E10.3)
   12 CONTINUE
      READ 46, W
      PRINT 3,W
    3 FORMAT(*-W=*E15.8)
```

```
C
C        READ MATERIAL DENSITY (KGM/METRE-3)
      READ 39,RHO
   39 FORMAT(E15.8)
      PRINT 43,RHO
   43 FORMAT(* MATERIAL DENSITY=*E15.8*KGM/M-3*/)
      READ 120,VSINCC
  120 FORMAT(E10.3)
      PRINT 121,VSINCC
  121 FORMAT(*-SMALLEST VELOCITY INCREMENT = *E10.3)
      READ 19,THETA,PSI
   19 FORMAT(2E15.8)
      PRINT 22,THETA,PSI
   22 FORMAT(*0THETA = *E15.8/* PSI = *E15.8/)
      PSI =PI*PSI/180.
      THETA =PI*THETA/180.
      CT=COS(THETA)
      ST=SIN(THETA)
      CP=COS(PSI)
      SP=SIN(PSI)
      V(1,1)=CP
      V(1,2)=-SP*ST
      V(1,3)=SP*CT
      V(2,1)=-SP
      V(2,2)=-CP*ST
      V(2,3)=CP*CT
      V(3,1)=0.
      V(3,2)=-CT
      V(3,3)=-ST
      PRINT 16
   16 FORMAT(/* DIRECTION COSINES*/)
      DO 17 I=1,3
      DO 17 J=1,3
      PRINT 20,I,J,V(I,J)
   20 FORMAT(* V(*I1*,*I1*)= *E15.8)
   17 CONTINUE
      READ 46, H
  46  FORMAT(E15.8)
      PRINT 18,H
  18  FORMAT(* H=*E15.8)
C
C     READ INITIAL VELOCITY, INCREMENTAL VELOCITY, AND NUMBER OF STEPS
C     (VELOCITY IN METRES PER SEC)
      READ 40,VS,VSINC,NSTEPS
   40 FORMAT(2(E15.8),I3)
      PRINT 42,VS,VSINC,NSTEPS
  42  FORMAT(*-VS= *E15.8/* VSINC= *E15.8/* NSTEPS= *I3/)
C        CONVERTING C(I,J) TO C1(I,J,K) ETC.
      C1(1,1,1)=C(1,1)
      C1(1,1,2)=C(1,6)
      C1(1,1,3)=C(1,5)
      C1(1,2,1)=C(1,6)
      C1(1,2,2)=C(1,2)
      C1(1,2,3)=C(1,4)
      C1(1,3,1)=C(1,5)
      C1(1,3,2)=C(1,4)
      C1(1,3,3)=C(1,3)
      C1(2,1,1)=C(1,6)
      C1(2,1,2)=C(6,6)
      C1(2,1,3)=C(5,6)
      C1(2,2,1)=C(6,6)
      C1(2,2,2)=C(2,6)
      C1(2,2,3)=C(4,6)
      C1(2,3,1)=C(5,6)
      C1(2,3,2)=C(4,6)
      C1(2,3,3)=C(3,6)
      C1(3,1,1)=C(1,5)
      C1(3,1,2)=C(5,6)
      C1(3,1,3)=C(5,5)
      C1(3,2,1)=C(5,6)
      C1(3,2,2)=C(2,5)
      C1(3,2,3)=C(4,5)
      C1(3,3,1)=C(5,5)
      C1(3,3,2)=C(4,5)
      C1(3,3,3)=C(3,5)
      C2(1,1,1)=C(1,6)
      C2(1,1,2)=C(6,6)
      C2(1,1,3)=C(5,6)
      C2(1,2,1)=C(6,6)
      C2(1,2,2)=C(2,6)
      C2(1,2,3)=C(4,6)
      C2(1,3,1)=C(5,6)
      C2(1,3,2)=C(4,6)
      C2(1,3,3)=C(3,6)
      C2(2,1,1)=C(1,2)
      C2(2,1,2)=C(2,6)
      C2(2,1,3)=C(2,5)
      C2(2,2,1)=C(2,6)
      C2(2,2,2)=C(2,2)
      C2(2,2,3)=C(2,4)
```

```
      C2(2,3,1)=C(2,5)
      C2(2,3,2)=C(2,4)
      C2(2,3,3)=C(2,3)
      C2(3,1,1)=C(1,4)
      C2(3,1,2)=C(4,6)
      C2(3,1,3)=C(4,5)
      C2(3,2,1)=C(4,6)
      C2(3,2,2)=C(2,4)
      C2(3,2,3)=C(4,4)
      C2(3,3,1)=C(4,5)
      C2(3,3,2)=C(4,4)
      C2(3,3,3)=C(3,4)
      C3(1,1,1)=C(1,5)
      C3(1,1,2)=C(5,6)
      C3(1,1,3)=C(5,5)
      C3(1,2,1)=C(5,6)
      C3(1,2,2)=C(2,5)
      C3(1,2,3)=C(4,5)
      C3(1,3,1)=C(5,5)
      C3(1,3,2)=C(4,5)
      C3(1,3,3)=C(3,5)
      C3(2,1,1)=C(1,4)
      C3(2,1,2)=C(4,6)
      C3(2,1,3)=C(4,5)
      C3(2,2,1)=C(4,6)
      C3(2,2,2)=C(2,4)
      C3(2,2,3)=C(4,4)
      C3(2,3,1)=C(4,5)
      C3(2,3,2)=C(4,4)
      C3(2,3,3)=C(3,4)
      C3(3,1,1)=C(1,3)
      C3(3,1,2)=C(3,6)
      C3(3,1,3)=C(3,5)
      C3(3,2,1)=C(3,6)
      C3(3,2,2)=C(2,3)
      C3(3,2,3)=C(3,4)
      C3(3,3,1)=C(3,5)
      C3(3,3,2)=C(3,4)
      C3(3,3,3)=C(3,3)
C        CONVERTING E(I,J) TO EE(I,J,K)
      EE(1,1,1)=E(1,1)
      EE(1,1,2)=E(1,6)
      EE(1,1,3)=E(1,5)
      EE(1,2,1)=E(1,6)
      EE(1,2,2)=E(1,2)
      EE(1,2,3)=E(1,4)
      EE(1,3,1)=E(1,5)
      EE(1,3,2)=E(1,4)
      EE(1,3,3)=E(1,3)
      EE(2,1,1)=E(2,1)
      EE(2,1,2)=E(2,6)
      EE(2,1,3)=E(2,5)
      EE(2,2,1)=E(2,6)
      EE(2,2,2)=E(2,2)
      EE(2,2,3)=E(2,4)
      EE(2,3,1)=E(2,5)
      EE(2,3,2)=E(2,4)
      EE(2,3,3)=E(2,3)
      EE(3,1,1)=E(3,1)
      EE(3,1,2)=E(3,6)
      EE(3,1,3)=E(3,5)
      EE(3,2,1)=E(3,6)
      EE(3,2,2)=E(3,2)
      EE(3,2,3)=E(3,4)
      EE(3,3,1)=E(3,5)
      EE(3,3,2)=E(3,4)
      EE(3,3,3)=E(3,3)
C
C        ROTATING COORDINATES FOR THE ELASTIC CONSTANTS TO C1R(I,J,K), ETC.
C        ROTATING PIEZOELECTRIC CONSTANTS TO EER(I,J,K)
      DO 21 J=1,3
      DO 21 K=1,3
      DO 21 L=1,3
      C1R(J,K,L)=0
      C2R(J,K,L)=0
      C3R(J,K,L)=0
      EER(J,K,L)=0
      DO 24 IS=1,3
      DO 24IT=1,3
      DO 24 IU=1,3
      C1R(J,K,L)=V(J,IS)*V(K,IT)*V(L,IU)*(V(1,1)*C1(IS,IT,IU)+V(1,2)*C2(
     1IS,IT,IU)+V(1,3)*C3(IS,IT,IU))+C1R(J,K,L)
      C2R(J,K,L)=V(J,IS)*V(K,IT)*V(L,IU)*(V(2,1)*C1(IS,IT,IU)+V(2,2)*C2(
     1IS,IT,IU)+V(2,3)*C3(IS,IT,IU))+C2R(J,K,L)
      C3R(J,K,L)=V(J,IS)*V(K,IT)*V(L,IU)*(V(3,1)*C1(IS,IT,IU)+V(3,2)*C2
     1(IS,IT,IU)+V(3,3)*C3(IS,IT,IU))+C3R(J,K,L)
      EER(J,K,L)=V(J,IS)*V(K,IT)*V(L,IU)*EE(IS,IT,IU)+EER(J,K,L)
   24 CONTINUE
   21 CONTINUE
```

```
      PRINT 30
   30 FORMAT(*0ROTATED ELASTIC CONSTANTS*/3X*I*2X*J*2X*K*5X*C1R(I,J,K)*5
     1X*C2R(I,J,K)*5X*C3R(I,J,K)*/)
      DO 27 J=1,3
      DO 27 K=1,3
      DO 27 L=1,3
      PRINT 31,J,K,L,C1R(J,K,L),C2R(J,K,L),C3R(J,K,L)
   31 FORMAT (I4,I3,I3,3(5X,E10.3))
   27 CONTINUE
      PRINT 32
   32 FORMAT(*0ROTATED PIEZOELECTRIC CONSTANTS*/3X*I*2X*J*2X*K*5X*EER(I,
     1J,K)*/)
      DO 33 I=1,3
      DO 33 J=1,3
      DO 33 K=1,3
      PRINT 34,I,J,K,EER(I,J,K)
   34 FORMAT(I4,I3,I3,5X,E10.3)
   33 CONTINUE
C        ROTATING THE DIELECTRIC CONSTANT TO EPSIR(I,J)
      PRINT 35
   35 FORMAT(*0ROTATED DIELECTRIC CONSTANT*/)
      DO 36 I=1,3
      DO 36 J=1,3
      EPSIR(I,J)=0
      DO 37 K=1,3
      DO 37 L=1,3
      EPSIR(I,J)=V(I,K)*V(J,L)*EPSI(K,L)+EPSIR(I,J)
   37 CONTINUE
      PRINT 38,I,J,EPSIR(I,J)
   38 FORMAT(* EPSIR(*I1*,*J1*)= *E10.3)
   36 CONTINUE
      NPROG=1
      NSTEP=0
      GO TO 101
  102 VS=VS-VSINC
  103 IF(VSINC.LT.VSINCC)200,104
  104 VSINC=VSINC/2
  105 VS=VS+VSINC
  101 IF(NSTEP.LT.NSTEPS)106,300
  106 NSTEP=NSTEP+1
      PRINT 112,VS,NSTEP
  112 FORMAT(*1VELOCITY= *E15.8/* NUMBER OF ITERATION = *I3)
C        THE ELEMENTS OF THE EQUATIONS OF MOTION ARE POLYNOMIALS IN S WITH REAL
C        COEFFICIENTS, WHERE S=*J*ALPHA.
C        A(I,J,K) IS THE COEFFICIENT OF S**(K-1)
      CALL STIME
      A(1,1,1)=-C1R(1,1,1)+RHO*VS*VS
      A(1,1,2)=C3R(1,1,1)+C1R(1,1,3)
      A(1,1,3)=-C3R(1,1,3)
      A(1,2,1)=-C1R(1,2,1)
      A(1,2,2)=C3R(1,2,1)+C1R(1,2,3)
      A(1,2,3)=-C3R(1,2,3)
      A(1,3,1)=-C1R(1,3,1)
      A(1,3,2)=C3R(1,3,1)+C1R(1,3,3)
      A(1,3,3)=-C3R(1,3,3)
      A(1,4,1)=-EER(1,1,1)
      A(1,4,2)=EER(1,3,1)+EER(3,1,1)
      A(1,4,3)=-EER(3,3,1)
      A(2,1,1)=-C1R(2,1,1)
      A(2,1,2)=C3R(2,1,1)+C1R(2,1,3)
      A(2,1,3)=-C3R(2,1,3)
      A(2,2,1)=-C1R(2,2,1)+RHO*VS*VS
      A(2,2,2)=C3R(2,2,1)+C1R(2,2,3)
      A(2,2,3)=-C3R(2,2,3)
      A(2,3,1)=-C1R(2,3,1)
      A(2,3,2)=C3R(2,3,1)+C1R(2,3,3)
      A(2,3,3)=-C3R(2,3,3)
      A(2,4,1)=-EER(1,1,2)
      A(2,4,2)=EER(1,3,2)+EER(3,1,2)
      A(2,4,3)=-EER(3,3,2)
      A(3,1,1)=-C1R(3,1,1)
      A(3,1,2)=C3R(3,1,1)+C1R(3,1,3)
      A(3,1,3)=-C3R(3,1,3)
      A(3,2,1)=-C1R(3,2,1)
      A(3,2,2)=C3R(3,2,1)+C1R(3,2,3)
      A(3,2,3)=-C3R(3,2,3)
      A(3,3,1)=-C1R(3,3,1)+RHO*VS*VS
      A(3,3,2)=C3R(3,3,1)+C1R(3,3,3)
      A(3,3,3)=-C3R(3,3,3)
      A(3,4,1)=-EER(1,1,3)
      A(3,4,2)=EER(1,3,3)+EER(3,1,3)
      A(3,4,3)=-EER(3,3,3)
      A(4,1,1)=-EER(1,1,1)
      A(4,1,2)=EER(1,1,3)+EER(3,1,1)
      A(4,1,3)=-EER(3,1,3)
      A(4,2,1)=-EER(1,2,1)
      A(4,2,2)=EER(1,2,3)+EER(3,2,1)
      A(4,2,3)=-EER(3,2,3)
      A(4,3,1)=-EER(1,3,1)
      A(4,3,2)=EER(1,3,3)+EER(3,3,1)
```

```
      A(4,3,3)=-EER(3,3,3)
      A(4,4,1)=EPSIR(1,1)
      A(4,4,2)=-(EPSIR(1,3)*EPSIR(3,1))
      A(4,4,3)=EPSIR(3,3)
C        LET SUBROUTINE PHCDET CALCULATE THE COEFFICIENTS OF THE POLYNOMIAL
C        IN S=J*ALPHA
C        PHCDET RETURNS COEFF(I)=THECOEFFICIENT OF S**(I-1) IN THE POLYNOMIAL.
      CALL PHCDET(A,COEFF)
C     POLYNOMIAL COEFFICIENTS ARE,
      PRINT 45
45    FORMAT(*-POLYNOMIAL COEFFICIENTS ARE*/)
      PRINT 44,((I,COEFF(I)),I=1,9)
   44 FORMAT(* C(*I1*)= *E15.8)
      CALL POLYR(COEFF,S,8,9)
C        TRANSFER COMPLEX ROOTS TO S(I) (I=1,8).
C        CHECK THAT WE HAVE 4 POSITIVE REAL DECAY CONSTANTS.
      ITE=0
      DO 50 I=1,8
      IF(AIMAG(S(I)).GT.0.) 51,50
51    ITE=ITE+1
      ALPHA(ITE)=-(0.,1.)*S(I)
50    CONTINUE
      IF(ITE.LT.4)107,108
108   CONTINUE
C
C        CHECK THAT ROOTS ARE IN SAME ORDER AS LAST ITERATION
      CALL RORD(ALPHA,NSTEP)
52    PRINT 55,(ALPHA(I),I=1,ITE)
55    FORMAT(*0DECAY CONSTANTS =*8(E12.3))
C        EVALUATE BETA(I,J) FOR EACH ALPHA(J) (USE CORRESPONDING S(I))
      DO 60 I=1,4
      S(I)=(0.,1.)*ALPHA(I)
60    CONTINUE
      PRINT 59
59    FORMAT(*-AMPLITUDE RATIOS ARE*)
      DO62 K=1,4
      DO 61 I=1,4
      DO 61 J=1,4
      AC(I,J)=A(I,J,1)+S(K)*(A(I,J,2)+S(K)*A(I,J,3))
61    CONTINUE
      CALL MATSOLV(AC,BETA)
      DO 63 I=1,4
      B(I,K)=BETA(I)
      PRINT 64,I,K,B(I,K)
64    FORMAT(* BETA(*I1*,*I1*)=*E12.3,4X,E12.3)
63    CONTINUE
62    CONTINUE
C        DEFINE TERMS OF THE BOUNDARY CONDITION MATRIX
      DO 71 J=1,4
      DO 70 K=1,3
      ACOM(K,J)=B(1,J)*((0.,1.)*C3R(K,1,1)+ALPHA(J)*C3R(K,1,3))
     *          +B(2,J)*((0.,1.)*C3R(K,2,1)+ALPHA(J)*C3R(K,2,3))
     *          +B(3,J)*((0.,1.)*C3R(K,3,1)+ALPHA(J)*C3R(K,3,3))
     *          +B(4,J)*((0.,1.)*EER(1,3,K)+ALPHA(J)*EER(3,3,K))
70    CONTINUE
      ACOM(4,J)=B(1,J)*((0.,1.)*EER(3,1,1)+ALPHA(J)*EER(3,1,3))
     *          +B(2,J)*((0.,1.)*EER(3,2,1)+ALPHA(J)*EER(3,2,3))
     *          +B(3,J)*((0.,1.)*EER(3,3,1)+ALPHA(J)*EER(3,3,3))
     *-B(4,J)*((0.,1.)*EPSIR(3,1)+ALPHA(J)*EPSIR(3,3)+EPSIO/TANH(W*H/VS)
     *)
71    CONTINUE
C        EVALUATE THE BOUNDARY CONDITION DETERMINANT
C        THE COMPLEX VALUE OF THE DETERMINANT IS RETURNED IN CCOM
      CALL PHCDETC(ACOM,CCOM)
C        DETERMINE THE REAL PART OF THE DETERMINANT
      PRINT 73,CCOM
73    FORMAT(*-BOUNDARY CONDITION DETERMINANT=*2(E12.3))
      X1=1.
      X2=CCOM
      X3=AIMAG(CCOM)
      MSIGN1=SIGN(X1,X2)
      MSIGN2=SIGN(X1,X3)
      IF(NPROG.LT.2) 109,110
109   NSIGN1=MSIGN1
      NSIGN2=MSIGN2
      NPROG=2
110   IF(MSIGN1.EQ.NSIGN1.AND.MSIGN2.EQ.NSIGN2)111,107
111   IF(NPROG.EQ.2)105,103
107   IF(NPROG-2)201,202,203
201   PRINT 113,ITE
113   FORMAT(*-ONLY *I3*DECAY CONSTANTS*)
      GO TO 1000
202   NPROG=3
203   GO TO 102
300   PRINT 301
301   FORMAT(*1PERMISSIBLE NUMBER OF ITERATIONS EXCEEDED--PROGRAM TERMIN
     CATED*)
      GO TO 1000
```

```
200   PRINT 114,VSINCC,VS
114   FORMAT(*-ITERATION COMPLETE*/* VSINC LESS THAN *E15.8/* VELOCITY=
     C*E15.8)
C
C        SOLVE FOR THE A(J) COEFFICIENTS IN  THE BOUNDARY CONDITION MATRIX
C
      CALL MATSOLV(ACOM,AMP)
      PRINT 304
304   FORMAT(*0AMPLITUDE COEFFICIENTS ARE */)
      PRINT 302,(AMP(I),I=1,4)
 302  FORMAT(2E15.3)

C        RESCALE THE B(I,J) WITH THE AMP(I) FROM THE BOUNDARY CONDITIONS
      DO 303 I=1,4
      DO 303J=1,4
 303  B(I,J)=AMP(J)*B(I,J)
C
C        COMPUTE THE POWER FLOW P1 PARALLEL TO THE WAVE VECTOR AND
C        P2 PERPENDICULAR TO THE WAVE VECTOR
      P1=CZERO
      P2=CZERO
      P3=CZERO
      DO 310 I=1,4
      ALPHAC(I)=CONJG(ALPHA(I))
      DO 310 J=1,4
 310  BC(I,J)=CONJG(B(I,J))
      DO 320 J=1,3
      DO 320 N=1,4
      BT1=(EER(1,1,J)-JAY*ALPHA(N)*EER(3,1,J))*B(4,N)
      BT2=(EER(1,2,J)-JAY*ALPHA(N)*EER(3,2,J))*B(4,N)
      BT3=(EER(1,3,J)-JAY*ALPHA(N)*EER(3,3,J))*B(4,N)
      DO 321 K=1,3
      BT1=BT1+(C1R(J,K,1)-JAY*ALPHA(N)*C1R(J,K,3))*B(K,N)
      BT2=BT2+(C2R(J,K,1)-JAY*ALPHA(N)*C2R(J,K,3))*B(K,N)
      BT3=BT3+(C3R(J,K,1)-JAY*ALPHA(N)*C3R(J,K,3))*B(K,N)
321   CONTINUE
      BTEMP=CZERO
      DO 322 M=1,4
322   BTEMP=BTEMP+ BC(J,M)/(ALPHA(N)+ALPHAC(M))
      P1=P1+BTEMP*BT1
      P2=P2+BTEMP*BT2
      P3=P3+BTEMP*BT3
320   CONTINUE
      P1=0.5*W*P1
      PRINT 312,P1
 312  FORMAT(*0POWER FLOW P1 = *2E12.3/)
      P2=0.5*W*P2
      PRINT 313,P2
 313  FORMAT(*0POWER FLOW P2 = *2E12.3/)
      P3=0.5*W*P3
      PRINT 316,P3
316   FORMAT(*0POWER FLOW P3 = *2E12.3/)
C
C        COMPUTE THE TOTAL POWER
      PR1=REAL(P1)
      PR2=REAL(P2)
      PTOT=SQRT(PR1*PR1+PR2*PR2)
      PRINT 314,PTOT
 314  FORMAT(*0TOTAL POWER FLOW = *E12.3*WATTS*/)
      GAMMA=ATAN2(PR2,PR1)*180./PI
      PRINT 315,GAMMA
315   FORMAT(*0MISALIGNMENT ANGLE= *E12.3*DEGREES*/)
C
C        NORMALISE WAVE COMPONENTS FOR ONE WATT/METRE
      PRINT 400
400   FORMAT(*0NORMALISED AMPLITUDES*/5X*I*9X*J*17X*BETA(I,J)*/)
      PTOT = SQRT(PTOT)
      DO 401 I=1,4
      DO 402 J=1,4
      B(I,J)=B(I,J)/PTOT
402   CONTINUE
      PRINT 323,I,(B(I,J),J=1,4)
 323  FORMAT(I6,9X*1-4*3X,4(E15.3,E11.3))
401   CONTINUE
      GO TO 1000
      DO 324 I=1,4
      PUNCH 325,ALPHA(I)
      DO 324 J=1,4
      PUNCH 325,B(I,J ),I,J
325   FORMAT(2E20.12,2I10)
324   CONTINUE
      PUNCH 326,VS
326   FORMAT(E20.12*VS*)
      PUNCH 327,W
327   FORMAT(E20.12*W*)
      PUNCH328,H
328   FORMAT(E20.12*H*)
      DO 340 I=1,3
      DO 340 J=1,3
      DO 340 K=1,3
```

```
      PUNCH 341,EER(I,J,K),I,J,K
341   FORMAT(E20.12,3I10)
340   CONTINUE
      DO 342 I=1,3
      PUNCH 343,EPSIR(I,1),EPSIR(I,3),I
343   FORMAT(2E20.12,I10)

342   CONTINUE
 1000 CONTINUE
      STOP
      END
      SUBROUTINE RORD(A,NSTEP)
C
C        THIS SUBROUTINE ATTEMPTS TO ENSURE THAT ROOTS OF THE POLYNOMIAL
C        APPEAR IN THE SAME ORDER IN SUCCESSIVE ITERATIONS
      COMPLEX A(4),S(4),X,Y
      DIMENSION C(4)
      DIFF(X,Y)=CABS(X-Y)
C
C        IS THIS THE FIRST ITERATION
      IF(NSTEP.EQ.1)1,2
1     DO 3 I=1,4
3     S(I)=A(I)
      GO TO 4
C
C        REORDER THE ROOTS
2     DO 5 N=1,3
      J=5-N
      DO 6 I=1,J
6     C(I)=DIFF(S(N),A(I))
      CMIN=C(1)
      MIN=1
      DO 7 I=2,J
      IF(C(I).LT.CMIN)8,7
8     CMIN=C(I)
      MIN=I
7     CONTINUE
      S(N)=A(MIN)
      A(MIN)=A(J)
5     CONTINUE
      S(4)=A(1)
      DO 9 I=1,4
9     A(I)=S(I)
4     RETURN
      END
      SUBROUTINE STIME
      CALL SECOND(T)
      PRINT 2000,T
2000  FORMAT(*-CP TIME= *F10.3//)
      RETURN $ END
      SUBROUTINE PHCDET(A,C)
      DIMENSION A(4,4,3),C(9)
      INTEGER E,P(4),R(4)
C
C     THIS SUBROUTINE DETERMINES THE EXPANDED POLYNOMIAL FORM OF A 4 BY
C     4 DETERMINANT WHOSE ELEMENTS ARE POLYNOMIALS OF SECOND ORDER
C     WITH REAL COEFFICIENTS
C
C     NOTATION
C     ---------------------------------------------------------------
C
C     A(I,J,K) IS A 4 BY 4 BY 3 ARRAY USED TO STORE THE MATRIX ELEMENTS
C     A(I,J,K) IS THE ELEMENT IN THE ITH ROW,JTH COLUMN AND THE (K-1)TH
C     POWER OF S
C
C     P(J) IS A PERMUTATION OF THE NUMBERS 1 TO 4
C
C     R(J) IS A VECTOR USED IN CALCULATING THE PARITY
C
C     E IS THE PARITY OF THE PERMUTATION
C
C     L1 TO L4 ARE LOOP COUNTERS USED TO GENERATE P
C
C     C(N) IS THE OUTPUT VECTOR OF THE POLYNOMIAL COEFFICIENTS
C     C(N) IS THE COEFFICIENT OF S TO THE POWER (N-1)
C
C     K1 TO K4 ARE LOOP COUNTERS USED TO ACCUMULATE C
C
C     N IS INDEX NUMBER - POLYNOMIAL POWER PLUS 1
C
C
C     SET INITIAL VALUES OF C TO ZERO
C     ---------------------------------------------------------------
C
      DO 1 N=1,9
      C(N)=0.
    1 CONTINUE
```

```
C
C     GENERATION OF PERMUTATION
C     -------------------------------------------------------------
C
C     MUST PUT EACH DIGIT 1 TO 4 IN TURN INTO SUCCESSIVE POSITIONS OF P
C     BUT MUST AVOID USING THE SAME DIGIT TWICE.LOOPS L1 TO L4 ARE
C     NESTED
C
      DO 2 L1=1,4
      P(1)=L1
      DO 3 L2=1,4
      IF (L2.EQ.L1) GO TO 3
      P(2)=L2
      DO 4 L3=1,4
      IF (L3.EQ.L1.OR.L3.EQ.L2) GO TO 4
      P(3)=L3
      DO 5 L4=1,4
      IF (L4.EQ.L1).OR.L4.EQ.L2.OR.L4.EQ.L3) GO TO 5
      P(4)=L4
C
C     THIS COMPLETES THE GENERATION OF THE PERMUTATION P
C
C     DETERMINATION OF THE PARITY
C     -------------------------------------------------------------
C
C     REQUIRE TWO RECORDS OF P AND SO PUT P INTO R
C
      DO 6 N=1,4
      R(N)=P(N)
    6 CONTINUE
C
C     MAKE AN INITIAL SETTING OF PARITY EQUAL TO 1
C
      E=1
C
C     NOW INTERCHANGE ELEMENTS OF R TO GET THEM INTO NUMERICAL ORDER
C     MULTIPLYING PARITY BY -1 EACH TIME AN INTERCHANGE IS NEEDED
C
      DO 7 I=1,4
      IF (R(I).EQ.I) GO TO 7
C
C     THE LAST STATEMENT ENSURES AVOIDING SUPERFLUOUS INTERCHANGES
C
      DO 8 J=1,4
      IF (R(J).EQ.I) 9,24
    9 CONTINUE
      R(J)=R(I)
      R(I)=I
C
C     THAT WILL PUT THE DIGIT I INTO ITS CORRECT PLACE BY EXCHANGING
C     IT WITH THE OCCUPANT OF THAT PLACE
C     ADJUST THE PARITY AS THE RESULT OF THIS EXCHANGE
C
      E=E*(-1)
   24 CONTINUE
    8 CONTINUE
    7 CONTINUE
C
C     HAVE NOW DETERMINED THE PARITY E
C
C     ACCUMULATION OF POLYNOMIAL COEFFICIENTS
C     -------------------------------------------------------------
C
C     CONSTRUCT NOW ONE TERM OF THE MATRIX EXPANSION.THE TERM WILL
C     HAVE 4 FACTORS WITH THE ROW AND COLUMN INDICES
C              1,P(1)   2,P(2)   3,P(3)   4,P(4)
C     IN EACH OF THESE 4 FACTORS ARE 3 TERMS.EACH CORRESPONDS TO A
C     POWER OF S AND IS GENERATED AS K RANGES OVER ITS 3 VALUES
C     THE FULL PRODUCT IS OBTAINED BY USING A FURTHER SET OF 4 NESTED
C     DO LOOPS AS BELOW
C
      DO 10 K1=1,3
      DO 11 K2=1,3
      DO 12 K3=1,3
      DO 13 K4=1,3
C
C     THE POWER OF THE POLYNOMIAL TO WHICH THIS PRODUCT OF TERMS WILL
C     CONTRIBUTE IS GIVEN BY
C
      N=K1+K2+K3+K4-3
C
C     ARE NOW READY TO ACCUMULATE C BY THE FOLLOWING
C
      IDUM1=P(1)
      IDUM2=P(2)
      IDUM3=P(3)
      IDUM4=P(4)
      C(N)=C(N)+E*A(1,IDUM1,K1)*A(2,IDUM2,K2)*A(3,IDUM3,K3)
     C*A(4,IDUM4,K4)
```

```
C
C     NOW THE LOOPS OVER K1 TO K4 ARE TO BE CLOSED
C
   13 CONTINUE
   12 CONTINUE
   11 CONTINUE
   10 CONTINUE
C
C     CLOSE THE LOOPS L1 TO L4 WHICH GENERATED THE PERMUTATION OF THE
C     ARRAY ELEMENTS
C
    5 CONTINUE
    4 CONTINUE
    3 CONTINUE
    2 CONTINUE
C
C     THE POLYNOMIAL COEFFICIENTS ARE NOW IN VECTOR C
C
      RETURN
      END
      SUBROUTINE POLYR(H,Z,N,K)
      COMPLEX B,Z,DZ,SZ,ZT
      DIMENSION H(K),Z(K),B(50),A(10)
      DO 990 I=1,9,1
      A(I)=H(I)
  990 CONTINUE
      N=N+1
      EPS=1.0E-10
      M=N
  400 ZT=(0.,0.)
      DO 401 I=1,M
  401 B(I)=A(I)
      IF(A(1)) 404,402,404
  402 M=M-1
      DO 403 I=1,M
  403 A(I)=A(I+1)
      Z(N-M)=(0.,0.)
      GO TO 434
  404 IF (A(M)) 406,405,406
  405 M=M-1
      Z(N-M)=(1.0E+100,0.)
      GO TO 434
  406 IF(M-2) 435,407,408
  407 Z(N-1)=-A(1)/A(2)
      GO TO 435
  408 D=.1
      L=0
      SZ=(0.,0.)
      GO TO 412
  409 DO 410 I=1,M
  410 B(I)=A(I)
      SZ=DZ
      DO 411 I=2,M
      DO 411 J=I,M
  411 B(M+I-J-1)=B(M+I-J-1)+ZT*B(M+I-J)
  412 RMAG=500.0
      BA=CABS(B(1))
      IF(BA) 426,426,413
  413 BA=ALOG(BA)
      DO 416 I=2,M
      BM=CABS(B(I))
      IF(BM) 416,416,414
  414 BM=(BA-ALOG(BM))/(I-1.)
      IF(BM-RMAG) 415,415,416
  415 RMAG=BM
      II=I
  416 CONTINUE
      IF(II-2) 417,417,418
  417 DZ=-B(1)/B(2)
      RMAG=CABS(DZ)
      GO TO 419
  418 RMAG=EXP(RMAG)
      DZ=-B(1)/B(II)
      X=REAL(DZ)
      Y=AIMAG(DZ)
      THE=ATAN2(Y,X)/(II-1.)
      X=RMAG*COS(THE)
      Y=RMAG*SIN(THE)
      DZ=CMPLX(X,Y)
  419 IF(CABS(DZ+SZ)-.1*RMAG) 420,421,421
  420 DZ=0.5*DZ
  421 ZT=ZT+DZ
      R=CABS(ZT)
      IF(RMAG-EPS*R) 426,422,422
  422 IF(RMAG-D*R) 423,424,424
  423 L=0
      D=0.1*D
      GO TO 422
```

```
  424 L=L+1
      IF(L-25) 409,425,425
  425 IF(CABS(DZ)-CABS(SZ)) 409,426,426
  426 X=REAL(ZT)
      Y=AIMAG(ZT)
      IF(ABS(X)-1.0E+8*ABS(Y)) 430,427,427
  427 M=M-1
      Z(N-M)=X
      DO 428 I=2,M
  428 A(M+2-I)=A(M+2-I)+X*A(M+3-I)
      DO 429 I=1,M
  429 A(I)=A(I+1)
      GO TO 434
  430 M=M-2
      Z(N-M-1)=ZT
      Z(N-M)=CONJG(ZT)
      IF(M-1) 435,435,431
  431 A(M+1)=A(M+1)+2*X*A(M+2)
      DO 432 I=2,M
  432 A(M+2-I)=A(M+2-I)+2*X*A(M+3-I)-R*R*A(M+4-I)
      DO 433 I=1,M
  433 A(I)=A(I+2)
  434 IF(M-1) 435,435,400
  435 N=N-1
      RETURN
      END
      SUBROUTINE PHCDETC(ACOM,CCOM)
      COMPLEX ACOM(4,4),CCOM
      INTEGER E,P(4),R(4)
      CCOM=(0.,0.)
C
C
C
C     P(J) IS A PERMUTATION OF THE NUMBERS 1 TO 4
C
C     R(J) IS A VECTOR USED IN CALCULATING THE PARITY
C
C     E IS THE PARITY OF THE PERMUTATION
C
C     L1 TO L4 ARE LOOP COUNTERS USED TO GENERATE P
C
C     GENERATION OF PERMUTATION
C     -------------------------
C
C     MUST PUT EACH DIGIT 1 TO 4 IN TURN INTO SUCCESSIVE POSITIONS OF P
C     BUT MUST AVOID USING THE SAME DIGIT TWICE.LOOPS L1 TO L4 ARE
C     NESTED
C
      DO 2 L1=1,4
      P(1)=L1
      DO 3 L2=1,4
      IF (L2.EQ.L1) GO TO 3
      P(2)=L2
      DO 4 L3=1,4
      IF (L3.EQ.L1.OR.L3.EQ.L2) GO TO 4
      P(3)=L3
      DO 5 L4=1,4
      IF (L4.EQ.L1.OR.L4.EQ.L2.OR.L4.EQ.L3) GO TO 5
      P(4)=L4
C
C     THIS COMPLETES THE GENERATION OF THE PERMUTATION P
C
C     DETERMINATION OF THE PARITY
C     ---------------------------
C
C     REQUIRE TWO RECORDS OF P AND SO PUT P INTO R
C
      DO 6 N=1,4
      R(N)=P(N)
    6 CONTINUE
C
C     MAKE AN INITIAL SETTING OF PARITY EQUAL TO 1
C
      E=1
C
C     NOW INTERCHANGE ELEMENTS OF R TO GET THEM INTO NUMERICAL ORDER
C     MULTIPLYING PARITY BY -1 EACH TIME AN INTERCHANGE IS NEEDED
C
      DO 7 I=1,4
      IF (R(I).EQ.I) GO TO 7
C
C     THE LAST STATEMENT ENSURES AVOIDING SUPERFLUOUS INTERCHANGES
C
      DO 8 J=1,4
      IF (R(J).EQ.I) 9,24
    9 CONTINUE
      R(J)=R(I)
      R(I)=I
```

```
C
C      THAT WILL PUT THE DIGIT I INTO ITS CORRECT PLACE BY EXCHANGING
C      IT WITH THE OCCUPANT OF THAT PLACE
C      ADJUST THE PARITY AS THE RESULT OF THIS EXCHANGE
C
       E=E*(-1)
   24  CONTINUE
    8  CONTINUE
    7  CONTINUE
C
C      HAVE NOW DETERMINED THE PARITY E
C
C
C      ARE NOW READY TO ACCUMULATE C BY THE FOLLOWING
C
       IDUM1=P(1)
       IDUM2=P(2)
       IDUM3=P(3)
       IDUM4=P(4)
       CCOM=CCOM+E*ACOM(1,IDUM1)*ACOM(2,IDUM2)*ACOM(3,IDUM3)*ACOM(4,IDUM4
      U)
C
C      CLOSE THE LOOPS L1 TO L4 WHICH GENERATED THE PERMUTATION OF THE
C      ARRAY ELEMENTS
C
    5  CONTINUE
    4  CONTINUE
    3  CONTINUE
    2  CONTINUE
C
C         THE VALUE OF THE DETERMINANT IS NOW IN CCOM
C
       RETURN
       END
       SUBROUTINE MATSOLV(AC,BETA)
C         THIS SUBROUTINE SOLVES A FOUR BY FOUR MATRIX EQUATION
       COMPLEX AC(4,4),BETA(4),B(3,3),ACC(4),C(2,2),DUM
       COMPLEX M42,M43,M32
       M42=-AC(2,4)/AC(4,4)
       M43=-AC(3,4)/AC(4,4)
       DO 2 I=1,3
       B(3,I)=AC(3,I)+M43*AC(4,I)
       B(2,I)=AC(2,I)+M42*AC(4,I)
2      CONTINUE
       M32=-B(2,3)/B(3,3)
       C(2,1)=B(2,1)+M32*B(3,1)
       C(2,2)=B(2,2)+M32*B(3,2)
C         FINDING SOLUTIONS
       BETA(1)=(1.,0.)
       BETA(2)=-BETA(1)*C(2,1)/C(2,2)
       BETA(3)=-(BETA(1)*B(3,1)+BETA(2)*B(3,2))/B(3,3)
       BETA(4)=-(BETA(1)*AC(4,1)+BETA(2)*AC(4,2)+BETA(3)*AC(4,3))/AC(4,4)
C         CHECKING SOLUTIONS
       DO 5 L=1,4
5      ACC(L)=(0.,0.)
       DO 3 I=1,4
       DO 3 J=1,4
       ACC(I)=AC(J,I)*ACC(I)
3      CONTINUE
       DUM=ACC(1)*BETA(1)+ACC(2)*BETA(2)+ACC(3)*BETA(3)+ACC(4)*BETA(4)
       PRINT 4,DUM
4      FORMAT(*0CHECK SUBSTITUTION IN SUM OF EQUATIONS=*E11.3,E11.3/)
       RETURN
       END
00000000000000000000000      END OF RECORD
  86.74E+9          C11
   6.99E+9          C12
  11.91E+9          C13
- 17.91E+9          C14
    .  E+9          C15
    .  E+9          C16
  86.74E+9          C22
  11.91E+9          C23
  17.91E+9          C24
    .  E+9          C25
    .  E+9          C26
 107.2 E+9          C33
    .  E+9          C34
    .  E+9          C35
    .  E+9          C36
  57.94E+9          C44
    .  E+9          C45
    .  E+9          C46
  57.94E+9          C55
- 17.91E+9          C56
  39.88E+9          C66
   1.71E-1          E11
-  1.71E-1          E12
    .  E-           E12
```

```
-  4.06E-2          E14
    .  E-           E15
    .  E-           E16
    .  E-           E21
    .  E-           E22
    .  E-           E23
    .  E-           E24
   4.06E-2          E25
-  1.71E-1          E26
    .  E-           E31
    .  E-           E32
    .  E-           E33
    .  E-           E34
    .  E-           E35
    .  E-           E36
 8.854E-12       EPSIO
 39.21E-12          EPSI 11
   .  E-12          EPSI 12
   .  E-12          EPSI 13
   .  E-12          EPSI 21
 39.21E-12          EPSI 22
   .  E-12          EPSI 23
   .  E-12          EPSI 31
   .  E-12          EPSI 32
 41.03E-12          EPSI 33
  3.14159265E 8     W
    2.65   E 3     RHO
 5.   E -3     VSINCC
   0.             0.              THETA     PSI
   1.      E-20    H
 3140.            10.          25   VS,VSINC,NS1EPS
00000000000000000000     END OF FILE
```

## A1.2 Program ASWPLOT - Surface-Wave Field Plots

### A1.2.1 Flow Chart

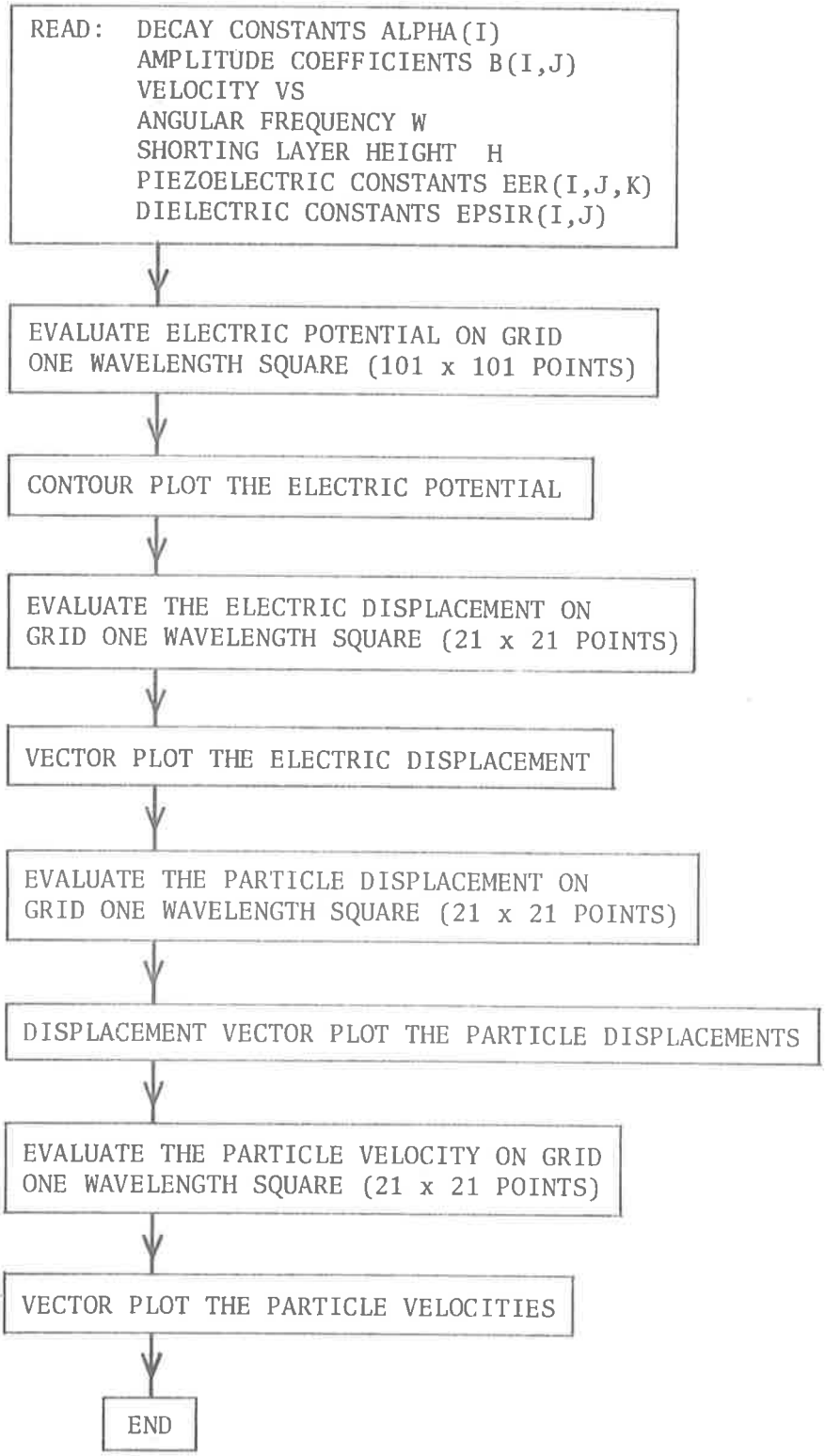

## A1.2.2 Program Listing

```
      PROGRAM ASWPLOT(INPUT,OUTPUT)
C
C        THIS PROGRAM PLOTS THE ---
C        ELECTRIC POTENTIAL
C        ELECTRIC DISPLACEMENT
C        PARTICLE DISPLACEMENT
C        PARTICLE VELOCITY
C        FIELDS FOR A PROPAGATING SURFACE WAVE
C     INPUT DATA NEEDED---
C        ALPHA(I ) = 4 DECAY CONSTANTS
C        B(I,J) = 16 AMPLITUDE COEFFICIENTS
C        VS = SURFACE WAVE VELOCITY
C        W = ANGULAR FREQUENCY
C        H = HEIGHT OF CONDUCTING PLANE
C        EER(I,J ) = 27 PIEZOELECTRIC CONSTANTS
C        EPSIR(I,J) = 6 DIELECTRIC CONSTANTS
C
      DIMENSION Z(51,51),CO(30),EER(3,3,3),EPSIR(3,3)
      DIMENSION LQ(51,51)
      COMPLEX B(4,4),ALPHA(4)
      COMPLEX JAY,BTEMP,XTEMP,D(3),BSUM
      COMPLEX CXTEMP
      COMPLEX A(21,21)
      COMPLEX AVEL(21,21),DUM
      DIMENSION TED(4),TPD(4),TPV(4)
      COMPLEX U(3)
      COMPLEX V(3)
      COMPLEX E(4)
      REAL LAMBDA
      REAL MOD
      COMMON/ /Z,LQ
      PI=3.14159265358979
      DATA TED/40HELECTRIC DISPLACEMENT ASW ON YX-QUARTZ  /
      DATA TPD/40HPARTICLE DISPLACEMENT OF ASW YX-QUARTZ  /
      DATA TPV/40HPARTICLE VELOCITY OF ASW ON YX-QUARTZ   /
      EPSIO =8.85E-12
      PRINT 99
99    FORMAT(1H1,9X*I*9X*J*17X*B(I,J)*/)
      DO 100 I=1,4
      READ 101,ALPHA(I)
      PRINT 103,I,ALPHA(I)
103   FORMAT(* ALPHA(*I1*)=*2E20.6)
      DO 100 J=1,4
      READ 101,B(I,J),II,JJ
101   FORMAT(2E20.12,2I10)
      PRINT 102,II,JJ,B(I,J)
102   FORMAT(I11,I10,2E20.6)
100   CONTINUE
      READ 113,VS,W,H
113   FORMAT(E20.12)
      PRINT 104,VS,W,H
104   FORMAT(* VS =*E20.6/* W =*E20.6/* H =*E20.6/)
      PRINT 105
105   FORMAT(*0PIEZOELECTRIC CONSTANTS*/)
      DO 106 I=1,3
      DO 106 J=1,3
      DO 106 K=1,3
      READ 107,EER(I,J,K),II,JJ,KK
107   FORMAT(E20.12,3I10 )
      PRINT 108,II,JJ,KK,EER(I,J,K)
108   FORMAT(I11,2I10,E20.6)
106   CONTINUE
      PRINT 109
109   FORMAT(*0DIELECTRIC CONSTANTS*/)
      DO 110 I=1,3
      READ 111,EPSIR(I,1),EPSIR(I,3),II
111   FORMAT(2E20.12,I10)
      PRINT 112,II,EPSIR(I,1),EPSIR(I,3)
112   FORMAT(I11,2E20.6)
110   CONTINUE
C
C        COMPUTE VALUE OF ELEC POTENTIAL OVER THE PLOTTING GRID
C        (101 X 101 POINTS) ONE WAVELENGTH SQUARE, AT T=0 AND X1=0 TO LAMBDA
      LAMBDA=2.*PI*VS/W
      PRINT 400,LAMBDA
400   FORMAT(*1SURFACE WAVELENGTH =*E12.3*METRES*/)
      XINC=LAMBDA/50.
      DO 401 I=1,51
      DO 403 J=1,38
      X1=(I-1)*XINC
      X3=(38.-J)*XINC
      Z(I,J)=0.
      DO 402 N=1,4
      BTEMP=-1.*W*(ALPHA(N)*X3+(0.,1.)*X1)/VS
      Z(I,J)=Z(I,J)+B(4,N)*CEXP(BTEMP)
```

```
 402  CONTINUE
 403  CONTINUE
      DO 404 J=39,51
      Z(I,J)=(0.,0.)
      X3=(38.-J)*XINC
      UT=W*H/VS
      UV=UT+W*X3/VS
      UTM=-1.*UT
      UVM=-1.*UV
      XTEMP=-1.*(0.,1.)*W*X1/VS
      IF(UT.GT.100.)405,406
 405  XTEMP=CEXP(XTEMP)*EXP(W*X3/VS)
      GO TO 407
 406  CONTINUE
      XTEMP=CEXP(XTEMP)*(EXP(UV)-EXP(UVM))/(EXP(UT)-EXP(UTM))
 407  CONTINUE
      Z(I,J)=(B(4,1)+B(4,2)+B(4,3)+B(4,4))*XTEMP
      GO TO 404
 404  CONTINUE
 401  CONTINUE
C
C        PLOT CONTOURS OF THE ARRAY Z
      CALL PLOT10(10HNEBC Bx142,10)
      CALL XLIMIT(100.)
      CALL PAUPLOT(30HBLANK PAPER + .4 BLACK INK PLS,30)
      CALL SYMBOL(-1.,2.,.1,18HPOTENTIAL CONTOURS,90.,18)
      CALL PLOT(0.,7.4,3)
      CALL PLOT(10.,7.4,2)
      CALL PLOT(0.,0.,3)
      CALL BCONTR(Z,51,51,5.,5.,30,0,LQ,CO,NONO)
      PRINT 410,NONO
 410  FORMAT(*0NUMBER OF CONTOURS =*I5/)
      PRINT 411,(I,CO(I),I=1,NONO)
 411  FORMAT(* CONTOUR*I2* =*E11.3)
C
C        COMPUTE THE ELECTRIC DISPLACEMENT
      WVEC=W/VS
      JAY=CMPLX(0.,1. )
      XINC=LAMBDA/20.
      DO 501 I=1,21
      DO 502 J=1,16
      X1=(I-1)*XINC
      X3=(16.-J)*XINC
      A(I,J)=(0.,0.)
      DO 506 N=1,4
      BTEMP=-1.*WVEC*(ALPHA(N)*X3+JAY*X1)
506   E(N )=CEXP(BTEMP)
      DO 503 N=1,3,2
      D(N)=(0.,0.)
      DO 504 K=1,4
      DUM=(0.,0.)
      DO 505 L=1,3
505   DUM =DUM +(JAY*EER(N,L,1)+ALPHA(K)*EER(N,L,3))*B(L,K)
      DUM =DUM -(JAY*EPSIR(N,1)+ALPHA(K)*EPSIR(N,3))*B(4,K)
      DUM=DUM*E(K)
504   D(N)=DUM+D(N)
503   D(N)=-WVEC*D(N)
      D1=REAL(D(1))
      D3=REAL(D(3))
      MOD=SQRT(D1*D1+D3*D3)
      ANGLE=ATAN2(-D3,D1)
      A(I,J)=CMPLX(MOD,ANGLE)
502   CONTINUE
C
C        COMPUTE THE FREE SPACE ELECTRIC DISPLACEMENT
      BSUM=(0.,0.)
      DO 509 K=1,4
509   BSUM=BSUM+B(4,K)
      DO 510 J=17,21
      A(I,J)=(0.,0.)
      X3=(16.-J)*XINC
      UT=WVEC*H
      UTM=-1.*UT
      UV=UT+WVEC*X3
      UVM=-1.*UV
      XTEMP=-JAY*WVEC*X1
      CXTEMP=CEXP(XTEMP)
      IF(UT.GT.100.)511,512
511   D(1)=EPSIO*JAY*WVEC*BSUM*CXTEMP*EXP(WVEC*X3)
      D(3)=-EPSIO*WVEC*BSUM*CXTEMP*EXP(WVEC*X3)
      GO TO 513
512   CONTINUE
      CUT=EXP(UT)
      CUTM=EXP(UTM)
      CUV=EXP(UV)
      CUVM=EXP(UVM)
      D(1)=(CUV-CUVM)*CXTEMP/(CUT-CUTM)
      D(1)=D(1)*EPSIO*JAY*WVEC*BSUM
      D(3)=(CUV+CUVM)*CXTEMP/(CUT-CUTM)
      D(3)=-D(3)*EPSIO *WVEC*BSUM
```

```
513   CONTINUE
      D1=REAL(D(1))
      D3=REAL(D(3))
      MOD=SQRT(D1*D1+D3*D3)
      ANGLE=ATAN2(-D3,D1)
      A(I,J)=CMPLX(MOD,ANGLE)
      GO TO 510
510   CONTINUE
501   CONTINUE
      VL=1.0
      CALL VECPLOT(A,21,21,2.,2.,TED,VL,0)
C
C        COMPUTE PARTICLE DISPLACEMENT FIELD
      WVEC=W/VS
      JAY=CMPLX(0.,1.)
      DO 600 I=1,21
      DO 601 J=1,16
      X1=(I-1 .)*XINC
      X3=(16.-J)*XINC
      A(I,J)=(0.,0.)
      DO 606 N=1,4
      BTEMP=-1.*WVEC*(ALPHA(N)*X3+JAY*X1)
606   E(N)=CEXP(BTEMP)
      DO 602 N=1,3,2
      U(N )=(0.,0.)
      DO 603 K=1,4
603   U(N)=U(N)+B(N,K)*E(K)
602   CONTINUE
      U1=REAL(U(1 ) )
      U3=REAL(U(3))
      MOD=SQRT(U1*U1+U3*U3)
      ANGLE=ATAN2(-U3,U1)
      A(I,J)=CMPLX(MOD,ANGLE)
C
C        COMPUTE PARTICLE VELOCITY
      DO 702 N=1,3,2
702   V(N)=U(N)*JAY*W
      V1=REAL(V(1))
      V3=REAL(V(3))
      MOD=SQRT(V1*V1+V3*V3)
      ANGLE=ATAN2(-V3,V1)
      AVEL(I,J)=CMPLX(MOD,ANGLE)
601   CONTINUE
      DO 604 J=17,21
      AVEL(I,J)=(0.,0.)
604   A(I,J)=(0.,0.)
600   CONTINUE
C
C        PLOT PARTICLE DISPLACEMENT
      VL=1.0
      CALL VECPLOT(A,21,21,2.,2 .,TPD,VL,1)
C
C        PLOT THE PARTICLE VELOCITY
      VL=1.0
      CALL VECPLOT(AVEL,21,21,2.,2.,TPV,VL,0)
      STOP
      END
      SUBROUTINE VECPLOT(A,M,N,XS,YS,T,VL,K )
C
C        THIS SUBROUTINE PLOTS A VECTOR FIELD SPECIFIED AT THE INTERSECTION
C        POINTS OF A RECTANGULAR GRID, AND DRAWS A BOUNDARY THROUGH THE OUTER
C        GRID POINTS.
C        A = A COMPLEX NUMBER, THE REAL PART HOLDING THE LENGTH OF THE VECTOR
C        AND THE IMAGINARY PART THE DIRECTION RELATIVE TO  THE X-AXIS (IN RADS).
C        T = ALPHABETIC TITLE (UP TO 40 CHARACTERS)
C
C
C        THE FIRST INDEX INDICATES THE X-VARIABLE MAGNITUDE AND THE SECOND
C        THE Y-VARIABLE I.E. OF THE FORM A(X,Y)
C        M = THE NUMBER OF COLUMNS IN THE GRID
C        N = THE NUMBER OF HORIZONTAL ROWS IN THE GRID
C        XS = NUMBER OF MESH POINTS/INCH
C              IN X DIRECTION
C        YS = NUMBER OF MESH POINTS/INCH IN Y DIRN.
C        T = AN ARRAY OF UP TO 40 HOLLERITH
C        CHARACTERS HOLDING A TITLE.
C        VL = ARROW LENGTH / HORIZONTAL MESH SPACING.
C        K = SETS PLOTTING MODE. K=1, THE ARROWS ORIGINATE AT THE GRID POINTS.
C             WITH K.NOT EQ.1 THE ARROWS ARE BISECTED BY A BAR INDICATING THE
C             GRID POINT LOCATION
C        VL RETURNS A SCALE FACTOR (IN INPUT UNITS/INCH) WHICH WHEN MULTIPLIED B
C        BY THE ARROW LENGTHS INDICATES THE MAGNITUDE OF THE PLOTTED QUANTITY
C        THE PEN IS ASSUMED TO BE AT THE LOWER L.H. CORNER OF THE GRID, AND THIS
C        POINT MUST HAVE BEEN DEFINED AS THE NEW ORIGIN
C        AFTER PLOTTING THE ORIGIN IS SHIFTED TO A POINT 2 INCHES TO THE RIGHT O
C        OF THE R.H. EDGE OF THE GRID
C
C
```

```
      DIMENSION T(4)
      DIMENSION TS(3)
      COMPLEX A(M,N)
      DATA (TS(I),I=1,3)/30HSCALE =              UNITS/INCH/
C        DRAW IN THE BORDER STARTING
C        FROM (0,0)
      X1=(M-1.)/XS
      X2 = X1
      X3=0.
      Y1 = 0
      Y2=(N-1.)/YS
      Y3 = Y2
      CALL PLOT (X1,Y1,2)
      CALL PLOT (X2,Y2,1)
      CALL PLOT (X3,Y3,1)
      CALL PLOT (0.,0.,1)
C        DRAW IN THE ARROWS AT THE
C        MESH POINTS
C        NORMALISE THE MAXIMUM ARROW LENGTHS
C        TO BE EQUAL TO VL * HORIZONTAL
      AM = 1.E-200
      DO 10 I=1,M
      DO 10 J=1,N
10    AM = AMAX1(AM,REAL(A(I,J)))
C        SCALE FACTOR THEN BECOMES
      VL=AM*XS/VL
      PRINT 1,AM,VL
1     FORMAT(* AM=*E11.3* VL=*E11.3)
      DO 11 I=1,M
      DO 11 J=1,N
      Z=REAL(A(I,J))/VL
      A(I,J) = CMPLX(Z,AIMAG(A(I,J)))
11    CONTINUE
      DO 20 I=1,M
      DO 20 J=1,N
      X=(I-1)/XS
      Y=(J-1)/YS
      CALL ARROW(X,Y,A(I,J),K)
20    CONTINUE
C        DRAW IN THE TITLE.
      CALL SYMBOL(-2.,2.,0.1,T,90 .,40)
      CALL SYMBOL(-1.5,2.0,0.1,TS,90.,30)
      CALL NUMBER(-1.5,2.6,0.1,VL,90 .,5HE10.3)
      CALL PLOT((M-1.)/XS+4.0,0.,-3)
      RETURN
      END
      SUBROUTINE ARROW(XX,YY,C,K)
      DIMENSION X(9),Y(9)
      COMPLEX C
C        GENERATE PLOTTING COORDS
      PI = 3.14159265358979
      AP=5.*PI/6.
      R = REAL (C)
      CA = AIMAG(C)
      R2=R/2
      R5 = R/5.
      R10=R/10
      ANGU = CA + AP
      ANGD=CA-AP
      SANGU=R5*SIN(ANGU)
      CANGU=R5*COS(ANGU)
      SANGD=R5*SIN(ANGD)
      CANGD=R5*COS(ANGD)
      CCA=COS(CA)
      SCA=SIN(CA)
C
C        TEST FOR PLOTTING MODE
      IF(K.EQ.1)20,21
C
C        PLOTTING MODE 1
20    N=5
      X(1 )=XX
      Y(1)=YY
      X(2)=XX+R*CCA
      Y(2)=YY+R*SCA
      X(3)=X(2)+CANGU
      Y(3)=Y(2)+SANGU
      X(4)=X(2)+CANGD
      Y(4)=Y(2)+SANGD
      X(5)=X(2)
      Y(5)=Y(2)
      GO TO 22
C        PLOTTING MODE 2
21    N=9
      X(1)=XX-R2*CCA
      Y(1)=YY-R2*SCA
      X(2)=XX
      Y(2)=YY
      X(3)=XX-R10*SCA
      Y(3)=YY+R10*CCA
```

```
      X(4)=XX+R10*SCA
      Y(4)=YY-R10*CCA
      X(5)=XX
      Y(5)=YY
      X(6)=XX+R2*CCA
      Y(6)=YY+R2*SCA
      X(7)=X(6)+CANGU
      Y(7)=Y(6)+SANGU
      Y(7)=Y(6)+RS*SIN(ANGU)
      X(8)=X(6)+CANGD
      Y(8)=Y(6)+SANGD
      X(9)=X(6)
      Y(9)=Y(6)
22    CONTINUE
C        DO PLOTTING
      CALL PLOT(X(1),Y(1),3)
      DO 10 I=2,N
      CALL PLOT(X(I),Y(I),2)
10    CONTINUE
      RETURN
      END
      SUBROUTINE BCONTR(H,M,N,XSCALE,YSCALE,NO,IFCO,LQ,CO,NONO)
C
C     CSIRO 3600 LIBRARY ROUTINE LIN MODIFIED FOR 6400

C     CHOICE OF CONTOUR VALUES IMPROVED
C     FRAME DRAWN TO INDICATE PLOTTING AREA BOUNDARY.
C
C     H(I, J)       IS THE ARRAY OF POINTS FOR WHICH A CONTOUR MAP IS TO
C     M,N           ARE THE DIMENSIONS OF THE ARRAY AT CALL TIME.
C                   M  MUST BE EQUAL TO  I , BUT  N  MAY BE SMALLER THAN
C                   IF DESIRED, RESULTING IN A SAVING OF CP TIME WHEN ONL
C                   OF ARRAY  H  IS OF INTEREST.
C     NO            IS EQUAL IN ABSOLUTE VALUE TO THE NUMBER OF CONTOURS
C                   UP TO 30 CONTOURS CAN BE REQUESTED.
C                   IF NO IS NEGATIVE THE CONTOURS ARE LABELLED 1-30 IN
C                   ASCENDING ORDER.
C     CO(NO)        ARE THE LEVELS OF THE CONTOURS IN ASCENDING ORDER, DI
C                   ( NO ). CO MAY BE SET AUTOMATICALLY OR PRESET.
C     NONO          IS THE NUMBER OF CONTOURS ACTUALLY DRAWN IF  CO  IS
C                   SET AUTOMATICALLY.  (NONO.LE.NO)  .
C     IFCO          IS AN INDICATOR.
C                   IF IFCO=1 ,THE PRESET VALUES OF CO WILL BE USED.
C                   IF IFCO = 0 , THEN THE VALUES OF CO ARE SET AUTOMATIC
C                   AT SUCCESSIVE SIMPLE NUMBERS BETWEEN THE LOWEST AND T
C                   HIGHEST VALUES IN  H  .
C                   (SIMPLE NUMBERS IN THIS CONTEXT ARE MEMBERS OF SOME S
C                     (K1*10.**K2*SIMPLE)
C                   WHERE K1 IS AN INTEGER RUNNING INDEX,
C                         K2 IS AN INTEGER SET BY THE SUBROUTINE, AND
C                         SIMPLE IS A PLEASING INTEGRAL SUBMULTIPLE OF 10
C     LQ(I, J)      IS WORKING SPACE, DIMENSIONED AT LEAST (M,N) IN CALLI
C     XSCALE, YSCALE ARE SCALES IN CELLS/INCH OF M, N RESPECTIVELY.
C
C     THE PEN IS TAKEN TO BE AT THE LOWER LEFT CORNER OF THE  M X N  GRI
C                   I.E. (1,1), AND THIS POINT MUST HAVE BEEN DEFINED AS
C                   BY A PREVIOUS  STATEMENT  CALL PLOT(X,Y,-3) .
C     AFTER ALL CONTOURS ARE DRAWN THIS S/R DEFINES A NEW ORIGIN FOR FUR
C                   PLOTTING, AT   ((M-1)/XSCALE+2., 0.)  .
C
      DIMENSIONH(M,N),LQ(M,N),CO(NO)
      DIMENSIONLABEL(30)
      DIMENSIONSIMPLE(5),JLIST(1)
      DIMENSIONLEQ(3),KSIDE(3)
      DIMENSIONINEW(23),JNEW(1),NIDLIST(1),KLIST(1),ILIST(1),KK(1),KL(1)
      EQUIVALENCE              (INEW(2),JNEW), (INEW(5),NIDLIST),
     =            (INEW(12),KLIST), (INEW(16),ILIST), (INEW(20),KK),
     =            (INEW(22),KL),(INEW(17),JLIST)
      DATA (INEW = 1, 0,-1,0,1,2,3,4,1,2,3,0,30,0,30,1,0,0,0, 1,0, 1,-1)
      DATA(SIMPLE=1.,2.,2.5,5.,10.)
      DATA(ONEBIT=4000000000B),(ALLBUT=777777777737777777778),(RIGHT=777
     177777777B)
      DATA(LABEL=1H1,1H2,1H3,1H4,1H5,1H6,1H7,1H8,1H9,2H10,2H11,2H12,2H13
     1,2H14,2H15,2H16,2H17,2H18,2H19,2H20,2H21,2H22,2H23,2H24,2H25,2H26,
     22H27,2H28,2H29,2H30)
      LOGICALEQ1,EQN
      LOGICALSTART,LOOKBK,G,LEQ,LQ,ONEBIT,ALLBUT,WORD,RESULT,MASK,RIGHT
C     MASKS AND FUNCTIONS FOR DEALING BIT-BY-BIT WITH LQ, LEQ.
      ASSIGN1000TONSET1
      ASSIGN1001TONSET0
      ASSIGN1002TONGET
      GOTO1004
 1000 MASK=ONEBIT
      CALLSHIFT(MASK,KBIT,LCO)
      RESULT=OR(WORD,MASK)
      GOTONCALL
 1001 MASK=ALLBUT
      GOTO1003
 1002 MASK=ONEBIT
```

```
 1003 CALL SHIFT(MASK,KBIT,LCO)
      RESULT=AND(WORD,MASK)
      GOTONCALL
 1004 CONTINUE
      NOABS=IABS(NO)
C     DRAW FRAME WITH TICKS
      IHALF=1
      XSTEP=1./XSCALE
      YSTEP=1./YSCALE
      X=0.
      Y=0.
   90 X=X+XSTEP
      CALLPLOT(X,Y,2)
      YTICK=Y-.04+.08*FLOAT(IHALF-1)
      DO91I=3,M
      CALLPLOT(X,YTICK,1)
      CALLPLOT(X,Y,1)
      X=X+XSTEP
   91 CALLPLOT(X,Y,1)
      XTICK=X+.04-.08*FLOAT(IHALF-1)
      Y=Y+YSTEP
      CALLPLOT(X,Y,1)
      DO92I=3,N
      CALLPLOT(XTICK,Y,1)
      CALLPLOT(X,Y,1)
      Y=Y+YSTEP
   92 CALLPLOT(X,Y,1)
      GOTO(93,94),IHALF
   93 XSTEP=-XSTEP
      YSTEP=-YSTEP
      IHALF=2
      GOTO90
   94 DO 61  J = 1, N
      DO 61 I = 1, M
   61 LQ(I,J)=0
      EQ1=0  $  EQN=0
      IF(IFCO)52,56
   52 NONO=NOABS
      GOTO55
C     FIND RANGE OF FUNCTION H
   56 HMIN=1.E304
      HMAX = -HMIN
      DO 57  I = 1, M
      DO 57  J = 1, N
      HMIN=AMIN1(HMIN,H(I,J))
57    HMAX=AMAX1(HMAX,H(I,J))
C     GENERATE SIMPLE CONTOUR INTERVAL
      SUBRNG=(HMAX-HMIN)/FLOAT(NOABS-1)
      RNGELG=ALOG10(SUBRNG)
      LGRNGE=RNGELG+SIGN(0.5,RNGELG)-0.5
      CHAR=10.**LGRNGE
      DO70I=1,5
      ADD=SIMPLE(I)*CHAR
      IF(ADD-SUBRNG)70,71,71
   70 CONTINUE
C     SET CONTOUR VALUES
71    COZERO=HMIN-AMOD(HMIN,ADD)
      IF(COZERO-HMIN)710,711,711
  710 COZERO=COZERO+ADD
  711 CO(1)=COZERO
      DO 72 NONO=2,NOABS
      CO(NONO)=COZERO+ADD*FLOAT(NONO-1)
      DIFFER=CO(NONO)-HMAX
      IF(DIFFER)72,72,73
   72 CONTINUE
      NONO=NOABS
      GOTO55
   73 DO741=NONO,NOABS
   74 CO(I)=0.
      NONO=NONO-1
C     CONSIDER THE BITS IN A WORD OF  LQ  TO BE NUMBERED FROM 60 AT LEFT
C     TO 1 AT RIGHT.
C     SET BIT LCO TO 1 IN EVERY  LQ(I,J)  SUCH THAT CONTOUR  LCO
C     PASSES TO RIGHT OF  (I,J)  BUT NOT TO RIGHT OF  (I+1,J) .
C     SET BIT (LCO+30) TO 1 IN EVERY  LQ(I,J)  SUCH THAT CONTOUR  LCO
C     PASSES ABOVE (I,J) BUT NOT ABOVE (I,J+1) .
C     KBIT=0 OPERATES ON BIT (LCO+30) AND VICE VERSA
   55 DO 66  K = 1, 2
         JS = 3 - K
      KBIT=KLIST(K)
      DO 66  J = JS, N
      DO 66  I = K , M
      DO66LCO=1,NONO
          IF      (CO(LCO).LT.H(I-K+1,J+K-2).AND.CO(LCO).GE.H(I,J)) 64,63
   63     IF      (CO(LCO).GE.H(I-K+1,J+K-2).AND.CO(LCO).LT.H(I,J)) 64,66
   64 WORD=LQ(I-K+1,J+K-2)
      ASSIGN641TONCALL
      GOTONSET1
  641 LQ(I-K+1,J+K-2)=RESULT .
   66 CONTINUE
```

```
      JJ=1
      II=1
      LOOKBK=0
      GOTO  11
   25 IF (START)  27, 11
   11 I = 0
C     SEARCH FOR UNPLOTTED CONTOUR IN NEIGHBOURHOOD OF  (II,JJ)  .
   51 I = I + 1
      J = 0
   49 DO 43  L0 = 1, 2
      DO 43  L1 = 1, 2
      DO 43  L2 = 1, 2
      IL = II + KL(L1)*KK(L0) * I  +  KL(L1)*KK(L0+1) * J
      JL = JJ + KL(L2)*KK(L0) * J  +  KL(L2)*KK(L0+1) * I
      IF (IL.LT.1. OR .IL.GT.M. OR .JL.LT.1. OR .JL.GT.N)  43, 41
   41 IF(LQ(IL,JL))42,43
   42 IF(AND(LQ(IL,JL),RIGHT))44,45
   43 CONTINUE
C     SEARCH UNSUCCESSFUL.  INCREMENT J AND/OR I IF PERMISSIBLE.
      J = J + 1
      IF (J.LE.I)  49, 53
   53 IF (I.LT.M+N)  51, 18
C     NEW CONTOUR(S) FOUND. IDENTIFY THE FIRST ONE.
C     LOCATE A STARTING POINT ON IT AND MOVE THERE, PEN UP.
C     THEN ENTER TRACKING SEQUENCE.
   44 NID = 2
      GOTO  46
   45 NID = 3
   46 II = IL
      JJ = JL
      JS = JL
      START = 1
      KBIT=KLIST(NID)  $  WORD=LQ(II,JS)  $  ASSIGN 470 TO NCALL
      DO47LCO=1,NONO
      GOTO NGET
  470 IF(RESULT)22,47
   47 CONTINUE
   22 CALL CONC (NID, II, JJ, CO(LCO), X, Y, M, N, H)
      IF(LCO.EQ.1 .AND. EQ1)221,222
  221 ISYM=15  $  GOTO224
  222 IF(LCO.EQ.NONO .AND. EQN)223,225
  223 ISYM=3
  224 CALLSYMBOL(X/XSCALE,Y/YSCALE,.04,ISYM,0.,-1)
      GOTO226
  225 IF(NO.LT.0)2251,2252
 2251 CALLSYMBOL(X/XSCALE,Y/YSCALE,.07,LABEL(LCO),0.,2)
 2252 CALLPLOT(X/XSCALE,Y/YSCALE,3)
  226 G = 0
      NED = NID
      GOTO  29
C     MAIN PLOTTING SEQUENCE.
C     A POINT HAS BEEN PLOTTED ON ONE SIDE OF A GRID UNIT CELL IN ARRAY
C     FIND ANOTHER SIDE OF THIS CELL CUT BY SAME CONTOUR.
   31 START = 0
    1 IF (II.LE.0.OR.JJ.LE.0.OR.II.GE.M.OR.JJ.GE.N)  10, 2
    2 DO 54  K = 1, 3
      NSUB=NIDLIST(NID+K)
      IM=II+ILIST(NSUB)
      JM=JJ+JLIST(NSUB)
      KSIDE(K)=KLIST(NSUB)
   54 LEQ(K)=LQ(IM,JM)
      KBIT=KSIDE(3)  $  WORD=LEQ(3)  $  ASSIGN540TONCALL  $  GOTONGET
  540 IF(RESULT)5,3
    3 KBIT=KSIDE(2)  $  WORD=LEQ(2)  $  ASSIGN300TONCALL  $  GOTONGET
  300 IF(RESULT)9,4
    4 KBIT=KSIDE(1)  $  WORD=LEQ(1)  $  ASSIGN400TONCALL  $  GOTONGET
  400 IF(RESULT)8,10
    5 KBIT=KSIDE(1)  $  WORD=LEQ(1)  $  ASSIGN500TONCALL  $  GOTONGET
  500 IF(RESULT)7,6
    6 KBIT=KSIDE(2)  $  WORD=LEQ(2)  $  ASSIGN600TONCALL  $  GOTONGET
  600 IF(RESULT)25,36
    7 KBIT=KSIDE(2)  $  WORD=LEQ(2)  $  ASSIGN700TONCALL  $  GOTONGET
  700 IF(RESULT)37,25
    9 KBIT=KSIDE(1)  $  WORD=LEQ(1)  $  ASSIGN900TONCALL  $  GOTONGET
  900 IF(RESULT)25,38
   36     NAD = 3
      GOTO  19
   38     NAD = 2
      GOTO  19
   37 CALL CONC  (NIDLIST(NID+1), II, JJ, CO(LCO), XR, YR, M, N, H)
      CALL CONC  (NIDLIST(NID+3), II, JJ, CO(LCO), XL, YL, M, N, H)
      IF(XL*XL+YL*YL-XR*XR-YR*YR.LE.2*X*(XL-XR)+2*Y*(YL-YR))  36, 8
    8     NAD = 1
   19 IF(LOOKBK)20,17
   17 NED = NIDLIST (NID + NAD)
C     PLOTTING SEQUENCE ENTRY POINT.
C     TEST COORDINATES OF GRID POINT ON WHICH INTERPOLATION WILL BE BASE
   29 IT = II + ILIST(NED)
      JT=JJ+JLIST(NED)
      KT=KLIST(NED)
```

```
      IF (START)  28, 12
C     CHECK WHETHER NEW CONTOUR STARTS ON PLOT BOUNDARY
   28 IF ((IT.EQ.1.AND.KT.EQ.0).OR.IT.EQ.M.OR.JT.EQ.N.OR.(JT.EQ.1.AND.KT
     1.EQ.30))  12,15
C     IF NOT, REVERSE DIRECTION OF TRACKING
   15 LOOKBK=1
      NAD = 0
      II = II + INEW(NID)
      JJ = JJ + JNEW(NID)
      NID = NIDLIST(NID + 2)
      GOTO  1
C     RETURN TO ORIGINAL TRACKING DIRECTION
   20 LOOKBK=0
      II = II + INEW(NID)
      JJ = JJ + JNEW(NID)
      NID = NIDLIST(NID + 2)
      IF (NAD)  31, 12
   12 KBIT=KT  $  WORD=LQ(IT,JT)  $  ASSIGN120 TO NCALL  $  GOTO NSET0
  120 LQ(IT,JT)=RESULT
   30 IF (START)  31, 21
C     INTERPOLATE AND PLOT.
   21      CALL CONC (NED, II, JJ, CO(LCO), X, Y, M, N, H)
      IF(LCO.EQ.1 .AND. EQ1)211,212
  211 ISYM=15  $  GOTO214
  212 IF(LCO.EQ.NONO .AND. FQN)213,215
  213 ISYM=3
  214 CALLSYMBOL(X/XSCALE,Y/YSCALE,.04,ISYM,0.,-1)
      GOTO216
  215 CALLPLOT(X/XSCALE,Y/YSCALE,2)
  216 G = 1
      NID = NIDLIST(NED + 2)
      II = II + INEW(NED)
      JJ = JJ + JNEW(NED)
      GOTO  31
   10 IF(LOOKBK)20,24
   24 IF (G)  11, 27
   27 II = II + INEW(NID)
      JJ = JJ + JNEW(NID)
      NID = NIDLIST(NID + 2)
      KBIT=KT  $  WORD=LQ(IT,JT)  $  ASSIGN270TONCALL  $  GOTO NSET0
  270 LQ(IT,JT)=RESULT
      GOTO  31
C     PREPARE NEW ORIGIN FOR ANY SUBSEQUENT PLOT
   18 XSTEP = ABS(XSTEP)
      XNEW=(FLOAT(M-1)*XSTEP)+4.0
      CALLPLOT(XNEW,0.,-3)
      RETURN
      END
      SUBROUTINE CONC      (NED, I, J, CON, X, Y, MM, NN, H)
      DIMENSIONH(MM,NN)
      IF (NED.EQ.2. OR .NED.EQ.4)  5, 1
    1 K = (NED - 1)/2
      X = I - K
      IF (H(I-K+1,J).EQ.H(I-K+1,J+1))  3, 2
    2 Y = (H(I-K+1,J+1)-CON)/(H(I-K+1,J)-H(I-K+1,J+1)) + J
                                                          GOTO  7
    3 Y = J - .5
                                                          GOTO  7
    4 X = I - .5
                                                          GOTO  7
    5 K = 2 - NED/2
      Y = J - K
      IF (H(I,J-K+1).EQ.H(I+1,J-K+1))  4, 6
    6 X = (H(I+1,J-K+1)-CON)/(H(I,J-K+1)-H(I+1,J-K+1)) + I
    7 RETURN
      END
0000000000000000000000     END OF RECORD
  1.621749908301E-01 -4.484155085839E-44
  9.558154227811E-12  0.                        1         1
  1.163052225444E-12 -1.139493623873E-26        1         2
 -6.076481211866E-11 -3.075016366715E-11        1         3
 -6.076481211866E-11  3.075016366715E-11        1         4
  9.738292254775E-01  3.587324068672E-43
 -7.627686219526E-52  9.675527835739E-11        2         1
 -2.701316017061E-26 -2.757164708471E-12        2         2
 -4.916616169091E-11 -1.955822154567E-11        2         3
  4.916616169091E-11 -1.955822154567E-11        2         4
  8.708095565656E-01 -6.165282179713E-01
  1.250170097892E-51 -1.546136244363E-10        3         1
 -6.783045511668E-27 -6.923282423311E-13        3         2
 -4.166259474779E-11 -5.265738206718E-12        3         3
  4.166259474778E-11 -5.265738206718E-12        3         4
  8.708095565656E-01  6.165282179713E-01
  2.685498673810E-01  1.749433876808E-42        4         1
  3.051508764834E-01 -2.989697886862E-15        4         2
 -4.508902605869E-01  3.845454451754E-01        4         3
 -4.508902605869E-01 -3.845454451754E-01        4         4
```

```
 3.160458984375E+03VS
 3.141592650000E+08W
 1.577000000000E-05H
 1.710000000000E-01          1          1          1
 0.                          1          1          2
 0.                          1          1          3
 0.                          1          2          1
 0.                          1          2          2
 4.060000000000E-02          1          2          3
 0.                          1          3          1
 4.060000000000E-02          1          3          2
-1.710000000000E-01          1          3          3
 0.                          2          1          1
 0.                          2          1          2
 0.                          2          1          3
 0.                          2          2          1
 0.                          2          2          2
 0.                          2          2          3
 0.                          2          3          1
 0.                          2          3          2
 0.                          2          3          3
 0.                          3          1          1
-4.060000000000E-02          3          1          2
-1.710000000000E-01          3          1          3
-4.060000000000E-02          3          2          1
 0.                          3          2          2
 0.                          3          2          3
-1.710000000000E-01          3          3          1
 0.                          3          3          2
 0.                          3          3          3
 3.921000000000E-11  0.                             1
 0.                  0.                             2
 0.                  3.921000000000E-11             3
00000000000000000000     END OF FILE
```

## A1.3 Subroutine BFAST - Fast-Fourier Transform

### A1.3.1 Flow Chart

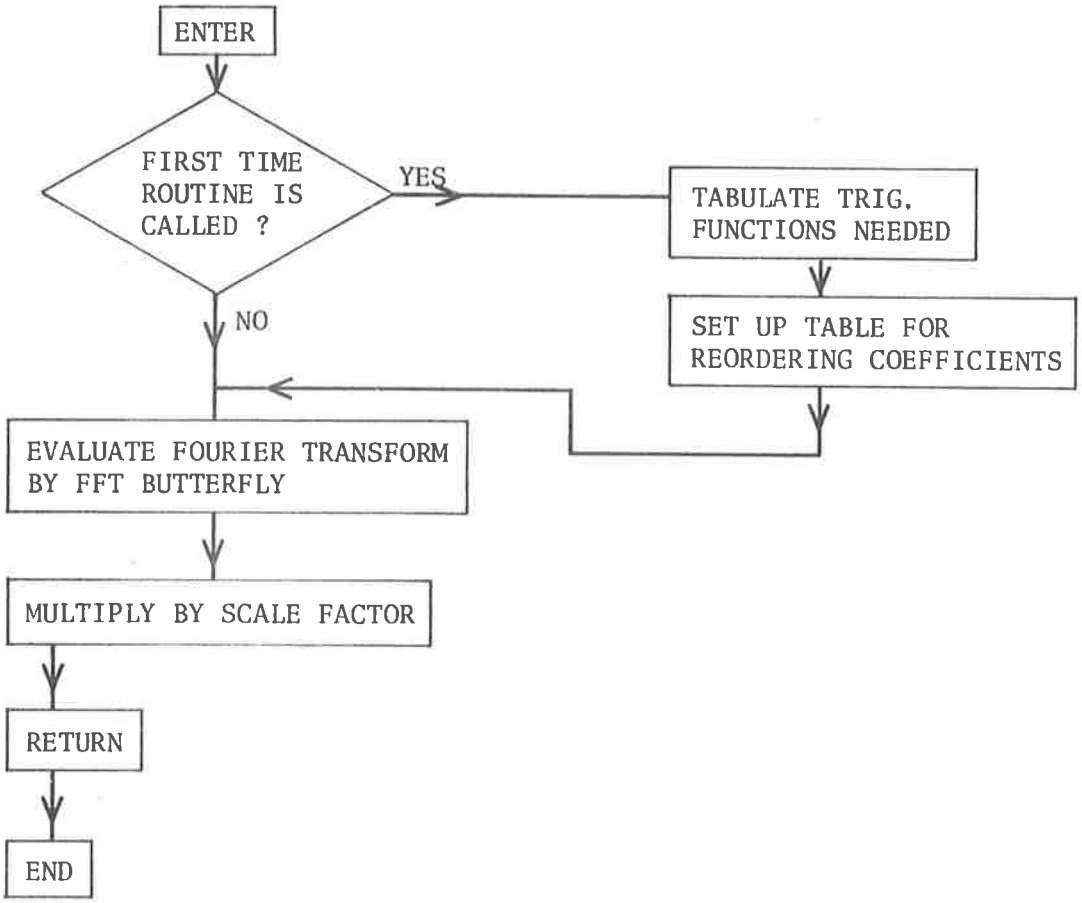


### A1.3.2 Program Listing

```
      SUBROUTINE BFAST(Y,M,SIGN,DXY)
*                                                                      FAST  20
*                                                                      FAST  30
*       SUBROUTINE FOR THE CALCULATION OF EITHER THE FORWARD OR        FAST  40
*       INVERSE FOURIER TRANSFORM OF A COMPLEX SEQUENCE  Y  USING THE  FAST  50
*       FAST FOURIER TRANSFORM (FFT) ALGORITHM.                        FAST  60
*                                                                      FAST  70
*                                        M
*       Y  IS A COMPLEX ARRAY OF DIMENSION 2   AND IS BOTH THE INPUT   FAST  90
*       AND OUTPUT SEQUENCE OF THE SUBROUTINE.                         FAST 100
*                                                                      FAST 280
*        PRESENT DIMENSIONS LIMIT=2**10
*                                                                      FAST 110
```

```
*       DXY = THE SAMPLE SPACING FOR THE INPUT ARRAY Y. THE CORRES-
*       PONDING SAMPLE SPACING IN THE TRANSFORM DOMAIN IS OUTPUT IN DXY
*                                                                      FAST 140
*       FOR TIME TO FREQUENCY TRANSFORMATION,     SIGN = -1.0          FAST 150
*       FOR FREQUENCY TO TIME TRANSFORMATION,     SIGN = +1.0          FAST 160
*                                                                      FAST 170
*       SUBROUTINE  CON  SETS UP A CONVERSION TABLE TO REARRANGE THE   FAST 190
*       INPUT ARRAY FOR PROCESSING.                                    FAST 190
*                                                                      FAST 200
*       SUBROUTINE  TABLE  SETS UP A TABLE OF ALL SINES AND COSINES    FAST 210
*       USED IN SUBROUTINE  FAST.                                      FAST 220
*                                                                      FAST 230
*       SUBROUTINE BFAST IS MODIFIED VERSION OF SUBROUTINE FAST WRITTEN 2/5/72
*       ON 2 MAY 1972
*
*                                                                      FAST 260
      COMPLEX A,U,W,T,Y                                                FAST 270
      DIMENSION A(1024),Y(2)                                           FAST 290
      COMMON /PERM/MM(1024)                                            FAST 300
      COMMON /TAB/TC(10),TS(10)                                        FAST 310
      DATA MSET/0/                                                     FAST 320
*                                                                      FAST 330
      IF (MSET.EQ.M) GOTO 1                                            FAST 340
      CALL TABLE(M)                                                    FAST 350
      CALL CON(M)                                                      FAST 360
      MSET=M                                                           FAST 370
    1 CONTINUE                                                         FAST 380
*                                                                      FAST 400
      N=2**M                                                           FAST 390
      DO 7 I=1,N                                                       FAST 430
      J=MM(I)
    7 A(I)=Y(J)
*
      DO 20 L=1,M                                                      FAST 470
      LE=2**L                                                          FAST 480
      LE1=LE/2                                                         FAST 490
      U=(1.0,0.0)                                                      FAST 500
      W=CMPLX(TC(L),TS(L)*SIGN)                                        FAST 510
      DO 20J=1,LE1                                                     FAST 520
      DO 10 I=J,N,LE                                                   FAST 530
      IP=I+LE1                                                         FAST 540
      T=A(IP)*U                                                        FAST 550
      A(IP)=A(I)-T                                                     FAST 560
      A(I)=A(I)+T                                                      FAST 570
   10 CONTINUE                                                         FAST 580
      U=U*W                                                            FAST 590
   20 CONTINUE                                                         FAST 600
*                                                                      FAST 610
      DO 30 I=1,N                                                      FAST 620
      Y(I)=A(I)*DXY                                                    FAST 660
   30 CONTINUE
      DXY=1./(DXY*N)                                                   FAST 680
*
      RETURN                                                           FAST 700
      END                                                              FAST 690
      SUBROUTINE TABLE(M)                                              FAST 760
      COMMON /TAB/TC(10),TS(10)                                        TABL  10
      PI=4.0*ATAN2(1.0,1.0)                                            TABL  20
      DO1I=1,M                                                         TABL  30
      TC(I)=COS(PI/(2**(I-1)))                                         TABL  40
    1 TS(I)=SIN(PI/(2**(I-1)))                                         TABL  50
      RETURN                                                           TABL  60
      END                                                              TABL  70
      SUBROUTINE CON(M)                                                TABL  80
      INTEGER A,T                                                      CON   10
      COMMON /PERM/ A(1024)                                            CON   20
      N=2**M                                                           CON   30
      NV2=N/2                                                          CON   40
      NM1=N-1                                                          CON   50
      J=1                                                              CON   60
      DO1I=1,N                                                         CON   70
    1 A(I)=I                                                           CON   80
      DO 7 I=1,NM1                                                     CON   90
      IF(I.GE.J)GOTO5                                                  CON  100
      T=A(J)                                                           CON  110
      A(J)=A(I)                                                        CON  120
      A(I)=T                                                           CON  130
    5 K=NV2                                                            CON  140
    6 IF(K.GE.J)GOTO7                                                  CON  150
      J=J-K                                                            CON  160
      K=K/2                                                            CON  170
      GOTO 6                                                           CON  180
    7 J=J+K                                                            CON  190
      RETURN                                                           CON  200
      END                                                              CON  210
                                                                       CON  220
```

## A1.4 Program SAWDLY 1 - Transadmittance Calculation

### A1.4.1 Flow Chart

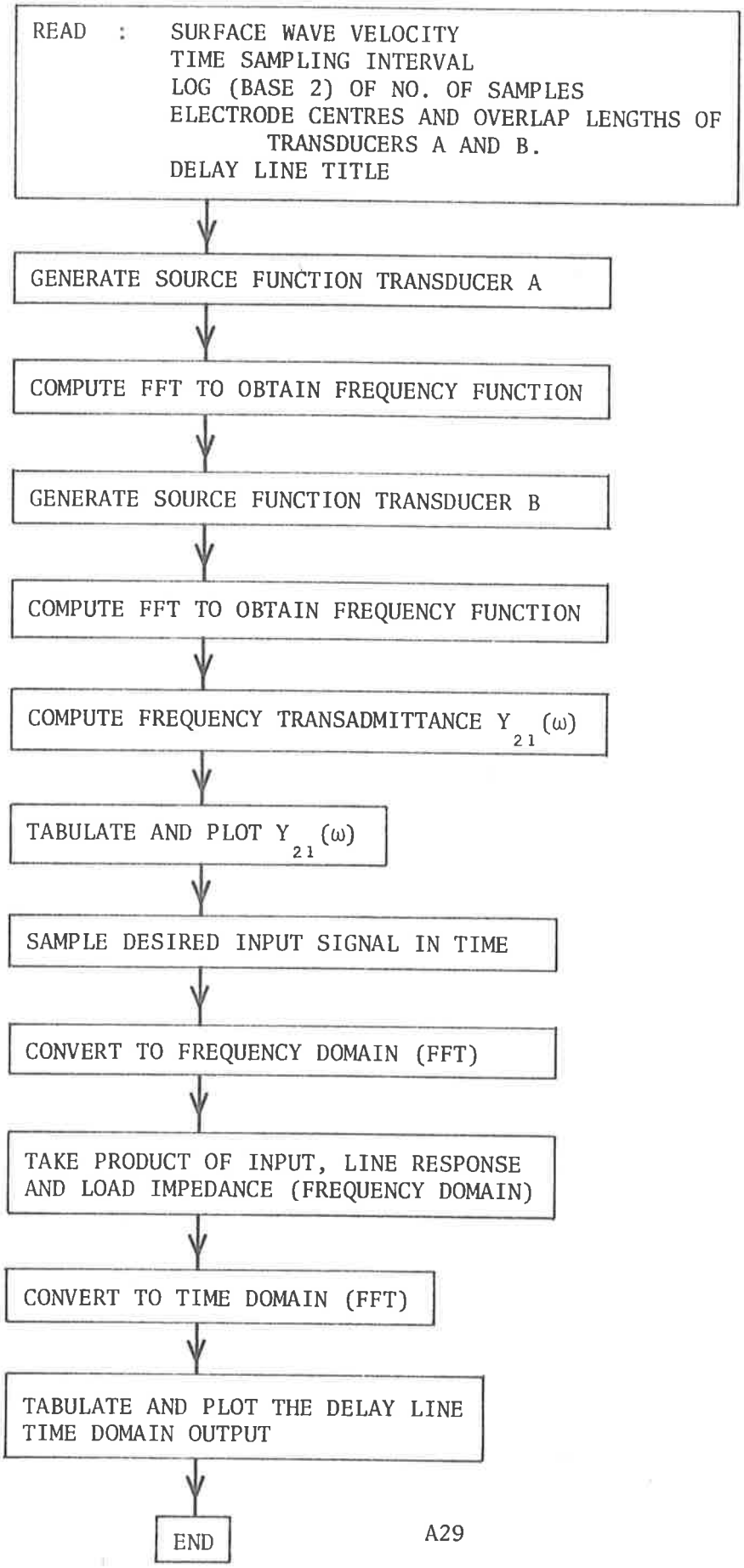

## A1.4.2 Program Listing

```
      PROGRAM SAWDLY1(INPUT,OUTPUT)
CC          THIS PROGRAM COMPUTES THE TRANSADMITTANCE Y21(W), Y21(T) AND THE
C          LINE IMPULSE RESPONSE VL/V1(T) FOR 2 TRANSDUCERS AND LOAD R.
C         THE BASIC EXCITATION CELL FOR THE TRANSDUCERS IS ASSUMED TO BE THE GAP
C         BETWEEN A PAIR OF ELECTRODES.
C         THE CELL INCLUDES AN ELECTRODE HALF WIDTH ON EACH SIDE SET EQUAL TO A
C         QUARTER CELL WIDTH.
C         THE REQUIRED INPUT DATA ARE=
*         XPA(I)= POSITION OF ELECTRODE I IN TRANSDUCER A (IN MILLIMETRES)
*         XPB(I)= DITTO TRANSDUCER B
*         XLA(I)= OVERLAP LENGTH OF CELL I (IN MILLIMETRES)
*         XLB(I)= DITTO TB
*         NA = NUMBER OF GAPS IN TA
*         NB = DITTO TB
*         VSAW= SURFACE VELOCITY (IN MM/SEC)
*         AGA = RATIO OF GAP(I+1)/GAP(I) FOR TA
*         ALA = RATIO OF XL(I+1)/XL(I)
*         AGB = DITTO AGA FOR TB
*         ALB = DITTO ALA FOR TB
*         GA = INITIAL GAP WIDTH (IN MM) TA
*         GB = DITTO FOR TB
*         TINC = SAMPLING TIME INTERVAL
*         M = LOG(BASE 2) OF NUMBER OF SAMPLES
C         TITLE= IDENTIFIER OF THE PARTICULAR DELAY LINE
*
C         ETA = CHARACTERISTIC IMPEDANCE OF FREE SPACE IN OHMS
$         EPSI = DIELECTRIC CONSTANT OF FREE SPACE
C         STEP = SPATIAL SAMPLING INTERVAL = TINC*VSAW
      DIMENSION XPA(100),XLA(100),XPB(100),XLB(100)
      DIMENSION XP(520),YP(520)
      COMPLEX A(1026),B(1026),Y(1026)
      REAL C(520),D(520),GD(520)
      COMMON / /A,B,Y
      PI=3.141592653589793
      ETA = 337.
      EPSI=8.85E-12
      EPSO=39.21E-12
      DELTA=-9.3E-4
      R=64
      GAIN=31.6
      Z=0
      READ 301,VSAW
      READ 302,TINC,M
      READ 401,NA,NB
      READ 402,XPA(1),XLA(1),GA
      READ 402,AGA,ALA
      READ 402,XPB(1),XLB(1),GB
      READ 402,AGB,ALB
      READ 411,TITLE
401   FORMAT(2I5)
402   FORMAT(3E10.3)
411   FORMAT(A10)
301   FORMAT(2(E10.3))
      TINC=1./8.192E8
302   FORMAT(E10.3,I10)
      STEP=TINC*VSAW
      PRINT 303,VSAW
303   FORMAT(*1SURFACE WAVE VELOCITY =*E10.3*MM/SEC*)
     C =*E10.3)
      N=2.**M
      PRINT 304,TINC,N
304   FORMAT(* SAMPLING INTERVAL =*E10.3,/* NUMBER OF SAMPLES =*I5,)

C        COMPUTE OVERLAP AND SPACING

      XPA(2)=XPA(1)+GA
      DO 403 I=2,NA
      GA=GA*AGA
      XPA(I+1)=XPA(I)+GA
      XLA(I)=XLA(I-1)*ALA
403   CONTINUE
      XPB(2)=XPB(1)+GB
      DO 404 I=2,NB
      GB=GB*AGB
      XPB(I+1)=XPB(I)+GB
      XLB(I)=XLB(I-1)*ALB
404   CONTINUE
      PRINT 405
405   FORMAT(*1TRANSDUCER A*/6X*INDEX*7X*ELECTRODE*5X*SUBSEQUENT*7X*OVER
     CLAP*/19X*POSITION*9X*GAP*11X*LENGTH*)
      PRINT 406
406   FORMAT(8X*I*10X*XPA(I)*24X*XLA(I)*/)
      DO 407 I=1,NA
      GA=XPA(I+1)-XPA(I)
```

```
      PRINT 408,I,XPA(I),GA,XLA(I)
408   FORMAT(I11,3E15.3)
407   CONTINUE
      NA1=NA+1
      PRINT 408,NA1,XPA(NA1)
      PRINT 409
409   FORMAT(1H0,7X*I*10X*XPB(I)*24X*XLB(I)*/)
      DO 410 I=1,NB
      GB=XPB(I+1)-XPB(I)
      PRINT 408,I,XPB(I),GB,XLB(I)
410   CONTINUE
      NB1=NB+1
      PRINT 408,NB1,XPB(NB1)
C        ASSUME THAT THE SIGN OF THE FIELD ALTERNATES IN EACH GAP AND THAT THE
C        FIRST GAP HAS POSITIVE ELECTRIC FIELD
C        ASSUME THAT THE GAP FUNCTION IS FORM SIN(PI/2) TO SIN(3PI/2)
C        THE FFT OPERATES ON 2**M POINTS
      SIGN=-1
      NSTEP=XPA(1)/STEP
      DO 600 NS=1,NSTEP
600   A(NS)=(0.,0.)
      ACON=(EPSQ*EPSI)*PI/(EPSI*1.854)
      DO 601 I=1,NA
      SIGN=-1.*SIGN
      NSTEP=XPA(I+1)/STEP-NS
      NSS=NS+1
      NSE=NS+NSTEP
      GA=XPA(I+1)-XPA(I)
      AMP=ACON*XLA(I)/GA
      DO 602 NS=NSS,NSE
      ARG=(NS*STEP-XPA(I))*PI/GA
      AR=AMP*COS(ARG)*SIGN
      A(NS)=CMPLX(AR,Z)
602   CONTINUE
601   CONTINUE
      NSS=NS+1
      DO 603 NS=NSS,N
603   A(NS)=(0.,0.)
C        PRINT GAP FUNCTION A
      PRINT 650
650   FORMAT(*0AMPLITUDE FUNCTION A*//)
      DO 651 I=1,NSS,4
      PRINT 652,I,(A(I+J-1),J=1,4)
 652  FORMAT(I5,8E15.3)
651   CONTINUE
C        GAP FUNCTION FOR TRANSDUCER B
      SIGN=-1
      NSTEP=XPB(1)/STEP
      NSB=NSTEP
      DO 700 NS=1,NSTEP
700   B(NS)=(0.,0.)
      DO 701 I=1,NB
      SIGN=-1*SIGN
      NSTEP=XPB(I+1)/STEP-NS
      NSS=NS+1
      NSE=NS+NSTEP
      GB=XPB(I+1)-XPB(I)
      BMP=ACON*XLB(I)/GB
      DO 702 NS=NSS,NSE
      BRG=(NS*STEP-XPB(I))*PI/GB
      BR=BMP*SIGN*COS(BRG)
      B(NS)=CMPLX(BR,Z)
702   CONTINUE
701   CONTINUE
      NSE1=NSE+1
      DO 703 NS=NSE1,N
703   B(NS)=(0.,0.)
C        PRINT GAP FUNCTION B
      PRINT 750
750   FORMAT(*0AMPLITUDE FUNCTION B*//)
      DO 751 I=NSB,NSE1,4
      PRINT 752,I,(B(I+J-1),J=1,4)
 752  FORMAT(I5,8E15.3)
751   CONTINUE
C        COMPUTE INTEGRAL TRANSFORM OF TRANSDUCER A
      DXY=STEP
      CALL BFAST(A,M,-1.,DXY)
      FINC=DXY*VSAW
      PRINT 800
800   FORMAT(* FREQUENCY RESPONSE TRANSDUCER A*/* FREQUENCY*10X*TRANSFOR
     CM OUTPUT*/)
      DO 801 I=1,N,40
      FREQ=(I-1)*FINC
      PRINT 802,FREQ,(A(I+J-1),J=1,4)
802   FORMAT(E11.3,8E15.3)
801   CONTINUE
C        COMPUTE INTEGRAL TRANSFORM OF TRANSDUCER B
      DXY=STEP
      CALL BFAST(B,M,+1.,DXY)
      FINC=DXY*VSAW
```

```
      PRINT 900
900   FORMAT(*1FREQUENCY RESPONSE OF TRANSDUCER B*/* FREQUENCY*10X*TRANS
     CFORM OUTPUT*/)
      DO 901 I=1,N,40
      FREQ=(I-1)*FINC
      PRINT 902,FREQ,(B(I+J-1),J=1,4)
902   FORMAT(E11.3,8E15.3)
901   CONTINUE

C         COMPUTE TRANSADMITTANCE Y(I) MHOS
      PRINT 1000
 1000 FORMAT(*1DELAY LINE TRANSADMITTANCE*/* FREQUENCY*10X*COMPLEX Y(I)*
     C5X*MAGNITUDE*5X*PHASE*9X*GROUP DELAY*)
      PRINT 1004
 1004 FORMAT(5X*HERTZ*7X*REAL*8X*IMAG*8X*MHOS*6X*DEGREES*7X*SECONDS*/)
      DELF= 2.*PI*FINC
      RADTDEG=180./PI
      CONKK=-PI*(EPSI**2)*DELTA/(XLA(1)*(EPSI+EPSQ))
      CONKK=CONKK*2./1000.
      C(1)=D(1)=Y(1)=(0.,0.)
      FREQ=0.
      PRINT 1002,FREQ,Y(1),C(1),D(1)
      N2=N/2
      N2P1=N2+1
      DO 1001 I=2,N2P1
      FREQ=(I-1)*FINC
      Y(I)=CONKK*FREQ*A(I)*B(I)
      C(I)=2*CABS(Y(I))
      XX=REAL(Y(I))
      YY=AIMAG(Y(I))
      D(I)=ATAN2(YY,XX)*RADTDEG
      GD(I)=(D(I-1)-D(I))/(DELF*RADTDEG)
1001  CONTINUE
      DO 1003 I=11,N2
      FREQ=(I-1)*FINC
      PRINT 1002,FREQ,Y(I),C(I),D(I),GD(I)
1002  FORMAT(5E12.3,E15.3)
 1003 CONTINUE
C
C         PLOT THE MAGNITUDE OF THE TRANSADMITTANCE FUNCTION
      CALL PLOT10(10HNEBCBOX142,10)
      CALL XLIMIT(100.)
      CALL PAUPLOT(17H0.4 BLACK INK PLS,17)
      YPM=-1000
      YP(1)=-1000
      DO 1102 I=2,501
      YP(I)=20.*ALOG10(C(I))
      YPM=AMAX1(YPM,YP(I))
1102  XP(I)=(I-1)*FINC
      XP(1)=0
      IPM=YPM/10.
      IPL=10.*IPM-90
      DO 1103 J=1,501
      IF(IPL-YP(J))1103,1103,1104
1104  YP(J)=IPL
1103  CONTINUE
      CALL PLOT(4.,0.,-3)
      CALL SCALE(XP,20.,501,1)
      YP(502)=IPL
      YP(503)=10.
      CALL AXIS(0.,0.,17HFREQUENCY (HERTZ),-17,20.,0.,XP(502),XP(503),0)
      CALLAXIS(0.,0.,31HDELAY LINE TRANSADMITTANCE (DB),31,10.,90.,YP(50
     C2),YP(503),-1)
      CALL LINE(XP,YP,501,1,0,0)
      CALL SYMBOL(3.,8.,0.2,10HDELAY LINE,0.,10)
      CALL SYMBOL(5.,8.,0.2,TITLE,0.,10)
      CALL PLOT(25.,0.,-3)
C
C          COMPUTE THE LINE IMPULSE RESPONSE
C
C         COMPUTE INPUT IMPULSE
      DO 1300 I=1,N
1300  A(I)=(0.,0.)
      A(10)=A(11)=A(12)=A(13)=(114.,0.)
      DXY=TINC
      CALL BFAST(A,M,+1.,DXY)
      DO 1204 I=1,N2P1
1204  Y(I)=A(I)*Y(I)
      DO 1203 I=2,N2
      Y(N+2-I)=CONJG(Y(I))
 1203 CONTINUE
      DXY=FINC
      CALL BFAST(Y,M,-1.,DXY)

C          INCLUDE PREAMP GAIN

      DO 1206 I=1,N
1206  Y(I)=-Y(I)*GAIN*R
```

```
      PRINT 1205
 1205 FORMAT('1LINE IMPULSE RESPONSE'/3X'1'3X'TIME(USEC)'11X'1'29X'2'29X
     C'3'29X'4'/)
      DO 1200 I=1,N2,4
      TIM=1.E6*(I-1)*TINC
      PRINT1201 ,I,TIM,(Y(I+J-1),J=1,4)
 1201 FORMAT(I5,F7.3,8E15.3)
 1200 CONTINUE
C
C        PLOT THE LINE IMPULSE RESPONSE
C
      DO 1202 I=1,401
      XP(I)=(I-1)*TINC
 1202 YP(I)=Y(I)
      CALL SCALE(XP,20.,401,1)
      CALL SCALE(YP,10.,401,1)
      XP(402)=0.
      XP(403)=2.5E-8
      YP(402)=-1.E-1
      YP(403)=2.E-2
      CALL AXIS(0.,0.,17HTIME (IN SECONDS),-17,20.,0.,XP(402),XP(403),0)
      CALL AXIS(0.,0.,16HVOLTAGE WAVEFORM,16,10.,90.,YP(402),YP(403),-1)
      CALL SYMBOL(3.,8.,0.2,10HDELAY LINE,0.,10)
      CALL SYMBOL(5.,8.,0.2,TITLE,0.,10)
      CALL LINE(XP,YP,401,1,0,0)
      CALL PLOT(25.,0.,-3)
      STOP
      END
      SUBROUTINE BFAST(Y,M,SIGN,DXY)
*                                                                      FAST  20
*                                                                      FAST  30
*        SUBROUTINE FOR THE CALCULATION OF EITHER THE FORWARD OR       FAST  40
*        INVERSE FOURIER TRANSFORM OF A COMPLEX SEQUENCE  Y  USING THE FAST  50
*        FAST FOURIER TRANSFORM (FFT) ALGORITHM.                       FAST  60
*                                                                      FAST  70
*                                          M
*        Y  IS A COMPLEX ARRAY OF DIMENSION 2   AND IS BOTH THE INPUT  FAST  90
*        AND OUTPUT SEQUENCE OF THE SUBROUTINE.                        FAST 100
*                                                                      FAST 280
*         PRESENT DIMENSIONS LIMIT=2**10
*                                                                      FAST 110
*        DXY = THE SAMPLE SPACING FOR THE INPUT ARRAY Y. THE CORRES-
*        PONDING SAMPLE SPACING IN THE TRANSFORM DOMAIN IS OUTPUT IN DXY
*                                                                      FAST 140
*        FOR TIME TO FREQUENCY TRANSFORMATION,     SIGN = -1.0         FAST 150
*        FOR FREQUENCY TO TIME TRANSFORMATION,     SIGN = +1.0         FAST 160
*                                                                      FAST 170
*        SUBROUTINE  CON  SETS UP A CONVERSION TABLE TO REARRANGE THE  FAST 180
*        INPUT ARRAY FOR PROCESSING.                                   FAST 190
*                                                                      FAST 200
*        SUBROUTINE  TABLE  SETS UP A TABLE OF ALL SINES AND COSINES   FAST 210
*        USED IN SUBROUTINE  FAST.                                     FAST 220
*                                                                      FAST 230
*        SUBROUTINE BFAST IS MODIFIED VERSION OF SUBROUTINE FAST WRITTEN 2/5/72
*        ON 2 MAY 1972
*                                                                      FAST 260
*                                                                      FAST 270
      COMPLEX A,U,W,T,Y                                               FAST 290
      DIMENSION A(1024),Y(2)                                          FAST 300
      COMMON /PERM/MM(1024)                                           FAST 310
      COMMON /TAB/TC(10),TS(10)                                       FAST 320
      DATA MSET/0/                                                    FAST 330
*                                                                     FAST 340
      IF (MSET.EQ.M) GOTO 1                                           FAST 350
      CALL TABLE(M)                                                   FAST 360
      CALL CON(M)                                                     FAST 370
      MSET=M                                                          FAST 380
    1 CONTINUE                                                        FAST 400
*                                                                     FAST 390
      N=2**M                                                          FAST 430
      DO 7 I=1,N
      J=MM(I)
    7 A(I)=Y(J)
*                                                                     FAST 470
      DO 20 L=1,M                                                     FAST 480
      LE=2**L                                                         FAST 490
      LE1=LE/2                                                        FAST 500
      U=(1.0,0.0)                                                     FAST 510
      W=CMPLX(TC(L),TS(L)*SIGN)                                       FAST 520
      DO 20J=1,LE1                                                    FAST 530
      DO 10 I=J,N,LE                                                  FAST 540
      IP=I+LE1                                                        FAST 550
      T=A(IP)*U                                                       FAST 560
      A(IP)=A(I)-T                                                    FAST 570
      A(I)=A(I)+T                                                     FAST 580
   10 CONTINUE                                                        FAST 590
      U=U*W                                                           FAST 600
   20 CONTINUE                                                        FAST 610
*                                                                     FAST 620
      DO 30 I=1,N                                                     FAST 660
      Y(I)=A(I)*DXY
```

```
 30   CONTINUE                                                          FAST 680
      DXY=1./(DXY*N)
*                                                                       FAST 700
      RETURN                                                            FAST 690
      END                                                               FAST 760
      SUBROUTINE TABLE(M)                                               TABL  10
      COMMON /TAB/TC(10),TS(10)                                         TABL  20
      PI=4.0*ATAN2(1.0,1.0)                                             TABL  30
      DO1I=1,M                                                          TABL  40
      TC(I)=COS(PI/(2**(I-1)))                                          TABL  50
 1    TS(I)=SIN(PI/(2**(I-1)))                                          TABL  60
      RETURN                                                            TABL  70
      END                                                               TABL  80
      SUBROUTINE CON(M)                                                 CON   10
      INTEGER A,T                                                       CON   20
      COMMON /PERM/ A(1024)                                             CON   30
      N=2**M                                                            CON   40
      NV2=N/2                                                           CON   50
      NM1=N-1                                                           CON   60
      J=1                                                               CON   70
      DO11=1,N                                                          CON   80
 1    A(I)=1                                                            CON   90
      DO 7 I=1,NM1                                                      CON  100
      IF(I.GE.J)GOTO5                                                   CON  110
      T=A(J)                                                            CON  120
      A(J)=A(I)                                                         CON  130
      A(I)=T                                                            CON  140
 5    K=NV2                                                             CON  150
 6    IF(K.GE.J)GOTO7                                                   CON  160
      J=J-K                                                             CON  170
      K=K/2                                                             CON  180
      GOTO 6                                                            CON  190
 7    J=J+K                                                             CON  200
      RETURN                                                            CON  210
      END                                                               CON  220
00000000000000000000      END OF RECORD
  3.06 E 6        VSAW
    1.              10   TINC        M
     8     8     NA    NB
  1.0         3.16        3.16E- 2     XPA     XLA     GA
   1.0         1.0         AGA     ALA
    2.         3.16        3.16E- 2    XPB    XLB    GB
   1.0         1.0         AGB        ALB
50MHZ VIDT     TITLE
  6.03 E-7      VT
00000000000000000000      END OF FILE
```

## A.1.5 Program INAD - Input Admittance Calculation

### A1.5.1 Flow Chart

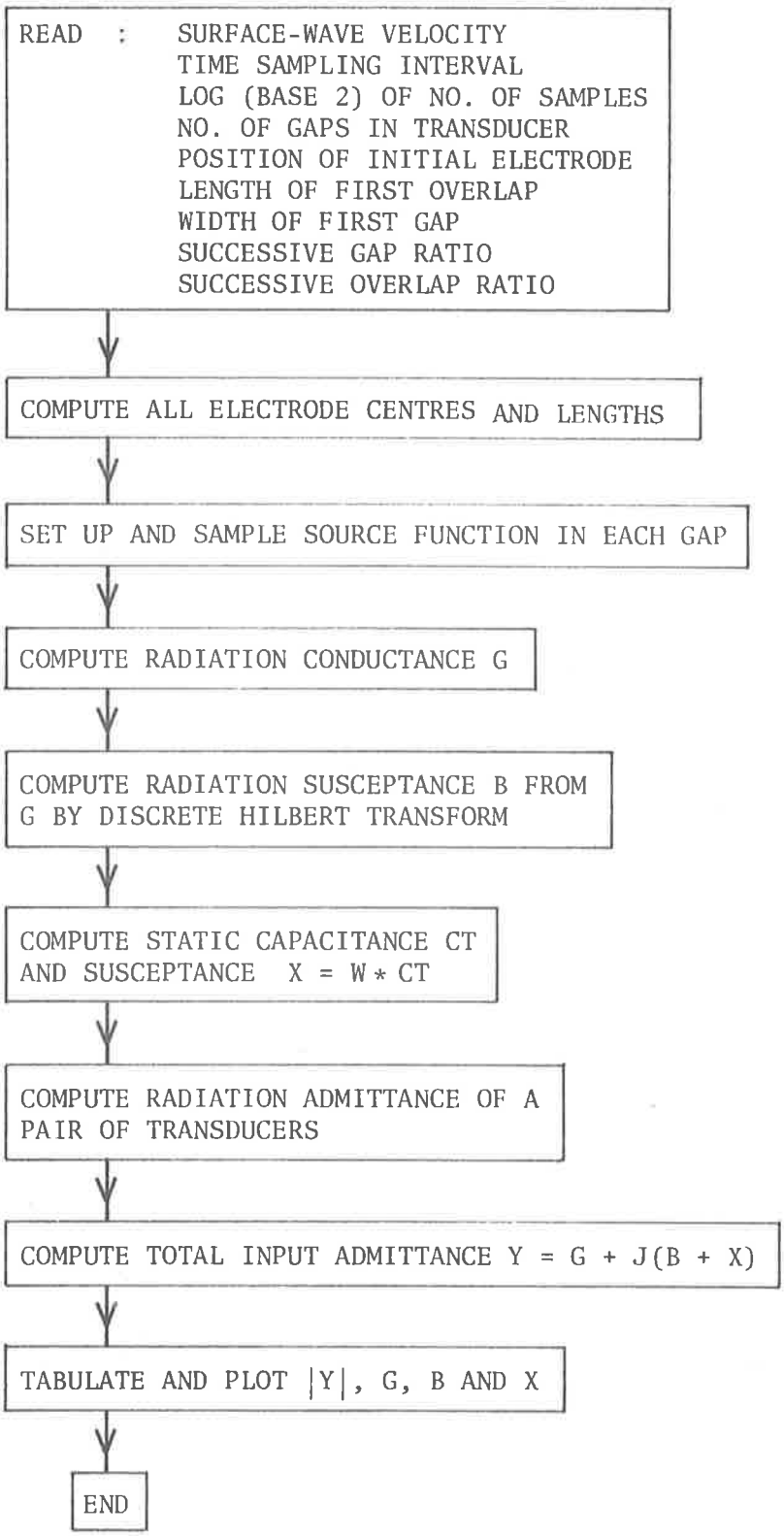

## A1.5.2 Program Listing

```
      PROGRAM INAD(INPUT,OUTPUT)
C        THIS PROGRAM COMPUTES THE RADIATION CONDUCTANCE (G) AND SUSCEPTANCE
C        (B) AND ALSO THE STATIC CAPACITIVE SUSCEPTANCE (X) OF ANY SURFACE WAVE
C        TRANSDUCER (ASSUMING THE FINGERS ALL HAVE EFFECTIVELY UNIFORM OVERLAP),
C        I.E. Y=G+J(B+X)
C        THE BASIC EXCITATION CELL FOR THE TRANSDUCERS IS ASSUMED TO BE THE GAP
C        BETWEEN A PAIR OF ELECTRODES.
C        THE CELL INCLUDES AN ELECTRODE HALF WIDTH ON EACH SIDE SET EQUAL TO A
C        QUARTER CELL WIDTH.
C        THE REQUIRED INPUT DATA ARE=
*        XPA(I)= POSITION OF ELECTRODE I IN TRANSDUCER A (IN MILLIMETRES)
*        XLA(I)= OVERLAP LENGTH OF CELL I (IN MILLIMETRES)
*        NA = NUMBER OF GAPS IN TA
*        VSAW = SURFACE WAVE VELOCITY (METRES/SEC)
*        AGA = RATIO OF GAP(I+1)/GAP(I) FOR TA
*        ALA = RATIO OF XL(I+1)/XL(I)
*        GA = INITIAL GAP WIDTH (IN MM) TA
*        TINC = SAMPLING TIME INTERVAL
*        M = LOG(BASE 2) OF NUMBER OF SAMPLES
*        TITLE = IDENTIFIER OF PARTICULAR TRANSDUCER
$        EPSI = DIELECTRIC CONSTANT OF FREE SPACE
*        EPSQ = DIELECTRIC CONSTANT OF THE MATERIAL
C        STEP = SPATIAL SAMPLING INTERVAL = TINC*VSAW
C        GL = TOTAL LENGTH OF OVERLAPPING GAPS
*
      DIMENSION XPA(100),XLA(100)
      DIMENSION XP(520),YP(520)
      COMPLEX A(1026),Y(1026)
      DIMENSION G(515),B(515),X(515)
      COMPLEX IMAG,IMAGM
      COMMON/ /A,Y,G,B,X
      U=1.
      UM=-1.
      PI=3.141592653589793
      EPSI=8.85E-12
      EPSQ=39.21E-12
      DELTA=-9.3E-4
      Z=0
      READ 301,VSAW
      READ 302,TINC,M
      READ 401,NA
      READ 402,XPA(1),XLA(1),GA
      READ 402,AGA,ALA
      READ 411,TITLE
411   FORMAT(A10)
301   FORMAT(2(E10.3))
      TINC=1./2.048E8
302   FORMAT(E10.3,I10)
      STEP=TINC*VSAW*1000.
      PRINT 303,VSAW
 303  FORMAT(*1SURFACE WAVE VELOCITY =*E10.3*METRE/SEC*/)
      N=2.**M
      PRINT 304,TINC,N
304   FORMAT(* SAMPLING INTERVAL =*E10.3,/* NUMBER OF SAMPLES =*I5,)

C        COMPUTE OVERLAP AND SPACING
401   FORMAT(2I5)
402   FORMAT(3E10.3)
      XPA(2)=XPA(1)+GA
      DO 403 I=2,NA
      GA=GA*AGA
      XPA(I+1)=XPA(I)+GA
      XLA(I)=XLA(I-1)*ALA
403   CONTINUE
      PRINT 405
405   FORMAT(*1TRANSDUCER A*/6X*INDEX*7X*ELECTRODE*5X*SUBSEQUENT*7X*OVER
     CLAP*/19X*POSITION*9X*GAP*11X*LENGTH*)
      PRINT 406
406   FORMAT(8X*I*10X*XPA(I)*24X*XLA(I)*/)
      DO 407 I=1,NA
      GA=XPA(I+1)-XPA(I)
      PRINT 408,I,XPA(I),GA,XLA(I)
408   FORMAT(I11,3E15.3)
407   CONTINUE
      NA1=NA+1
      PRINT 408,NA1,XPA(NA1)

C        ASSUME THAT THE SIGN OF THE FIELD ALTERNATES IN EACH GAP AND THAT THE
C        FIRST GAP HAS POSITIVE ELECTRIC FIELD
C        ASSUME THAT THE GAP FUNCTION IS FORM SIN(PI/2) TO SIN(3PI/2)
C        THE FFT OPERATES ON 2**M POINTS
      SIGN=-1
      NSTEP=XPA(1)/STEP
      DO 600 NS=1,NSTEP
600   A(NS)=(0.,0.)
      ACON=(EPSQ*EPSI)*PI/(EPSI*1.854)
      DO 601 I=1,NA
```

```
      SIGN=-1.*SIGN
      NSS=NSTEP+1
      NSE=XPA(I+1)/STEP
      GA=XPA(I+1)-XPA(I)
      AMP=ACON*XLA(I)/GA
      DO 602 NS=NSS,NSE
      ARG=(NS*STEP-XPA(I))*PI/GA
      AR=AMP*COS(ARG)*SIGN
      A(NS)=CMPLX(AR,Z)
602   CONTINUE
601   CONTINUE
      NSS=NSE+1
      DO 603 NS=NSS,N
603   A(NS)=(0.,0.)
C        PRINT GAP FUNCTION A
      PRINT 650
650   FORMAT(*0AMPLITUDE FUNCTION A*//)
      DO 651 I=1,NSS,4
      PRINT 652,I,(A(I+J-1),J=1,4)
 652  FORMAT(I5,8E15.3)
651   CONTINUE

C        COMPUTE INTEGRAL TRANSFORM OF TRANSDUCER A
      DXY=STEP*0.001
      CALL BFAST(A,M,-1.,DXY)
      FINC=DXY*VSAW
      PRINT 800
800   FORMAT(* FREQUENCY RESPONSE TRANSDUCER A*/* FREQUENCY*10X*TRANSFOR
     CM OUTPUT*/)
      DO 801 I=1,N,40
      FREQ=(I-1)*FINC
      PRINT 802,FREQ,(A(I+J-1),J=1,4)
802   FORMAT(E11.3,8E15.3)
801   CONTINUE
C
C        COMPUTE RADIATION CONDUCTANCE G.
      CONK=-2.*PI*(EPSI**2)*DELTA/(XLA(1)*(EPSI+EPSQ))
      CONK=1000.*CONK
      N2=N/2
      N2P=N2+1
      G(1)=0.
      DO 1001 I=2,N2P
      FREQ=(I-1)*FINC
 1001 G(I)=CONK*FREQ*A(1)*CONJG(A(I))
$
C        COMPUTE RADIATION SUSCEPTANCE B.
      DO 1002 I=2,N2
      A(I)=CMPLX(G(I),Z)
 1002 A(N+2-I)=A(I)
      A(1 )=CMPLX(Z,Z)
      A(N2P)=CMPLX(G(N2P),Z)
      DXY=FINC
      CALL BFAST(A,M,-1.,DXY)
      IMAG=CMPLX(Z,U)
      IMAGM=CMPLX(Z,UM)
      DO 1003 I=2,N2
      A(I)=IMAG*A(I)
      NC=N+2-I
1003  A(NC)=IMAGM*A(NC)
      A(1)=IMAG*A(1)
      A(N2P)=IMAG*A(N2P)
      DXY=TINC
      CALL BFAST(A,M,1.,DXY)
      PRINT 1006
 1006 FORMAT(*1HILBERT A(I) ARE*/)
      DO 1005 I=1,N2,40
      PRINT 1004,(A(I+J-1),J=1,4)
 1004 FORMAT(4(E15.3,E11.3))
 1005 CONTINUE
      DO 1007 I=1,N2
 1007 B(I)=A(I)
C
C        COMPUTE THE TRANSDUCER STATIC CAPACITANCE AND SUSCEPTANCE (ASSUMING
C        UNITY ELECTRODE GAP RATIO AND Y-CUT QUARTZ).
C
C        ADD OVERLAP LENGTHS OF ALL GAPS
C
      GL=XLA(1)
      DO 1010 I=2,NA
      XLA(I)=XLA(I-1)*ALA
 1010 GL=GL+XLA(I)
      CT=(EPSI+EPSQ)*1.E-3*GL/2.
      PRINT 1011,CT
 1011 FORMAT(*1TRANSDUCER CAPACITANCE=*E11.3/)
C
C        COMPUTE TRANSDUCER SUSCEPTANCE
C
      WINC=2.*PI*FINC
      DO 1012 I=1,N2
      OMEGA=(I-1)*WINC
1012  X(I)=OMEGA*CT
      PRINT 1013
 1013 FORMAT(*0CAPACITIVE SUSCEPTANCE*/)
```

```
      DO 1014 I=1,N2,40
 1014 PRINT 1015,I,(X(I+J-1),J=1,4)
 1015 FORMAT(I11,4(E15.3,E11.3))
      GO TO 200
200   CONTINUE

C        COMPUTE THE INPUT ADMITTANCES FOR A PAIR OF TRANSDUCERS
C
      BL=-60.*PI*2.*GA/VSAW
      BL=BL*1.E-3
      PRINT 202,G(250)
202   FORMAT(*0G(250)=*E15.3)
      DO 70 I=1,N2
      AI=BL*(I-1)*FINC
      G(I)=2.*G(I)*(1.+COS(AI))
      B(I)=2.*B(I)*(1.+SIN(AI))
70    X(I)=2.*X(I)
      CLAST=COS(AI)
      PRINT 201,BL,AI
201   FORMAT(* BL=*E15.3/* AI=*E15.3)
      PRINT 203,CLAST,G(250)
203   FORMAT(* CLAST=*E15.3/* G(250)=*E15.3/)

C
C        PRINT G,B,X AND Y.
      PRINT 900
  900 FORMAT(1H1,34X*TRANSDUCER INPUT ADMITTANCE*/)
      PRINT 901
  901 FORMAT(*  FREQUENCY*10X*G*19X*B*19X*X*19X*Y=G+J(B*X)*)
      PRINT 902
  902 FORMAT(4X*(MHZ)*9X*(MHOS)*14X*(MHOS)*14X*(MHOS)*12X*(MHOS)*7X*(DEG
     CREES)*)
      Y(1)=(0.,0.)
      DO 903 I=2,N2
      G(I)=2.*G(I)
      DUM=2.*B(I)+X(I)
      Y(I)=CMPLX(G(I),DUM)
      CA=CABS(Y(I))
      DEG=ATAN2(DUM,G(I))*180./PI
      Y(I)=CMPLX(CA,DEG)
      FREQ=(I-1)*FINC*1.E-6
      PRINT 904,FREQ,G(I),B(I),X(I),Y(I)
904   FORMAT(F8.1,E18.3,2E20.3,E18.3,E16.3)
 903  CONTINUE
      GO TO 100
100   CONTINUE
C
C        PLOT THE MODULUS OF THE INPUT ADMITTANCE
C
      CALL PLOT10(10HNEBC BX142,10)
      CALL XLIMIT(100.)
      CALL PAUPLOT(17H0.4 BLACK INK PLS,17)
      CALL PLOT(4.,0.,-3)
      DO 1020 I=1,501
      XP(I)=(I-1)*FINC
 1020 YP(I)=REAL(Y(I))
      XP(501)=AINT(XP(501))
      CALL SCALE(XP,10.,501,1)
      CALL SCALE(YP,4.,501,1)
      CALL AXIS(0.,0.,17HFREQUENCY (HERTZ),-17,20.,0.,XP(502),XP(503),0)
      CALL AXIS(0.,0.,38HMODULUS OF TRANSDUCER INPUT ADMITTANCE,38,10.,9
     C0.,YP(502),YP(503),-1)
      CALL SYMBOL(3.,8.,0 .2,10HTRANSDUCER,0.,10)
      CALL SYMBOL(5.,8.,0.2,TITLE,0.,10)
      CALL LINE(XP,YP,501,1,0,0)
C
C        PLOT G,B AND X.
      CALL SCALE(G,4.,501,1)
      CALL AXIS(20.,0.,5HG (*),5,10.,90.,G(502),G(503),-1)
      CALL LINE(XP,G,501,1,5,3)
      CALL SCALE(B,4.,501,1)
      CALL AXIS(22.,0.,5HB (X),5,10.,90.,B(502),B(503),-1)
      CALL LINE(XP,B,501,1,5,4)
      CALL SCALE(X,4.,501,1)
      CALL AXIS(24.,0.,1HX,1,10.,90.,X(502),X(503),-1)
      CALL LINE(XP,X,501,1,0,0)
      CALL PLOT(30 .,0.,-3)
      STOP
      END
      NOLIST
      SUBROUTINE BFAST(Y,M,SIGN,DXY)
*                                                                      FAST  20
*                                                                      FAST  30
*        SUBROUTINE FOR THE CALCULATION OF EITHER THE FORWARD OR       FAST  40
*        INVERSE FOURIER TRANSFORM OF A COMPLEX SEQUENCE  Y  USING THE FAST  50
*        FAST FOURIER TRANSFORM (FFT) ALGORITHM.                       FAST  60
*                                                                      FAST  70
*                                          M
*        Y  IS A COMPLEX ARRAY OF DIMENSION 2   AND IS BOTH THE INPUT  FAST  90
*        AND OUTPUT SEQUENCE OF THE SUBROUTINE.                        FAST 100
*                                                                      FAST 280
*         PRESENT DIMENSIONS LIMIT=2**10
*                                                                      FAST 110
```

```
*       DXY = THE SAMPLE SPACING FOR THE INPUT ARRAY Y. THE CORRES-
*       PONDING SAMPLE SPACING IN THE TRANSFORM DOMAIN IS OUTPUT IN DXY
*                                                                      FAST 140
*       FOR TIME TO FREQUENCY TRANSFORMATION,     SIGN = -1.0          FAST 150
*       FOR FREQUENCY TO TIME TRANSFORMATION,     SIGN = +1.0          FAST 160
*                                                                      FAST 170
*       SUBROUTINE  CON  SETS UP A CONVERSION TABLE TO REARRANGE THE   FAST 180
*       INPUT ARRAY FOR PROCESSING.                                    FAST 190
*                                                                      FAST 200
*       SUBROUTINE  TABLE  SETS UP A TABLE OF ALL SINES AND COSINES    FAST 210
*       USED IN SUBROUTINE  FAST.                                      FAST 220
*                                                                      FAST 230
*       SUBROUTINE BFAST IS MODIFIED VERSION OF SUBROUTINE FAST WRITTEN 2/5/72
*       ON 2 MAY 1972
*
*                                                                      FAST 260
      COMPLEX A,U,W,T,Y                                                FAST 270
      DIMENSION A(1024),Y(2)                                           FAST 290
      COMMON /PERM/MM(1024)                                            FAST 300
      COMMON /TAB/TC(10),TS(10)                                        FAST 310
      DATA MSET/0/                                                     FAST 320
*                                                                      FAST 330
      IF (MSET.EQ.M) GOTO 1                                            FAST 340
      CALL TABLE(M)                                                    FAST 350
      CALL CON(M)                                                      FAST 360
      MSET=M                                                           FAST 370
 1    CONTINUE                                                         FAST 380
*                                                                      FAST 400
      N=2**M                                                           FAST 390
      DO 7 I=1,N                                                       FAST 430
      J=MM(I)
 7    A(I)=Y(J)
*
      DO 20 L=1,M                                                      FAST 470
      LE=2**L                                                          FAST 480
      LE1=LE/2                                                         FAST 490
      U=(1.0,0.0)                                                      FAST 500
      W=CMPLX(TC(L),TS(L)*SIGN)                                        FAST 510
      DO 20J=1,LE1                                                     FAST 520
      DO 10 I=J,N,LE                                                   FAST 530
      IP=I+LE1                                                         FAST 540
      T=A(IP)*U                                                        FAST 550
      A(IP)=A(I)-T                                                     FAST 560
      A(I)=A(I)+T                                                      FAST 570
 10   CONTINUE                                                         FAST 580
      U=U*W                                                            FAST 590
 20   CONTINUE                                                         FAST 600
*                                                                      FAST 610
      DO 30 I=1,N                                                      FAST 620
      Y(I)=A(I)*DXY                                                    FAST 660
 30   CONTINUE
      DXY=1./(DXY*N)                                                   FAST 680
*
      RETURN                                                           FAST 700
      END                                                              FAST 690
      SUBROUTINE TABLE(M)                                              FAST 760
      COMMON /TAB/TC(10),TS(10)                                        TABL  10
      PI=4.0*ATAN2(1.0,1.0)                                            TABL  20
      DO11=1,M                                                         TABL  30
      TC(I)=COS(PI/(2**(I-1)))                                         TABL  40
 1    TS(I)=SIN(PI/(2**(I-1)))                                         TABL  50
      RETURN                                                           TABL  60
      END                                                              TABL  70
      SUBROUTINE CON(M)                                                TABL  80
      INTEGER A,T                                                      CON   10
      COMMON /PERM/ A(1024)                                            CON   20
      N=2**M                                                           CON   30
      NV2=N/2                                                          CON   40
      NM1=N-1                                                          CON   50
      J=1                                                              CON   60
      DO11I=1,N                                                        CON   70
 1    A(I)=I                                                           CON   80
      DO 7 I=1,NM1                                                     CON   90
      IF(I.GE.J)GOTO5                                                  CON  100
      T=A(J)                                                           CON  110
      A(J)=A(I)                                                        CON  120
      A(I)=T                                                           CON  130
 5    K=NV2                                                            CON  140
 6    IF(K.GE.J)GOTO7                                                  CON  150
      J=J-K                                                            CON  160
      K=K/2                                                            CON  170
      GOTO 6                                                           CON  180
 7    J=J+K                                                            CON  190
      RETURN                                                           CON  200
      END                                                              CON  210
000000000000000000000      END OF RECORD                               CON  220
 3.204E  3   VSAW
    1.              10   TINC        M
    8   NA
   1.0         3.16      3.16E- 2   XPA        XLA        GA
   1.0         1.0        AGA     ALA
50MH7 UIDT    TITLE
000000000000000000000      END OF FILE
```

## A1.6 Program PCODE - Binary Code Listing

### A1.6.1 Flow Chart

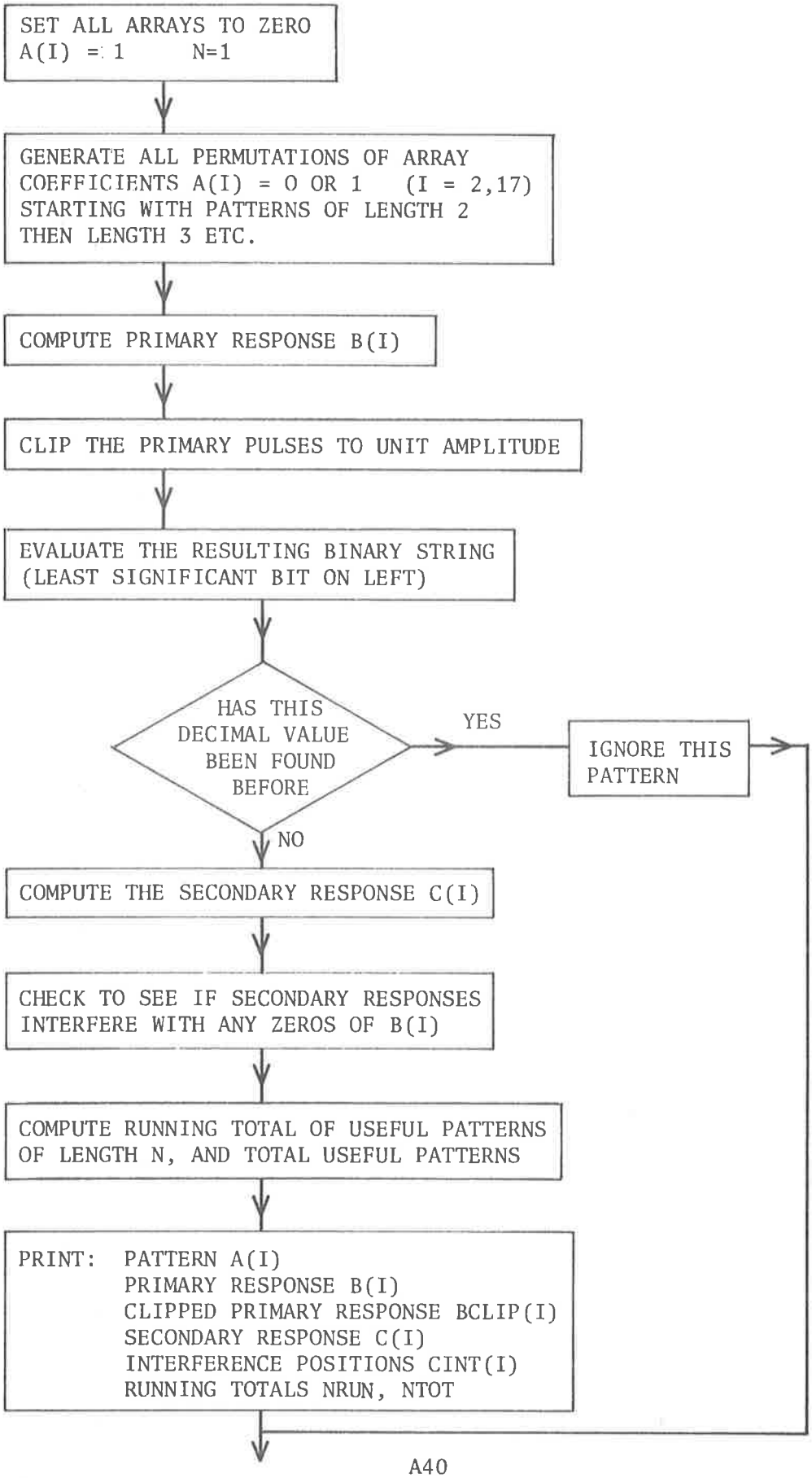

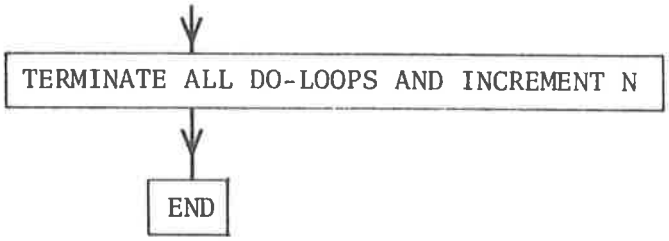


## A1.6.2 Program Listing

```
      PROGRAM PCODE(INPUT,OUTPUT)
C
C        THIS PROGRAM COMPUTES THE PRIMARY AND SECOND ORDER REGENERATED
C        RESPONSES FOR A DELAY LINE WITH IDENTICAL TRANSDUCERS SEPARATED IN TIME
C        BY INTEGRAL MULTIPLES OF THE BASIC TIME INTERVAL T.
C        A(I)= THE TRANSDUCER DESCRIPTOR
C        B(I)= THE PRIMARY RESPONSE CODE
C        BCLIP(I)= THE BINARY CODE OBTAINED BY CLIPPING B(I).
C        C(I)= THE SECONDARY (REGENERATED) RESPONSE.
C        NADD= THE NUMBER OF UNIQUE CODES OBTAINED BY ADDING 1 MORE TRANSDUCER
C        NTOT= THE TOTAL NUMBER OF UNIQUE CODES
C
C
      REAL B(20),C(40)
      INTEGER A(20),BCLIP(20),CINT(40)
      INTEGER DEC(10000),IH(20)
      DATAK1,K2,K3,K4,K5,K6,K7,K8,K9/0,0,0,0,0,0,0,0,0/
      DATA K10,K11,K12,K13,K14,K15,K16/0,0,0,0,0,0,0/
      COMMON / /DEC
C
C        PRINT THE HEADINGS
      PRINT 1
1     FORMAT(1H1,6X*TRANSDUCER*24X*RESPONSES    B(I),BCLIP(I),C(I),CINT(
     1I)*33X*DECIMAL    CODES  TOTAL*)
      DO 2 I=1,17
2     IH(I)=I-1
      PRINT 3,(IH(I),I=1,17)
3     FORMAT(*ON*6X*PATTERN*11X,17I5,* EQUIVALENT ADDED CODES*)
C
C        SET UP THE TRANSDUCERS
      DO 9 I=1,16
      A(I)=0
      B(I)=0
      BCLIP(I)=0
      C(I)=0
9     CINT(I)=0
      A(1)=1
      N=1
      NTOT=0
      DEC(1)=0
      NTEMP=0
```

```
      DO 26 NQ=1,2
      A(17)=NQ-1
      DO 25 NP=1,2
      A(16)=NP-1
      DO 24 NN=1,2
      A(15)=NN-1
      DO 23 NM=1,2
      A(14)=NM-1
      DO 22 NL=1,2
      A(13)=NL-1
      DO 21 NK=1,2
      A(12)=NK-1
      DO 20 NJ=1,2
      A(11)=NJ-1
      DO 19 NI=1,2
      A(10)=NI-1
      DO 18 NH=1,2
      A(9)=NH-1
      DO 17 NG=1,2
      A(8)=NG-1
      DO 16 NF=1,2
      A(7)=NF-1
      DO 15 NE=1,2
      A(6)=NE-1
      DO 14 ND=1,2
      A(5)=ND-1
      DO 13 NC=1,2
      A(4)=NC-1
      DO 12 NB=1,2
      A(3)=NB-1
      DO 11 NA=1,2
      A(2)=NA-1
      IF(K1.EQ.0)30,31
30    K1=1
      N=2
      GO TO 11
31    CONTINUE
C
C        COMPUTE IMPULSE RESPONSE B(I).
C
      DO 50 I=1,N
      B(I)=0.
50    B(1)=B(1)+0.5*A(I)*A(I)
      DO 501 L=2,N
      L1=N-L+1
      DO 501 J=1,L1
501   B(L)=B(L)+A(J)*A(J+L-1)
C
C        CLIP PULSES IN A(I) TO UNIT AMPLITUDE
      DO 51 I=1,N
      IF(B(I).EQ.0)511,512
511   BCLIP(I)=0
      GO TO 51
512   BCLIP(I)=1
51    CONTINUE
C
C        EVALUATE THE BINARY CODE(LEAST SIGNIFICANT DIGIT TO THE LEFT)
      NDEC=0
      DO 52 I=2,N
52    NDEC=NDEC*2+BCLIP(N+2-I)
C
C        HAS THIS DECIMAL VALUE BEEN FOUND BEFORE
      DO 53 I=1,NTOT
      IF(DEC(I).EQ.NDEC) GO TO 11
53    CONTINUE
      NTOT=NTOT+1
      DEC(NTOT)=NDEC
C
C        COMPUTE THE SECONDARY RESPONSE C(I)
      L2=2*N-1
      DO 60 I=1,L2
      C(I)=0.
60    CINT(I)=0.
      DO 601 L=1,N
      DO 601 M=1,L
601   C(L)=C(L)+B(M)*B(L-M+1)
      L3=N+1
      DO 602 L=L3,L2
      L4=L-N+1
      DO 602 M=L4,N
602   C(L)=C(L)+B(M)*B(L-M+1)
C
C        CHECK TO SEE IF THE SIGNAL INTERFERES WITH ANY ZEROS IN BCLIP(I)
      DO 61 I=2,N
      IF (BCLIP(I).EQ.0)62,61
62    IF(C(I).EQ.0) 61,63
63    CINT(I)=1
61    CONTINUE
```

```
C        COMPUTE RUNNING TOTAL OF TRANSDUCERS ADDED FOR FIXED N

      IF(NTEMP.EQ.N)701,702
701   NRUN=NRUN+1
      GO TO 703
702   NRUN=1
      NTEMP=N
703   CONTINUE
C        PRINT TRANSDUCERS AND CODE
      PRINT 70,N,(A(I),I=1,17),(B(I),I=1,17)
70    FORMAT(1H0,I2,X,17I1,5X,17F5.1)
      PRINT 71,(BCLIP(I),I=1,17),NDEC
71    FORMAT(26X,17I5,I10)
      PRINT 72,(C(I),I=1,17),(CINT(I),I=1,17),NRUN,NTOT
72    FORMAT(26X,17F5.1/26X,17I5,11X,2I7)
11    CONTINUE
      IF(K2.EQ.0)32,12
32    K2=1
      N=3
12    CONTINUE
      IF(K3.EQ.0)33,13
33    K3=1
      N=4
13    CONTINUE
      IF(K4.EQ.0)34,14
34    K4=1
      N=5
14    CONTINUE
      IF(K5.EQ.0)35,15
35    K5=1
      N=6
15    CONTINUE
      IF(K6.EQ.0)36,16
36    K6=1
      N=7
16    CONTINUE
      IF(K7.EQ.0)37,17
37    K7=1
      N=8
17    CONTINUE
      IF(K8.EQ.0)38,18
38    K8=1
      N=9
18    CONTINUE
      IF(K9.EQ.0)39,19
39    K9=1
      N=10
19    CONTINUE
      IF(K10.EQ.0)40,20
40    K10=1
      N=11
20    CONTINUE
      IF(K11.EQ.0)41,21
41    K11=1
      N=12
21    CONTINUE
      IF(K12.EQ.0)42,22
42    K12=1
      N=13
22    CONTINUE
      IF(K13.EQ.0)43,23
43    K13=1
      N=14
23    CONTINUE
      IF(K14.EQ.0)44,24
44    K14=1
      N=15
24    CONTINUE
      IF(K15.EQ.0)45,25
45    K15=1
      N=16
25    CONTINUE
      IF(K16.EQ.0)46,26
46    K16=1
      N=17
26    CONTINUE
      STOP
      END
00000000000000000000      END OF RECORD
00000000000000000000      END OF FILE
00000000000000000000      END OF FILE
```

## A1.7 Program PATBL2 - Electrode Pattern Generation

### A1.7.1 Flow Chart

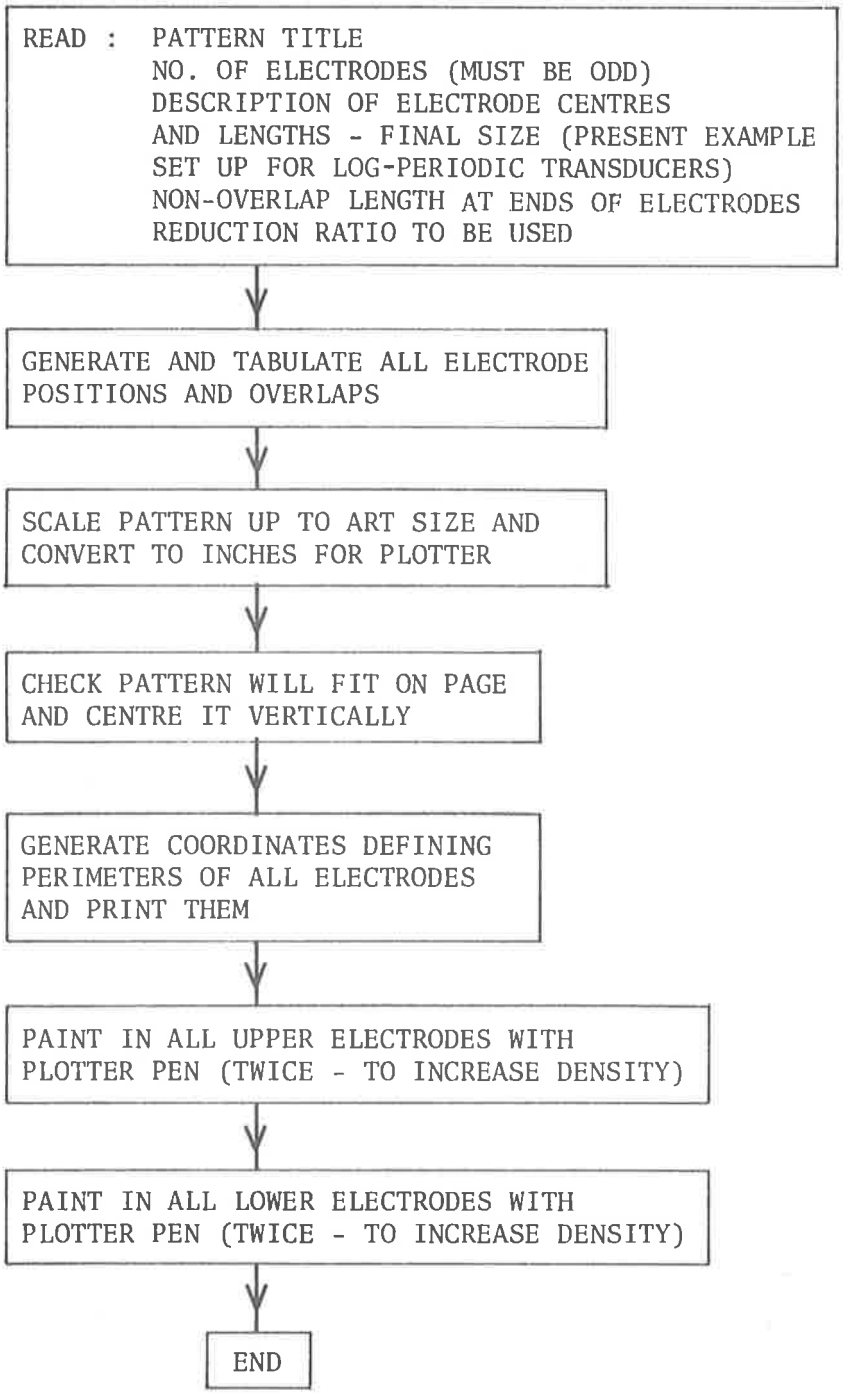

## A1.7.2 Program Listing

```
      PROGRAM PATBL2(INPUT,OUTPUT)
C        THIS PROGRAM PRODUCES A BLACK AND WHITE ELECTRODE PATTERN SUITABLE
C        FOR PHOTOGRAPHY
C
C         PEN TIP WIDTH IS 0.3 MILLIMETRES
C        AVERAGE PEN TRACE OVERLAP = .1544 = .006 INCH
C        ALLOWANCE IS MADE FOR PEN TIP WIDTH
C
C              INPUT DATA REQUIRED =
*        NA=ODD NUMBER OF FINGERS IN THE TRANSDUCER
*        GA= SIZE OF FIRST GAP IN MILLIMETRES
*        XPA(1)= POSITION OF FIRST FINGER CENTRE IN MM.
*        XLA(1)= SIGNED MAGNITUDE OF FIRST OVERLAP IN MM.
*        AGA= RATIO OF SUCCESSIVE GAP WIDTHS
*        ALA= RATIO OF  SUCCESSIVE OVERLAPS (UNSIGNED)
*        WNO= MINIMUM NON-OVERLAP LENGTH IN MM.
C        NOTE OVERLAP I IS BETWEEN FINGER I AND FINGER I+1
*        REDR= TOTAL REDUCTION RATIO((DEFINED GREATER THAN 1)
*        TITLE = IDENTIFYING NAME OF THE PATTERN
C        PROGRAM ASSUMES EACH GAP DIVIDED INTO QUARTERS AND RIGHT AND LEFT
C        QUARTERS METALLIZED
C        THE PROGRAM ASSUMES THE SUM OF THE SIGNED OVERLAPS IS SMALL
C
C
      DIMENSION XPA(100),XLA(100)
      DIMENSIONX(400),Y(400)
      READ 200,TITLE
200   FORMAT(A10)
      READ 305,NA,GA
305   FORMAT(I10,E10.3)
      READ 300,XPA(1),XLA(1)
300   FORMAT(2E10.3)
      READ 300,ALA,AGA
      READ 300,WNO
      READ 300,REDR
C
C        TEST THAT NA IS ODD
      AN=NA
      AN=AN/2
      ANT=AN-AINT(AN)
      IF(ANT.EQ.0)301,302
301   PRINT 303
303   FORMAT(*1NUMBER OF FINGERS MUST BE ODD*)
      STOP
302   CONTINUE
      PRINT 320,TITLE,NA,GA
320   FORMAT(*1TITLE=*A10/* NA=*I10/* GA=*E10.3)
      PRINT 321,XPA(1),XLA(1)
321   FORMAT(* XPA(1)=*E10.3/* XLA(1)=*E10.3)
      PRINT 322,ALA,AGA
322   FORMAT(* ALA=*E10.3/* AGA=*E10.3)
      PRINT 323,WNO,REDR
323   FORMAT(* WNO=*E10.3/* REDR=*F10.3)
C        GENERATE GAPS AND OVERLAPS
      XPA(2)=XPA(1)+GA
      NA1=NA-1
      DO 304 I=2,NA1
      GA=GA*AGA
      XPA(I+1)=XPA(I)+GA
304   XLA(I)=-XLA(I-1)*ALA
C
C        PRINT ELECTRODE POSITIONS AND OVERLAPS
      PRINT 306
306   FORMAT(*0ELECTRODE  POSITIONS AND OVERLAPS (IN MM)*/)
      DO 307 J=1,NA1
307   PRINT 308,XPA(J),XLA(J)
308   FORMAT(E22.3,E13.3)
      PRINT 308,XPA(NA)
C        SCALE UP TO ARTWORK SIZE (IN INCHES)
      SCALE=REDR/25.4
      DO 309 I=1,NA
      XPA(I)=XPA(I)*SCALE
309   XLA(I)=XLA(I)*SCALE
C        FIND THE MAXIMUM OVERLAP
      XM=0
      DO 400 I=1,NA1
400   XM=AMAX1(XM,XLA(I))
C        FIND TOTAL PATTERN WIDTH
      WT=XM+2*WNO
C        TEST PATTERN DOES NOT EXCEED 28 INCHES HIGH
      IF(WT.LT.28)GO TO 402
      PRINT 403
403   FORMAT(*1PATTERN TOO HIGH*)
      STOP
```

```
C        GENERATE PLOTTING COORDS - ELECTRODE 1
402   CL=14
      G3=(XPA(2)-XPA(1))/4
      X(1)=X(2)=XPA(1)
      X(3)=X(4)=XPA(1)+G3
      YMAX=CL+WT/2
      YMIN=CL-WT/2
      Y(1)=Y(4)=YMAX
      Y(2)=Y(3)=CL-XLA(1)/2
C        GENERATE PLOTTING COORDS FOR REMAINING ELECTRODES
      DO 401 J=2,NA1,2
      J4=4*J
      G1=G3
      G2=(XPA(J+1)-XPA(J))/4
      G3=(XPA(J+2)-XPA(J+1))/4
      X(J4-3)=X(J4-2)=XPA(J)-G1
      X(J4-1)=X(J4)=XPA(J)+G2
      Y(J4-3)=Y(J4)=YMIN
      Y(J4-2)=Y(J4-1)=Y(J4-5)+XLA(J-1)
      X(J4+1)=X(J4+2)=XPA(J+1)-G2
      X(J4+3)=X(J4+4)=XPA(J+1)+G3
      Y(J4+1)=Y(J4+4)=YMAX
      Y(J4+2)=Y(J4+3)=Y(J4-1)+XLA(J)
401   CONTINUE
      X(J4+3)=X(J4+4)=XPA(J+1)
C        PRINT OUT COORDINATES
      PRINT 502
502   FORMAT(35X*PLOTTING COORDINATES (IN INCHES)*//* ELECTRODE*7X*X1*6X
     C*Y1*10X*X2*6X*Y2*10X*X3*6X *Y3*10X*X4*6X*Y4*)
      DO 503 I=1,NA
      I4=4*I
      PRINT 504,I,X(I4-3),Y(I4-3),X(I4-2),Y(I4-2),X(I4-1),Y(I4-1),X(I4),
     CY(I4)
504   FORMAT(I10,4(F12.3,F8.3))
503   CONTINUE
C
C        PLOT THE ELECTRODE PATTERN
      CALL PLOT30(10HNEBC B0X34,10)
      CALL XLIMIT(55.)
      CALL PAUPLOT(30HWHITE PAPER + 0.3BLACK INK PLS,30)
C
C        PLOT PATTERN DATA
       CALL SYMBOL(0.,5.,0.3,9HPATTERN =,90.,9)
      CALL SYMBOL(0.,8.,0.3,TITLE,90.,10)
      CALL SYMBOL(1.,5.,0.3,17HREDUCTION RATIO =,90.,17)
      CALL NUMBER(1.,10.,0.3,REDR,90.,4HF6.2)
      CALL PLOT(10.,0.,-3)
C        PLOT UPPER HALF OF PATTERN
C
C        NOTE DIMENSIONS NOW IN INCHES
      P=0.3/25.4
      P2=P/2
      OLAP=0.006
      NTEMP=0
1000  CONTINUE
      NTEMP=NTEMP+1
      DO 601 I=1,NA,2
      J=4*I
C         IS LINE WIDTH LESS THAN PEN TIP WIDTH
      IF((X(J)-X(J-3)).LT.P)602,603
602   PRINT 604
604   FORMAT(*1LINE WIDTH LESS THAN PEN WIDTH*)
      STOP
603   XD=X(J-3)+P2
      YD=Y(J-3)
      CALL PLOT(XD,YD,3)
      YD=Y(J-2)
      CALL PLOT(XD,YD,2)

      YD=Y(J)
      CALL PLOT(XD,YD,1)

C
C        IS THERE ROOM FOR A FULL STROKE DOWN
608    CONTINUE
      IF((X(J)-(XD+P2-OLAP)).LT.P)606,607
606   XD=X(J)-P2
      CALL PLOT(XD,YD,1)
      YD=Y(J-1)
      CALL PLOT(XD,YD,1)
      YD=Y(J)
      CALL PLOT(XD,YD,1)
      GO TO 601
607   XD=XD+P-OLAP
      CALL PLOT(XD,YD,1)
      YD=Y(J-1)
      CALL PLOT(XD,YD,1)
      YD=Y(J)
      CALL PLOT(XD,YD,1)
      GO TO 608
```

```
601   CONTINUE
$
C        PLOT THE LOWER HALF OF THE PATTERN
C
      CALL PLOT(0.,YD,3)
      CALL PLOT(0.,Y(5),3)
      DO 610 I=2,NA1,2
      J=4*I
      XD=X(J-3)+P2
      YD=Y(J-3)
      CALL PLOT(XD,YD,3)
      YD=Y(J-2)
      CALL PLOT(XD,YD,2)

      YD=Y(J)
      CALL PLOT(XD,YD,1)
C
C        IS THERE ROOM FOR A FULL STROKE DOWN
618    CONTINUE
      IF((X(J)-(XD+P2-OLAP)).LT.P)616,617
616   XD=X(J)-P2
      CALL PLOT(XD,YD,1)
      YD=Y(J-1)
      CALL PLOT(XD,YD,1)
      YD=Y(J)
      CALL PLOT(XD,YD,1)
      GO TO 610
617   XD=XD+P-OLAP
      CALL PLOT(XD,YD,1)
      YD=Y(J-1)
      CALL PLOT(XD,YD,1)
      YD=Y(J)
      CALL PLOT(XD,YD,1)
      GO TO 618
610   CONTINUE
      DO 999 I=1,NA
      DO 999 J=1,4
      K=4*(I-1)+J
999   X(K)=X(K)+11.2
      IF(NTEMP.GE.2) GO TO 1001
      GO TO 1000
1001  CONTINUE
      CALL PLOT(40.,0.,-3)
      STOP
      END
00000000000000000000      END OF RECORD
 LG-15/20  1ITLE
         5  .105         NA       GA
   5.       9.         XPA        XLA
   1.        0.9        ALA         AGA
   2.       WNO
   20.        REDR
00000000000000000000      END OF FILE
```

## A1.8 Program INTER - Receiver System Model

### A1.8.1 Flow Chart

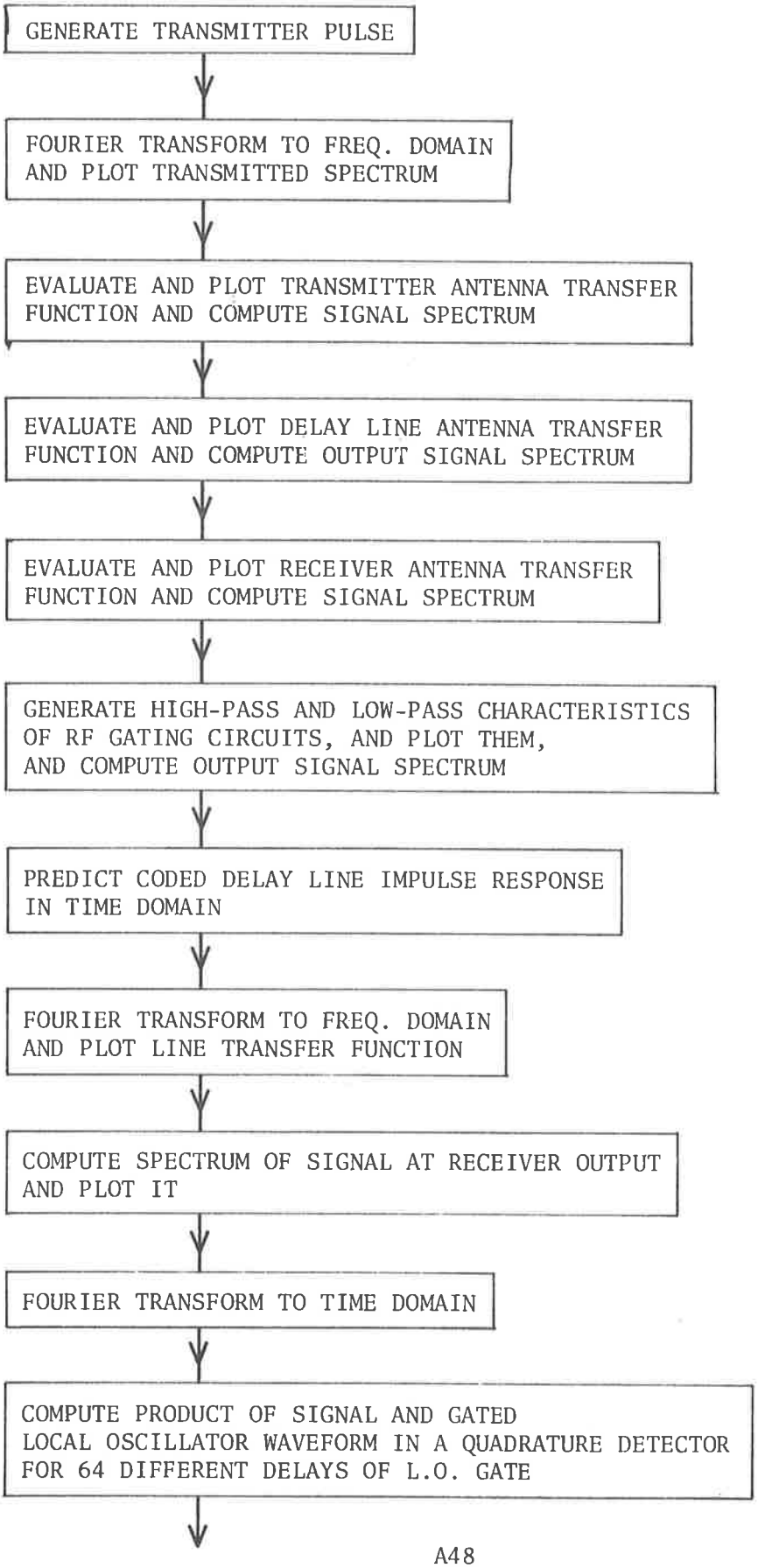

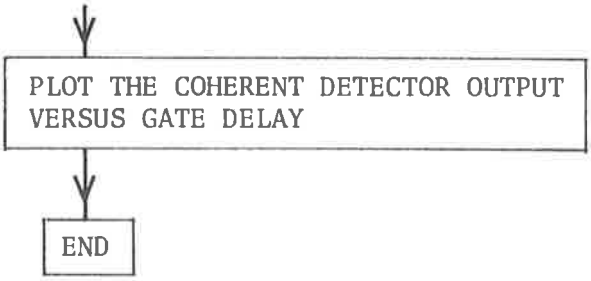


## A1.8.2 Program Listing

```
      PROGRAM INTER(INPUT,OUTPUT)
C        HAVE 1024 SAMPLES SPACED 5NSEC (QUARTER WAVELENGTH) AND ALL TIME
C        FUNCTIONS PERIODIC ON LENGTH 1024.
C        V(T) = VOLTAGE WAVEFORM
C        NT = LO GATE INCREMENTS MEASURED FROM ZERO
C        F(I) =CENTRE FREQUENCY OF TUNED CIRCUIT I - IN HERTZ
C        Q(I) = Q-FACTOR OF TUNED CIRCUIT I
C        H(I,J) = TRANSFER FUNCTION I AT FREQUENCY INCREMENT J.
C
C        INPUT DATA NEEDED
C        F(I),Q(I),I=1,4     -  2(E10.3)
C        NT,NF,NS,NC    -  4(I5)
C        LE(I),I=1,NT     -  10(I5)
      DIMENSION C(1024),D(1024),F(4),Q(4)
      DIMENSION X(100),Y(100),XV(1024),YV(1024)
      COMPLEX V(1024),PT(1024),W,WINCC
      REAL LL,CC,R(150),S(150),U(150)
      COMPLEX H(513)
      COMMON /A1/H
      COMMON V,PT,C,D
      PI=3.14159265358979
      CALL TIME
C        SET UP TRANSMITTER PULSE
      DO 1 IA=1,1024
1     V(IA)=(0.,0.)
      DO 10 IA=1,17,4
      V(IA+1)=(1.,0.)
10    V(IA+3)=(-1.,0.)
C        CONVERT V TO FREQUENCY DOMAIN
      CALL FAST(10,V,-1.,10)
C        PLOT TRANSMITTER SPECTRUM - AMPLITUDE
      CALL PLOT10(10HNEBC BX142,10)
      CALL XLIMIT(140.)
      CALL PAUPLOT(30H0.38LACK INK * BLANK PAPER PLS,30)
      WINC=2*PI*1.E6/5.12
      DO 120 J=1,512
      XV(J)=J*1.E6/5.12
120   YV(J)=CABS(V(J))
      CALL SCALE(XV,10.,512,1)
```

```
      CALL SCALE(YV,4.,512,1)
      CALL AXIS(0.,0.,20HTRANSMITTER SPECTRUM,20,10.,90.,YV(513),YV(514)
     C,-1)
      CALL PLOT(6.,0.,-3)
      CALL LINE(XV,YV,512,1,0,0)
C        COMPUTE TUNED CIRCUIT TRANSFER FUNCTIONS
      PRINT 23
23    FORMAT(*1TUNED CIRCUIT PARAMETERS*/)
      DO 20 IB=1,4
      READ 21,F(IB),Q(IB)
21    FORMAT(2(E10.3))
      PRINT 22,IB,F(IB),IB,Q(IB)
22    FORMAT(* CENTRE FREQUENCY (*I1*)=*E10.3,5X,*Q(*I1*)=*E10.3)
20    CONTINUE
C        TRANSMITTER ANTENNA TRANSFER FUNCTION
      CALL BPASS(F(1),Q(1),2)
      DO 122 J=1,513
      V(J)=H(J)*V(J)
122   YV(J)=CABS(H(J))
C        PLOT ANTENNA TRANSFER FUNCTION
      CALL PLOT(-4.,0.,-3)
      CALL SCALE(YV,4.,512,1)
       YVO=YV(513)
      CALL AXIS(0.,0.,13HTUNED CIRCUIT,13,10.,90.,YV(513),YV(514),-1)
      CALL PLOT(4.,0.,-3)
      CALL LINE(XV,YV,512,1,5,2)
      CALL SYMBOL(1.,9.,0.15,19HTRANSMITTER ANTENNA,0.,19)
      CALL SYMBOL(5.1,9.1,.15,2,0.,-1)
C        CARD ANTENNA TRANSFER FUNCTION
      CALL BPASS(F(2),Q(2),2)
      DO 123 J=1,513
      V(J)=H(J)*H(J)*V(J)
123   YV(J)=CABS(H(J))
      YV(513)=YVO
      CALL LINE(XV,YV,512,1,5,3)
      CALL SYMBOL(1.,8.5,0.15,12HCARD ANTENNA,0.,12)
      CALL SYMBOL(5.1,8.6,0.15,3,0.,-1)
C        RECEIVER ANTENNA TRANSFER FUNCTION
      CALL BPASS(F(4),Q(4),2)
      DO 130 J=1,513
      V(J)=V(J)*H(J)
130   YV(J)=CABS(H(J))
      YV(513)=YVO
      CALL LINE(XV,YV,512,1,5,4)
      CALL SYMBOL(1.,8.,0.15,16HRECEIVER ANTENNA,0.,16)
      CALL SYMBOL(5.1,8.1,0.15,4,0.,-1)
C        COMPUTE RECEIVER FILTER TRANSFER FUNCTIONS
C        LOW PASS NETWORKS
      CALL BPASS(1.E8,0.,1)
      DO 131 J=1,513
      H(J)=H(J)**4
      V(J)=V(J)*H(J)
131   YV(J)=CABS(H(J))
      YV(513)=YVO
      CALL LINE(XV,YV,512,1,5,5)
      CALL SYMBOL(1.0,7.5,0.15,16HLOW-PASS FILTERS,0.,16)
      CALL SYMBOL(5.1,7.6,0.15,5,0.,-1)
C        HIGH PASS NETWORKS
      CALL BPASS(2.E7,0.,3)
      DO 132 J=1,513
      H(J)=H(J)**4
      V(J)=V(J)*H(J)
132   YV(J)=CABS(H(J))
      YV(513)=YVO
      CALL LINE(XV,YV,512,1,5,6)
      CALL SYMBOL(1.0,7.0,0.15,17HHIGH-PASS FILTERS,0.,17)
      CALL SYMBOL(5.1,7.1,0.15,6,0.,-1)
C        COMPUTE LINE IMPULSE RESPONSE  - PT(I)
      CALL IMPULSE(PT)
C        CONVERT TO FREQUENCY DOMAIN
      CALL FAST(10,PT,-1.,10)
C        PLOT DELAY LINE SPECTRUM - AMPLITUDE
      CALL PLOT(-2.,0.,-3)
      DO 124 J=1,512
124   YV(J)=CABS(PT(J))
      CALL SCALE(YV,4.,512,1)
      CALL AXIS(0.,0.,19HDELAY LINE SPECTRUM,19,10.,90.,YV(513),YV(514),
     C-1)
      CALL PLOT(2.,0.,-3)
      CALL LINE(XV,YV,512,1,0,0)
C        COMPUTE OUTPUT SPECTRUM OF TUNED CIRCUITS AND DELAY LINE
      DO 40 IE=1,513
40    V(IE)=V(IE)*PT(IE)
      DO 41 IE=1,511
41    V(513+IE)=CONJG(V(513-IE))
C        PLOT SPECTRUM OF INPUT TO MIXER - AMPLITUDE
      DO 126 J=1,512
126   YV(J)=CABS(V(J))
      CALL SCALE(YV,4.,512,1)
      CALL AXIS(0.,0.,17HFREQUENCY (HERTZ),-17,20.,0.,XV(513),XV(514),0)
```

```
      CALL AXIS(0.,0.,20HMIXER INPUT SPECTRUM,20,10.,90.,YV(513),YV(514)
     C,-1)
      CALL LINE(XV,YV,512,1,0,0)
      CALL PLOT(14.,0.,-3)
C        CONVERT TO TIME DOMAIN
      CALL FAST(10,V,+1.,10)
C        PLOT WAVEFORM INTO MIXER
      DO 80 K=1,1024
      XV(K)=K*5
80    YV(K)=V(K)
      CALL SCALE(XV,25.,1000,1)
      CALL SCALE(YV,5.,1000,1)
      CALL AXIS(0.,0.,7HVOLTAGE,7,10.0,90.0,YV(1001),YV(1002),-1)
      CALL AXIS(0.,0.,17HTIME(NANOSECONDS),17,50.,0.,XV(1001),XV(1002),0
     C)
      CALL LINE(XV,YV,1000,1,0,0)
      CALL SYMBOL(20.0,9.0,0.2,22HVOLTAGE INPUT TO MIXER,0.,22)
      CALL PLOT(50.,0.,-3)
C        COMPUTE LOCAL OSCILLATOR SIGNALS
      DO 50 IF=1,1021,4
      C(IF)=D(IF+1)=1.
      C(IF+2)=D(IF+3)=-1.
50    C(IF+1)=D(IF)=C(IF+3)=D(IF+2)=0.
C        PERFORM GATED MIXING OVER 64 TIME INTERVALS
      DO 60 NT=70,133
      NS=5*NT
      R(NT)=S(NT)=0
      DO 70 NA=1,20
      N=NS+NA
      R(NT)=R(NT)+V(N)*C(N)
70    S(NT)=S(NT)+V(N)*D(N)
      U(NT)=SQRT(R(NT)*R(NT)+S(NT)*S(NT))
      X(NT-69)=NT
      Y(NT-69)=U(NT)
60    CONTINUE
C        PRINT OUTPUT
      PRINT 110
110   FORMAT(*0MIXER OUTPUT AS FUNCTION OF TIME SLOT*/* LO GATE OPENING
     C(X25NSEC)*10X*MIXER OUTPUT*)
      PRINT 111,((NT,U(NT)),NT=70,133)
111   FORMAT(I15,E22.2)
C        PLOT SYSTEM OUTPUT
      CALL SCALE(X,10.,64,1)
      CALL SCALE(Y,4.,64,1)
      CALL AXIS(0.,0.,12HMIXER OUTPUT,+12,10.0,90.0,Y(65),Y(66),-1)
      CALL AXIS(0.,0.,13HGATE POSITION,-13,15.,0.0,X(65),X(66),0)
      CALL LINE(X,Y,64,1,1,1)
      CALL SYMBOL(4.,9.,0.2,33HBASIC SYSTEM - LINE CODE 11010011,0.,33)
      CALL PLOT(19.0,0.0,-3)
      CALL PAUPLOT(22HPLOT COMPLETE THANKYOU,22)
      STOP
      END
      SUBROUTINE FAST(M,Y,SIGN,NN)                                        FAST  10
*                                                                         FAST  20
*                                                                         FAST  30
*        SUBROUTINE FOR THE CALCULATION OF EITHER THE FORWARD OR          FAST  40
*        INVERSE FOURIER TRANSFORM OF A COMPLEX SEQUENCE  Y  USING THE    FAST  50
*        FAST FOURIER TRANSFORM (FFT) ALGORITHM.                          FAST  60
*                                                                         FAST  70
*                                          NN                             FAST  80
*        Y  IS A COMPLEX ARRAY OF DIMENSION 2   AND IS BOTH THE INPUT     FAST  90
*        AND OUTPUT SEQUENCE OF THE SUBROUTINE.                           FAST 100
*                                                                         FAST 110
*                                                  M                      FAST 120
*        THE NUMBER OF POINTS TO BE USED IN THE FFT = 2  WITH M ≤ 10.     FAST 130
*                                                                         FAST 140
*        FOR TIME TO FREQUENCY TRANSFORMATION,     SIGN = -1.0            FAST 150
*        FOR FREQUENCY TO TIME TRANSFORMATION,     SIGN = +1.0            FAST 160
*                                                                         FAST 170
*        SUBROUTINE  CON  SETS UP A CONVERSION TABLE TO REARRANGE THE     FAST 180
*        INPUT ARRAY FOR PROCESSING.                                      FAST 190
*                                                                         FAST 200
*        SUBROUTINE  TABLE  SETS UP A TABLE OF ALL SINES AND COSINES      FAST 210
*        USED IN SUBROUTINE  FAST.                                        FAST 220
*                                                                         FAST 230
*        SUBROUTINE  FAST  WAS LAST MODIFIED ON  11 /  8 / 71  AND        FAST 240
*        SUPERSEDES ALL PREVIOUS VERSIONS.                                FAST 250
*                                                                         FAST 260
*                                                                         FAST 270
*                                                                         FAST 280
      COMPLEX A,U,W,T,Y                                                   FAST 290
      DIMENSION A(1024),Y(2)                                              FAST 300
      COMMON /PERM/MM(1024)                                               FAST 310
      COMMON /TAB/TC(10),TS(10)                                           FAST 320
      DATA MSET/0/                                                        FAST 330
*                                                                         FAST 340
      IF (MSET.EQ.M) GOTO 1                                               FAST 350
      CALL TABLE(M)                                                       FAST 360
      CALL CON(M)                                                         FAST 370
      MSET=M                                                              FAST 380
*                                                                         FAST 390
```

```
 1    CONTINUE                                                          FAST 400
      NNMM=NN-M                                                         FAST 410
      J1=2**NNMM                                                        FAST 420
      N=2**M                                                            FAST 430
      DO 7 I=1,N                                                        FAST 440
      J=(MM(I)-1)*J1+1                                                  FAST 450
 7    A(I)=Y(J)                                                         FAST 460
*                                                                       FAST 470
      DO 20 L=1,M                                                       FAST 480
      LE=2**L                                                           FAST 490
      LE1=LE/2                                                          FAST 500
      U=(1.0,0.0)                                                       FAST 510
      W=CMPLX(TC(L),TS(L)*SIGN)                                         FAST 520
      DO 20 J=1,LE1                                                     FAST 530
      DO 10 I=J,N,LE                                                    FAST 540
      IP=I+LE1                                                          FAST 550
      T=A(IP)*U                                                         FAST 560
      A(IP)=A(I)-T                                                      FAST 570
      A(I)=A(I)+T                                                       FAST 580
 10   CONTINUE                                                          FAST 590
      U=U*W                                                             FAST 600
 20   CONTINUE                                                          FAST 610
*                                                                       FAST 620
      IF (SIGN.GT.0.0) GOTO 40                                          FAST 630
*                                                                       FAST 640
      RFLN=1.0/N                                                        FAST 650
      DO 30 I=1,N                                                       FAST 660
      Y(I)=A(I)*RFLN                                                    FAST 670
 30   CONTINUE                                                          FAST 680
      RETURN                                                            FAST 690
*                                                                       FAST 700
 40   DO 50 I=1,N                                                       FAST 710
      Y(I)=A(I)                                                         FAST 720
 50   CONTINUE                                                          FAST 730
      RETURN                                                            FAST 740
*                                                                       FAST 750
      END                                                               FAST 760
      SUBROUTINE TABLE(M)                                               TABL  10
      COMMON /TAB/TC(10),TS(10)                                         TABL  20
      PI=4.0*ATAN2(1.0,1.0)                                             TABL  30
      DO 1 I=1,M                                                        TABL  40
      TC(I)=COS(PI/(2**(I-1)))                                          TABL  50
 1    TS(I)=SIN(PI/(2**(I-1)))                                          TABL  60
      RETURN                                                            TABL  70
      END                                                               TABL  80
      SUBROUTINE CON(M)                                                 CON   10
      INTEGER A,T                                                       CON   20
      COMMON /PERM/ A(1024)                                             CON   30
      N=2**M                                                            CON   40
      NV2=N/2                                                           CON   50
      NM1=N-1                                                           CON   60
      J=1                                                               CON   70
      DO 11 I=1,N                                                       CON   80
 1    A(I)=I                                                            CON   90
      DO 7 I=1,NM1                                                      CON  100
      IF(I.GE.J)GOTO5                                                   CON  110
      T=A(J)                                                            CON  120
      A(J)=A(I)                                                         CON  130
      A(I)=T                                                            CON  140
 5    K=NV2                                                             CON  150
 6    IF(K.GE.J)GOTO7                                                   CON  160
      J=J-K                                                             CON  170
      K=K/2                                                             CON  180
      GOTO 6                                                            CON  190
 7    J=J+K                                                             CON  200
      RETURN                                                            CON  210
      END                                                               CON  220
      SUBROUTINE BPASS(F,Q,ILBH)
C        F=CENTRE OR TURNOVER FREQUENCY (IN HERTZ)
C        Q=Q FACTOR FOR BANDPASS NETWORKS
C        ILBH=1 FOR LOW PASS NETWORK
C            =2 FOR BANDPASS
C            =3 FOR HIGH PASS
      COMPLEX H(513),WINCC,W
      REAL LL
      COMMON /A1/H
      PI=3.14159265358979
      WC=2*PI*F
      W=(0.,1.E-50)
      WINC=2.*PI*1.E6/5.12
      WINCC=CMPLX(0.,WINC)
      IF(ILBH-2)1,2,3
C        LOW PASS NETWORK
1     CC=1.E100
      LL=1./WC
      GO TO 4
C        BAND PASS NETWORK
2     CC=1./(WC*Q)
      LL=Q/WC
      GO TO 4
```

```
C         HIGH PASS NETWORK
3       CC=1/WC
        LL=0.
4       CONTINUE
        DO 25 IC=1,513
        H(IC)=1./(1.+W*LL+(1./(W*CC)))
25      W=W+WINCC
        RETURN
        END
        SUBROUTINE TIME
        CALL SECOND(T)
        PRINT 2000,T
2000    FORMAT(* CP TIME = *F6.3)
        RETURN
        END
        SUBROUTINE IMPULSE(PEAK)
C         THIS SUBROUTINE COMPUTES DELAY LINE RESPONSE FOR AN IMPULSE AT T=0
C         NT=NUMBER OF TRANSDUCERS
C         NF= NUMBER OF TRANSDUCER FINGER GAPS
C         NS=FINGER SPACING (TIME UNITS)
C         GAPS ARE ASSUMED TO BE HALF-WAVELENGTH APART
C         NC = NOT USED
C         LE(I)=LOCATION OF FIRST GAP OF TRANSDUCER I
C         NUMBER OF ELECTRODE GAPS IS N
C         LENGTH OF ELECTRODE PATTERN IS M
C         NUMBER OF POINTS ON THE TIME SCALE IS M
C          NGP(I) IS POSITION OF GAP I
C          NGS(I) IS SIGN OF GAP I
C         OUTPUT PULSE HEIGHTS ARE STORED IN OPEAKS
        INTEGER OPEAKS
        DIMENSION NGP(1000),NGS(1000),OPEAKS(1000)
        COMPLEX PEAK(1024)
        DIMENSION LE(20)
        READ 10,NT,NF,NS,NC
   10   FORMAT(4(I5))
        PRINT 15,NT,NF,NS,NC
   15   FORMAT(*1NT=*I5/* NF=*I5/* NS=*I5/* NC=*I5/)
        READ 11,(LE(I),I=1,NT)
   11   FORMAT(10(I5))
        DO 16 ID=1,NT
        PRINT 17,ID,LE(ID)
   17   FORMAT(* LE(*I2*)=*I5)
   16   CONTINUE
C         COMPUTE ALL FINGER POSITIONS
        IA=0
        DO 12 IB=1,NT
        LEB=LE(IB)
        NGSC=1
        DO 13 IC=1,NF
        IA=IA+1
        NGP(IA)=LEB
        LEB=LEB+NS
        NGS(IA)=NGSC
        NGSC=NGSC*(-1)
   13   CONTINUE
   12   CONTINUE
        N=NT*NF
        M=NGP(N)
        PRINT 8,N,M
    8   FORMAT(* NUMBER OF ELECTRODES=*I10/* LINE LENGTH=*I10/)
         PRINT 9,((NGP(I),NGS(I)),I=1,N)
    9   FORMAT (* ELECTRODE*/* POSITION   SIGN*/(I8,I6))
        DO 3 I=1,M
    3   OPEAKS(I)=0
C         COMPUTE TIME LAGS BETWEEN GAPS
         K=N-1
         DO 4 I=1,K
         KK=I+1
         DO 4 J=KK,N
        NTAU=NGP(J)-NGP(I)
    4   OPEAKS(NTAU)=NGS(I)*NGS(J)  +OPEAKS(NTAU)
        DO 30 J=1,M
        DUP=OPEAKS(J)
        DUM=0.
30      PEAK(J)=CMPLX(DUP,DUM)
        MM=M+1
        DO 40 J=MM,1024
40      PEAK(J)=(0.,0.)
        RETURN
        END
0000000000000000000000      END OF RECORD
 5.000E  7 5.000E  0
  5.0 E  7   5.0
  5.0 E  7   5.0
 5.000E  7 5.000E  0
    6     8     2     1
    1   361   401   481   601   641
0000000000000000000000      END OF FILE
```

APPENDIX A2

# PHOTOFABRICATION TECHNIQUES

To supplement the outline given in Chapter 6 of the procedures developed for the manufacture of the surface-wave delay lines, further details of the photographic equipment and procedures used are documented below. Apart from the substrate heater, (Section A2.3.3) which was supplied by Dr. P.V.H. Sabine, and assistance in the design of the two reduction cameras (Sections A2.1.3 and 2.1.4) and the laminar-flow cabinet (Section 2.3.1) from the author's supervisor, Dr. P.H. Cole, all the equipment and techniques described in this Appendix A2 were developed by the author.

## A2.1 Photographic Reduction

### A2.1.1 Artwork

EITHER

| | | |
|---|---|---|
| Hand-cut masking film | : | Rubylith D3R 40" wide |

OR

| | | |
|---|---|---|
| XY-plotter | : | 30" Calcomp drum-plotter with incremental drive at 250 steps/inch |
| Drawing surface | : | Matte cellulose triacetate |
| Drawing ink | : | Calcomp GP1 black ink |

### A2.1.2 Copy board

| | | |
|---|---|---|
| Working Area | : | 30" x 40" |
| Illumination | : | 6 apple-green 48" fluorescent tubes |
| Filter | : | Kodak Yellow Sheeting |
| Diffuser | : | ¼" white opalescent perspex 4" behind glass (must be out of focus) |
| Screen | : | 3/8" plate glass |

### A2.1.3 First Stage Reduction Camera

| | | |
|---|---|---|
| Lens | : | Wray 12" f/10 process copying optimised for 4:1 |
| Reduction range | : | 2½X to 5X |
| Film size | : | 10" x 8" sheets |

| | | |
|---|---|---|
| Film type | : | Kodalith ortho Type 3 on .007" estar base |
| Film support | : | Vacuum hold-down |
| Working area | : | 9" x 7" |
| Processing | : | |

| | | |
|---|---|---|
| Clean film | - | clean blower brush |
| Expose | - | 1 sec. at f32 |
| Develop | - | 5 min. in Kodak D19 developer (undiluted) at 20°C |
| Stop | - | 30 sec. in Kodak Stop Bath |
| Fix | - | 2 min. in Kodak Fixer |
| Rinse | - | 5 min. running water |
| Wetting Agent | - | 30 sec. in Kodak Photoflo |
| Dry | - | dry suspended in laminar-flow clean cabinet |

### A2.1.4 Second Stage Reduction Camera

| | | |
|---|---|---|
| Lens | : | Wray 3" f4 process copying optimised for 25:1 |
| Reduction range | : | 20X to 35X |
| Plate size | : | 2" x 2" glass plates |
| Plate type | : | Kodak High Resolution Plate |
| Plate support | : | Spring pressure against 3-point support studs defining image plane |
| Working area | : | $1\frac{3}{8}$" x $1\frac{3}{8}$" (radiused corners) |
| Processing | : | |

| | | |
|---|---|---|
| Filtration | - | chemicals vacuum filtered through No. 1 paper |
| Clean plates | - | gas-blast from 50 p.s.i. filtered dry-nitrogen supply |
| Expose | - | 100 sec. at f5.6 |
| Develop | - | 5 min. in Kodak D19 developer at 20°C |
| Stop | - | 30 sec. in Kodak Stop Bath |
| Fix | - | 1 min. in Kodak Fixer |
| Wash | - | 30 sec. in distilled water |
| Clear | - | 2 min. in Hypo Clearing Agent |
| Rinse | - | 2 min. in running distilled water |
| Wetting agent | - | 30 sec. in Kodak Photoflo |
| Dry | - | air-dry standing vertical in laminar-flow clean cabinet |

## A2.2 Substrate Preparation

### A2.2.1 Polishing

The substrates were obtained as unpolished rectangular blanks and polished professionally using cerium oxide on a pitch lap

with water as the coolant. The polishing specification was usually to obtain a scratch-free optically polished surface, flat to within one wavelength of light.

### A2.2.2 Cleaning

The standard cleaning procedure, adopted after a number of experiments, was

Ultrasonic Cleaning Bath

2 minutes in trichloroethylene
2 minutes in Decon 75 detergent solution
2 minutes in distilled water
2 minutes in isopropyl alcohol

Vapour Degreasing Bath

Immediately prior to vacuum coating the crystals were loaded into the coating jig and lowered into the refluxing bath (containing analytic quality trichloroethylene) three times for 30 seconds each time, withdrawing the jig between insertions to allow the crystals to cool. At this stage it was found the cleanliness of the crystal surface could be judged visually by watching the 'evaporation line' with the crystals held at a slight angle to the horizontal while the solvent evaporated (in a fume cupboard for safety reasons). This evaporation line should be a smooth curve which progresses steadily down the crystal surface, and any irregularity in this line or its rate of motion usually indicates the presence of contaminant material on the surface and the need for a repeat of the previous cleaning steps.

### A2.2.3 Metal Coating

The crystals, in an aluminium supporting jig, were transferred from the refluxing bath, straight into the vacuum coating unit, which had been previously brought into operating readiness. The coating procedure then followed the steps,

(1) Pump down to $2 \times 10^{-1}$ torr with the rotary pump, switch in the diffusion pump, and maintain this pressure with an air-bleed.

(2) Clean the surface by running the glow discharge (3kV $AC_{RMS}$ at 8mA between high-purity aluminium electrodes) for 10 minutes.

(3) Heat the crystals to $200^{o}C$. The heater upon which the crystal jig was placed was an aluminium block containing 4 quartz-iodide lamps each rated at 100W and run at 10V 15A DC. The block temperature was monitored using a chrome-alumel thermocouple.

(4) Shut-off the air bleed and pump down to $5 \times 10^{-5}$ torr.

(5) Heat the filament (made from 3 twisted strands of 0.5 mm tungsten wire formed into a 3 turn 1 cm dia. helix) slowly to melt the aluminium loops (0.3 mm wire) crimped to it.

(6) Evaporate the aluminium quickly (to avoid grain growth) using 30A for 5 seconds.

(7) Close off pumps and bleed in air to accelerate substrate cooling.

(8) Transfer crystals under glass to laminar flow bench.

## A2.3 Photolithography

### A2.3.1 Clean Cabinet

A clean cabinet suitable for the photoresist work was obtained by modifying a commercial laminar-flow bench fitted with HEPA filters such that the filtered air-flow went past the operator from right to left instead of straight towards the operator. To prevent accumulation of the toxic solvent vapours associated with resist processing in the darkroom, the air in the cabinet was then vented through the wall of the darkroom (through another filter and fan to prevent ingress of dust when the cabinet was not in use). This arrangement gave a working volume of 150 x 50 x 50 cm., with access by sliding doors along one side as shown in Figure 6.5(a). All the steps in the work described in this section, except resist exposure, were performed in the clean cabinet.

### A2.3.2 Resist Coating

(1) Mount substrate on spinner head (which is mounted directly on the shaft of a ½ H.P. 3-phase 3000 R.P.M. induction motor which can reach 90% speed in approximately 0.5 sec.) and screw the symmetrically opposed rotating jaws (see Figure 6.5(b)) up tightly.

(2) Flood with isopropyl alcohol, filtered through 1.2μm filter in 13 mm Swinney filter holder on the end of a syringe.

(3) Fit safety cover, run spinner for 30 sec., wait for spinner to run down and remove cover.

(4) Dilute 1 volume of Kodak Thin Film Resist (KTFR) with 2 volumes of KTFR Thinner and mix thoroughly.

(5) Assemble a carefully cleaned stainless steel 13 mm. Swinney filter-holder by placing, in order, upon the stainless steel support screen a 1.2μm Gelman Acropor filter membrane (AN-1200), a 10μm Millipore Mitex filter (LCWPO 1300) and a Millipore glass prefilter (AP2501300). Fit the filter to a glass syringe.

(6) Eject 2 ml. of diluted resist through the filter nozzle to waste and then flood the surface of the metallized substrate with filtered resist.

(7) Fit the safety cover, run the spinner for 30 sec., wait for it to stop and remove cover. (Film thickness should be about 5μm.)

(8) Transfer substrate to a hotplate and bake for 15 min. at 90°C. (Set hotplate thermostat to maximum and use a Variac and thermocouple probe to monitor the temperature.)

(9) Allow substrate to cool.

A2.3.3 Contact Printing

(1) Place contact printing jig (Figure 6.6(a)) under alignment microscope (Figure 6.5(a)).

(2) Insert glass plate, emulsion side up, and clean with blower and filtered dry nitrogen blast.

(3) Invert substrate and lower carefully onto glass plate and check alignment with pattern marks on glass slide through microscope.

(4) Close the top cover over the exposure jig and evacuate the interior.

(5) Run lamphouse for at least 10 mins. with cover on top to stablize the operating temperature of the lamp.

(6) Place exposure jig over the exposure aperture in the lamphouse (Figure 6.6(b)) for 50 sec. and return it to clean cabinet (lamp is Philips MLU-300).

(7) Release the vacuum with the needle-valve, remove crystal, place resist side up and allow to cool.

(8) Develop by immersion sequentially in 2 beakers of KTFR Developer, 20 sec. each with continuous agitation. (Beaker 2 should have clean developer and when slightly used should replace beaker 1 which is discarded and a new beaker 2 is obtained etc.)

(9) Flood the surface immediately after development with a good flow of KTFR Rinse from a squeeze bottle or syringe.

(10) Allow to dry with the substrate surface near-vertical.

(11) Examine resist image under microscope - if not acceptable stop and repeat from (1).

A2.3.4 Etching

(1) Bake crystal on hotplate to remove all traces of solvents at 120°C for 20 min. and allow to cool.

(2) Make up etch solution using

| | |
|---|---|
| 16 parts | concentrated $H_3PO_4$ |
| 2 parts | glacial $CH_3COOH$ |
| 1 part | concentrated $HNO_3$ |
| 1 part | $H_2O$ |

(Recipe believed to originate at I.I.T., U.S.A.)

(3) Immerse the substrate in the etchant warmed to 50°C and agitate steadily.

(4) Observe crystal surface carefully and withdraw immediately clear areas of pattern appear clear, at approximately 90 sec. Further etching will produce undercutting of the pattern beneath the resist.

(5) Immediately transfer the substrate into a beaker of distilled water, then rinse under running distilled water.

(6) Dry in the clean cabinet.

(7) Immerse in the resist-stripping bath warmed to 50°C and agitate gently for 2 mins. (Stripper is Type JL1 from Chemical Processes Co., U.K.: do not allow this solution to contact operator's skin.)

(8) Remove the substrate from the solution and flood it with a quick flow of distilled water to sweep the stripped material off the surface.

(9) Dry the substrate in the clean cabinet.

REFERENCES


1. KALLMANN, H.E. 'Transversal Filters'. Proc. I.R.E., vol. 28, 1940, pp.302-310.

2. RAYLEIGH, LORD. 'On Waves Propagated Along the Plane Surface of an Elastic Solid'. Proc. London Math. Soc., vol.17, 1885, pp.4-11.

3. STONELEY, R. 'The Propagation of Surface Elastic Waves in a Cubic Crystal'. Proc. Roy. Soc. (London), vol. A232, 1955, pp.447-458.

4. GOLD, L. 'Rayleigh Wave Propagation in Anisotropic (Cubic) Media'. Phys. Rev., vol. 104, 1956, pp.1532-1536.

5. DERESIEWICZ, H. and MINDLIN, R.D. 'Waves on the Surface of a Crystal'. J. Appl. Phys., vol. 28, 1957, pp.669-671.

6. SYNGE, J.L. 'Elastic Waves in Anisotropic Media'. J. Mathematics and Physics, vol. 35, 1956, pp.323-334.

7. GAZIS, D.C., HERMAN, R. and WALLIS, R.F. 'Surface Elastic Waves in Cubic Crystals'. Physical Review, vol. 119, 1960, pp.533-544.

8. BUCHWALD, V.T. 'Rayleigh Waves in Transversely Isotropic Media'. Quart. Journ. Mech. and Applied Math., vol. XIV, 1961, pp.293-317.

9. ——— . 'Rayleigh Waves in Anisotropic Media'. Quart. Journ. Mech. and Applied Math., vol. XIV, 1961, pp.461-469.

10. COOK, C.E. and VAN VALKENBURG, H.E. 'Surface Waves at Ultrasonic Frequencies'. ASTM Bulletin, May 1954, pp.81-84.

11. VIKTOROV, I.A. 'Investigation of Methods for Exciting Rayleigh Waves'. Soviet Physics-Acoustics, vol. 7, 1962, pp.236-244.

12. ———. 'Rayleigh Waves in the Ultrasonic Range'. Soviet Physics-Acoustics, vol. 8, 1962, pp.118-129.

13. PRESS, F. and HEALY, J. 'Absorption of Rayleigh Waves in Low-Loss Media'. J. Appl. Phy., vol. 28, 1957, pp.1323-1325.

14. LAMB, J., REDWOOD, M. and SHTEINSHLEIFER, Z. 'Absorption of Compressional Waves in Solids from 100 to 1000 Mc/sec'. Phys. Rev. Letters, vol. 3, 1959, pp.28-29.

15. VINOGRADOV, K.N. and UL'YANOV, K.G. 'Measurement of the Velocity and Attenuation of Ultrasonic Surface Waves in Hard Materials'. Soviet Phys. Acoustics, vol. 5, 1960, pp.296-299.

16. MORTLEY, W.S. British Patent 988102, Application date August 1962.

17. ——— . 'Pulse Compression by Dispersive gratings on crystal quartz'. Marconi Rev., vol. 28, 1965, pp.273-290.

18. WHITE, R.M. and VOLTMER, F.W. 'Direct Piezoelectric Coupling to Surface Elastic Waves'. Appl. Phys. Lett., vol. 7, 1965, pp.314-316.

19. ASH, E.A. 'Realization of Microwave Circuit Functions Using Acoustic Waves'. Paper 8-1, 1967 G-MTTT Intl. Microwave Symposium, Boston, Mass., 1967.

20. COQUIN, G.A. and TIERSTEN, H.F. 'Analysis of the Excitation and Detection of Piezoelectric Surface Waves in Quartz by Means of Surface Electrodes'. J. Acoust. Soc. Amer., vol. 41, 1967, pp.921-939.

21. CAMPBELL, J.J. and JONES, W.R. 'A Method for Estimating Optimal Crystal Cuts and Propagation Directions for the Excitation of Piezoelectric Surface Waves'. IEEE Trans. Sonics and Ultrasonics, vol. SU-15, 1968, pp.209-217.

22. LIM, T.C. and FARNELL, G.W. 'Search for Forbidden Directions of Elastic Surface-Wave Propagation in Anisotropic Crystals'. J. Appl. Phys., vol. 39, 1968, pp.4319-4325.

23. ——— . 'Character of Pseudo Surface Waves on Anisotropic Crystals'. J. Acoust. Soc. Amer., vol. 45, 1969, pp.845-851.

24. LOVE, A.E.H. 'Some Problems in Geodynamics'. Cambridge University Press: Cambridge, 1911.

25. STONELEY, R. 'Elastic Waves at the Surface of Separation of Two Solids'. Proc. Roy. Soc., vol. A106, 1924, pp.416-428.

26. BLEUNSTEIN, J.L. 'A New Surface Wave in Piezoelectric Materials'. Appl. Phys. Letters, vol. 13, 1968, pp.412-413.

27. GULYAEV, Y.V. "Electroacoustic Surface Waves in Solids'. Sov. Phys. - JETP, vol. 9, 1969, pp.63-65.

28. MAERFELD, C. and TOURNOIS, P. 'Pure Shear Elastic Surface Wave Guided by the Interface of Two Semi-Infinite Media'. Appl. Phys. Letters, vol. 19, 1971, pp.117-118.

29. ROWEN, J.H. 'High Frequency Dispersive Ultrasonic Delay Lines'. Paper J-6, presented at the 1964 Ultrasonic Symp., Santa Monica, California, Oct. 14-16 (unpublished).

30. ARTZ, R.M., SALZMANN, E. and DRANSFELD, K. 'Elastic Surface Waves in Quartz at 316 MHz'. Appl. Phys. Letts., vol.10, 1967, pp.165-167.

31. BAHR, A.J., LEE, R.E. and PODELL, A.F. 'The Grating Array: A New Surface Acoustic Wave Transducer'. Proc. IEEE., vol. 60, 1972, pp.443-444.

32. HARTMANN, C.S., JONES, W.S. and VOLLERS, H. 'Wideband Unidirectional Interdigital Transducers'. IEEE Trans. Sonics and Ultrasonics, vol. SU-19, 1972, pp.378-381.

33. LEE, R.E. and WHITE, R.M. 'Excitation of Elastic Surface Waves by Surface Heating'. Appl. Phys. Lett., vol.12, 1968, pp.12-14.

34. VOLTMER, F.W., WHITE, R.M. and TURNER, C.W. 'Magnetostrictive Generation of Surface Elastic Waves'. Appl. Phys. Lett., vol. 15, 1969, pp.153-154.

35. LEE, R.E. and WHITE,R.M. 'Elastic Wave Generation by a Gunn Effect Oscillator Coupled to a Piezoelectric'. Appl. Phys. Lett., vol. 16, 1970, pp.343-346.

36. IMSAKUN, K. and WILKINSON, C.D.W. 'Generation of Surface Acoustic Waves Using the Electrostrictive Effect'. Electronics Letters, vol. 8, 1972, pp.555-557.

37. SERAFIN, R.J., FRYBERGER, D. and EPSTEIN, M. 'Measurement of Strain and Velocity of Ultrasonic Surface Waves'. Rev. Sci. Instrum., vol. 38, 1967, pp.1395-1397.

38. IPPEN, E.P. 'Diffraction of Light by Surface Acoustic Waves'. Proc. IEEE (Letters), vol. 55, 1967, pp.248-249.

39. KORPEL, A., LAUB, L.J. and SIEVERING, H.A. 'Measurement of Acoustic Surface Wave Propagation Characteristics by Reflected Light'. Appl. Phys. Lett., vol. 10,1967,pp.295-297.

40. ENGAN, H. 'Experiments with Elastic Surface Waves in Piezoelectric Ceramics'. Elab. Rept. TE-128, Electronics Research Lab., Norwegian Institute of Technology, Trondheim, Norway, 1969.

41. DAVIS, L.E. and CHAMBERS, J. 'Optical Scattering in a Nematic Liquid Crystal Induced by Acoustic Surface Waves'. Electronics Letters, vol. 7, 1971, p.287.

42. BRUUN, M., LUDVIK, S. and QUATE, C.F. 'Field Effect Transistors on Epitaxial Ga As as Transducers for Acoustic Surface Waves'. Appl. Phys. Lett., vol. 18, 1971, pp.118-120.

43. RICHARDSON, B.A. and KINO, G.S. 'Probing of Elastic Surface Waves in Piezoelectric Media'. Appl, Phys. Lett., vol. 16, 1970, pp.82-84.

44. BLACKLEDGE, V.O. and KAUFMAN, I. 'Control of Electron Emission by Elastic Surface Waves'. Appl. Phys. Lett., vol. 15, 1969, pp.127-128.

45. GLOERSEN, P.G. and WHITE, R.M. 'Bolometer Detector for Surface Elastic Waves'. J. Appl. Phys., vol. 42, 1971, pp.1086-1088.

46. WHITE, R.M. 'Surface Elastic-Wave Propagation and Amplification'. IEEE Trans. Electron Devices, vol. ED-14, 1967, pp.181-189.

47. SMITH, W.R., GERARD, H.M., COLLINS, J.H., REEDER, T.M. and SHAW, H.J. 'Analysis of Interdigital Surface Wave Transducers by Use of an Equivalent Circuit Model'. IEEE Trans. Microwave Theory and Tech., vol. MTT-17, 1969, pp.856-864.

48. ——— . 'Design of Surface Wave Delay lines with Interdigital Transducers'. IEEE Trans. Microwave Theory and Tech., vol.MTT-17, 1969, pp.865-873.

49. BERLINCOURT, D.A., CURRAN, D.R. and JAFFE, H., in 'Physical Acoustics', W.P. MASON, Ed., vol. 1A. Academic Press, New York, 1964, pp.233-242.

50. AULD, B.A. 'Application of Microwave Concepts to the Theory of Acoustic Fields and Waves in Solids'. IEEE Trans. Microwave Theory and Tech., vol. MTT-17, 1969, pp.800-811.

51. ——— . 'Surface Wave Theory'. Invited Proceedings of 1970 IEEE Ultrasonics Symposium (LW. Kessler, Ed.), IEEE, New York, 1971, pp.1-15.

52. WHITE, R.M. 'Surface Elastic Waves'. Proc. IEEE, vol. 58, 1970, pp.1238-1276.

53. KINO, G.S. and MATTHEWS, H. 'Signal Processing in Acoustic Surface-Wave Devices'. IEEE Spectrum, vol. 8, 1971, pp.22-35.

54. AULD, B.A. and KINO, G.S. 'Normal Mode Theory for Acoustic Waves and its Application to the Interdigital Transducer'. IEEE Trans. Electron Devices, vol.ED-18, 1971, pp.898-908.

55. FARNELL, G.W. 'Properties of Elastic Surface Waves', in 'Physical Acoustics', vol. VI, W.P. MASON and R.M. THURSTON, Eds. Academic Press, New York, 1970, pp.157-158.

56. Ref. 49, p.190.

57. INGEBRIGTSEN, K.A. 'Surface Waves in Piezoelectrics'. J. Appl. Phys., vol. 40, 1969, pp.2681-2686.

58. 'I.R.E. Standard on Piezoelectric Crystals, 1949'. Proc. I.R.E., vol. 37, 1949, pp.1378-1395.

59. SPIEGEL, M.R. 'Vector Analysis and an Introduction to Tensor Analysis'. Schaum Publishing Co., New York, 1959, pp.166-207.

60. Ref. 49, p.59.

61. BECHMANN, R. 'Elastic and Piezoelectric Constants of Alpha-Quartz'. Phys. Rev., vol.110, 1965, pp.1060-1061.

62. ENGAN, H., INGEBRIGTSEN, K.A. and TONNING, A. 'Elastic Surface Waves in α-Quartz: Observation of Leaky Surface Waves'. Appl. Phys. Lett., vol. 10, 1967, pp.311-313.

63. Ref. 55, p.153.

64. SLOBODNIK, A.J.,JR. and CONWAY, E.D. 'Microwave Acoustics Handbook, vol. 1: Surface Wave Velocities'. USAF Cambridge Res. Labs., Bedford, Mass., Physical Science Research Paper 414, March 1970. (unpublished).

65. SABINE, P.V.H.S. 'Surface Acoustic Wave Scattering at a Periodically Mass-Loaded Surface'. Ph.D. Thesis, Elec. Eng. Dept., Adelaide University, 1973, p.41.

66. TANCRELL, R.H. and HOLLAND, M.G. 'Acoustic Surface Wave Filters'. Proc. IEEE, vol. 59, 1971, pp.393-409.

67. TSENG, C.C. 'Frequency Response of an Interdigital Transducer for Excitation of Surface Elastic Waves'. IEEE Trans. Electron Devices, vol. ED-15, 1968, pp.586-594.

68. ATZENI, C. 'Sensor Number Minimization in Acoustic Surface-Wave Matched Filters'. IEEE Trans. Sonics and Ultrasonics, vol. SU-18, 1971, pp.193-201.

69. HARTMANN, C.S. 'Impulse Response Model for Surface-Wave Transducers'. Texas Instruments Advanced Technology Laboratory Technical Report no. TR-08-72-50, 1972.

70. KRAIROJANANAN, T. and REDWOOD, M. 'Piezoelectric Generation and Detection of Ultrasonic Surface Waves by Interdigital Electrodes: An Electrical Equivalent Circuit'. Electronics Letters, vol. 5, 1969, pp.134-135.

71. COLLINS, J.H., GERARD, H.M. and SHAW, H.J. 'High-Performance Lithium Niobate Acoustic Surface Wave Transducers and Delay Lines'. Appl. Phys. Lett., vol. 13, 1968, pp.312-313.

72. MITCHELL, R.F., WILLIS, W. and REDWOOD, M. 'Electrode Interactions in Acoustic Surface-Wave Transducers'. Electronics Letters, vol. 5, 1969, pp.456-457.

73. KRAIROJANANAN, T. and REDWOOD, M. 'Equivalent Electrical Circuits of Interdigital Transducers for Piezoelectric Generation and Detection of Rayleigh Waves'. Proc. IEE, vol. 118, 1971, pp. 305-310.

74. MILSOM, R.F. and REDWOOD, M. 'Interdigital Piezoelectric Rayleigh-Wave Transducer: An Improved Equivalent Circuit'. Electronics Letters, vol. 7, 1971, pp.217-218.

75. ——— . 'Generation of Acoustic Waves by Single Pair of Electrodes on Surface of Piezoelectric Ceramic'. Electronics Letters, vol. 7, 1971, pp.541-542.

76. SKEIE, H. 'Electrical and Mechanical Loading of a Piezoelectric Surface Supporting Surface Waves'. J. Acoust. Soc. Amer., vol. 48, 1970, pp.1098-1109.

77. ——— . 'Development and Evaluation of an Equivalent Circuit Model for Acoustic Surface Wave Transducers'. Proc. European Microwave Conference, 1971.

78. JONES, W.S., HARTMANN, C.S. and STURDIVANT, T.D. 'Second Order Effects in Surface Wave Devices'. IEEE Trans. Sonics and Ultrasonics, vol. SU-19, 1972, pp.368-377.

79. JOSHI, S.G. and WHITE, R.M. 'Excitation and Detection of Surface Elastic Waves in Piezoelectric Crystals'. J. Acoust. Soc. Amer., vol. 46, 1969, pp.17-27.

80. ENGAN, H. 'Excitation of Elastic Surface Waves by Spatial Harmonics of Interdigital Transducers'. IEEE Trans. Electron Devices, vol. ED-16, 1969, pp.1014-1017.

81. LAKIN, K.M. 'Perturbation Theory for Electromagnetic Coupling to Elastic Surface Waves on Piezoelectric Substrates'. J. Appl. Phys., vol. 42, 1971, pp.899-906.

82. MILSOM, R.F. and REDWOOD, M. 'Piezoelectric Generation of Surface Waves by Interdigital Array'. Proc. IEE, vol. 118, 1971, pp.831-840.

83. BURGESS, A.S. and COLE, P.H. 'Second Order Response Prediction in Acoustic Surface Wave Devices using an Admittance Model'. Proc. 14th National Radio and Electronics Engineering Convention, 1973, pp.144-145.

84. BRACEWELL, R.M. 'The Fourier Transform and its Applications'. McGraw-Hill, New York, 1965, pp.267-273.

85. PAPOULIS, A. 'The Fourier Integral and its Applications'. McGraw-Hill, New York, 1962, p.198.

86. KINO, G.S. and REEDER, T.M. 'A Normal Mode Theory for the Rayleigh Wave Amplifier'. IEEE Trans. Electron Devices, vol. ED-18, 1971, pp.909-920.

87. NALAMWAR, A.L. and EPSTEIN, M. 'Immittance Characterization of Acoustic Surface-Wave Transducers'. Proc. IEEE (Letters), vol. 60, 1972, pp.336-337.

88. ABRAMOWITZ, M. and STEGUN, I.A. 'Handbook of Mathematical Functions'. Dover Publications, New York, 1965, Chapter 17, pp.587-626.

89. HARTMANN, C.S., BELL, D.T. and ROSENFELD, R.C. 'Impulse Model Design of Acoustic Surface-Wave Filters'. IEEE Trans. Microwave Theory and Techniques, vol. MTT-21, 1973, pp.162-175.

90. SMITH, W.R., GERARD, H.M. and JONES, W.R. 'Analaysis and Design of Dispersive Interdigital Surface-Wave Transducers'. IEEE Trans. Microwave Theory and Techniques, vol. MTT-20, 1972, pp.458-471.

91. SUGIYAMA, K. and YOSHIKAWA, S. 'Transient Response of Interdigital Surface Wave Transducers'. IEEE Trans. Sonics and Ultrasonics, vol. SU-20, 1973, pp.34-38.

92. Ref.85, Appendix 1 and Equation 1-32, pp.269-282.

93. BURGESS, A.S. 'Numerical Computation of Fourier Transforms'. Proc. 14th National Radio and Electronics Engineering Convention, 1973, pp.38-39.

94. COOLEY, J.W. and TUKEY, J.W. 'An Algorithm for the Machine Calculation of Complex Fourier Series'. Math. of Comput., vol. 19, 1965, pp.297-301.

95. COOLEY, J.W., LEWIS, P.A.W. and WELCH, P.D. 'The Fast Fourier Transform and Its Applications'. IEEE Trans. Education, vol. 12, 1969, pp.27-34.

96. DOWNING, A.R. Private communication.

97. CIZEK, V. 'Discrete Hilbert Transform'. IEEE Trans. Audio and Electroacoustics, vol. AU-18, 1970, pp.340-343.

98. GENTLEMAN, W.M. and SANDE, G. 'Fast Fourier Transforms - for Fun and Profit'. 1966 Fall Joint Computer Conf., AFIPS Proc., vol. 29, Spartan, Washington, D.C., 1966, pp.563-578.

99. WEINSTEIN, C.J. 'Roundoff Noise in Floating Point Fast Fourier Transform Computation'. IEEE Trans. Audio and Electroacoustics, vol. AU-17, 1969, pp.209-215.

100. Ref.84, pp.189-194.

101. JAFFE, H. and BERLINCOURT, D.A. 'Piezoelectric Transducer Materials'. Proc. IEEE, vol. 53, 1965, pp.1372-1386.

102. MITCHELL, R.F. 'Some New Materials for Ultrasonic Transducers'. Ultrasonics, 1968, pp.112-116.

103. COLLINS, J.H., HAGON, P.J. and PULLIAM, G.R. 'Evaluation of New Single Crystal Piezoelectric Materials for Surface Acoustic-Wave Applications'. Ultrasonics, 1970, pp.218-226.

104. SCHULZ, M.B. and MATSINGER, J.H. 'Rayleigh-Wave Electro-mechanical Coupling Constants'. Appl. Phys. Letters, vol. 20, 1972, pp.367-369.

105. VIKTOROV, I.A. and TALASHEV, A.A. 'Transducers Fabricated by Engraving for the Generation and Reception of High-Frequency Surface Waves'. Sov. Phys.-Acoustics, vol.17, 1971, pp.261-262.

106. 'Techniques of Microphotography'. Eastman Kodak Company, Rochester, New York, 1967, pp.17-28.

107. BROERS, A.N., LEAN, E.G. and HATZAKIS, M. '75-GHz Acoustic-Surface-Wave Transducer Fabricated by an Electron Beam'. Appl. Phys. Letters, vol. 15, 1969, pp.98-101.

108. DAMON, G.F. 'The Effect of Whirler Acceleration on the Properties of Photoresist Film'. Proc. of the Second Kodak Seminar on Microminiaturisation, 1966, Eastman Kodak Company, Rochester, New York, 1967, pp.36-43.

109. GRIFFIN, D.W. Private communication.

110. COOK, C.E. and BERNFELD, M. 'Radar Signals, an Introduction to Theory and Application'. Academic Press, New York, 1967, pp.34-37.

111. SALZMANN, E., PLIENINGER, J. and DRANSFELD, K. 'Attenuation of Elastic Surface Waves in Quartz at Frequencies of 316 MHz and 1047 MHz'. Appl. Phys. Letters, vol. 13, 1968, pp.14-15.

112. DANIEL, M.R. and DE KLERK, J. 'Temperature-Dependent Attenuation of Ultrasonic Surface Waves in Quartz'. Appl. Phys. Letters, vol. 16, 1970, pp.30-31.

113. SLOBODNIK, A.J.JR., CARR, P.H. and BUDREAU, A.J. 'Microwave Frequency Acoustic Surface Wave Loss Mechanisms on $LiNbO_3$'. J. Appl. Phys., vol. 41, 1970, pp.4380-4387.

114. LEAN, E.G.H. and POWELL, C.G. 'Optical Probing of Surface Acoustic Waves'. Proc. IEEE, vol. 58, 1970, pp.1939-1947.

115. BUDREAU, A.J. and CARR, P.H. 'Temperature Dependence of the Attenuation of Microwave Frequency Elastic Surface Waves in Quartz'. Appl. Phys. Letters, vol. 18, 1971, pp.239-241.

116. POMERANTZ, M. 'Ultrasonic Attenuation by Phonons in Insulators'. Proc. 1972 Ultrasonics Symposium, IEEE, New York, 1972, pp.479-485.

117. SINCLAIR, R. 'Velocity Dispersion of Rayleigh Waves Propagating along Rough Surfaces'. J. Acoust. Soc. Amer., vol. 50, 1971, pp.841-845.

118. SABINE, P.V.H. 'Rayleigh-Wave Propagation on a Periodically Roughened Surface'. Electronics Letters, vol. 6, 1970, pp.149-151.

119. BELL, D.T. 'Growth, Orientation, and Surface Preparation of Quartz'. Proc. 1972, Ultrasonics Symposium, IEEE, New York, 1972, pp.206-210.

120. LEAN, E.G. and POWELL, C.G. 'Nondestructive Testing of Thin Films by Harmonic Generation of Dispersive Rayleigh Waves'. Appl. Phys. Letters, vol. 19, 1971, pp.356-359.

121. CAMBON, G. and ROUZEYRE, M. 'Attenuation of Dispersive Rayleigh Waves on Quartz'. Electronics Letters, vol. 6, 1970, pp.539-541.

122. BRADFIELD, G. 'Damping of Surface (Sound) Waves by the Air'. Electronics Letters, vol. 4, 1968, pp.95-96.

123. SLOBODNIK, A.J.,JR. 'Attenuation of Microwave Acoustic Surface Waves Due to Gas Loading'. J. Appl. Phys., vol. 43,1972, pp.2565-2568.

124. SZABO, T.L. and SLOBODNIK, A.J.,JR. 'The Effect of Diffraction on the Design of Acoustic Surface Wave Devices'. IEEE Trans. Sonics and Ultrasonics, vol. SU-20, 1973, pp.240-251.

125. TANCRELL, R.H. and WILLIAMSON, R.C. 'Wavefront Distortion of Acoustic Surface Waves from Apodized Interdigital Transducers'. Appl. Phys. Letters, vol. 19, 1971, pp.456-459.

126. GERARD, H.M., JUDD, G.W. and PEDINOFF, M.E. 'Phase Corrections for Weighted Acoustic Surface-Wave Dispersive Filters'. IEEE Trans. Microwave Theory and Techniques (Corresp.), vol. MTT-20, 1972, pp.188-192.

127. WALDRON. R.A. 'Power Transfer Factors for Nonuniformly Irradiated Interdigital Piezoelectric Transducers'. IEEE Trans. Sonics and Ultrasonics, vol. SU-19, 1972, pp.448-453.

128. JONES, W.S., HARTMANN, C.S. and HARRIS, J.L. 'Matching Optimisation to Interdigital Surface-Wave Devices'. Electronics Letters, vol. 6, 1970, pp.333-335.

129. REEDER, T.M. and SPERRY, W.R. 'Broad-Band Coupling to High-Q Resonant Loads'. IEEE Trans. Microwave Theory and Techniques, vol. MTT-20,1972, pp.453-458,

130. REEDER, T.M., SHREVE, W.R. and ADAMS, P.L. 'A New Broadband Coupling Network for Interdigital Surface Wave Transducers'. IEEE Trans. Sonics and Ultrasonics, Vol.SU-19,1972, pp.466-470.

131. HEIGHWAY, J., TARRANT, D.W. and OXLEY, C.H. 'Simple Approach to the Design of Interface Networks for Acoustic-Surface-Wave Filters'. Electronics Letters, vol. 8, 1972,pp.642-643.

132. SCHMIDT, R.V. 'Excitation of Shear Elastic Waves by an Interdigital Transducer Operated at Its Surface-Wave Centre Frequency'. J. Appl. Phys., vol. 43,1972,pp.2498-2501.

133. RISTIC, V.M. 'Bulk Mode Generation in Surface Wave Devices'. Proc. 1972 Ultrasonics Symposium, IEEE, New York,1972,pp.424-428.

134. DANIEL, M.R., EMTAGE, P.R. and DE KLERK, J. 'Acoustic Radiation by Interdigital Grids on $LiNbO_3$'. Proc. 1972 Ultrasonics Symposium, IEEE, New York, 1972, pp.392-395.

135. LAMB, J. and SEGUIN, H. 'Surface Treatment of Quartz Crystals for Hypersonic Applications'. J. Acoust. Soc. Amer. (Letters), vol. 39, 1966, pp.752-753.

136. CARR, P.H. 'Measurement of the Piezoelectric Constant of Quartz at Gigacycle Frequencies'. J.Acoust. Soc. Amer., vol. 41, 1967, pp.75-83.

137. GRAHAM, G.M. and PEREIRA, F.N.D.D. 'Temperature Variation of the Piezoelectric Effect in Quartz'. J. Appl. Phys. (Communications), vol. 42, 1971, p.3011.

138. JOSHI, S.G. and WHITE, R.M. 'Dispersion of Surface Elastic Waves Produced by a Conducting Grating on a Piezoelectric Crystal'. J. Appl. Phys., vol. 39, 1968, pp.5819-5827.

139. CARR, P.H. 'Reduction of Reflections in Surface-Wave Delay Lines with Quarter-Wave Taps'. Proc. IEEE (Letters), vol. 60, 1972, pp.1103-1104.

140. LOPEN, P.O. 'Second-Harmonic Generation in a Elastic Surface Wave in α-Quartz'. J. Appl. Phys., vol. 39, 1968, pp.5400-5404.

141. LEAN, E.G. and TSENG, C.C. 'Nonlinear Effects in Surface Acoustic Waves'. J. Appl. Phys., vol. 41, 1970, pp.3912-3917.

142. SCHULZ, M.B., MATSINGER, B.J. and HOLLAND, M.G. 'Temperature Dependence of Surface Acoustic Wave Velocity on α-Quartz'. J. Appl. Phys., vol. 41, 1970, pp.2755-2765.

143. SCHULZ, M.B. and HOLLAND, M.G. 'Surface Acoustic Wave Delay Lines with Small Temperature Coefficient'. Proc. IEEE (Letters), vol. 58, 1970, pp.1361-1362.

144. LEWIS, M.F., BELL, G. and PATTERSON, E. 'Temperature Dependence of Surface Elastic Wave Delay Lines'. J. Appl. Phys. (Communications), vol. 42, 1971, pp.476-477.

145. ZELENKA, J. and LEE, P.C.Y. 'On the Temperature Coefficients of the Elastic Stiffnesses and Compliances of Alpha-Quartz'. IEEE Trans. Sonics and Ultrasonics, vol. SU-18, 1971, pp.79-80.

146. CAMBON, G. and QUATE, C.F. 'Dispersive Rayleigh Waves on Quartz'. Electronics Letters, vol. 5, 1969, pp.402-403.

147. ALSOP, L.E., GOODMAN, A.S. and ASH, E. 'Surface Wave Dispersion in a Mass-Loaded Half-Space'. J. Acoust. Soc. Amer., vol. 50, 1971, pp.176-180.

148. BUCARO, J.A. and DAVIS, C.M. 'Rayleigh Wave Dispersion on Surface-Treated Glass'. J. Appl. Phys., vol. 43, 1972, pp.2151-2153.

149. Ref. 110, pp.18-24.

150. LAWSON, J.L. and UHLENBECK, G.E. 'Threshold Signals'. McGraw-Hill, New York, 1950, Figure 8.11, p.208.

151. Ref. 85, pp.226-233.

152. ——. pp.62-74.

153. SASAKI, H., CHUBACHI, N. and KIKUCHI, Y. 'Thickness Dependence of Effective Coupling Factors of ZnO Thin-Film Surface-Wave Transducers'. Electronics Letters, vol. 9, 1973, pp.92-93.

154. HICKERNELL, F.S. 'DC Triode Sputtered Zinc Oxide Surface Elastic Wave Transducers'. J. Appl. Phys., vol. 44, 1973, pp.1061-1071.

155. SCHNITZLER, P., BERGSTEIN, L. and STRAUSS, L. 'Elastic Surface Waves: Thin-Film Transducers and Layered-System Dispersion'. IEEE Trans. Sonics and Ultrasonics, vol. SU-17, 1970, pp.185-188.

156. SANDBANK, C.P. and BUTLER, M.B.N. 'Acoustic Surface Waves on Isopaustic Glass'. Electronics Letters, vol. 7, 1971, pp.499-501.

157. WAUK, M.T. 'Suppression of Spurious Triple-Transit Signals in Acoustic Surface-Wave Delay Lines'. Appl. Phys. Letters, vol. 20, 1972, pp.481-483.

158. LEWIS, M.F. 'Triple-Transit Supression in Surface-Acoustic-Wave Devices'. Electronics Letters, vol. 8, 1972, pp.553-554.

159. PANTER, P.F. 'Modulation, Noise, and Spectral Analysis'. McGraw-Hill, New York, 1965, pp.705-710.

160. Ref.110, pp.5-9.

161. BARKER, R.H. 'Group Synchronizing of Binary Digital Systems'. in Communication Theory, W. Jackson, Ed., Butterworth, London, 1953, pp.273-287.

162. SQUIRE, W.D., WHITEHOUSE, H.J. and ALSUP, J.M. 'Linear Signal Processing and Ultrasonic Transversal Filters'. IEEE Trans. Microwave Theory and Techniques, vol. MTT-17, 1969, pp.1020-1040.

163. COSTANZA, S.T., HAGON, P.J. and MACNEVIN, L.A. 'Analog Matched Filter Using Tapped Acoustic Surface Wave Delay Line'. IEEE Trans. Microwave Theory and Techniques (Correspondence), vol. MTT-17, 1969, pp.1042-1043.

164. JONES, W.S., HARTMANN, C.S. and CLAIBORNE, L.T. 'Evaluation of Digitally Coded Acoustic Surface-Wave Matched Filters'. IEEE Trans. Sonics and Ultrasonics, vol. SU-18, 1971, pp.21-27.

165. GANGULY, A.K. and VASSELL, M.O. 'Frequency Response of Acoustic Surface Wave Filters. I'. J. Appl. Phys., vol. 44, 1973, pp.1072-1085.

166. ZUCKER, J. and GANGULY, A.K. 'Frequency Response of Acoustic Surface Wave Filters. II'. J. Appl. Phys., vol. 44, 1973, pp.1086-1088.

167. MITCHELL, R.F. and REILLY, N.H.C. 'Equivalence of δ-Function and Equivalent-Circuit Models for Interdigital Acoustic-Surface-Wave Transducers'. Electronics Letters, vol. 8, 1972, pp.329-331.

PUBLICATIONS BY THE AUTHOR


1. BURGESS, A.S. 'Underwater Sound Propagation: a Bibliography'. Library Bibliography No. 296, Ministry of Technology, London, WC2, April 1968.

2. ——. 'Communication Applications of Surface Acoustic Waves - Two-Dimensional Launching Schemes'. Technical Report 1-70, University of Adelaide, Electrical Engineering Department, April 1970.

3. ——. 'Design Problems with Broadbanding Techniques for Surface Wave Transducers'. Presented to 13th National IREEA Convention, Melbourne, May 1971.

4. BURGESS, A.S. and COLE, P.H. 'Second-Order Response Prediction in Acoustic Surface Wave Devices Using an Admittance Model'. Presented to 14th National IREEA Convention, Melbourne, August 1973.

5. BURGESS, A.S. 'Numerical Computation of Fourier Transforms'. Presented to 14th National IREEA Convention, Melbourne, August 1973.

6. BURGESS, A.S. and COLE, P.H. 'Design of Acoustic Surface-Wave Devices Using an Admittance Formalism'. IEEE Transactions on Microwave Theory and Techniques, vol. MTT-21, October 1973, pp.611-618.